UNIFIED AND HETEROGENEOUS MODELING OF WATER VAPOR SORPTION IN DOUGLAS-FIR WOOD WITH ARTIFICIAL NEURAL NETWORKS

by

Anteneh Tesfaye Tekleyohannes

M.Sc. (Ing.), Technical University in Zvolen, 1995

A THESIS SUBMITTED IN PARTIAL FULFILLMENT OF THE REQUIREMENTS FOR THE DEGREE OF

DOCTOR OF PHILOSOPHY

in

The Faculty of Graduate Studies

(Forestry)

THE UNIVERSITY OF BRITISH COLUMBIA
(Vancouver)

March 2010

ABSTRACT

The objective of this study was firstly to investigate and understand sorption properties of earlywood, latewood, annual rings and gross wood. Secondly, to develop a heterogeneous sorption model for earlywood, latewood and annual rings by taking into consideration unified complex interactions of anatomy, chemical composition and thermodynamic parameters. Thirdly, to upscale the annual ring level model to gross wood by applying artificial neural networks (ANNs) modeling tools using dimensionally reduced inputs through dimensional analysis and genetic algorithms.

Four novel physical models, namely, dynamical two-level systems (TLS) model of annual rings, sorption kinetics, sorption isotherms and TLS model of physical properties and chemical composition were derived and successfully validated using experimental data of Douglas-fir. The annual ring's TLS model was capable to generate novel physical quantities, namely, golden ring volume (GRV) and golden ring cube (GRC) to which the sorption properties are very sensitive, according to the validation tests. A new heterogeneity test criterion (HTC) was also derived. Validations of the TLS sorption models revealed new evidence showing a transient nature of sorption hysteresis in which boundary sorption isotherms asymptotically converged to a single isotherm at large time limit. A novel method for the computation of internal surface area of wood was also validated using the TLS model of sorption isotherms. The fibre saturation point prediction of the model was also found to agree well with earlier reports. The TLS model of physical properties and chemical composition was able to reveal the self-organization in Douglas-fir that gives rise to allometric scaling. The TLS modeling revealed existence of self-organizing criticality (SOC) in Douglas-fir and demonstrated mechanisms by which it is generated.

Ten categories of unified ANNs Douglas-fir sorption models that predict equilibrium moisture content, diffusion and surface emission coefficients were successfully developed and validated. The network models predict sorption properties of Douglas-fir using thermodynamic variables and parameters generated by the four TLS models from chemical composition and physical properties of annual rings. The findings of this study contribute to the creation of a decision support system that would allow predicting wood properties and processing characteristics based on chemical and structural attributes.

TABLE OF CONTENTS

LIST OF TABLES

LIST OF FIGURES

ACKNOWLEDGEMENTS

I owe the successful completion of this graduate research to many people. First and foremost I am very much indebted to my graduate and research supervisor Dr. Stavros Avramidis, for his patience, support, immense knowledge and resourceful guidance. I would also like to thank my graduate supervisory committee, Drs. Shawn Mansfield, Simon Ellis and Luiz Oliveira for their constant encouragement, advice and constructive criticism. Dr. Oliveira has been instrumental in inspiring me to undertake this honourable task of solving the complex water vapour sorption in wood and I consider him as the motive force behind the obtained solutions.

Indeed, a graduate research of this magnitude can not be successful without active support of many professionals and close associates. The vital and timely delivery of Douglas-fir samples from Malcolm Knapp University research forest would not have been possible without the kind and unconditional co-operation of Paul Lawson and Ionut Aron. I have enjoyed all rounded technical support of Bob Myronuk from specimen preparation to scientific equipment maintenance and his refined skill enabled me to solve unprecedented technical problems. The assistance of Tom Wray was also vital in meeting accurate specimen specifications. The fast and timely delivery of research supplies and consumables was possible mainly due to conscientious and very dutiful support of Diana Hastings.

I would like to extend further my sincere gratitude to Slobodan Bradic, Kyu Yang (former postdoc from wood characterization lab) and Linoj Kumar, Pablo Chung and Sharon Ewanik (from biotechnology lab) for their kind help during density profile measurement and the chemical analysis of Douglas-fir, respectively**.** Dr Marek Pawlik and Sally Finora were very kind in allowing me to use their surface area measurement equipment and were also very resourceful for every of the assistance I sought for. I would also like to thank Dave Munro of Forintek for providing me with Douglas-fir densitometry data without which results of this graduate research would have been very difficult to achieve timely. I am also indebted to Diane Jones for editing and proof reading the final thesis. Last but not least, I would like to extend my sincere gratitude to crew of SMS-North America, Terry Hopes, Dan Burnett, Phil Hopes, Greg Faucon and Armando Garcia whose instant responses have been decisive in adapting the DVS equipment to water vapour sorption in wood.

DEDICATION

Dedicated to the memory of my much loved parents Tariqua and Tesfaye who unfortunately passed away during the early years of this graduate research.

May their souls rest in peace

1.0. INTRODUCTION

Wood is created in an aqueous medium and maintains its close association with water (aqua) in various forms through out its existence as lignocellulosic material. Sawn wood is usually kiln dried to service conditions before its use in applications such as structural members or re-manufactured items like furniture, doors, windows, cabinets and floorings. Any change in ambient conditions related to temperature and/or humidity causes gain or loss of water vapour by wood until equilibrium is attained. This phenomenon, termed "sorption", is a dynamic process that accompanies every change in ambient conditions when water is either adsorbed or desorbed by wood. The rate of moisture gain or loss and the level of equilibrium moisture content (M_{emc}) are not exact and vary depending on wood attributes and environmental conditions. Knowledge of the exact sorption properties is important since moisture directly affects most physical and mechanical properties of wood.

Many thermodynamic theories and prediction models of water vapour sorption exist that are applicable to wood and wood products. Most are developed for the estimation of moisture content within a certain range of relative humidity or temperature, and some are proposed as improvements over others for a given application. After certain parameter tuning, the models predict M_{emc} based on ambient conditions, however, they cannot provide explanations for variations in M_{emc} at given ambient conditions and neither do most of them sufficiently explain the theoretical reasoning for the parameters tuning required for satisfactory prediction.

The variations in M_{emc} are linked to the heterogeneities in chemical composition and structure of each wood species in general and individual wood pieces in particular. Model parameters are also emergent properties that are attributes of the complex wood-water thermodynamic interactions. Ideally, sorption models should incorporate information about the structure and composition of wood for satisfactory prediction in a wide range of applications, in addition to parameters solely adjusted to given ambient conditions and highly specific experimental data. Incorporation of the various factors that affect water vapour sorption in wood is a complex and challenging task as it means multidimensional integration of sorption theories. Owing to the heterogeneous complexity of the interaction between water

vapour and wood, the existing conventional physical models in their current theoretical formulation become very complex and are hardly solvable if they are required to include detailed properties of wood. The requirement of simplifying assumptions about the similarity of adsorption layers is a typical challenge one should always face while including thermodynamic heterogeneity in molecular layering. Indeed, simplification of thermodynamic problems by neglecting property heterogeneity is the well known and generic reason that is limiting the prediction power of sorption models. It is, therefore, necessary to introduce and implement non-conventional systemic approaches of the emerging science of complexity which utilizes powerful tools that can deal with the challenges of heterogeneity.

Many of the assumptions required in model derivation could be minimized if modeling is carried out at the least heterogeneous level with the minimum number of components rather than neglecting the inherent heterogeneity. Identification and characterization of the least homogeneous level is a demanding task since it may mean a study at the atomic level. Moreover, characterization of micro-sorption properties is still an ambitious frontier even at cell-wall level. Due to these technical constraints, earlywood and latewood were taken as the least heterogeneous levels for sorption properties of wood in this study. Earlywood and latewood mostly possess definite transversal anatomical boundaries and are also suitable for reliable localized measurements of physical properties and chemical composition.

The task of generalizing earlywood and latewood sorption properties to gross wood is also a formidable one because the sorption properties of the latter are not in a linear relation with the former. Earlywood and latewood are representations of wood formed as a result of complex interactions of growth parameters whose variability is difficult to predict. Their definite characteristics can combine in infinite ways giving rise to infinite variations of gross wood properties. This implies the highly complicated nature of generalizing studies made on earlywood and latewood properties to gross-wood. The multidimensional interactions in multi-component systems are complex. The best tool that could facilitate prediction of properties of such a complex system is knowledge of mechanisms of self-organization of characteristic parameters or lengths by which the system could be described. Self-organization is a mechanism by which systems spontaneously create internal structures and patterns in response to changes caused by external agents. But external agents do not have

the ability of controlling the spontaneous internal changes. Knowledge of the scaling behaviour of characteristic lengths could guide systematic selection of the most probable possibilities in the space of infinite variations by reducing dimensionality or complexity. However, this does not always give rise to the ability of predicting gross wood sorption properties. Complex systems, except in some special cases of one-dimensional numerical or computational integrability, are not usually amenable to analytical solutions. Nonetheless, self-organization can still render a solution through computational tools. Artificial Neural Networks (ANNs) are such tools, inspired by the assumed self-organization in human brain that can learn, classify and predict very complex and nonlinear mechanisms.

Implementation of this task requires two steps. Firstly, developing a sorption prediction model at the annual ring level and secondly, upscaling the model to gross wood that is applicable for all wood species. The simplest way of executing these tasks may be, to carry out matched property measurements at annual ring and gross wood levels and then use the matched data for training, testing and validation of the ANNs model. Although this approach seems simple, it requires a vast amount of matched data for each measured property at both levels. This is because ANNs can not create a cognitive and computationally efficient system which is close to the human brain due to the multitude of neuronal connections required (the human brain have more than 100 billion neurons and each of them can have up to 3000 connections). In addition to that, more connections of neurons mean more parameters that will deplete the explanatory capability of ANNs prediction thereby reducing our limited opportunity of gains in understanding the mechanisms of sorption. Therefore, the number of connected parameters (neurons) needed to create a universal cognitive system is not within the bounds of present computational power. The demand for excessive computational power can be offset or minimized by providing large numbers of training data that are assumed to be sufficient to explore and discover the governing input-output relationships. However, in most situations it is difficult or impossible to have the required amount of matched datasets that contain all variables of interest. As a result of this, the neural networks are trained with available limited amount of data. A neural network model developed in this way may work well for the data domain from which it is obtained, but is difficult to prove its validity to the modeling and prediction of similar phenomena at large.

The problem of validity is caused by the high dimensional nature of multivariate data modeling in general and ANNs modeling in particular. Some dimensional reduction tools such as dimensional analysis and genetic algorithms have been implemented to tackle and solve similar problem situations. Dimensional analysis and reduction becomes an effective tool if the participating variables and the output can enter into some relations that can be scale dependent or invariant. Empirical evidence revealed existence of scale dependent and invariant mechanisms during sorption of water vapour in wood, consequently dimensional analysis has been applied in this study. Empirical evidences further indicate existence of chaotic phenomena similar to self-organizing criticality (SOC) in the wood-water vapour interaction. SOC is governed by slowly driven scale invariant mechanisms, thus, the tendency of wood properties and sorption to display this type of long-range temporal and spatial evolution is utilized in this study to explain sorption hysteresis and associated prediction inconsistencies.

A close microscopic examination of an annual ring reveals a gradual, but stepwise transition from earlywood to latewood that macroscopically may coarse-grain into two distinct phases. The reason for phase separation in an annual ring into earlywood and latewood can obviously be attributed to growth conditions that are partly affected by seasonal changes which in a physical sense can be likened to periodic external parameter switching. In dynamical systems, similar mechanisms are studied by introducing various paradigms of driven physical systems. The scope of this study does not allow us to go deeper and study details of growth mechanisms and trajectories that give rise to earlywood and latewood. Therefore, our task is restricted to finding average magnitudes of trajectories from the paths of growth ensembles in an annual ring. In this way, we can introduce a concept of ensemble average which in case of earlywood and latewood can be given as a two-level system (TLS) description since there are two distinct phases or components in an annual ring.

The concept of TLS and ensemble energy average is suitable to explain transversal interactions in wood and their time evolution from which various parameters can be obtained. The parameter modeling can be performed first by exploring and proving types of self organizations existing at annual ring level with respect to major explanatory variables of wood properties. Therefore, the TLS self-organization in the interaction of major chemical

components of wood and the corresponding physical properties is applied in this study to explain intra and inter annual rings transversal interactions. The TLS property is similarly applied to describe and model parameters governing sorption mechanisms.

The objective of this dissertation is, therefore, firstly to investigate and understand sorption properties of wood at annual ring and gross wood level. Secondly, to develop a heterogeneous sorption model for earlywood, latewood and annual ring level by taking into consideration a unified complex interaction of anatomy, chemical composition and thermodynamic parameters that is based on valid mechanisms of self-organization. And thirdly, to coarse-grain (upscale) sorption properties of earlywood, latewood and annual rings to gross wood sorption properties. The sorption prediction models are developed by applying ANNs modeling tools using dimensionally reduced parameters through theory of similarity and dimensional analysis. The objectives of this study are fulfilled by the following deliverables validated based on experiments done Douglas-fir:

- Self-organization and scaling of Douglas-fir wood properties and chemical composition.
- TLS behaviour and scaling properties of earlywood latewood and growth rings of Douglas-fir.
- TLS behaviour of sorption kinetics of earlywood, latewood and annual rings of Douglas-fir.
- TLS behaviour of sorption isotherms of earlywood, latewood and annual rings of Douglas-fir.
- ANNs sorption prediction model for earlywood, latewood, annual rings and gross wood of Douglas-fir.

The deliverables are expected to positively contribute to the creation of a decision support system that will allow predicting wood properties from the structure and chemistry of physically, chemically or biologically modified or native wood. Should the latter are possibly simulated by tree/forest growing models then the ability to grow forest that will be capable of yielding wood of specific properties in addition to the density ones would become a reality in the future.

1.1. Scope and limitations of this graduate research

The scope and limitations of this graduate research are given in two subtopics. The first subtopic describes the scope based on the objectives stated in the introduction part. The second subtopic describes the limitations as those arising from the bottom-up approach and those that are caused by constraints of experimental conditions and resources.

1.1.1 Scope of this graduate research

The scope of this study ranges from investigating and understanding sorption properties of earlywood, latewood, annual rings to the development of a coarse-grained sorption model of gross wood. All pertinent models are developed by considering unified complex interactions of anatomy, chemical composition and thermodynamic parameters. Due to time and experimental resources constraints, sorption, anatomical, chemical composition and physical properties related experimental data were generated and collected only for Douglas-fir species using three breast height disks obtained from three trees that originated from the same forest site. The modeling and coarse graining is carried out using artificial neural networks. Four additional physical models are developed to help the network models compensate for reduced generalization due to much localized sampling and the small sample size. Therefore, the modeling of sorption properties of Douglas-fir consists of experimental data collection, physical and neural network models development.

1.1.2. System level limitations arising from the reductionism resembling bottom-up approach

The complexity in wood water vapour interaction is well documented. Complexity is an emergent collective property, which is difficult to understand by reductionism based traditional approach that is prevalent in natural science (Anderson, 1972; Abe and Suzuki, 2009). Spatial as well as temporal correlations between elements in a complex system are so strong that it is essential to treat the relation between the system and its components in a holistic manner. The interaction and correlation of elements at several and in some instances at infinite length scales are the main limitations of current theories and tools which usually

assume independence of system dynamics controlling variables (characteristic lengths). It is therefore difficult to explain the effect of a single assumed controlling variable on the system without due consideration of the complex interaction (influence) from other variables.

In a complex system, complete knowledge of interactions between components or variables can not be warranted. Therefore, the synergy and complimentarity of given variables that are justified to contribute to the prediction of Douglas-fir gross wood sorption properties cannot be warranted to be absolute in representing the complex interactions necessary for sufficient prediction of the state and dynamics of water vapour in wood. They are first and foremost applicable to conditions that are identical to the experimental conditions of validations datasets. As a matter of fact, species wide and generic generalization should always be done after due retesting and revalidation.

In this graduate research the sorption properties of Douglas-fir are modeled to be predicted based on anatomical, physical properties and chemical composition of earlywood, latewood and annual rings in a bottom-up approach. The other system level limitation arises just from the risk of considering the bottom (component) as an independent element of the wood-water vapour interaction. It can be assumed that the collective behaviour of the bottom components (earlywood and latewood) are large enough not to cause frequent symmetry breaking or bifurcation in their manifested gross wood properties. The gross wood properties can be assumed as having permanent configurations as juvenile wood and mature wood or sapwood and heartwood. If this assumption can hold true always, then the number of bifurcations can be assumed to be finite and predictable. However, this is not always true since there are anomalies that disrupt this seemingly permanent configuration. Occurrence of reaction wood and false heartwood can be cited as examples. These anatomical features are known for extreme or significantly deviating properties in chemical composition that can not be accounted by simple local fluctuations in earlywood and latewood properties. These outliers are attempted to be simulated/accounted for by taking Douglas-fir samples from transversal locations where properties usually appear to take minima and maxima. To be specific, the sampling was done at the beginning of mature wood and sapwood. However, it is not possible to account for every extreme transversal configuration that has casual link to complex interactions just by making the sampling at the two locations. Therefore, it is

necessary to scrutinize prediction accuracies in situations where there appears to be deviations from normally observed behaviours. The best strategy in dealing with this type of the unexpected is it to retest and revalidate developed models as new dataset are available.

1.1.3 Limitations arising from sampling and sample size

The raw experimental data used for development of the neural network models had undergone standard statistical analysis regarding the significance of transversal properties variations in physical properties (including sorption) and chemical composition. There are two behaviours of a complex system that are displayed while moving from micro- to global-scale. The first behaviour is the invariance (universal behaviour) displayed across many scales while going up the scaling ladder. The second one is the randomness that arises due to symmetry breaking or bifurcation which makes systems behaviour chaotic (sensitive to small differences in initial conditions) while going up the scale ladder (Marchetti, 2009). This shows that there are two aspects that require attention, behaviours that are long range and that transcend scale and those which are scale dependent with spatial and temporal constraint that mainly display Markovian dynamics.

In this study both behaviours are attempted to be incorporated using statistical and nonlinear physics. Anatomical, physical properties and chemical composition descriptions are modeled as two level systems to capture both behaviours as two components. For example, chemical composition and basic density are coupled in a way to capture the randomness in the occurrence of density (that can be described by deterministic Hamiltonian) that can take many values for scale invariant behaviour of the physical description for aggregated chemical composition. In any case the models are statistical and hence may require detailed description or knowledge of structural elements of earlywood and latewood. This means that there is a need to assure the representativeness of the statistics obtained from the samples of earlywood and latewood of Douglas-fir. The best assurance exists when the sample size is equivalent to the population size which is impossible to achieve in one graduate research. The best that could be done in this graduate research was to incorporate as much of the transversal properties variation as possible in the samples obtained from the three trees. The number of samples used to obtain chemical composition data was only 36 due to the limited number of

configuration of earlywood and latewood used for the sorption properties measurements. It is well known that 36 samples are the minimum number of samples that enable us to do inferential statistics but there is no assurance that the conclusions obtained are definitive. The results are not warranted to be immediately applicable in conditions which are different from the description in the experiment. There is a need to retest and revalidate.

The sorption experiments are done only at two temperatures (25^0C and 50^0C). It is well known that the temperature dependence of wood properties is amenable to a description using Arrhenius equation. However, the measurements done at only two temperatures are not sufficient to be generalized using the Arrhenius equation. Therefore, the temperature dependence of the sorption properties was quantified using the experimental sorption results and data obtained from Wood Handbook of FPL (Simpson and TenWolde, 1999). It can not be warranted that this approach is generally valid unless a validation experiment is done at lower and higher temperatures with similar specimens as used in this graduate research. Hence, the validity of the network model regarding temperature below 25 and above 50^0C should be treated cautiously. There is a need to retrain the network models with sorption data obtained below 25 and above 50^0C to assure the prediction reliability.

Since models derived from data generally depend on database size, it is always recommended that the neural networks developed should be updated as new datasets that are unseen by them during training are available. The datasets that require further incorporation are Douglas-fir and other softwood species. The approach implemented in the development of the network models makes possible their use for the prediction of sorption properties for hardwood species. However, the prediction accuracy must first be tested and validated before any practical use. It can be concluded that the neural network models should be allowed to evolve with availability of new datasets and it is only in this way their prediction reliability can be assured.

2.0. REVIEW OF LITERATURE

2.1. Sorption and its dual nature

Sorption describes the phenomenon of gain, retention and loss of vapour by polymeric, porous or powdery materials (Crank and Park, 1968; Gregg and Sing, 1982). It is a broad term used to describe phenomena that could be of physical (physisorption) or chemical (chemisorption) in nature. Water vapour sorption by wood is considered a physisorption consequence of weak intermolecular forces of interaction energies (Mangel, 2000). The state and dynamics of these energies are determined based on the variables of equilibrium thermodynamics which are temperature, pressure, molar concentration or volume of water vapour in the air and in the wood (Skaar, 1988). Temperature, pressure and molar concentration are macroscopic observables that do not require detailed knowledge about forces of interaction at molecular level (Adkins, 1968). Due to existence of sorption hysteresis, a phenomenon in which the amount of water vapour content is greater during drying (desorption) than moisture gain (adsorption) at similar ambient conditions, some scholars cautioned application of equilibrium thermodynamics to describe sorption in general (Skaar, 1988).

When water vapour is taken up by wood, energy that is called heat of sorption is released and the process is termed adsorption. Similarly, when water vapour is lost from wood the evaporating water absorbs energy that is called heat of vaporization, and the process is termed desorption. Assuming existence of thermodynamic equilibrium conditions, the magnitude of heat of sorption can be obtained from the difference between the enthalpy of free and adsorbed water. It can be measured calorimetrically as heat released when one gram of wood of known moisture content is completely wetted in excess of water. It can also be calculated from Clausius-Clapeyron equation using the relation given in equation (2.1) that requires knowledge of isotherms of sorption at two temperatures for given moisture content (Skaar, 1988):

$$\Delta H_s = R \cdot \frac{d\, ln\left(p / p_0\right)}{d\left(\frac{1}{T}\right)} \tag{2.1}$$

where ΔH_s [J mol^{-1}] is the change in enthalpy of sorbed water, R [8.314 472 J K^{-1} mol^{-1}] is the gas constant, p_0 [kPa] is the saturated vapour pressure, p [kPa] is the partial vapour pressure and T is the temperature in degrees Kelvin.

The equilibrium thermodynamic description of sorption allows satisfactory prediction of the state and dynamics of water vapour in wood without the complications arising from the microscopic details. The enthalpy (heat content), entropy (a measure of disorder) and the Gibb's free energy of water vapour are obtained based on thermodynamic equilibrium consideration (Skaar, 1988; Siau, 1995). However, microscopic processes and interaction forces are fundamental to the understanding of the mechanisms of sorption at any level and can yield consistent theories. Mechanisms of sorption at molecular level are described by studying and simulating all molecular interaction energies such as flexing, vibration and rotation. The intermolecular forces have been studied using newer and continuously improving techniques aimed at probing the structure of water and polymers along with their mutual interaction. However, their use as elementary basis of sorption modeling for exact prediction and description of mechanisms of sorption is not yet within grasp (Monson, 2005; Vesely, 2008). Sorption properties are still, therefore, being determined mainly by macro-level phenomenological studies.

The sorption phenomenon is described by sorption kinetics and isotherms. The sorption kinetics is expressed by a time dependent mass uptake or loss relation while the equilibrium relation of water activity and water vapour concentration in wood at given temperature determines the sorption isotherm. The moisture content, M [%], in wood is determined gravimetrically based on percentage of the mass of the oven-dry wood (ASTM, 2000; Siau, 1995; Skaar, 1988). Sorption isotherms describe moisture contents up to fibre or cell-wall saturation point (M_{fsp}), defined as a point at which moisture content dependent properties of wood show abrupt change when the relative humidity is kept close to 100% (Skaar, 1988).

Babiak and Kúdela (1995) have shown the wide disparity of magnitudes of M_{fsp} that can range from 13-70% of moisture content based on measuring method thus proving how illusive this point is. The mathematical relationships obtained by changing relative humidity and temperature as external stimuli and the corresponding material response as a change in vapour concentration have been used for physical description of sorption isotherms and kinetics. Although, the mathematical expression of sorption is derived based on theories of sorption, the actual sorption isotherms and kinetic models are finally determined based on case-by-case empirical curve fitting.

Sorption is usually described with reference to two variables such as temperature and vapour pressure, adsorption and desorption, isotherms and kinetics, or adsorbate and adsorbent. Although scholars tend to consider sorption as equilibrium thermodynamics, they are not able to refute its non-equilibrium nature, making it possible to describe sorption as a phenomenon involving multiple levels or modes in stable or metastable states (Masaro and Zhu, 1999; Klopffer and Flaconnè, 2001).

The consequence of this study is a physical description that reveals the inherent unity in the two-level or two-component nature of sorption, nevertheless, for the sake of familiarity and convenience in dealing with existing literature, sorption isotherms will be discussed first and then will follow sorption kinetics. Nonetheless, a discourse will be made from one to the other as the need arises.

2.2. Sorption isotherms and their classification

For a wide variety of solids, thousands of isotherms can be obtained by experimental curve fitting (Gregg and Sing, 1982). The widely accepted isotherm classification methods are those of the IUPAC (1972) (International Union of Pure and Applied Chemistry) that were originally proposed by Brunauer, *et al.*, (1940) (BDDT) which groups isotherms into six categories based on porosity and adsorbate-adsorbent system interaction (Figure 2.1). There are other classifications that complement or improve the IUPAC and BDDT. Donohue and Aranovich (1998, 1999) proposed a new classification of isotherms that is supposed to expand the IUPAC to include vapour adsorption in both the sub-critical and critical state.

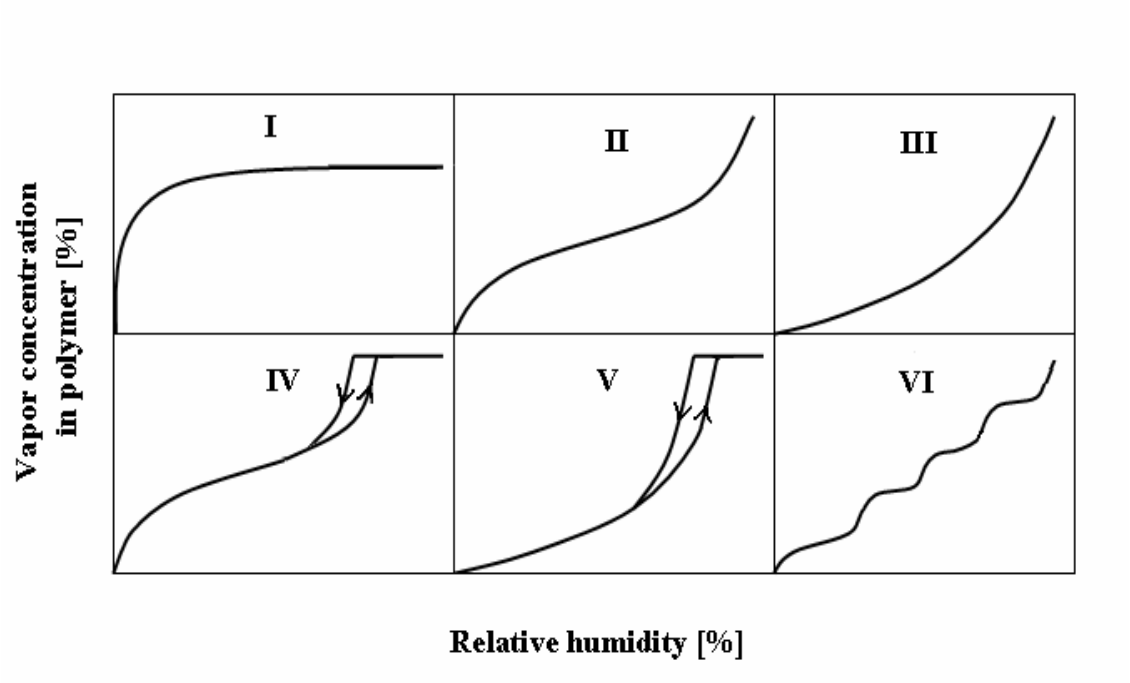

Figure 2.1 The diagrammatic representation of the six types of sorption isotherms drawn to match the IUPAC (1972) classification

One of the benefits of the IUPAC classification is that while empirically determined parameters of models enable prediction of water vapour concentration in a polymer matrix and sorption energies, the shape of fitted isotherms characterize the porosity of adsorbents and strength of interactions in the vapour-polymer system. Specific surface area, pore volume, pore sizes and distribution can be determined if inert molecular probe gases like N_2, Ar, CO_2, and low molecular alkenes used for isotherms measurement (Gregg and Sing, 1982; Groen *et al.*, 2003). Isotherms indicated as type I in Figure 2.1 are typical of microporous sorption while II, III and VI are indicators of nonporosity or macroporosity. The ones indicated as IV and *V* show presence of mesoporosity. The shape of isotherms further indicates the prevailing type of interaction between adsorbates and adsorbents. Type-II and IV denote strong adsorbate-adsorbent interaction over type-III and type-V. The last sorption isotherm of type-VI shows a step wise multilayer adsorption with metastable phases of equilibrium.

Based on the dominant types of interactions in the vapour-polymer system, Klopffer and Flaconnè (2001) categorized sorption into five modes. Mode of sorption describes the prevailing interaction in the adsorbate-adsorbent system. They considered the Henry, Langmuir and Florry-Huggins sorption isotherms as mechanisms defining basic modes of sorption with two more resulting from their combinations. The first basic mode is the Henrian sorption in which the vapour is assumed to have ideal behaviour with no preference either to adsorbate-adsorbate or adsorbate-adsorbent interactions. The isotherm shows a linear relationship between vapour pressure and concentration of the adsorbate in the adsorbent. When the adsorbate-adsorbent interaction dominates, the Langmuirian mode with final saturation state prevails. The combination of Henrian and Langmuirian mode is classified as the dual mode sorption and describes sorption of low-activity vapour in glassy polymers. When the adsorbate-adsorbate interaction dominates then there will be a tendency for clustering or plasticization of the adsorbent. In this case the sorption mode takes the form of Florry-Huggins basic mode with exponential trend in higher vapour pressure. The last class of mode of sorption is obtained by the combination of Langmuirian and Florry-Huggins modes and describes sorption in highly hydrophilic adsorbents.

Sorption of water vapour in wood is represented both by the IUPAC (1972), and Donohue and Aranovich (1999) using the type-II isotherm (sigmoid). According to Klopffer and Flaconnè (2001) the type-II isotherm is represented by a combination of Langmuirian and Florry-Huggins mode. They considered the Florry-Huggins mode as an isotherm that denotes multilayer sorption as described by multilayer BET (Brunauer, *et al.*, (1938)) theory of sorption in which there is a prevailing and step wise adsorbent-adsorbate and adsorbate-adsorbate interaction. IUPAC classifies pores with diameter of less than 5 Å as ultramicropore, 5-20 Å as micropore, 20-500 Å as mesopore and those having diameter greater than 500 Å as macropore. Therefore, based on the size of voids in the cell-wall, diameter of lumens and shape of the sigmoid type isotherm, it can be concluded that, wood is according to IUPAC, mainly ultra microporous and macroporous (Stamm 1964; IUPAC 1972,).

The interaction in a heterogeneous polymer-water system is complex. Hence it has not been amenable to exhaustive theoretical modeling. Many theories have been proposed based on

various assumptions about the mechanisms of adsorbate and adsorbent interactions. However, none of these theories so far is capable of describing and predicting sorption behaviour for all possible variations in material properties and thermodynamic conditions (Avramidis and Iliadis, 2005). Generally, they can be analyzed on the basis of assumptions made about the adsorbent surface geometry and the thermodynamic heterogeneity in the adsorbed film. Initially, most classical sorption theories, including BET, considered the sorption as if taking place on planar surface and implicitly or explicitly assume the adsorbent to be resistant to modifying effect of adsorbates, an assumption which is far from the real world (Cerofolini and Meda, 1998). The inadequacy of BET and similar monolayer sorption models later on lead to a wider acceptance for the existence of at least two non-equivalent adsorbate-adsorbent interaction domains.

With advances in surface probing methods, it has also been shown that the real geometry of adsorbing surfaces is not planar, but a geometric feature that lies between a plane and spatial geometry (Pfeifer *et al.*, 1989). Most sorption theories concur in accepting the existence of thermodynamic differences at least between the first monolayer and subsequently adsorbed molecules. However, they still differ in the concept of the mechanism by which adsorption beyond the monolayer is taking place, and the involved thermodynamic heterogeneity. Sorption theories can thus be generally categorized into two major groups, namely, theories based on molecular layering and those which are based on water-polymer solution formation analogy (Skaar, 1988).

Molecular layering based theories accept the monolayer as primarily adsorbed with the highest energy of interaction. The analogy for subsequent layers in this theory can further be divided into two groups. In the first group are models based on the BET (Brunauer, Emmett, Teller) that assume the primary monolayer sorption to take place on a planar surface and additional molecules to be sorbed in secondary layers with further assumption of equal energy of sorption to that of the enthalpy of bulk molecules (Brunauer *et al*., 1938 and 1940). According to this theory, adjacent molecules in a layer are restricted from interacting with each other or the interaction can be neglected. It recognizes existence of sorption sites that are vacant, with one or multiple layers under equilibrium conditions. The original form of the BET model is given by

$$\frac{V}{V_m} = \frac{C \cdot h}{(1 - h)} \cdot \frac{1 - (n + 1) \cdot h^n + n \cdot h^{(n+1)}}{1 + (C - 1) \cdot h - C \cdot h^{(n+1)}} \quad (2.2)$$

where V_m [$cm^3\ mol^{-1}$] represents the total volume of water in the monolayer, V [$cm^3\ mol^{-1}$] is the total volume of water in all layers, h [kPa] is the vapour pressure, C is the BET constant and n is the number of layers. The BET model was an extension of the monolayer sorption isotherms of Langmuir, but had not been sufficient to describe the majority of sorption isotherms especially at higher vapour pressure. Dent (1977) proposed a model that is based on the same concept of primary and secondary sorbed layers, but with additional consideration of the sorption energy in the secondary layer to be different from bulk molecules.

In the continued endeavour of expanding the BET model to describe all the IUPAC classes of sorption isotherms, the basic assumptions have constantly been modified to various degrees. For example, Le and Ly (1992) model is the one in which some modifications were made and the sorption heterogeneity was considered. However, this model was not capable of sufficiently differentiating the concepts of fractality, molecular clustering and non-interacting columns of sorbed molecules. Boquet *et al*., (1980) demonstrated the similarity among the various models proposed despite the novelty claimed in each. Assuming incremental and decremental variations in heats of sorption in consecutive layers, Augure *et al.*, (1989) showed the possibility of deriving families of BET-like sorption models that can cause over- or underestimation of sorption based on the respective assumptions at higher relative humidity. This includes the three-parameter GAB (Guggenheim, Anderson and de Boer) model which was obtained when the heat of sorption in the multilayer was confined to constancy. Therefore, the magnitude of fitted parameters obtained under various assumptions should be carefully scrutinized as to their validity and conditions of applicability before they are used to explain different energy quantities.

The clustering theory of adsorbed molecules in polymers was proposed to explain some of the thermodynamic inconsistencies in multilayer sorption theories first by Zimm (1953), Zimm and Lundberg (1956) and later by Starkweather (1963, 1974). It has considerably impacted the improvement of analyzing the problems of sorption in polymers associated with

the concept of multilayering. Hartley and Avramidis (1993) used water vapour clustering to successfully describe the potential differences in the mechanisms of adsorption and desorption of water vapour in wood. The actual realization of clustering theory as a tool for analytical solution remains still only a future aspiration due to the associated complexity, except in simulation of numerical solution for the theory of percolation. Of course, application of percolation theory requires a detailed knowledge of the structure and properties of both polymer and adsorbate that are most inaccessible in heterogeneous materials. The work by Perré and Turner (2001) is conspicuous with this regard, specifically in characterizing anatomical features of earlywood and latewood for the purpose of developing a coarse-grained model for bound water diffusivity and thermal conductivity.

Generally, despite satisfactory result obtained in reproducing experimental data, incorporating some aspects of clustering in the BET-type models did not yield theoretical benefits as many parameters were required to form a working model for which there is no clear physical meaning (Cerofolini and Meda, 1998). The multilayer theory predicts monolayer capacity consistently, and in this regard the validity of BET theory is not disputed. However, transfer of the BET monolayer analogy to the multilayer has not shown much success. Models which are consistent in the higher relative humidity range lack the same capability in lower ranges. This typical weakness has been a case for the GAB model that appears to give a satisfactory prediction at higher relative humidity and which is consistently predicting higher monolayer capacity than the BET model (Timmermann, 2003). In any case, a sufficient explanation for sorption beyond the vapour pressure of 0.3, especially close to unity, remains difficult to achieve.

Hailwood and Horrobin (H-H) (1946) successfully applied a concept of two-species or two-domain physical mechanisms to describe vapour sorption in polymers. The H-H model described the sorption process in which the vapour-polymer interaction creates a distinct polymer-hydrate and polymer-solution components in addition to the bare polymer network. The interesting feature in this model is its consideration of phase change analogies in the wood-water interaction. It explicitly recognizes the existence of wood in two phases, namely, dry and hydrated solid, and liquid (solution). The model in its polyhydrate form is given as

$$c = \frac{K \cdot a}{(1 - K \cdot a)} + \frac{K \cdot a \cdot K_1 + 2 \cdot (K \cdot a)^2 K_1 \cdot K_2 + ...}{1 + K \cdot a \cdot K_1 + K \cdot K_2 \cdot (K \cdot a)^2 + ...} \quad (2.3)$$

in which c [g mol^{-1}] is the mole fraction of water on the basis of net weight of polymer, K_i is a corresponding equilibrium empirical constant between the different phases of water and the variable a is the dimensionless water activity. The first and second functional terms of equation (2.3) represent the fraction of dissolved water and that of the polyhydrates respectively.

Equation (2.3) has been satisfactorily applied to wood, but with contradictory prediction of heats of sorption in addition to its weakness in predicting sorption at higher vapour pressure (Simpson, 1979). Feng (2007) introduced a new type of dual-mode sorption (DMS) model to describe a two-domain or two-species sorption mechanism. The model is basically a hybrid of the classical DMS (dual-mode sorption) and ENSIC (engaged species induced clustering) sorption models. The ENSIC was developed as an improvement of the Florry-Huggins model (Favre *et al*., 1996). Based on the new DMS model, all molecules which are sorbed in the matrix region and which are equivalent to dissolved water molecules described in the H-H model are assumed to be in a thermodynamic equilibrium state and have the same partition function. Sorption in microvoid was assumed to be a non-equilibrium property having immobilized water molecules with a sorption mechanism behaving based on assumptions of the GAB model. Despite the explicit assumptions made, the model claims were similar to those achieved by the GAB model.

2.3. Critical behaviours that bridge sorption isotherms to kinetics

In principle, additional numbers of sorption parameters enable more accurate prediction in any domain of interest. Nonetheless, every additional parameter comes with extra complexity to the computational procedure and the gains obtained are offset by computational difficulty, especially when more than three parameters are used. The higher order parameters are associated with long-range interactions and thus it is difficult to confine their role only to higher vapour pressure domain. Analytical solutions usually assume the dependence of mechanisms of sorption on the structure and properties of both the adsorbent and adsorbate.

Many studies revealed that this dependence in many cases takes complex form due to multiple-component and multiphase interaction.

Water displays anomalous behaviour and exhibits polymorphism which is assumed to have been caused by co-existence of two-species or two domains in its chemical and physical properties with possible inter-domain transitions (Poole *et al.*, 1992; McMillan, 2004). These two-state properties are observed in amorphous ice and liquid water and the same properties are confirmed to exist for super cooled crystalline ice and for water vapour (Cerveny *et al*., 2007; Hedström *et al*., 2007; Winkel *et al*., 2008; Greaves *et al*., 2008; Hedges *et al*., 2009). The anomalies that are observed, therefore, are due to first order phase transitions between components or domains. It is known that covalent and hydrogen bonds are involved in the interaction of water molecules. However, it is problematic to view the two bonds as separate and interacting states with a transition from one to another. Because Compton scattering studies revealed the intermingling or overlapping feature of covalent and hydrogen bonds in water which is against prior assumption that considered the two bonds in water as separate (Isaacs *et al.,* 1999).

A similar behaviour that can be compared to two-level and two-component system which is in a state of self-organizing criticality (phase transition) is demonstrated to exist in wood (Tekleyohannes and Avramidis, 2009). The magnitude of the product between the non-dimensionalized value of specific gravity and the non-dimensionalized value of carbohydrate and lignin content is found to scale with the reciprocal value of its own cumulative occurrence (f^{1}). The magnitudes of the scaling exponent ranged from -1.5 to 1.5 that can be linked to self-organizing criticality (SOC). SOC explains the mechanism by which dynamical systems self-organize into a complex but general physical structure that can be described by some statistical properties and simple power laws (Bak *et al*., 1987 and 1988). The SOC behaviour was strong for specific gravity of wood with some amount of moisture present in it and was stronger for specific gravity in saturated state. The state of wood in terms of its chemical composition and magnitudes of its dimensional shrinkage as an expression for the associated moisture content (which is lost) also displayed similar behaviour.

Thermodynamic sorption equilibrium assumes full reversibility; however, existence of sorption hysteresis indicates the equilibrium predicted by sorption isotherms plausibly to be in a metastable state which is far from equilibrium. This brings forth the prime question whether it is proper to treat sorption isotherms as equilibrium state as it is defined in thermodynamics and whether it is justified to neglect the effect of non-stationary or non-saturating kinetics on sorption isotherms (Pan and Liss, 1998). Referring to Morton and Hearle (1962, 1975), Skaar (1988) cautioned the application of equilibrium thermodynamics for modeling of water vapour sorption in wood due to hysteresis.

The association of hysteresis with power laws and some form of criticality was reported by Dahmen *et al*. (2001) based on a decade long study of Barkhausen noise in magnetic systems. The underlying physical mechanism resembled (SOC). Sornette (1994) argued that observed critical behaviour with the hysteretic acoustic emission does not comply with the definition of SOC because the controlling parameter is a sweeping force rather than a slowly and gently driving parameter. However, in the case of sorption hysteresis it can be counter argued that the conditions for SOC are fulfilled. The phase changes associated with pure water and that of adsorbed in polymers, and the self-organizing behaviour that is existing in the chemical composition of wood with regard to moisture content are indicators of phenomena in a critical state (Poole *et al.*, 1992; McMillan, 2004; Cerveny *et al*., 2007; Hedström *et al*., 2007; Greaves *et al*., 2008; Winkel *et al*., 2008; Tekleyohannes and Avramidis, 2009).

In describing water vapour transport in wood, Frandsen and Svensson (2007) summarized and implemented a model which they called multi-Fickian that is inspired by the double porosity model of Krabbenhøft and Damkilde (2004). In addition to the usual moisture transport in cell-wall and cell-lumen that are assumed to be Fickian, the model incorporated another parameter to account for non-Fickian behaviour and it was separately named as "sorption", a name which is usually significant if there is transport of a solute in addition to the solvent (water). The constitutive coupled gradient equations of diffusion for bound and vapour phase water were

$$\frac{\partial c_b}{\partial t} = \nabla \cdot (D_b \nabla c_b) + \dot{c} \ \text{[mol m}^{-3}\text{s}^{-1}\text{]} \tag{2.4}$$

$$\frac{\partial c_v}{\partial t} = \nabla \cdot (D_v \nabla c_v) - \dot{c} \ \text{[mol m}^{-3}\text{s}^{-1}\text{]} \tag{2.5}$$

where c_b [mol L^{-1} or mol m^{-3}] is concentration of water in the bound-water phase, c_v [mol L^{-1} or mol m^{-3}] is concentration of water in water-vapour phases based on oven dried volume of wood, D_b [m^2s^{-1}] diffusion coefficient for bound water, D_v [m^2s^{-1}] is diffusion coefficients water in vapour phase, ∇ is the gradient operator and $\dot{c}$ [mol $m^{-3}s^{-1}$] is given as a correction term named "sorption rate". According to the assumption made, sorption should cease at equilibrium, but it was introduced to describe the non-Fickian mechanism that is similar to non-equilibrium critical behaviour. Although it is claimed that a good agreement is obtained between experimental and numerical values it is commendable that the model should also be tested against long range effects based on anticipated final state at long time limit. In the implementation of the same model, while predicting sorption hysteresis, the scanning curves are regarded as equilibrium paths while they can also be chaotic non-stationary trajectories. In real time, the trajectories may become dependent on their long range history in addition to being Markovian due to the casual relationship of hysteresis to criticality as described by Dahmen *et al*. (2001).

2.4. The origin of non-Fickian and critical behaviour of sorption kinetics

Existence of sorption hysteresis and criticality clearly indicates the inconsistencies and inaccuracies in the prediction of sorption equilibrium and kinetics to be traceable to the separate treatment of kinetics and isotherms as dynamic and equilibrium state values, respectively. When sorption kinetics is treated separately it is described by definition of diffusion which is in turn defined as the movement of matter from places of higher potential or concentration to lower ones. Theoretical explanation of diffusion in solids is complicated and difficult; however, the governing parameter of the process is accepted to be the diffusion constant which is computed based on Fick's first and second laws of diffusion (Masaro and Zhu, 1999). The basic principle of these laws is that the rate of diffusion across any plane at

right angles to the direction of diffusion is quantitatively definable by a linear relation to diffusion constant and concentration gradient. Although the term gradient in diffusion process can be linked to partial vapour pressure, chemical potential and spreading pressure, it can be generally expressed as rate of mass transfer (Stamm, 1964; Jacobs, 1967; Siau, 1995). In steady-state diffusion, concentration is assumed to be constant with time and as a result, the flux is also constant. The actual mathematical relation is known as Fick's first law of diffusion and its one dimensional representation reads

$$J = -D\frac{\partial c}{\partial x} \quad [\text{mol m}^{-2}\text{s}^{-1}] \tag{2.6}$$

where J [mol $m^{-2}s^{-1}$] is the flux, D [m^2s^{-1}] is the coefficient of diffusion, c [mol L^{-1} or mol m^{-3}] is the concentration of molecules and x [mm or m] is the thickness in the direction of diffusion or mass flow. In unsteady-state diffusion where the boundary conditions in terms of concentration and flux are continuously changing, the process of diffusion is more complicated. It is expressed in terms of rate of change of concentration and takes up the form of Fick's second law of diffusion that reads

$$\frac{\partial c}{\partial t} = D \cdot \frac{\partial^2 c}{\partial x^2} \ [\text{mol m}^{-3}\text{s}^{-1}] \tag{2.7}$$

where t [s] is time. Equation (2.6) can be solved by setting corresponding boundary conditions for the transport problem. The diffusion coefficient *D* varies with changes of concentration and temperature (Robertsen and Lönnberg, 1991; Siau, 1995). This can be confirmed from diffusion studies performed using gravimetric and various electromagnetic methods in steady and unsteady state (Skaar, 1954; Iotov, 1998; Masaro and Zhu, 1998; Vesely, 2008).

Fick's laws given by equations (2.6) and (2.7) fall short in describing the process of diffusion in viscoelastic, semi-crystalline and amorphous polymers and hence are not always obeyed (Kalospiros *et al*. 1991; Wadsö, 1992; Roy *et al.*, 2000). In Fickian diffusion, the sorption rate has comparatively very small relaxation effect on the polymer matrix, hence equilibrium

is achieved fast and the boundary conditions are independent of time. However, when viscoelastic phenomena are significant, the rate of sorption is affected by swelling kinetics (relaxation of the polymer matrix). In this case, the overall diffusion process deviates very much from Fick's law resulting in a phenomenon commonly known as non-Fickian.

Non-Fickian diffusion differs from its Fickian counterpart by the shape of sorption half-time curves and relative rates of adsorption and desorption. Originally, Crank and Park (1951) suggested three possible causes of non-Fickian diffusion, namely, variable surface concentration, localized swelling and stresses and memory effect of the diffusion process on the coefficient. Masaro and Zhu (1999) proposed identification of sorption as Fickian (Case-I) and non-Fickian (anomalous and Case-II) diffusion. The case-I diffusion is observed when rate at which the advancing front of penetrant is faster than the polymer molecular structure relaxation and rearrangement process. When magnitudes of the two processes become close to each other then the diffusion becomes case-II. Anomalous diffusion is considered as a state between case-I and case-II diffusion (Roy *et al.*, 2000). Diffusion can also be divided into the three classes based on equation (2.8) (Crank and Park, 1968; Aminabhavi and Aithal, 1988; Masaro and Zhu, 1999).

$$\frac{w_t}{w_\infty} = k \cdot t^n \tag{2.8}$$

where w_t [g or kg] is mass uptake at time t, w_∞ [g or kg] is equilibrium mass uptake, k is an empirical constant and n is an empirical constant that provides information about the nature of the diffusion process. If n has a value of 0.5 then the diffusion is Fickian and a value of n close to 1 implies case-II diffusion. An intermediate value may indicate anomalous diffusion. Many investigators have studied the qualitative aspect of non-Fickian behaviour and the commonly observed trends are summarized in Figure 2.2. Non-Fickian diffusion was observed by Nikolas *et al.*, (1991) and Alfrey *et al.*, (1966) and they attributed the case to the very thin sample size. The non-Fickian diffusion manifested itself as two-stage sorption, sorption overshoot and diffusion with non-overlapping kinetic plots. The observed behaviours are assumed to have been caused by penetrant-polymer interaction that involves

bond breakage and molecular rearrangement associated with relaxation of stresses developed during polymer's swelling (Bagley and Long, 1955; Christensen, 1965; Joshi and Astarita, 1979; Nikolas *et al.*, 1991).

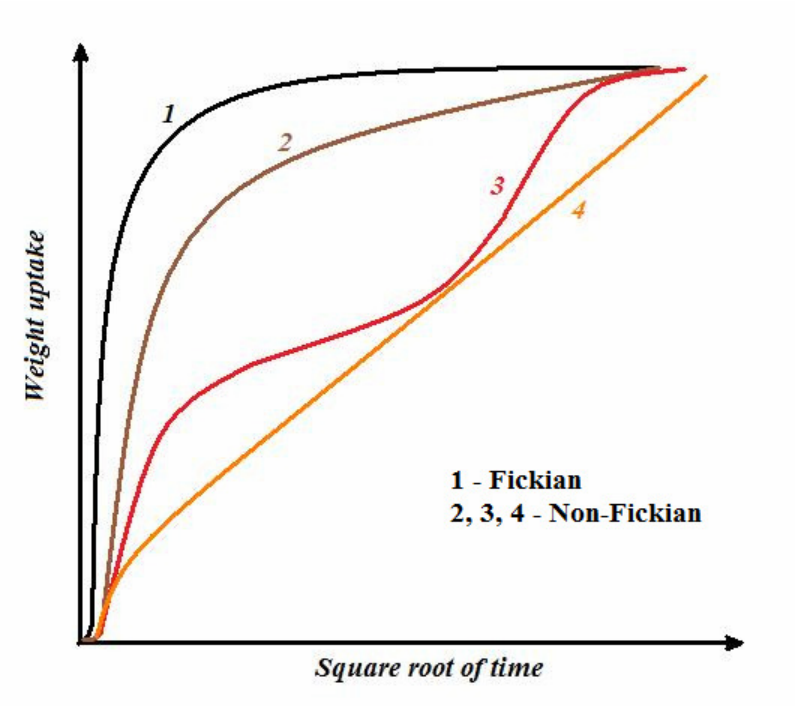

Figure 2.2 Dependence of water vapour weight uptake on the square root of time for Fickian and non-Fickian diffusion

2.5. Models of non-Fickian diffusion

Wadsö (1992) had already listed thirty non-Fickian models which he classified under eight categories. Masaro and Zhu (1999) considered the diffusion process in glassy polymers to be practically non-Fickian since it usually takes place below T_g. They proposed four major categories of diffusion that consist of a number of models based on obstruction effects, hydrodynamic and free volume. Most of the empirical models are formulated in a sense of scaling relationship between the diffusion coefficient, concentration, and the interaction between the polymer and diffusant having a general and simple mathematical relationship that can be implicitly given as

$$D = f(D_0, E_a, w) \cdot f(c, \mu, T, V, l) \tag{2.9}$$

where D [$m^2 s^{-1}$] is diffusion coefficient, $f(D_0,T,w)$ is a function characterizing the polymer, D_0 [$m^2 s^{-1}$] is diffusion coefficient of pure solvent, E_a [J mol^{-1}] is activation energy, w [g mol^{-1} or g g^{-1}] is weight fraction, $f(c,\mu,T,V,l)$ is usually an exponential or power function describing the complex interaction of potentials between the polymer and solvent, c [g mol^{-1}] is penetrant concentration, μ [J mol^{-1}] is chemical potential, T [K] is temperature, V [mL, L, cm^3or m^3] is volume and l [cm or m] is linear length. The relationship is made to accommodate both Fickian and non-Fickian diffusion.

2.6. Non-Fickian diffusion in wood

The slow rate of moisture absorption at higher relative humidity was the first observation of non-Fickian behaviour in wood (Christensen and Kelsey; 1959, 1965). Later on, Wadsö (1992) reported experimental observation of non-Fickian behaviour in wood that he described qualitatively and linked the cause to the samples' thickness. Diffusion in wood has been studied extensively both by isothermal and non-isothermal experimental methods. The Fickian and non-Fickian behaviour was studied by separating diffusion as internal and surface emission (Avramidis and Siau, 1987). The internal diffusion can take two values either based on anatomical direction or porosity. Based on anatomy, it can be determined as transversal and longitudinal. Diffusion has two components in both the transversal and longitudinal directions, namely, bound-water and water vapour diffusion. An empirical formula that gives the relationship between effective diffusion coefficient and diffusion of bound water in the cell-wall and water vapour diffusion in the lumen is given as (Siau 1995)

$$D = \frac{1}{(1-a^2)} \cdot \frac{D_B \cdot D_V}{D_B + D_V(1-a)} \text{ [m}^2\text{s}^{-1}\text{]} \tag{2.10}$$

where D_B [$m^2 s^{-1}$] is bound-water diffusion coefficient of the cell-wall, D_V [$m^2 s^{-1}$] is water-vapour diffusion coefficient of air in the lumens and a [m] is double cell-wall thickness.

Equation (2.10) is derived on the basis of an effective pore and in analogy with electrical conductance by envisioning series-parallel connections of electrical circuits. However, the slowing down (resistance) of vapour diffusion is caused by the delay of the diffusing particles in the dangling ends (attracting ends), bottlenecks and backbends existing in the disordered fractal structure (Havlin *et al.*, 2002). How equation (2.10) relates to the fractal structure of wood and to the chaotic nature of diffusion is still an open question.

Methods that are geared towards separating internal diffusion and surface emission coefficients were developed and implemented. Despite satisfactory agreements of experimental and analytical results on internal diffusion and surface mass transfer reported by individual investigators, there have been inter report disparities (Avramidis and Siau, 1987; Liu, 1988; Avramidis *et al.*, 1992; Siau and Avramidis, 1993; Avramidis *et al.*, 1994; Liu and Simpson, 1996; Siau and Avramidis, 1996).

The qualitative aspect of non-Fickian diffusion at higher moisture contents in the relative humidity range of 75% to 84% was experimentally explored (Wadsö 1994). Cunningham (1994) developed a mathematical model to explain anomalous moisture sorption in wood. Krabbenhøft and Damkilde (2004) also proposed a model describing the delayed sorption of water vapour based on the prior works and recommendations of Wadsö (1994). They suggested a diffusion model with two coupled water transfer processes assuming concentration of bound water and water vapour as driving potentials for the overall diffusion process. Frandensen (2005) stated that he would prefer to call the model that is derived from these two coupling by Krabbenhøft and Damkilde (2004) as "multi-Fickian" rather than non-Fickian moisture transport. Krabbenhøft and Damkilde (2007) reported a model renamed as multi-Fickian that was aimed to be applicable to the non-Fickian domain, too. Recently Yeo *et al*. (2008) determined internal diffusion and surface emission coefficients for Eastern white pine based on Siau and Avramidis (1996), and reported that their results agreed well with that of Siau's (1995). The formula derived by Siau and Avramidis (1996) based on Newman's (1931) solution to diffusion and surface emission coefficient reads as follows

$$\frac{a}{D_a} = \frac{a}{D} + \frac{3.5}{S} \tag{2.11}$$

where D_a [m^2 s^{-1}] is total (effective) diffusion coefficient, D [m^2 s^{-1}] internal diffusion, S [m s^{-1}] is surface emission coefficient and a [m] is half-thickness. Liu *et al.* (1989, 1996) also proposed another method for the separation of diffusion coefficient into surface emission and internal diffusion coefficient applicable to sorption measurements obtained from a single thickness specimen that can be formulated as follows.

$$D = -\left.\frac{0.1654 \cdot a^2}{0.701 \cdot (dt/dE) + 2.05 \cdot t}\right|_E \qquad [m^2 s^{-1}] \tag{2.12}$$

$$S = \left.\frac{0.7010 \cdot D}{D \cdot t / l - 0.1964 \cdot l}\right|_E \qquad [m s^{-1}] \tag{2.13}$$

where D [m^2 s^{-1}] is internal diffusion and S [m s^{-1}] is surface emission coefficient evaluated at time corresponding to selected moisture potential E (usually E=0.5), a [m] is half-thickness and t [s] is the half sorption time. Siau (1995) discussed the wide disparity of reported magnitudes of surface emission coefficient and stated that the mechanisms which lead to the development of surface resistance are little understood. Hence the root causes for these disparities are not exactly identifiable. Therefore, there is no an exact solution so far that enables us to place the surface emission coefficient in the external domain only. Indeed, transport phenomenon is an emergent property that is governed not only by coupling of internal diffusion and surface emission coefficients, but it is also a complex physical mechanism affected by internal and external interacting variables (Wadsö, 1992; Siau and Avramidis, 1995, 1996). Ideal investigations deal with transport phenomena starting from molecular, if possible from atomic, to gross wood with detailed structural characterization of each level with successive coarse-graining.

2.7. Characterization of wood at various structural length scales

It is long known that most materials are heterogeneous; however, during wood physical characterization and development of properties prediction/description models, existing heterogeneities are neglected to obtain analytic solutions. If some aspects of a problem are to

be neglected, then it should be done at a level where those aspects are assumed to have little effect on the description of the system under investigation. In physical systems, levels are usually characterized by length scales. Lu and Kaxiras (2004) categorized possible material characterization levels based on four length scales, namely atomic (~10^{-9}m), microscopic (~10^{-6}m), mesoscopic (~10^{-4}m) and macroscopic (~10^{-2}m). In the case of wood, the macroscopic domain shows typical repetitive (transversally periodic) properties and introduces at least two characteristic length scales, namely, earlywood and latewood, that coarse-grain into consecutive annual rings. The consecutive annual rings further coarse-grain into juvenile heartwood, mature heartwood and sapwood, and they finally emerge together as gross wood.

Categorization of gross wood into juvenile, mature and sapwood is problematic since there is no clear demarcation delineating one category from the other and the transition from one to the other is usually gradual. The transition from juvenile to mature wood is especially troublesome. Juvenile and mature wood have been demarcated using qualitative methods such as dullness for juvenile wood, visual examination of transversal properties trend using width of annual rings or density profile. Optimized demarcation method that employed nonlinear regression techniques has also been developed for some particular species. However, none of these methods are consistent due to high degree of variability of adopted controlling variables (Abdel-Gadir and Krahmar, 1993). This comes as no surprise because growth includes constant phase transition characterized by absence of characteristic length scale as in the case of SOC. Mansfield *et al*, (2009) showed how the demarcation of the transition from juvenile to mature wood quantitatively changed in lodgepole pine when wood density, which is the commonly used variable, was substituted for major fibre traits, namely, microfibril angle (MFA) and fibre length. MFA and fibre length are more directly related to primary growth trends in addition to having a higher correlation and therefore are recommended as better variables to be used in mature-juvenile wood demarcation.

The atomic scale includes the length scale domain for nanoscale. Characterization of the crystalline structure of cellulose from wood and similar materials at nanoscale revealed valuable information that is contributing to the understanding of how wood components are assembled. Cellulose is the major chemical component responsible for hygroscopic

properties of wood which has a crystalline and amorphous component. Recent CP/MAS (Cross Polarization/Magnetic Angle Spinning) NMR studies revealed that the crystalline component has at least two types of crystalline allomorphs (I_α and I_β) that led to the proposal of a model called composite crystal (Horii, 2001). Hydrothermal treatment experimentally proved to affect crystallinity (Dwianto *et al*., l996; Bhuiyan *et al*., 2000; Rayirath *et al*., 2008). Similar type of treatment at high temperature using saturated steam was able to cause a transition between I_α and I_β allomorphs (Horii, 2001). All these patterns of phase transitions along with the hygro-interactions agree with the analogy of two-level and two-component SOC already discussed in section 2.3 (Tekleyohannes and Avramidis, 2009). This is an important finding because the gross wood properties are the result of complex and successively coarse-grained manifestations of the properties of wood from the various structural levels.

The evidence for critical behaviour could imply existence of scale invariant properties which do not require detailed micro-characterization for the description of macro-wood properties. This means that few critical dimensions can explain the physical behaviours of complex and interacting components without a need to have complete knowledge of micro characteristics. In state of criticality, dimensions of all size are present and the system can not be represented by a single characteristic length (Cardy, 1996; Christensen and Moloney, 2005).

A complete knowledge and understanding of gross wood starting from its constituents' atomic structure and ranging up to interacting polymeric components is indispensable for those properties which are scale dependent. However, problems relating to getting pure polymeric isolates have made characterization of cell-wall chemical constituents of wood difficult. This is due to the complex associations between cell-wall chemical components. Nonetheless, there are various standard analytical procedures developed by CPPA (Canadian Pulp and Paper Association), ASTM, TAPPI and ISO that can be used for separation, analysis and chemical characterization of polymeric components, functional groups and linkage of building units (Baezza and Freer, 2001). Owing to the objective and scope of this study, discussions about chemistry of wood can be only up to polymeric composition of cell-wall in earlywood, latewood and gross wood in general.

2.7.1. Variation in chemical composition, criticality and scale invariance in timber species

Variations in chemical composition exist not only between hardwood and softwood but also within the same species. Chemical composition further varies within the same tree longitudinally and radialy from pith to bark. It also varies within an annual ring between earlywood and latewood. These variations are also accompanied by corresponding variations in other wood properties such as anatomical, physical and mechanical (Christensen and Kelsey, 1958; Kennedy and Warren, 1970; Ahlgren *et al.*, 1972; Rawat and Khali, 1990; Pang and Herritsch, 2005). Measurements of chemical composition done on important timber species showed a global variability of alpha-cellulose ranging 39-49%, pentosans 7-20%, lignin 20-37%, extractives soluble in mixture of ethanol-benzene 1-14% (exceptionally up to 24%) and extractives soluble in ether 0.1-7.7% for all timber species.

The chemical composition in softwood species differs slightly from the value given for all timber species. The range for percentage composition of extractives remains the same as previously given while alpha-celluloses content range changes to 38-49%, pentosans 7 to 14.5% and lignin 26-36%. The chemical composition values reported by Forest Products Laboratory in Madison for hardwood and softwood species from a similar climate of the temperate region of North America and Russia including CIS (Commonwealth of Independent States) are summarized in Table 2.1 (Pettersen, 2005). The variability of lignin for both species and glucan content for hardwood species was minimal. Pentosans for both species and glucan content for softwood species showed the maximum variation occurred.

Tekleyohannes and Avramidis (2009) have shown that despite the observed wide variations, the coupled two-level description of chemical composition and physical properties exhibit scale invariance as a result of critical behaviour. The reasons for differences in chemical composition between hardwoods and softwoods are long known. They have cells that are only specific to them or they can have certain types of cells composition with particular quantities. The tracheids in softwoods and fibres in hardwoods are dominant cell types that can control 80% of the gross wood properties. Occurrence of certain growth defects such as compression and tension wood can be a cause for some larger deviation from the average.

Reaction wood results in a decrease in the content of cellulose in softwoods while its effect is the opposite in hardwoods (Saka, 2001).

Table 2.1 Main cell-wall chemical components of hardwoods and softwoods grown in North America and Russia summarized from Pettersen (2005) (From public domain database of FPL)

Region	Chemical composition [%]		
	Glucan	Pentosans	Klason lignin
North America			
Hardwood	44.6±4.1	31.7±3.8	22.5±1.8
Softwood	41.9±1.8	28.5±1.7	29.2±2.0
Russia & CIS			
Hardwoods	44.3±5.1	24.2±3.4	21.9±3.2
Softwoods	48.3±4.8	18.8±2.5	29.0±1.6

Generally, there is an increase in cellulose content from juvenile (pith) to sapwood. In Douglas-fir, two-third of the increment is achieved in the first 16 to 25 rings which are within the range of juvenile wood. Hemicelluloses are assumed to decrease from juvenile to sapwood based on clues obtained from less pronounced increase in holocellulose than that of obtained for simultaneously coupled alpha-cellulose content. As a matter of fact the lignin and extractives contents decline from pith to sapwood (Hale and Clermont 1962).

2.7.2. Variation in chemical composition, specific gravity in annual rings and signatures of criticality

Chemically, earlywood and latewood differ mainly in the content of hemicelluloses with latewood having more than 4% of glucomanan and less glucuronoarabinoxylan. The content of cellulose in Scots pine remained almost constant with earlywood (57%) having higher value than latewood (56%). The reverse was true for balsam-fir with more of it in latewood (50%) than earlywood (45%) (Saka, 2001). Analysis of earlywood and latewood of Douglas-fir showed more alpha-cellulose content in latewood than earlywood, specifically 56% and 48%, respectively. Earlywood has more hemicelluloses and lignin content than latewood (Hale and Clemont, 1963). Similar quantitative values were obtained by Bertaud and Holmbom (2004) from earlywood and latewood chemical composition analysis. Latewood is

consistently observed to have higher content of hemicelluloses, cellulose and less of lignin. Earlywood had more extractives and wider scatter of magnitudes of chemical composition than latewood.

In species with distinct annual rings, the intra annual ring density variation can reach two to three folds (Zobel, 1989). According Mork's definition the part of annual ring becomes latewood when the lumen diameter becomes less than the double cell-wall thickness (Panshin and De Zeeuw, 1980). Although some demarcation methods were proposed based on threshold magnitudes of density ranging 0.40 to 0.55 g cm^{-3}, the transition from earlywood to latewood is gradual in most softwood species (Koubaa *et al*., 2002). Density has been a promising predictor for fibre quality but its control over variability in chemical composition is also weak.

Kennedy and Jaworsky (1990) investigated what controls variation in cellulose content and concluded that it is not controlled by any of the physical variables they had considered and rather attributed the explanation to genetic variation. Zobel (1989) in his comprehensive book on variations of wood properties asserted many wood properties are not correlated or are only slightly correlated. Genetic variations do not give full explanation for all observed variations (Zobel and Jett, 1995). Since polysaccharides are the major cell-wall components, their weak relationship to specific gravity defies rational reasoning unless the relationship is complex and nonlinear. The review so far discussed implies that if we want to use specific gravity as a kind of powerful predictor to properties such as sorption isotherms, kinetics or polysaccharides composition then it is better to deal with wood as a network of complex and nonlinear systems rather than considering it as a simple aggregate of components.

2.8. Network behaviour of wood complex interactions

In view of the discussion in the previous sections, characterizing wood as a multi-component bio-composite with multiple properties having high degree of variability, and incorporating their interaction into theoretical models is necessary. However, obtaining consistent analytical solutions based on conventional theoretical approaches become computationally demanding, perhaps impossible at present due to lack of matching analytical tools.

Especially, if the interaction between wood components and also with water is to be taken as close as to reality, then the computation of interactions becomes difficult. However, in conditions of very complex interactions involving real networks there are some scale invariant features that give a simple description of transport mechanisms. Gallos *et al.* (2007) have shown that metabolic and protein interaction networks, despite their complexity, exhibit scale invariance under length scale renormalization. They were able to characterize the transport properties with a set of critical exponents and they also confirmed a scaling relationship between the degree of nodes and volume of the network. In complex networks with details of connectivity or interaction paths, a transport problem can be expressed in terms of two parameters. The parameters are $T(\ell;k_1,k_2)$ and $R(\ell;k_1,k_2)$ in which T [s] is the average first passage time needed by a random walker to cover a distance ℓ [m] between two nodes with degrees k_1 and k_2 and R [V A^{-1}] is the resistance between the nodes. Gallos *et al.* (2007) used the ohmic resistance in the network simulation while quantifying conductance. It is shown that the following scaling relationship can be obtained using arguments of dimensional analysis:

$$R(\ell;k_1,k_2) = k_2^{\xi/dk} f_R\left(\frac{\ell}{k_2^{1/dk}}, \frac{k_1}{k_2}\right) \tag{2.14}$$

$$T(\ell;k_1,k_2) = k_2^{d_w/dk} f_T\left(\frac{\ell}{k_2^{1/dk}}, \frac{k_1}{k_2}\right) \tag{2.15}$$

where d_k is the exponent describing the scaling of the degree of the network. The resistance exponent ξ and random walk exponent d_w are related through the Einstein relation:

$$d_w = \xi + d_B \tag{2.16}$$

In the homogeneous case equations (2.14) and (2.15) were reduced to $R \approx \ell^{\xi}$ and $T \approx \ell^{dw}$. A similar report was presented by Condamin *et al*. (2007) confirming a scaling dependence of the mean first passage time of the transport phenomenon both on volume of the network and the distance between the source and target. In the case of isothermal heterogeneous

interaction of components in wood, Tekleyohannes and Avramidis (2009) also showed that there is a scale invariant relationship in wood components that is governed by two parameters characterizing the ground state (C_1 - a physical property such as density, weight or volume fraction) and a state that results from complex interactions of components (C_2 – weight fraction of networks of polymeric components) without predefined interaction paths. The relationship reads

$$p\,(b_2/b_1) = A \cdot \left(\left(\frac{C_1}{C_{0_1}} \right)^{b_1} \cdot \left(\frac{C_2}{C_{0_2}} \right)^{b_2} \right)^{b} \tag{2.17}$$

where b_i are scaling exponents, C_{0i} are system threshold magnitudes for the respective variable given as C_i and $p(b_2/b_1)$ is conditional probability for mutual occurrence of scaling exponent describing the active (state of complex interaction) and inactive (ground) state respectively. The exponent b converged to a value of -1 or remained bound to values -1±0.5 as b_2 increased from zero to magnitudes beyond a value of six.

The validity of equation (2.17) confirms the absence of characteristic lengths in the way wood polymeric components combine which is a signature of criticality. Its consequence is two-fold, namely, it demonstrates that the combination of wood components has scale invariant features. The scale invariance can be utilized in scaling without full description of the parameters that govern the wood-components-water system and circumvents the requirement for classical dimensional analysis. It also shows the possibility of applying the renormalization group theory for the purpose of scaling by considering physical properties, wood components and water as heterogeneous interacting networks as given by Gallos *et al*. (2007), which can be demonstrated even by using two components only. A similar principle that utilizes a two-component and two-level self organization has been recently applied to obtain induced pluripotent stem cells (iPS) from skin cells using only two factors and low molecular chemical (Huangfu *et al*., 2008). The two interacting wood components (C_1 and C_2) are the analogy for the two factors or classes and the water is analogous to the low molecular chemical. The low molecular chemical or the water molecules interact with the

two components (C_1 and C_2) and trigger an emergent property through a mechanism similar to phase transition.

The scaling property that emerges while wood is considered as a system comprised of interacting networks helps to describe the wood-water relations with reduced complexity. Moreover, there are effective computational tools that utilize a similar analogy of complex interactions, like the one existing in the networks of the nervous system, to solve problems of prediction, classification and association. Artificial Neural Networks (ANN) are such tools that can be combined with the self-organizing features of the complex and interacting networks in wood components and water vapour to bring about sufficient solutions for prediction and description of sorption in wood. This is a non-conventional approach but, with the necessary complex physical mechanisms, it has the ability to incorporate detailed properties of components.

2.9. Artificial neural networks

ANNs are computation methods inspired by the human brain which can process multidimensional information in parallel or they can be considered as simple models of the brain (Patterson, 1996; Bailer-Jones and Bailer-Jones, 2002). The idea of mimicking the information processing analogy of the human brain using artificial neurons came to light in 1940 by McCulloch and Walter (1943) that were using symbolic binary logic operators. These early concepts were far from the way human brain is believed to function. The anatomy and functional analogies adopted from human brain are shown in Figure 2.3. The soma or cell-body does part of information processing. The short extensions shown as dendrites are input devices while the axon along with all of its extensions is an output device. The square contact devices at the end of extensions of the axon that touch mostly the dendrites of another neuron are the synapses. It is this transfer device that is believed to be adaptive and capable of learning. A synapse is either excitatory or inhibitory. The sensory inputs are propagated in a form of electric potential in the order of 0.1mV. The magnitude of the propagating signal is variable based on the state of the synapse and it determines the

synaptic strength. Incoming electrical signals are integrated and the neuron fires when threshold is achieved (Geszti, 1990).

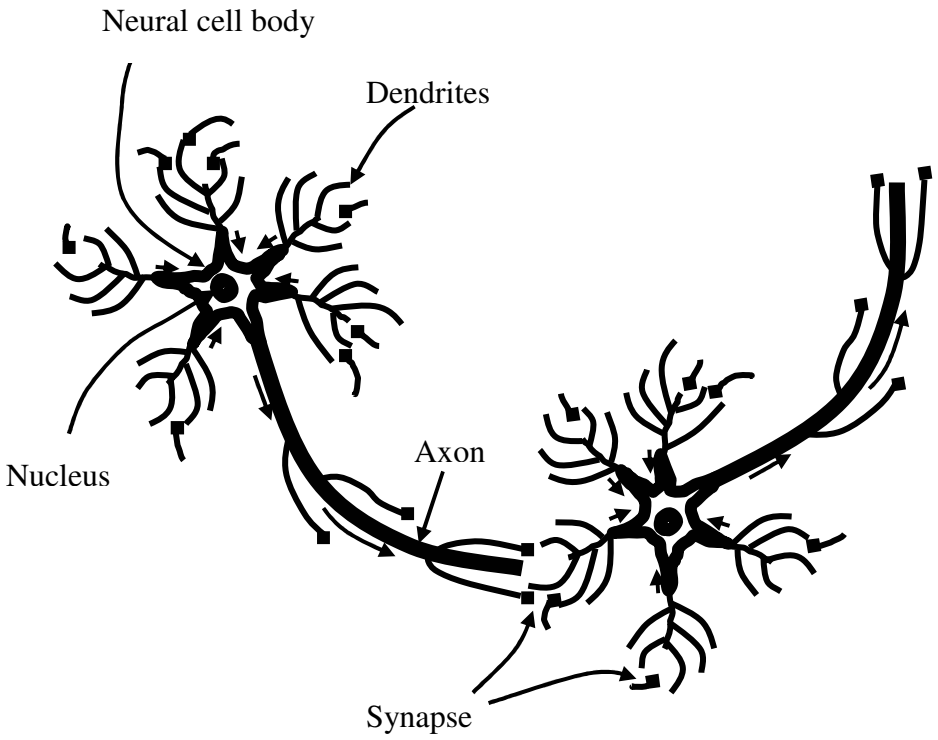

Figure 2.3 Schematic diagram of anatomical feature of biological neurons involved in information processing redrawn in line with the description by Patterson (1996)[*]

Having noticed the setback of binary neuron invented by McCulloch and Walter (1943), Rosenblatt (1958) came up with the early type of neural network that he named perceptron. He demonstrated that a perceptron can learn through supervised and reinforcement methods and can also generalize as the human brain does. Supervised learning is a method where the network is provided both with the sensory inputs and the correct output. On the other hand, during reinforcement learning, the network is provided with sensory inputs and gets feedbacks only about the correctness of its computed output. The perceptron adjusts the weight imposed at each input using a method of gradient descent error correction. A typical

[*] *PATTERSON, DAN, ARTIFICIAL NEURAL NETWORKS, 1st Edition, © 1995. Reprinted by permission of Pearson Education, Inc., Upper Saddle River, NJ*

neuron which is the building block of a perceptron is shown in Figure 2.4. Each input *I* received is multiplied by its weight and summed. The sum is then transformed using a nonlinear function before it is obtained as a target output or an input to another neuron.

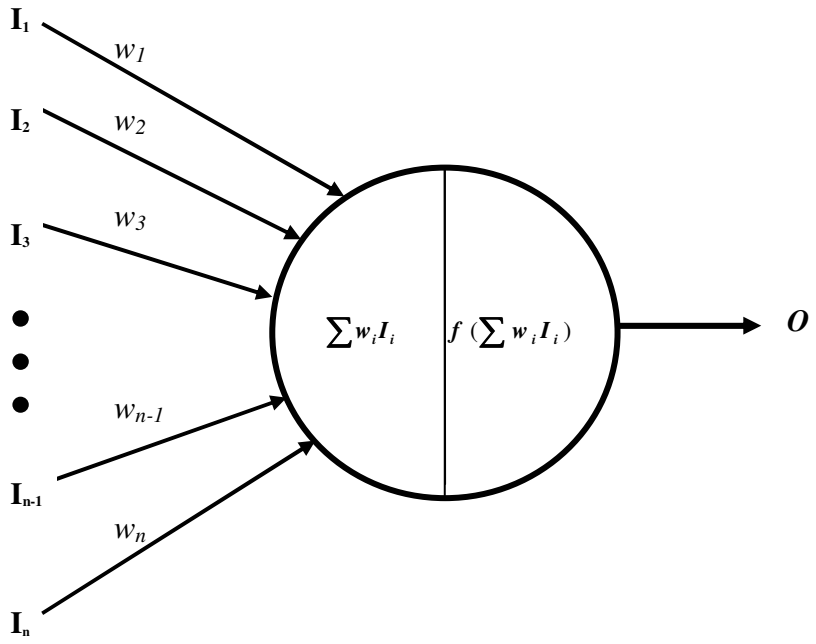

Figure 2.4 Main components and functions of artificial neuron with inputs-I_i and weights w_i summation after multiplication and functional transfer operation that give rise to an output *O*

Despite the inspiring success of the perceptron, in early 1960's, Minsky and Papert (1969) proved that a perceptron itself is far from mimicking the human brain since it can learn only linearly separable categories. The problem associated with the limited capacity of the perceptron reduced the interest in neural networks and stagnated their evolution for two decades. The revival and adoption of neural networks as efficient computational tools is attributed to Kohnen (1977, 1982 and 1984) based on his work on associative memory. Hopefield (1982, 1984 and 1985) and Rumelhart *et al*. (1986) also have a large share in helping the technical progress of neural networks. The discovery of backpropagation by Rumelhart *et al*., (1986) renewed interest in neural networks and triggered evolutionary leap that perfected ANNs to the present day reliable computational tool.

2.10. Artificial neural networks for material properties prediction

There are various multiple inputs and multiple outputs traditional nonlinear regression statistical models which are applied in material property prediction. Nonlinear empirical modeling methods such as projection pursuit regression (PPR), nonlinear principal component regression (NLPCR), nonlinear partial least squares regression (NLPLS), classification and regression trees (CART) and multivariate regression splines (MARS) are some of the statistical tools that are applied (Bakshhi and Chatterjee, 1998). It has been shown that multilayer ANNs outperform the traditional regression tools in every respect (Blank and Brown, 1993). In their review of ANNs, Basheer and Hajmeer (2000) distinguished neural networks as universal, nonlinear, multivariate and nonparametric to super regression tools where the modeling is relatively independent of *a priori* assumptions of mathematical relations.

ANNs are the best choice for modeling where there is sufficient data and unclear theory or in cases where there is sufficient data and theory, but the model is complex to formulate. They can approximate any arbitrary function and predict material property (Belli *et al*. 1999). In some studies it has been shown that the nonlinear and nonparametric feature of ANNs can be incorporated into traditional regression techniques by creating ANNs-regression hybrids. However, this approach has not yet found wider practical applications (Holcomb and Morari, 1992; Joseph *et al.,* 1992; Quin and McAvoy, 1992; Blanco *et al.*, 2000; Marengo *et al.,* 2006). Practical use and potential applications of various forms of ANNs in material property prediction have been proven (Kränz *et al*., 1996; Chen *et al*., 1998; Ripa and Frangu, 2004; Avramidis and Iliadis, 2005; Lightfoot *et al*., 2005; Avramidis *et al.*, 2006; Avramidis and Wu, 2007; Mansfield *et al*., 2007)

ANNs are widely applied in control, optimization, data compression, diagnostics, pattern recognition, prediction and generally in functional approximation. Basically, they are composed of many interconnected nodes called processing elements (PE) or neurons. The way their interconnections are made determines their architecture. The strength of their interconnection is adjusted through algorithmic training to achieve the desired network behaviour and this ability to learn through training is the defining property of ANNs. There

are two major training methods for networks, namely, the supervised and unsupervised. In the supervised training the network is made to learn both the input and output patterns based on representative examples. In a typical ANNs, the supervised training is done on a predetermined network by randomly initializing small weights for each PE. Each training input is presented to the network for computation and the result is compared with the target output to determine the error. The error is then made to back propagate through some predetermined rules so that the weights at each PE are adjusted to reduce the error at the output. The process is repeated until the error drops below an acceptable level. The usual method of error correction is the gradient descent algorithm; however, for some networks stochastic methods are suitable (Patterson, 1996).

Networks trained by the supervised method can be categorized into multilayer feedforward, recurrent, stochastic, and self-growing. A typical feedforward network with input layer of many dimensions, one hidden and a layer with three outputs is shown in Figure 2.5. The middle layer is called hidden because it receives only internal inputs and provides internal outputs. Each input I_i is connected to every node (H_j) of the first hidden layer through a connection weight w_{ij}. At each node of the first hidden layer, the inputs are multiplied by connection weights and summed up based on Figure 2.4. The sum is then computed using nonlinear transfer or mapping function to obtain outputs of the first hidden layer. This operation is repeated in a similar way until the final outputs O_y are obtained. In the backpropagation learning method the network outputs are compared with the target value and the difference is then iteratively back propagated starting from the outer hidden layer towards the first hidden layer. Weight adjustments are made at each hidden node based on predetermined rules so that the error is minimized. The operation is repeated as long as the difference between the network output and the target value is reduced below an acceptable level.

Recurrent neural networks have the output of one or more PEs connected to the inputs of one or more PE in the same or preceding layer including self feedback and lateral connections. They are good at describing spatiotemporal processes; however, the mechanism by which they work is chaotic and there are network stability and convergence issues that are difficult to tackle. They can be described only as dynamical systems and hence are poorly understood

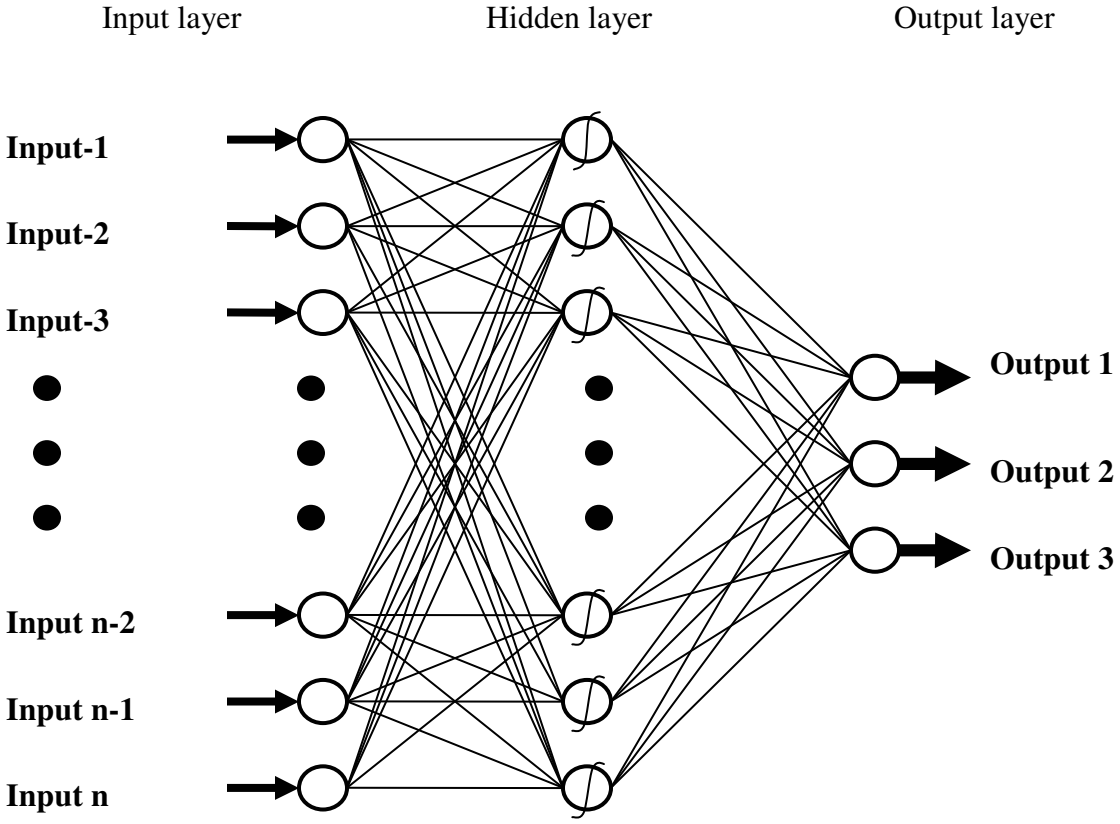

Figure 2.5 Fully interconnected multilayer feed forward (MLF) ANN with one hidden layer

with limited application. Stochastic networks known as Boltzmann machines are a type of recurrent ANNs with a network dynamics in an analogy known as "simulated annealing", a term borrowed from condensed matter physics (Bailer-Jones and Bailer-Jones, 2002). They have hidden PEs and visible PEs that are either input or output units. The Boltzmann machine was proposed to overcome the problem of trapping in local minima during gradient descent error backpropagation training method. However, the network takes long time to attain the required states of energy minima and this limits its utility (Donald, 1992; Gerhard, 1992). Recently, Hinton and Salakhutdinov (2006) reported on the use of the Boltzmann machine in image analysis for dimensionality reduction with improved speed of computation. The self growing networks were proposed to overcome both the trial-and-error way of finding the architecture of a network and local minima trapping. Cascade correlation

networks are typical representative for this category that are commonly applied (Fahlman and Lebiere, 1990). The network is built incrementally starting from the required inputs and outputs by adding one or more hidden PE at a time through a supervised training method. The final result of network building is MLF ANN.

In unsupervised training, the network is not provided with a correct output, but it rather discovers and learns it from regular features of the input. The training is usually done by adjusting the weight of PEs to match features of representative patterns of a group or cluster. The weight at the PEs is adjusted usually through a competitive way. The weight of the PE that responded more is strengthened to match the feature of the input, while the weights of the other PEs are either kept constant or decreased in a form of penalty. Through the principle of "winner-takes-all", more weight is assigned to the active input link to the sensitive PE, while the total sum of weights connected to the same PE remains constant. Self organizing maps (SOM), the Hopefield networks and learning vector quantization (LVQ) are typical networks which are trained through unsupervised way (Rumelhart and Mclelland, 1986; Kohnen, 1989).

Multilayer feed-forward (MLF) ANNs, with a backpropagation learning algorithm are the most widely used for functional approximation, prediction, control, data compression and pattern recognition owing both to their versatility and simplicity (Patterson, 1996; Scarselli and Tsoi, 1998). These are the ANNs selected to be used in this study to fulfill the general objective of the dissertation, which is to understand and model sorption properties of wood. The literature on the different variations of ANNs is now vast and detailed characterization of each of them needs a lot of space. Therefore, the remaining review will be mainly focused on multilayer feedforward neural networks.

2.11. The generalized delta rule for gradient descent backpropagation algorithm

Let H denote the hidden node state in the first layer of ANN. If the hidden node H_l is connected to the input node I_k and output node O_y of the hidden or output layer then the following expressions can be made (Gesszti, 1990; Suykens, 1996).

$$H_l^j = \beta_k + \sum_k w_{kl}^j I_k \tag{2.18}$$

where j represents the number of hidden layers, w_{kl} represents the synaptic strength or connection weight of the k^{th} input to l^{th} hidden nodes in the j^{th} hidden layer, β_k is the state of node at rest or it is the so called bias term. The forward and backpropagation computation procedures take a nested highly nonlinear functional form. The y^{th} output of the network is a function of the nonlinear combinations of states of all hidden nodes.

$$O_y = f\left(\sum_y^v \sum_{x=1}^u w_{yx} \cdot f\left(\sum_{l=1}^q \sum_{k=1}^m w_{kl}^j I_k + \beta_k \right) + \beta_y \right) \tag{2.19}$$

where m is the number of inputs, j is the number of hidden layers, q is the number of processing elements or nodes in the j^{th} hidden layer, u is the number of nodes in the last hidden layers and v is the number of outputs. During the training phase the weight matrix is iteratively updated based on the magnitude of error derivative. The mean squared error (E) is commonly used as measure of the difference between the network output and the target value. E in all training patterns is commonly given

$$E = \frac{1}{2P} \sum_{i=1}^P \sum_{y=1}^V (t_y - O_y)^2 \tag{2.20}$$

where P is the number of training patterns and t_y is the target output value. Let us consider the gradient descent backpropagation training method in which weights are updated after each of computational iteration. The weight updating mathematical relation of each training pattern is obtained from the error derivatives using the following relation

$$\Delta w_{(z+1)} = -\eta \frac{\partial E^p}{\partial w_z} \tag{2.21}$$

in which E^p is the error of a training pattern and η is the learning rate. Generally, the weight updating rule at the output layer that is back propagated layer-by-layer is given as

$$\Delta \boldsymbol{w}_{(z+1)} = \boldsymbol{\eta} \cdot \boldsymbol{\delta}_z \cdot \boldsymbol{t}_y \tag{2.22}$$

where the delta δ_z is error parameter that can be obtained from equations (2.19) and (2.20). It is quantitatively given by

$$\boldsymbol{\delta}_z = \boldsymbol{O}_y \cdot (\mathbf{1} - \boldsymbol{O}_y) \cdot (\boldsymbol{t}_y - \boldsymbol{O}_y) \tag{2.23}$$

The weight updating rule as given in equation (2.22) is computed based on the y^{th} network output and is similarly applied backward until the first hidden layer by invoking the chain rule (Patterson, 1996; Suykens, 1996).

The backpropagation algorithm is executed based on equation (2.19) firstly by initializing small random weights from a range $\mathrm{W} \in \langle -w, +w \rangle$. In subsequent iterations the weights are updated applying the rule given by equation (2.22). Generally, the input's main function is updating their activation level according to externally incoming information (independent variables). The output units generate activation that is used by other systems for interpretation and execution. The network output from j^{th} hidden nodes which is given by equation (2.18) is partly a result of mathematical operation using a transfer function argument, for example in the form of hyperbolic tangent function

$$\boldsymbol{h}^j = \boldsymbol{tanh}\left(\sum_k \boldsymbol{w}_{kl}^j \boldsymbol{I}_k + \boldsymbol{\beta}_k \right) \tag{2.24}$$

or using the most commonly applied sigmoid transfer function (Haykin 1994)

$$\boldsymbol{h}^j = \frac{\mathbf{1}}{\mathbf{1} + \boldsymbol{e}^{\sum_k \boldsymbol{w}_{kl}^j \boldsymbol{I}_k + \boldsymbol{\beta}_k}} \tag{2.25}$$

In practice, it is possible to use other continuous and differentiable linear and nonlinear functions. The collective effect at each hidden node is summed up by performing the dot

products of all values of input nodes and their corresponding interconnection weight w_i. Since the weights and the constants β_i are chosen at random at the beginning, the value of the output will not exactly match with experimental data right at the beginning. During network training, weights are systematically changed until a best-fit description of the output is obtained as a function of the inputs based on gradient descent error optimization algorithm (Bhadesha, 1999).

Data pre-processing aimed at noise removal, dimensionality reduction and elimination of outliers is important for swift ANNs convergence. Multilayer feed forward backpropagation neural networks require a dataset of the same problem domain partitioned into training, testing and validation subsets. The input and output data should be transformed into binary or normalized values in the range zero to one. When data are partitioned, assigning larger test data subset may be helpful to demonstrate the generalization capability of ANNs but it should not be done at the expense of smaller training dataset. General recommendations for allocation of the training datasets range from seventy to eighty percent of the total, while test dataset sizes can range from ten to thirty percent. Validation datasets usually account for about ten percent of the total data.

There are no hard and fast rules regarding the exact size of each data subset. While some suggest an example to weight ratio to be at least greater than four, others opt in favour of a value greater than ten (Basher and Hajmeer, 2000). ANN training starts by the initial selection and application of the randomly chosen weights. It is necessary to determine and decide on optimum learning rate (η) for changing the weight vector and weight updating momentum (δ) that can have values from 0.1 to 1.

The number of training patterns required to attain acceptable level of network performance increases with the number of inputs as the number of parameters or hidden nodes to be estimated increases. The required number of hidden nodes increases exponentially with an increasing number of outputs. However, the number of available labelled datasets is generally limited in most cases. Moreover, an increase in the network parameters makes the model more obscure and very confounded for possible physical explanation. The number of inputs can be reduced through two methods of dimensional reduction which are based on

differing assumptions. One of the methods is based on the selection of variables that contribute most to the outputs using genetic algorithms or in some cases linear regression methods such as principal components analysis (PCA) (Breuckner and Rudolph. 2000;Verleysen *et. al.,*2003; Sánchez-Maroñoz, *et. al*, 2005; Bellamine and Elkamel, 2008).

The other method is dimensional analysis and reduction. The method of dimensional analysis considers all of the physically quantifiable variables to be capable of affecting the output in a way that is complex and nonlinear. It nonlinearly combines as many of the variables as possible for full description of a physical system. This method has the benefit of obtaining some physical explanation for the group of variables that are nonlinearly combined into a single or fewer parameters. An important feature of dimensional analysis and reduction is that it can create models and sub-models that can be as powerful as the ANNs model. ANNs developed and trained using dimensionally reduced variables can generalize, extrapolate and predict better with more explanatory power. Genetic algorithms and dimensional analysis are synergistically applied in this study and are discussed in subsequent sections.

2.12. Reducing the number of inputs using evolutionary tools of artificial intelligence

The idea of evolutionary computing was first introduced in 1960 by Rechenberg. However, it was a decade later that the genetic algorithm was for the first time described by Holland (1973) regarding how the principles of natural selection can be applied to solve optimization problems. Since then, genetic algorithms have been adopted fast and are now being applied to optimize the performance of ANNs models in selecting salient inputs that significantly affect model output. This is done by using a data representation that allows variation operators which maintain a direct behavioural link between parent and offspring as observed in biology. Similar to the biological evolution, small changes in parental structure can lead to small changes in offspring and similarly large parental changes can lead to drastic alterations in offspring (Sivanandam and Deepa, 2008).

In genetic algorithms, a population of individuals is first created and stored in a computer as binary strings and then, the population is evolved by applying principles of variation, selection and inheritance. There are many ways of implementation that can generally be

described as simple iterative algorithmic sequences. The sequences start by initializing a population and subsequently proceed to vary individuals randomly. The fitness of individuals is evaluated at each of iterations and those with better fitness are retained while the rest are discarded. The algorithmic procedures are iteratively executed until a population satisfying the preset fitness criterion is achieved or when the maximum limit of iterations is reached (Forrest, 1993). Generally, genetic algorithms are a good selection tool when nothing is known about the search space or are worth to rely on when other tools have failed. Genetic algorithms have recently been successfully applied in automated selection and discovery of non linear differential equations and conservation laws. This is a breakthrough that will change the nature of research especially in mathematical and physical sciences (Bongard and Lipson, 2007; Schmidt and Lipson, 2009).

2.13. Dimensional analysis and reduction

Fundamental and derived units of measurement are used to quantify properties of any system. The number of fundamental units of measurement is seven. However, meter, kilogram and second are the most commonly used units to describe magnitude of a physical system. They can be used individually or in combination. During quantitative description, the fundamental units or their combinations (derivations) are used in such a way that it would always be possible to arbitrarily change numerical values of measures when it is necessary to move from one system of units to another since any of the units used to describe dimensions or dimension function are from the same class of phenomena. The dimension function of a given physical system is valid only for a corresponding class and is differently expressed if the system of units used is different. Only numerical values of dimensionless quantities remain invariant under changes in measurement units. The behaviour that is valid for dimensional quantities is their ability to be transformed into nondimensional quantities. It is just this ability that enables us to move from one system of measurement to another through a multipurpose tool known as dimensional analysis (Barenblatt, 2003).

The dimension function is a power-law monomial and remains invariant in homogeneous mathematical operations, mainly under multiplication, where it is always possible to integrate many of the dimensions using dimensional analysis. Dimensional analysis can also be used

as a method of reducing complex physical problems with many degrees of freedom to their simplest form (Sonin, 2004). From this point of view, dimensional analysis can be defined as a physical method by which the number of dimensional parameters describing a physical system is reduced to fewer nondimensional ones. The sufficient condition for a physical parameter for dimensional reducibility is dimensional homogeneity (Hutter and Jöhnk, 2004). It is basically formulated based on Buckingham's (1914) Π-Theorem stated as follows: let the following mathematical relation represent an equation that completely describes the given physical system a_0, determined by n parameters, which is the sum of the total number of parameters k and m

$$a_0 = f(a_1, a_2, \ldots, a_k ; b_1, b_2, \ldots, b_m) \tag{2.26}$$

where a_0 is a physical quantity obtained as a solution to the matrix of parameters a_i and b_i. The Π-Theorem states that a physical system that is described by a set of n governing parameters which are formulated using k independent parameters can be described by a different set of m dimensionless parameters whose number can be reduced by as many parameters as the number of the k independent parameters. The independent parameters a_i and some of the b_i can be transformed into the following form through dimensional analysis if they fulfill conditions of dimensional homogeneity

$$\Pi = f(a_1, a_2, \ldots, a_k ; \Pi_1, \Pi_2, \ldots, \Pi_m) \tag{2.27}$$

Equation (2.27) can take the generalized homogeneous form as shown by Barenblatt (2003)

$$f(a_1, a_2, \ldots, a_k ; \Pi_1, \Pi_2, \ldots, \Pi_m) = a_1^p \ldots a_k^r \cdot f\left(\frac{b_1}{a_1^{p_1} \ldots a_k^{r_1}}, \ldots, \frac{b_m}{a_1^{p_m} \ldots a_k^{r_m}}\right) \tag{2.28}$$

where any of the independent parameters a_i is allowed to be a monomial of any power $a_1^p \ldots a_k^r$. However, dimensionally homogeneous parameters Π_1, Π_2,…Π_m are independent of the a_i terms. This means that any change of a_i by an arbitrary factor will affect neither the other independent parameters nor the dimensionless parameters π_i.

Therefore equation (2.28) can simply read in a compact mathematical representation of the Π-*Theorem*

$$\Pi = f(\Pi_1, \Pi_2, \ldots, \Pi_m) \tag{2.29}$$

Equation (2.28) is a functional notation expressing (*i*x*n*) matrix with a rank of *k* formed using *i* fundamental quantities and *n* dimensional quantities. The consequence of equations (2.27) to (2.29) is the Π-Theorem and according to Tolman (1914) it can also be interpreted as a corollary to the principle of similitude. Recently, Assis (2004) introduced the principle of physical proportions (PPP) in which he explains how a true macro system can be constructed from the miniature system. He gave five statements of PPP. In his argument that signifies computational utility of ratios as dimensionless numbers, he showed the potential of using physical proportions to describe any physical system without a discourse to physical constants. His theory does not violate any physical laws and can simply be regarded as the trivial form of theory of similarity.

Sometimes, simple rules of dimensional analysis may not be sufficient to arrive at the minimum number of dimensionally reduced parameters. This may arise due to various reasons. Dimensional analysis is based on existence of characteristic lengths and in physical phenomena such as phase transition there is no a single characteristic length, using which the dimensional analysis can be performed. At phase transition, characteristic lengths of all sizes are at work. The physical system is characterized by scale invariant critical exponents that cannot be obtained through dimensional analysis. The other common situation in which dimensional analysis may become weak is when micro details of a physical system are considered in heterogeneous conditions and the system must be modeled as close to reality as possible. In this case, fractal natures dominate that can not be determined through simple dimensional analysis except in some trivial instances (Barenblatt, 2003; Christensen and Moloney, 2005). Fractal is a word coined by Benoit Mandelbrot in 1975 to describe shapes that are self-similar or that look the same at several levels of magnifications. Their defining characteristic is their very nature of repeating themselves at every scale and can not be sufficiently defined by Euclidian geometry (Mandelbrot, 1977 and 1982).

2.13.1 Monofractals

Monofractals are geometric structures or processes that can be characterized by a single dimension. If there is a geometric set that is formed by strings, two or three dimensional irregular objects and if N(r) is the minimum number of circles, squares, spheres or cubes required to fill, cover or measure the object and if the following power law relation holds true then the set is called fractal

$$N(r) \sim r^{-D} \tag{2.30}$$

where D is a non-integer exponent called the fractal dimension. The dimension D can be obtained by fitting equation (2.30) using regression methods (Hergarten, 2002). Monofractals have a constant Hölder exponent that does not vary either spatially or temporally. The Hölder exponent describes the local regularity of the fractal object.

2.13.2 Multifractals

Most fractal structures and processes can not be sufficiently characterized by a single dimension and require many local Hölder exponents to obtain their full scaling behaviour. Multifractal structures or processes are characterized by a multifractal singularity spectrum that associates the singularity measure or the Hausdorff dimension $f(\alpha)$ to the support of a measure μ. The support of a measure represents the location where the strength of singularity measure α is non-zero. The singularity measure of the Hausdorff dimension $f(\alpha)$ is given by (Muzy *et al.*, 1993)

$$f(\alpha) = dim_H \{ x \setminus \mu(B_x(\varepsilon)) \sim \varepsilon^{\alpha} \} \tag{2.31}$$

where $\dim_H$ denotes Hausdorff dimension and $B_x(\varepsilon)$ is a square (box) with a dimension of ε centered at x. Presently, there are two methods of multifractal analysis, namely the wavelet transform modulus maxima (WTMM) and multifractal detrended fluctuation analysis (MFDFA) (Kantelhardt *et al.*, 2002; Arianos and Carbone, 2007) . The multifractal

singularity spectrum is obtained from the power law scaling relation existing between the partition function Z_q that is fully characterized by all moments of the statistical distribution, the support of singularity measure μ and a box with a size of ε that scales with a dimension of an observable spectrum τ(q).

$$Z_q(\varepsilon) = \sum_i \mu(B_i(\varepsilon))^q \sim \varepsilon^{\tau(q)} \tag{2.32}$$

τ(q) is directly related to the generalized fractal dimension D_q through the following relation

$$D_q = \frac{\tau(q)}{q-1} \tag{2.33}$$

and when $\varepsilon \to 0$, τ(q) and $f(\alpha)$ are related through equation (2.34) and Legendre transform

$$f(\alpha) = min_\alpha [q \cdot \alpha - \tau(q)] \tag{2.34}$$

The plot of q versus τ(q) and α versus $f(\alpha)$ yields two curves that can be schematically shown as given in Figure 2.6. The two curves fully characterize the multifractal scaling behaviour.

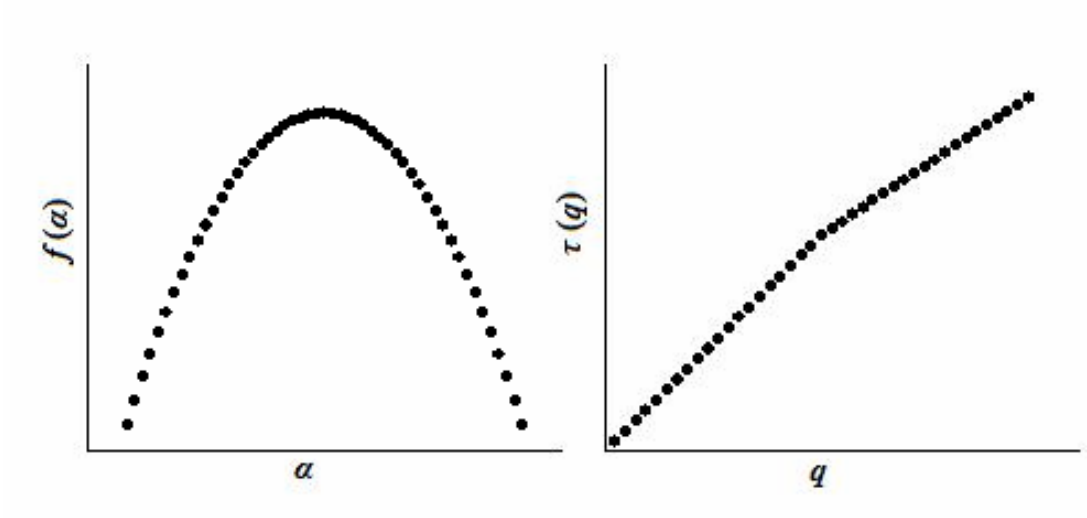

Figure 2.6 Schematic representation of multifractal spectra of $f(\alpha)$ based on the local holder exponent α and that of τ (q) based on order of the moment q

2.14. Scaling for macro-system prediction from micro-elements

When micro-details of a physical system are investigated it is not always possible to apply macro level governing physical equations and parameters as they are and without any modification. As sizes are reduced characteristic lengths and forms of governing parameters change due to appearance of new physical phenomena and effects. The changes occurring in characteristic lengths and their scaling exponents that appear while going from macro to micro or nanoworld was shown by Wautelet (2001). It is therefore necessary to establish conditions by which macro level governing physical parameters can be applied at micro level and vice versa. The macro-micro relationship is a complex topic that has been dealt with as issue of scaling involving scale dependent and invariant features in all scientific disciplines. Scaling gives a prediction how systems properties change with change of size which is usually based on power laws (Auraulit, 1991, 2002; Wu and Li, 2006).

One of the objectives of this research is to use a representative elementary volume (REV) that includes most of the heterogeneities in the wood-water vapour relationship. The micro-scale or fine-scale sorption prediction model that is developed for the REV is then to be coarse-grained to macro-level. In conventional coarse-graining, the fine-scale and macro-scale physical properties are assumed to be equivalent. The fine-scale is first approximated by a system of partial differential equations. Since the coarse-scale and fine-scale are equivalent, the coarse-scale can be described by differential equations of the same form that have the same parameters. However, the fine-scale and coarse-scale differ in the magnitudes of numerical values of their physical properties. In heterogeneous media this is usually related to homogenization whereby an average or effective physical value or parameter of the fine-scale is projected to the coarse-scale (Auriault, 2002). The basic tenet for this approach is the assumption that relates macro-scale to fine-scale physical properties through some scaling factors. These scale factors can be related to the similarity or dimensionless numbers obtained based on Buckingham's Π-Theorem (1914).

The transformation of micro physical properties to macro-scale is based on an assumption of physical similarity between fine-scale and coarse-scale. Two physical phenomena are similar if they are described by one and the same system of differential equations and have the

similarity conditions of single valuedeness. This similarity description is extendable to a group of phenomena that differ only by scale and meet the earlier definition of similarity (Luikov, 1966). Similar physical phenomena differ from each other only in numerical values of the quantities they are describing, but not in their distribution law (Gukhman, 1965). The similarity based scaling has been widely applied in hydro mechanics, both in kinematics and dynamics (Hutter and Jöhnk, 2004).

The concept of similarity is based upon the fact that the spatial and temporal arrangement of a physical system is determined by dimensionless magnitudes within the system itself and does not depend on the size or nature of units in which these magnitudes are measured. Similarity is often defined by specifying the equivalence of different measurements in the same body or of corresponding measurements in different bodies. If in a point-to-point matched mapping or transformation between two systems, the intrinsic ratios between the two systems can be equated, then for the two systems any corresponding values will be equal throughout. These intrinsic ratios, which are the same as the Buckingham π-numbers, are the dimensionless groups that define similarity between two states. Applications of geometrical, mechanical, thermal, chemical and biological similarity are most common in engineering and systems modeling (Johnstone and Thring, 1957; Stahl 1962; De La Barra and Günter, 1965; Rouvray, 1992; Günter *et al.*, 2003).

The Π-numbers obtained through dimensional analysis can be used as scaling factors. Scale factors are simple conversion parameters which relate characteristics of one system to corresponding characteristics of another. This in the simplest case means that a second physical system is obtainable as a scaled product of the quantitative value of the first. Scale factors are derived from knowledge of physical quantities that are known to govern specific processes of interest through dimensional methods and functional normalization (Tillotson and Nielson, 1984). In the latter, scale factors are determined based on various regression techniques from experimentally measured dependencies between two variables (Simmons *et al.*, 1979; Tillottson and Donald, 1984). In this method, all relationships between variables are brought into a single reference functional representation or curve that describes the set as a whole. Relationships to the reference curve are established based on experimentally determined scale factors.

The physical dimensional methods consider geometric, kinematics (rate dependent) and dynamic (inertia dependent) similarities (Hutter and Jöhnk, 2004). Within the realm of physical chemistry these groups can be extended to include chemical similarity (Johnstone and Thring, 1957). General dimensional methods include dimensional and inspectional analysis. The latter requires complete specification of the physical laws (equations) governing the system. Π-terms are then formed by inspection from the non-dimensional equations governing the physical system and scaling factors are determined from the Π-terms. In this approach, although scale invariance is accepted, existence of multiple characteristic lengths that are results of local heterogeneities are implicitly admitted.

In thermodynamic equilibrium systems that are at criticality or phase transition, scale invariant critical exponents are determined applying statistical physics. In statistical physics, once the partition function is determined it becomes simple to calculate the magnitude of the ensemble average of the observable $\langle A \rangle$ based on equation (2.35) that uses Boltzmann distribution from which all thermodynamic parameters can be found:

$$\langle A \rangle = \sum_{S_i} \frac{exp(-\beta E_{s_i})}{\sum_{S_i} exp(-\beta E_{s_i})} \cdot A_{S_i} \tag{2.35}$$

where S_i is the particular micro state, E_{s_i} [J mol^{-1}] is energy of the observable or physical quantity A_{S_i} and β is the reciprocal of the product of the Boltzmann constant k_b [m^2 mol s^{-2} K^{-1}] and temperature [K]. Unlike the case of scaling using Π-numbers, the critical exponents are insensitive to micro-details or do not require a complete knowledge of the governing physical equations of the system and depend mainly on dimensionality of the system as a whole (Christensen and Moloney, 2005). The critical exponent is dimension of the system that can be determined based on the renormalization group (RG) theory and cannot be obtained through simple dimensional analysis.

In RG studies, parameters defining the problem are re-expressed in a larger, but simpler domain while keeping unchanged those aspects of the problem under consideration (Cardy, 1996). The important idea that is incorporated into the RG is that all length scales are present

at the critical point as a result of which the system looks the same on any of its length scales. This property is called self-similarity. The renormalization group is therefore a general approach for extracting quantitative information from the self-similarity. The RG theory is applied in the Ising model that has been employed even in ANNs (Hopefield, 1982). The biggest challenges in the application of the RG theory are determining the partition function and tracing all micro states that the system visits. Once the partition function is determined, finding the average thermodynamic quantities becomes trivial. For systems in self-organizing criticality that are composed of a large number of interacting components which in essence are also slowly driven and far from equilibrium, finding the partition function is practically impossible. However, the behaviour of such a system can be described by critical exponents that are scale invariant and can be determined based on some statistical properties that can be displayed by the system, i.e. spatial and temporal algebraic correlations (Christensen and Molony, 2005).

Ecological modeling is one of the scientific disciplines that commonly require application of locally studied physical, chemical and biological interactions to large scale ecosystems. In ecological modeling, similarity analysis is applied for the purpose of finding coarse-scale properties from properties of the REV. Similarity analysis can be used to predict coarse-scale properties of a local ecosystem based on two basic approaches. In the first approach the coarse-scale properties are assumed to be under the same physical effects as the fine-scale, and physical processes are governed by the same parameters. The fine-scale inputs are first averaged and then submitted to the fine-scale model and are finally extrapolated to coarse-scale as average or effective parameters. Alternatively, instead of assuming the local models as applicable to coarse-scale, every fine-scale input can first be submitted to local models and then model outputs can be extrapolated to coarse-scale by averaging or summing up (Wu and Li, 2006).

In heterogeneous media, coarse-graining of the fine-scale is done through a computation process called homogenization. Homogenization is obtaining macro-scale properties based on properties at the scale of heterogeneity or REV (Auriault, 1991). It is a technique to tackle heterogeneities in the simplest way possible while respecting their presence and effect. The homogenized macro-scale description is assumed to be intrinsic to the porous media and the

physical processes or perturbation (Auriault, 2002). The unit of modeling is usually the REV which should be sufficiently large for representing the heterogeneity scale but very small compared to the macroscopic volume. The core principle is separation of the fine and coarse-scale as expressed by the following mathematical proposition in which *l* and *L* are the characteristics lengths at the REV and macroscopic levels respectively.

$$\frac{l}{L} = \varepsilon << 1 \tag{2.36}$$

The homogenization method has been enjoying successes over numerical methods in describing transport phenomena in porous media (Hollister and Kikuchi, 1992). However, the separation of scale requires $\varepsilon \to 0$, which is an assumption for the macro-scale media to be infinite or the fine-scale to be close to the nano level and the porous media is required to be periodic at REV. Furthermore, there is a need for a complete knowledge of the physical parameters and details of the geometry of REV which is practically impossible.

Homogenization in actual terms is a method of fine-scale properties averaging as representation of the macro-scale properties. Statistical modeling, self consistent modeling and volume averaging techniques are widely applied in coarse-graining (Auriault, 2002). In most of these techniques the transformation from REV to macro-scale is considered to be ergodic. Farmer (2002) in his review of upscaling, divided the upscaling procedure into two stages. The first stage is the step at which the fine grid experiment is done (local). The second stage is the step at which the coarse grid calibration (global) is done. Considering these two stages as basis for categorization, he introduced coupled methods termed as local-local, global-local, local-global and global-global. The problem with homogenization is that the REV is not always homogenizable when assumptions of periodicity and separation of scale cannot be fulfilled (Auriault, 1991).

Wood, by its nature, displays certain periodic properties as outlined in various parts of this review. It mostly contains two-components or involves two-levels. When it comes to the particular application of homogenization on wood properties, we can find some works done in mass transfer. Perré and Turner (2001) developed a tracheids model of softwood for

description of mass flow based on local density variation. They developed REV based image analysis that they used to model bound water diffusivity and thermal conductivity as a function of local density. Perré and Badel (2003) also presented a work in which they demonstrated the elastic and shrinkage properties of oak to be determined from properties of anatomical tissues through image analysis. Pérre (2007) further investigated the application of homogenization for multiscale coarse-graining using finite element methods. Hofstetter *et al.* (2004) demonstrated the possibility of predicting anisotropic elasticity of wood from micro composition or from what they called universal building blocks found in all trees. Despite the obvious difficulty in having a detailed characterization of wood properties, the results were encouraging.

The homogenization methods so far applied on wood explicitly depend on anatomical details which require detailed characterization. However, there are scale invariant behaviours of wood that may not explicitly depend on detailed characteristics. Growth is affected by climate conditions such as sunlight and rain that display SOC which is a signature for pink noise (f^{1}). The periodicity required for homogenization can be affected more by SOC phenomena than periodic growth trends. Normal growth trends can be scale dependent and more predictable, but the one that is much affected by climate signals is less likely to depend on scale. The latter can rather be governed by scale invariant parameters or critical exponents. The scale invariant features exist embedded in wood cells and growth rings. Close observation of cell-wall thickness, lumen sizes and their distributions can clearly indicate the prevailing fractal nature in the cross section of wood.

Widths of growth rings have been used in dendrochronology to extract and use such signals to reconstruct past millennial climate events (Cook and Kairiukstis, 1990; Von Storch *et al.*, 2004). Climate factors in some circumstances can cause exceptional changes in wood property. This fact was utilized to modify the acoustic properties of wood of Norway spruce and sycamore to obtain resonance wood with low density, but high modulus of elasticity (Francis *et al.*, 2008). In this case, the climate impact resulted in good resonance qualities and in other circumstances the effect can be the opposite. In conclusion, it is essential to point out that climate factors can cause emergent properties that are not related to inherent growth trends of the species in question but that cannot be simply left out as outliers

(Geoffrey *et al*., 2002). Therefore, any prediction models should deal not only with scale dependent geometric or anatomical features, but also with those that are scale invariant and possess long-range behaviours which arise due to interactions with the environment or other agents.

3.0. MODELS DERIVATION AND DEVELOPMENT

The methodology of this study was conceived in order to reveal and utilize the self-organizing behaviour in wood composition and its physical properties. It was implemented

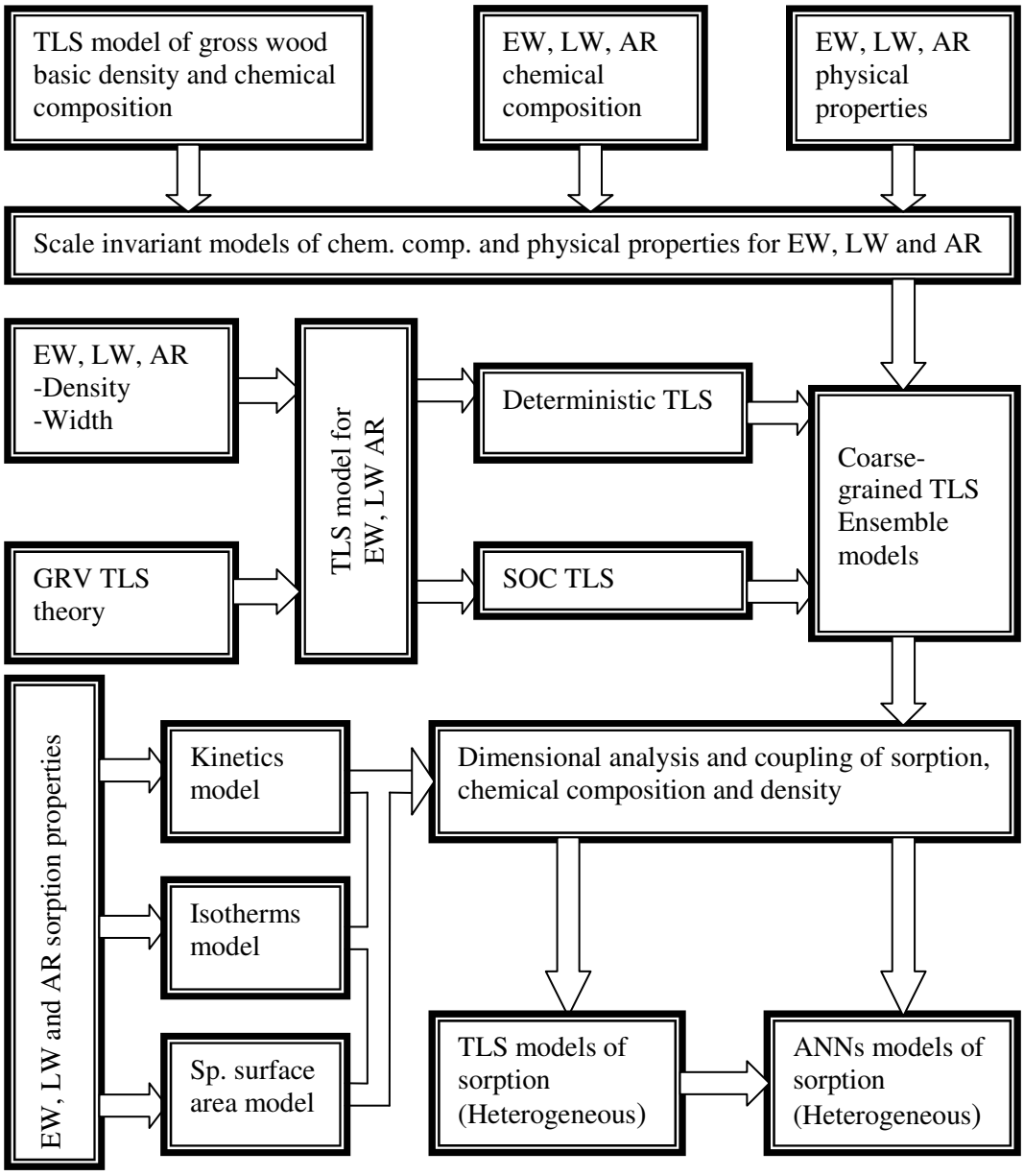

Figure 3.1 Block diagram of data collection and models development in which the acronyms denote the following: EW-earlywood, LW-latewood, AR-annual ring, TLS-two-level systems self-organization, GRV- golden ring volume and SOC-self-organizing criticality

by identifying two primary tasks. Firstly, deriving and validating meso-level prediction models for wood chemical composition and secondly, transforming and coupling these models with wood density for the development of a heterogeneous sorption prediction model for earlywood, latewood and annual rings Douglas-fir. Two-level or two-component self-organization is implemented in all model derivations that were used at the end to build the final artificial neural networks sorption prediction models. The block diagram that outlines the research is given in Figure 3.1.

The four models that are derived for the first time and from scratch have a dual purpose owing to their direct applications for prediction and their use as components to describe more complex or multi-component wood-water systems. The derivation process started from the coarse-scale observable description of a growth ring by its earlywood and latewood components. Originating from first principles (fundamental facts), the following were introduced and developed.

I. Two-level system (TLS) based dynamical coarse-graining model for earlywood, latewood and annual rings.
II. Demonstration of the two-component and two-level nature of water vapour sorption in gross wood and derivation of the TLS model of sorption kinetics.
III. Derivation of the TLS model of sorption isotherm.
IV. Extension of the two-level systems model to the description of wood in terms of its physical properties and chemical composition.
V. Creation of systems of dimensional and dimensionless parameters which are applicable to scaling and unified modeling of sorption using neural networks.

3.1. Derivation of two-level systems model of growth rings (coarse-graining)

Let the variables l_1, l_2, and l be widths of earlywood, latewood and annual ring, respectively, in unit of linear measures such as micrometer, millimetre or meter. Then Equation (3.1) is used to establish volume of an annual ring that is employed to find the relations of l_1, l_2 and l to density.

$$l = l_1 + l_2 \tag{3.1}$$

When both sides of equation (3.1) are cubed then equation (3.2) that describes volume of an annual ring and that will be named in this study as the golden ring cube (GRC) is obtained.

$$l^3 = l_1^3 + 2 \cdot l_1^2 \cdot l_2 + l_1^2 \cdot l_2 + 2 \cdot l_2^2 \cdot l_1 + l_2^2 \cdot l_1 + l_2^3 \tag{3.2}$$

After rearrangements of the terms, equation (3.3) can be established.

$$l^3 = \underset{I}{l_1^3} + \underset{II}{2 \cdot l_1^2 \cdot l_2} + \underset{III}{l_2^2 \cdot l_1} + \underset{IV}{2 \cdot l_2^2 \cdot l_1} + \underset{V}{l_1^2 \cdot l_2} + \underset{VI}{l_2^3} \tag{3.3}$$

Each of the terms in equation (3.3) is described by Figure 3.2b as components of a cube of an annual ring described by a dimension that is equal to its width. The first term is a component equivalent to the maximum cubic volume of earlywood that is described by width of earlywood and it is represented by the part bordered with red edges in the rear of Figure 3.2b. The second term represents the volume of earlywood in ring-width cube that is described by the product of a square cross section having its sides equal to the width of earlywood and a third dimension that is equal to the width of latewood. The third term represents the volume of earlywood in ring-width cube that is described by the product of a square having its sides equal to the width of latewood and a third dimension equivalent in magnitude to the width of earlywood. The sixth, fifth and fourth terms can be described symmetrically in the same manner as the volume of latewood in a ring-width cube created by the cube of width of latewood, the product of a square with sides having a magnitude equivalent to the width of latewood and width of earlywood, and by the product of the square of width of earlywood and width of latewood. The component that is created by the cube of latewood width is shown with thickened blue line edges at the front-bottom of Figure 3.2b.

If the weight of wood substance in each of the terms of equation (3.3) is known then it can be used to develop a *heterogeneity test criterion* (HTC). The dynamical fluctuations of each of the volumes shown in Figure 3.2b should be incorporated in the description for the test of

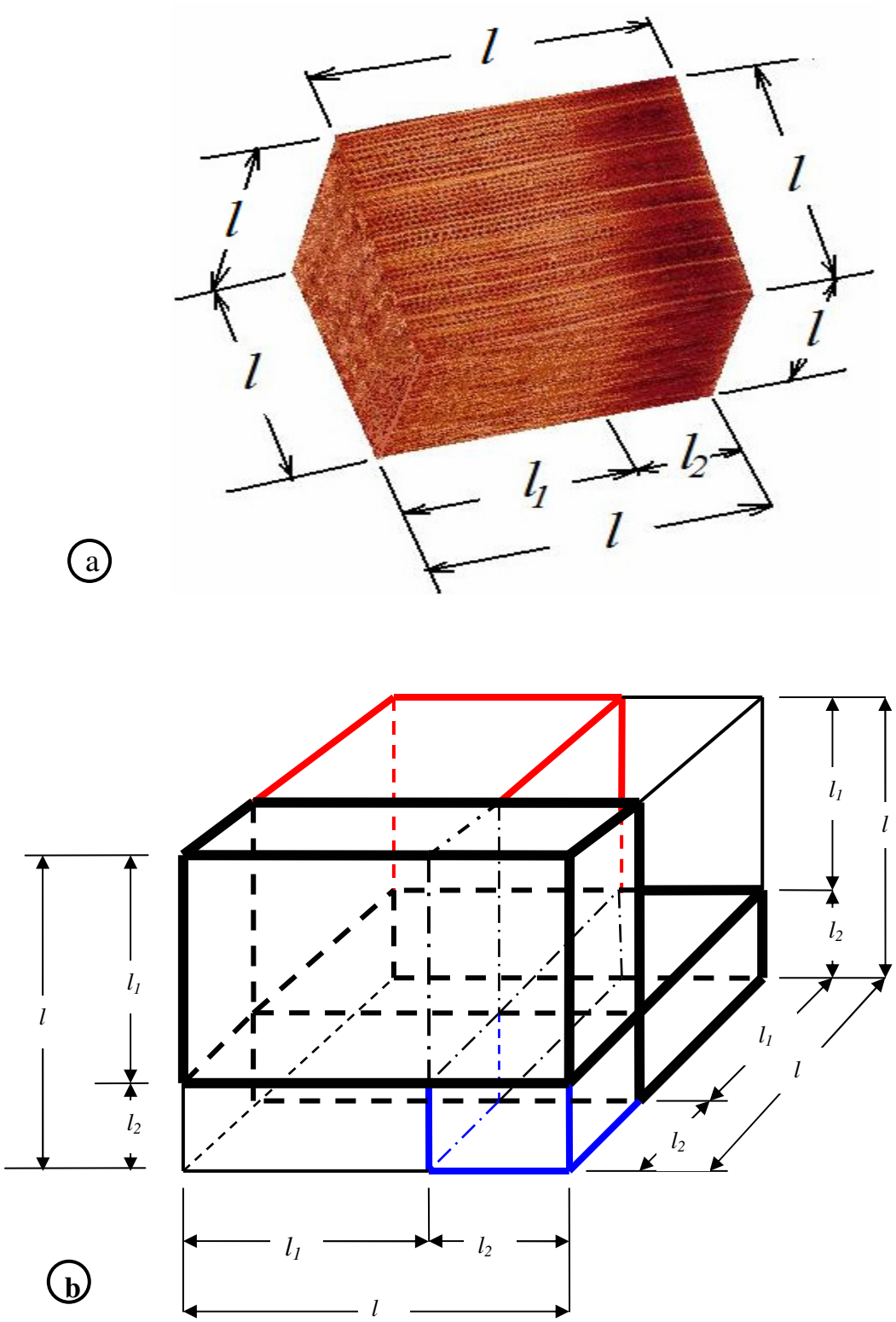

Figure 3.2 Cubic annual ring: a. cubic annual ring of a Douglas-fir b. a schematic representation of an annual ring with its width as cubic dimension and its geometrical relation to width of earlywood and latewood with GRV having the black thicker edges

heterogeneity. If earlywood and latewood are assumed to have uniform density then equation (3.4) holds true.

$$\rho_r \cdot l^3 = \underbrace{\left(\rho_e \cdot \left(\underbrace{l_1^3}_{I} + \underbrace{2 \cdot l_1^2 \cdot l_2}_{II} + \underbrace{l_2^2 \cdot l_1}_{III} \right) \right)}_{A} + \underbrace{\left(\rho_l \cdot \left(\underbrace{l_2^3}_{VII} + \underbrace{2 \cdot l_2^2 \cdot l_1}_{V} + \underbrace{l_1^2 \cdot l_2}_{VI} \right) \right)}_{B} \tag{3.4}$$

where ρ_r, ρ_e and ρ_l are mean densities in unit of weight per cubic linear length measure of the annual ring, earlywood and latewood, respectively. If the grand terms A (I+II+III) and B (IV+V+VI) are very close to each other in magnitude with the additional condition of equality for terms paired as I with IV, II with V, and III with VI then the annual ring can be considered homogeneous.

The more the grand terms A and B differ, the more heterogeneous will the annual ring be. In species with distinct earlywood and latewood the heterogeneity is obvious and arises as their names simply imply, from the interaction of growth factors and the environment. This interaction is well known and has widely been utilized to reconstruct dendrochronology since the inception of the concept at the turn of the twentieth century (Robinson, 1990; Downes *et al*., 2002; Vaganov *et al*., 2006; Deslauriers *et al.*, 2007). The outcome of this interaction is chaotic (disordered) to be described by a simple Euclidean geometry alone as it is given in Figure 3.2b. However, the chaotic behaviour can be described by fractal dimensions. In chaos, a fractal dimension is usually associated with non-integer dimensions that are used to describe similarity, capacity, information and correlation (Williams, 1997). The fractal dimension is used in this study to extract information on similarity, capacity (wood substance content) and the correlation between major ring-parameters. Despite its Euclidean nature, Figure 3.2b illustrates how a simplified fractal geometry analysis could be applied to an annual ring and its components. Equation (3.4) practically establishes characteristic lengths that are suitable for fractal characterization based on major annual ring parameters.

The fractal characterization of annual rings becomes simplified if, for this purpose, a unique unit of an annual ring is defined and a new term, golden ring volume (GRV) is introduced. The GRV is a result of self-organization and it is created by the width of annual ring,

earlywood and latewood. The half magnitude of the sum of term-II and term-V or term-III and term-VI in equations (3.3) or (3.4) is equivalent to the GRV. The GRV is located in the front of Figure 3.2b or it is also the one in the bottom-rear side of the rectangular prism which is also contrasted with thick black edges. This optimized ring volume could further be described as an annual ring having its cross-section formed by the width of earlywood and latewood and with a length equal to the width of the annual ring. There is an equal amount of weight of wood substance in the earlywood and latewood of the GRV for a homogeneous annual ring. The same holds true for the wood substance content in the ring-width cube which is a cube of an annual ring having all of its dimensions equal to its width. The GRV can generally be written as quantitatively equal to

$$\boldsymbol{GRV} = \boldsymbol{l}_1^2 \cdot \boldsymbol{l}_2 + \boldsymbol{l}_2^2 \cdot \boldsymbol{l}_1 \tag{3.5}$$

When the right hand side of equation (3.5) is multiplied by the respective densities of earlywood and latewood then a GRV that distinctly identifies earlywood and latewood as two-level system is obtained.

$$\boldsymbol{GRV}_{\boldsymbol{TLS}} = \boldsymbol{\rho}_{\boldsymbol{e}} \cdot \boldsymbol{l}_1^2 \cdot \boldsymbol{l}_2 + \boldsymbol{\rho}_{\boldsymbol{l}} \cdot \boldsymbol{l}_2^2 \cdot \boldsymbol{l}_1 \tag{3.6}$$

The magnitude of the wood substance contained in the GRV given by equation (3.6) is directly related to the transversal growth which could be translated as work done by the tree in one growth year. The short range growth trajectory shows a transition from earlywood to latewood and then from latewood to earlywood that continues repetitively. The coarse features of earlywood and latewood can be considered as the regions of stability for an annual ring that can be assumed to be in a quasi-equilibrium state. For a transition from earlywood to latewood to occur, a perturbation should take place that is capable of tipping the state of earlywood and enabling a nonequilibrium transition path to latewood. The transition paths can be chaotic with infinite trajectories. The infinite trajectories can be considered as repetitive work done in transferring earlywood to latewood. The mean of repetitive work done in the non-equilibrium transition from earlywood to latewood can be

equated to the free energy differences between the mean of preferred states of earlywood and latewood as it has generally been shown by Jarzynski (1997) and Crooks (2000).
The equality of nonequilibrium free energies has been applied to solve physical problems of two level systems by Ritort (2004), Chvosta (2007), and for the description of the glass phase transition by Garrahan *et al*. (2007 and 2009) and Hedges *et al*. (2009). Assuming immediate reversibility of work done or relaxation of a system that is far from equilibrium, the following relation was proved to be valid by Crooks (2000).

$$\left\langle \boldsymbol{\Phi} \right\rangle_{F} = \left\langle \hat{\boldsymbol{\Phi}} \cdot e^{-\beta \cdot W_d} \right\rangle_{R} \tag{3.7}$$

where $\left\langle \boldsymbol{\Phi} \right\rangle_{F}$ [J or kg m^2s^{-2}] is the average work through the path ensemble function $\boldsymbol{\Phi}$ in the forward direction and the right hand side of equation (3.7) is the reverse work of $\boldsymbol{\Phi}$ [J or kg m^2s^{-2}] weighted by the exponential of βW_d . According to Crooks (2000), equation (3.7) states the equivalence of ensemble properties generated due to a perturbation done on a system that was initially at equilibrium to those properties of ensembles generated while reversing it to its original state. The explicit dependence of the probability distribution of a non-equilibrium ensemble on the dynamics and history of its system is utilized in order to address the problem of finding ensembles which contain growth trajectories that satisfy equation (3.7). If the partition function of a given system is known then the probability of an ensemble in a trajectory can generally be given by equation (3.8).

$$p(Ens) = e^{-\beta \cdot w_d} \tag{3.8}$$

where $p(Ens)$ is the probability distribution of an ensemble of annual rings or growth trajectory. Equation (3.8) can be used to describe a GRV that physically behaves as a two-level system (GRV_{TLS}) and can be described by the probability distribution of single annual rings as follows

$$p_i(GRV) = e^{-\beta_i \cdot \langle GRV \rangle} \tag{3.9}$$

where the GRV in angle bracket means the configuration of wood substance in terms of its weight. The major physical observable (physical quantity) that represents heterogeneity in annual ring is the difference between the state of earlywood and latewood. Knowledge of the mechanism of transition from earlywood to latewood enables explanation and prediction of heterogeneity in annual ring that can simply be based on the analysis of differences between the two states. Describing the GRV as two-level system (TLS) requires identification of the inactive (ground) and active (excited) state**.** It is the amount of wood substance contained in the GRV that has a physical significance in this study. Since there is more wood substance in latewood than in earlywood per unit volume, and as a consequence of the definition of GRV, earlywood could be assumed as the inactive and latewood as the active state. This is slightly counter intuitive because it is during the formation of earlywood that there is increased growth rate. Nevertheless, let the assumption for latewood as the active state hold true. The probability distribution of occurrence for the inactive and active states in terms of wood substance in earlywood and latewood can be obtained by combining equations (3.6) and (3.9).

$$p_e(GRV) = e^{-\beta(GRV_{TLS} - \rho_l \cdot l_2^2 \cdot l_1)} = e^{-\beta \cdot \rho_e \cdot l_1^2 \cdot l_2} \tag{3.10}$$

$$p_l(GRV) = e^{-\beta \cdot (GRV_{TLS} - \rho_e \cdot l_1^2 \cdot l_2)} = e^{-\beta \cdot \rho_l \cdot l_2^2 \cdot l_1} \tag{3.11}$$

where β is a parameter analogous to the reciprocal of the product of the Boltzmann constant k_b [$m^2kgs^{-2}K^{-1}$] and temperature [K], p_e and p_l are probability distributions of the wood substance in the GRV consisting earlywood and latewood. Equations (3.10) and (3.11) can be normalized by GRV to give equations (3.12) and (3.13).

$$p_e(GRV) = e^{-\beta\left(1 - \frac{\rho_e \cdot l_1^2 \cdot l_2}{GRV_{TLS}}\right)} \tag{3.12}$$

$$p_l(GRV) = e^{-\beta\left(1 - \frac{\rho_l \cdot l_2^2 \cdot l_1}{GRV_{TLS}}\right)} \tag{3.13}$$

A chain of GRV representing a growth trajectory displays similar exponential probability distribution as follow.

$$p_i\left(\sum_{i=1}^{n}\langle GRV\rangle\right) = e^{-\beta_i\cdot\sum_{i=1}^{n}\langle GRV\rangle} \tag{3.14}$$

Equation (3.14) meets the following condition of invariance with respect to the number of annual rings n and the thermodynamic constant β.

$$n\cdot\beta_i = constant \tag{3.15}$$

Equation (3.15) describes an identity or conserved quantity. Therefore, an increase in the number of annual rings should be accompanied by a proportional decrease in the magnitude of β. This shows that the maximum interaction length can be obtained when the probability for the occurrence of a single annual ring (GRV) is considered. Equation (3.14) provides the most probable magnitude of β around which the ensemble self-organizes when the value of n is unity. Equation (3.15) gives the power law's dependence between the number of annual rings in a trajectory (consecutive series of annual rings) and the magnitude of β. These two could be sufficient to find the partition function describing the GRV as TLS. Therefore, equations (3.9) to (3.15) can be used to calculate the thermodynamic parameters of the GRV as an equilibrium/ quasi-equilibrium ensemble of TLS.

If earlywood is considered as the inactive state, then the energy difference from its own state is zero. The energy level of latewood could be obtained from the difference between weight of wood in latewood and that of earlywood in the GRV. Identification of the energy level of latewood is sufficient to obtain the equilibrium partition function Z_{eq} and describe the accompanying thermodynamic parameters as given in the following equations.

$$Z_{eq} = 1+e^{-\beta\cdot\left(1-\frac{\rho_l\cdot l_1^2\cdot l_2}{GRV_{TLS}}\right)} = 1+e^{-\beta\cdot\frac{\rho_l\cdot l_2^2\cdot l_1}{GRV_{TLS}}} \tag{3.16}$$

The expectation value of the GRV can be obtained from equation (3.14), (3.15) and equation (3.16) that could then simply be coarse-grained as consecutive GRVs which will form series of annual rings. However, the GRV as a dissipative system should be characterized differently by taking into consideration two factors, namely, the long range interaction that will affect the partition function and the short range phenomenon which has an effect on the expectation value of given GRV. The long range phenomena that affects the partition function can be incorporated into the TLS description by following the recent formalism given by Garrahan *et al*. (2009) while the expectation value of the GRV could be modified based on the Markov dynamics given by Lecomte *et al.* (2005). The dynamical partition function for trajectories of an annual ring is identifiable by the trace sum of the products of all configurations of trajectories and their probabilities (*p*). The probabilities are obtained in terms of widths and densities of earlywood and latewood normalized by maximum threshold values (the magnitude of wood substance in the GRV). The probability of magnitude of wood substance in the dynamical TLS can be given as follow:

$$p(TLS_D) = \frac{1}{Z_D(\beta, TLS_D)} \cdot e^{-\sum_i \beta_i \cdot (GRV_D)} \tag{3.17}$$

where the subscript *D* means dissipative, GRV_D is a GRV from *TLS* of annual rings and the partition function Z_D is given by the following equation:

$$Z_D(\beta, TLS_D) = \sum_{trajectory} TLS(trajectory) \cdot e^{-\sum \beta \cdot TLS(\beta)} \tag{3.18}$$

where β represents the thermodynamic parameter that has a direct relation to the number of annual rings. The most challenging part of finding the partition function in equation (3.18) is to establish the probability of the ensemble history or growth trajectory.

Earlywood and latewood of a given annual ring interact with each other. They also interact with adjacent latewood and earlywood, respectively. This interaction can be regarded as Markovian based on Figure 3.3. By using Figure 3.3 and the maximum interaction number

that can be obtained through equations (3.9) and (3.14), and according to the scale invariant relation in equation (3.15), a new variation of self-organizing criticality in wood formation and description of interaction in annual rings is introduced. A ring series can be characterized by fluctuations and threshold magnitudes of wood substance in a GRV. An ensemble of annual rings with the interaction length satisfying equation (3.15) contains the probable thresholds that can be obtained from fractal characterization of a ring series. The threshold dynamics can be characterized both temporally and by their magnitudes of fluctuations, if the characteristic interaction length is used as a moving ensemble. The moving ensemble is a new approach that is being introduced by this study and will enable incorporation of the long and short range interactions discussed earlier.

Let the following relation describe a TLS ensemble based on the interaction in Figure 3.3.

$$\boldsymbol{TLS}_i = \boldsymbol{Level}\,1_i + \boldsymbol{Level}\,2_i \tag{3.19}$$

where *i* denotes a ring sub-series under consideration. The probabilities of occurrence for *Level 1* (Earlywood) and *Level 2* (Latewood) in equation (3.19) can be determined from the invariant property of equation (3.15). Assuming weak interaction between earlywood and latewood, the interaction energy term β can be determined from the probability distribution function (PDF) of the configuration of earlywood and latewood in the GRV and Figure 3.3 which yields equation (3.20) in the following form

$$\left[\boldsymbol{TLS}\right]_i = \left[\left(\boldsymbol{GRV}_l\right)_m \cdot \left(\boldsymbol{GRV}_e\right)_{m+1} \cdot \left(\boldsymbol{GRV}_l\right)_{m+1}\right]_i + \left[\left(\boldsymbol{GRV}_e\right)_{m+1} \cdot \left(\boldsymbol{GRV}_l\right)_{m+1} \cdot \left(\boldsymbol{GRV}_e\right)_{m+2}\right]_i \tag{3.20}$$

The best way to see the connection between equation (3.19) and (3.20) is to consider the $\boldsymbol{l}_m$, $\boldsymbol{e}_{(m+1)}$ and $\boldsymbol{l}_{(m+1)}$ alternatively $\boldsymbol{e}_{(m+1)}$, $\boldsymbol{l}_{(m+1)}$ and $\boldsymbol{e}_{(m+2)}$ of the half GRV components as dimensions of a contracted golden ring volume (GRV_C). Then, the Jarzynski's (1997) identity can be utilized to envision the quantal nature of equation (3.20) from which follows the two-level or two-state equation of (3.19) and the symmetric (integral) meaning of equation (3.20).

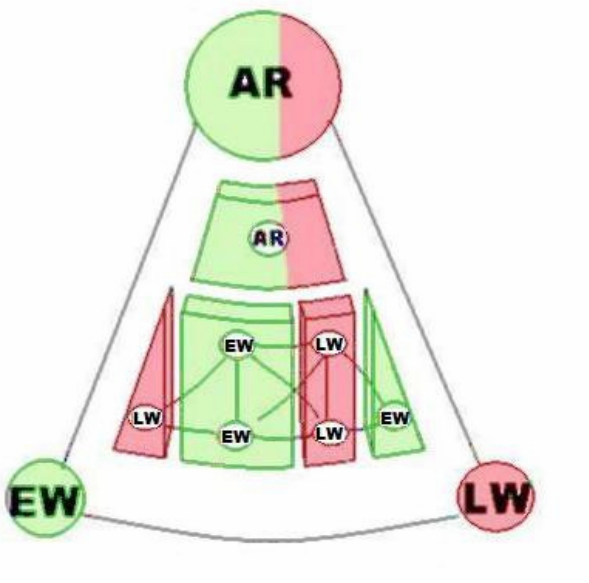

Figure 3.3 Schematic diagram of interactions in annual ring between earlywood and latewood with a simple two-component interaction network and with abbreviations denoting: AR-annual ring, EW-earlywood and LW-latewood

The mean configuration of m^{th} GRV in terms of the content of wood substance is given in equation (3.21) based on equations (3.19) and (3.20).

$$\overline{[TLS]}_m = \left\{ \begin{array}{l} \left[\left(\rho_{l(m-1)} \cdot l^2_{2(m-1)} \cdot l_{1(m-1)} \right) \cdot \left(\rho_{em} \cdot l^2_{1m} \cdot l_{2m} \right) \cdot \left(\rho_{lm} \cdot l^2_{2m} \cdot l_{1m} \right) \right]_i + \\ \\ + \left[\left(\rho_{em} \cdot l^2_{1m} \cdot l_{2m} \right) \cdot \left(\rho_{lm} \cdot l^2_{2m} \cdot l_{1m} \right) \cdot \left(\rho_{e(m+1)} \cdot l^2_{1(m+1)} \cdot l_{2(m+1)} \right) \right]_i \end{array} \right\} \tag{3.21}$$

where m indicates the m^{th} annual ring with values spanning from one (1) to the number of annual rings (β) in given growth rings trajectory. The TLS under the bar indicates the mean m^{th} configuration, e and l denote earlywood and latewood, respectively. The following scaling relation results from the probability distribution obtained based on equations (3.14) and (3.21).

$$\overline{[TLS(\beta)]}_i = p[TLS(\beta)] = n^{-\lambda} \tag{3.22}$$

where the term $\overline{[TLS(\beta)]}$ represents the expectation value of the right-hand-side of equation (3.21) obtained based on Figures 3.2b and 3.3, and λ is a scaling exponent. Equation (3.23) gives the scaling behaviour of the probability of occurrence for the maximum threshold magnitude of the TLS (TLS_{max}) for an interaction length with a value of β.

$$p[TLS_{max}(\beta)] = \overline{[TLS(\beta)]}^{-\frac{1}{\lambda}} \quad TLS_{max} \in TLS(\beta),\ \beta = 3\ to\ n\ and\ i = 1\ to\ r - n \tag{3.23}$$

$$F_i^q(TLS_i) = \left(\left(\left(\frac{1}{\beta}\cdot\sum_{i=1}^{\beta} TLS_i\right) - TLS_i\right)^q\right)^{\frac{1}{q}} \qquad for\ i = 1\ to\ r - n \tag{3.24}$$

$$p[TLS(\beta)] = n^{-\alpha} = F_i^q[TLS(\beta)]^{-\frac{1}{\alpha}}, \qquad for\ i = 1\ to\ n \tag{3.25}$$

where F_i^q is the q^{th} order fluctuation. The magnitudes of λ and α vary with change of β with a power laws scaling relation that can generally be given by equation (3.26).

$$\frac{ln\left(F_i^q[TLS(\beta)]\right)}{ln\left([TLS_{max}(\beta)]\right)} = \frac{\alpha}{\lambda} \tag{3.26}$$

Equation (3.26) is the same as

$$F_i^q[TLS(\beta)] = [TLS_{max}(\beta)]^{\frac{\alpha}{\lambda}} \tag{3.27}$$

where TLS $(\beta)_i$ is an ensemble of annual rings characterized by an interaction parameter β that indicates the number of annual rings in one instance of growth trajectory. F_i is the second fluctuation moment for n number of consecutive growth rings in a growth trajectory corresponding to the parameter β. Equation (3.27) establishes a scaling function that directly relates threshold magnitudes in a ring series characterized by β. The general dynamical partition function given in equation (3.18) can now formally be given by equation (3.28). The

probability for the history of the trajectory is given by equation (3.26). The scaling exponent α can be obtained from the number of annual rings in the trajectory by equation (3.27).

$$\boldsymbol{Z_D = \sum \left[f\left(F_i^q [TLS(\beta)], TLS_{max}(\beta)\right)\right] \cdot e^{-\sum \beta_n \cdot GRV_{TLS}}} \tag{3.28}$$

The magnitude or expectation value of the dynamical observable GRV can be obtained based on the partition function of equation (3.28) and reads as given in equation (3.29).

$$\boldsymbol{\left\langle GRV_D \right\rangle = \frac{TLS_D \cdot e^{-\sum \beta_n \cdot GRV_{TLS}}}{\sum \left[f\left(F_i^q [TLS(\beta)], TLS_{max}(\beta)\right)\right] \cdot e^{-\sum \beta_n \cdot GRV_{TLS}}}} \tag{3.29}$$

However, a special property of the GRV to GRC ratio renders an alternative and simple approach to equation (3.28) and (3.29) in obtaining magnitude of the dynamical golden ring volume (GRV_D). If for the sake of simplicity only volume of an annual ring is considered then the volume component of the GRC is given by equation (3.2) and that of GRV by equation (3.5) which yield

$$\boldsymbol{\frac{GRV}{GRC} = \frac{l_1^2 \cdot l_2 + l_2^2 \cdot l_1}{l_1^3 + 3 \cdot l_1^2 \cdot l_2 + 3 \cdot l_2^2 \cdot l_1 + l_2^3}} \tag{3.30}$$

The right hand side of equation (3.30) simplifies further to

$$\boldsymbol{\frac{l_1}{(l_1 + l_2)} \cdot \frac{l_2}{(l_1 + l_2)} = p(l_1) \cdot p(l_2)} \tag{3.31}$$

The GRV to GRC ratio is therefore

$$\boldsymbol{\frac{GRV}{GRC} = p(l_1) \cdot p(l_2)} \tag{3.32}$$

Therefore, the GRV to GRC ratio simplifies to the product of the probability of occurrence of earlywood and latewood. The probability occurrence of given earlywood and latewood is directly related to the GRV of earlywood and latewood. And by comparing equation (3.10), (3.11) and (3.32) the following holds true

$$\boldsymbol{GRV = (GRC)\cdot e^{-(\beta_e\cdot\rho_e\cdot l_1^2\cdot l_2+\beta_l\cdot\rho_e\cdot l_1^2\cdot l_2)}} \tag{3.33}$$

when β_e and β_l are very close to a magnitude of unity then Eq 33-I can be approximated by

$$\boldsymbol{GRV = (GRC)\cdot e^{-(GRV)}} \tag{3.34}$$

after rearrangement

$$\boldsymbol{GRC = (GRV)\cdot e^{(GRV)}} \tag{3.35}$$

Equation (3.34) is equivalent to equations (3.7) that was obtained from Crooks (2000). It also agrees with Jarzynski's (1997) identity obtained based on the nonequilibrium equality of free energy difference and gives a description both for the long range and Markovian nature of transversal growth increment. Equation (3.35) states that the GRC or the transversal ring width cubic increment is the exponential average of the GRV, from which follows the short and long range nonlinear relationship between earlywood, latewood and annual ring.

Equations (3.34) and (3.35) are valid in describing earlywood and latewood in annual ring as TLS and let us call this first degree TLS. If every succeeding annual ring is divided by the preceding annual ring according to equation (3.34) then a second degree TLS of consecutive annual rings is created. The third level probably would be cluster of annual rings that create the conventional transversal categories of juvenile wood, mature heartwood and sapwood. However, for equation (3.20) to be valid based on the concept of TLS of collapsed GRV (GRV_c) given in Figure 3.3, it is necessary to have either juvenile or mature heartwood as a component which has two distinct regions. If we consider the transversal density profile in

which density first decreases while going from pith towards bark before it starts to increase with its final plateau stage, then it can be assumed that the wood near pith has magnitudes of GRV equivalent to mature wood in its old stage (plateau or flattening). This can enable us to assume the later part of juvenile wood to be equivalent to the earlywood given in Figure 3.3, assuming existence of the same symmetry both at annual ring level and in gross wood transversal interaction. In this sense sapwood can be assumed to have close properties of the GRV to that of the late part of juvenile wood. The transversal categories of wood types are, therefore, early juvenile wood, late juvenile wood, mature wood and sapwood. Assuming this analogy is applicable to radial density profiles in which there is a monotonous increasing or decreasing magnitudes of density, too, this new classification along with TLS description of transversal density profile can mitigate the long standing juvenile-mature wood demarcation problem.

This study found a simple and alternative route for the quantification of parameters of equation (3.7). The derived scaling properties of the GRV presented in equations (3.22) to (3.27) further simplify the sufficient thermodynamic characterization of annual rings series.

3.2. Derivation of two-level systems models of water vapour sorption in wood

The general procedure of TLS description and modeling of sorption is similar to the TLS modeling of annual rings. However, determining the characteristic length is not as simple as the annual ring. The issue of characteristic interaction length with regard to kinetics was solved first and the obtained scaling behaviours were then transferred to the modeling of isotherms. The moisture potential given in section 4.6 by equation (4.1) was used to determine coefficients of the Fickian diffusion and this equation is modified to a form suitable for fractal characterization, which also signifies the contribution of the content of wood substance in heterogeneous sorption.

$$k(t) = \frac{w(t)}{w(t) - w(t_0)} \tag{3.36}$$

Equation (3.36) diverges at the beginning of the sorption and any numerical manipulation of the numerator does not help in avoiding the singularity. However, investigating the behaviour of $k(t)$ in the vicinity of $w(t_o)$ reveals important dynamics. The initial weight $w(t_o)$ is generic in a sense that it represents weight of wood at the beginning of sorption and hence can have a value different from oven dried weight based on initial value of equilibrium relative humidity. When $w(t_o)$ is different from oven dried or weight with no moisture that is represented below as $w(t_{oi})$ and when it is multiplicatively reduced by infinitesimally small values x as shown in equation (3.37), then the PDF of $k(t)$ follows power law distribution that diverges at the onset of the kinetics when x is numerically equal to one.

$$k(t) = \frac{w(t)}{w(t) - x \cdot w(t_{0i})} \quad and \left\{ \frac{w(t_{0i})}{w(t_0)} \leq x < 1 \right\} \tag{3.37}$$

Decreasing the value of x results in an increase in the scaling exponent of the PDF. The increase is linear for values of x going down to the magnitude of initial weight at time t to oven dry weight ratio. The decrease in the power law exponents of the PDF is another behaviour of $k(t)$ that is displayed when the denominator is raised to the powers of $y>1$ as given in equation (3.38):

$$k(t) = \frac{w(t)}{[w(t) - x \cdot w(t_{0i})]^y} \tag{3.38}$$

There is a power law dependence between the PDF of the power law exponents and the increasing powers to which the denominator is raised, that displays a scaling relation with a value close to -1 (a renormalization exponent). On one hand, increasing the magnitude of y in equation (3.38) makes the power laws exponent of its PDF decay to zero. On the other hand, allowing the value of x to remain close to one yields lower threshold value of the scaling exponent, while decreasing the magnitude of x below a value of one increases the exponent of the PDF. Decreasing the value of x based on equation (3.39) from unity by more than eighty five to ninety percent may result in a value less than the oven dry weight that

results in a distribution different from power laws. Equation (3.39) describes the scaling behaviour of sorption kinetics and its singularity.

$$p[w(t)]^{1-x} = \frac{w(t)}{[w(t) - x \cdot w(t_{0i})]^{y}} \tag{3.39}$$

If there is no sorption or if it is infinitesimally small and the value of x is kept close to zero then equation (3.38) diverges. If w_i is decreased to very small values and y is increased at the same time then equation (3.39) gives indeterminate (0/0) value. When the value of y is allowed to become negative then equation (3.39) approaches zero as the value of y becomes increasingly a smaller negative number. This special singularity behaviour is similar to the description of Hausdorff dimension. The spectrum of exponents that can be obtained by the power law displayed by varying values of y can be considered as equivalent to spectrums of interaction lengths in the wood-water-vapour system. Multifractal behaviour of the overall dynamics can be deduced from this. The Hausdorff dimension was once considered useful only for mere numerical exercise, but it is now being widely used in characterizing singularity spectrum of chaotic physical system that simplified analysis of attractor dynamics based on lately developed multifractal formalism.

For the derivation of scaling parameters and models for TLS description of sorption, the knowledge of the interaction length is just sufficient. The multifractal behaviour, which means many if not infinite dimensions, is detrimental to the purpose of this study as its main intent is finding concise scaling parameters. Therefore, the focus is mainly on the general scaling behaviour of the two cut-offs, which are the singularity scaling exponent of equation (3.39), the value of x beyond which the PDF of equation (3.39) stops behaving as power law, and the general scaling dynamics of other exponents located between the two. A simple scaling sorption model can be formed using the threshold scaling exponents based on power law criterion of x given in equation (3.37). A scaling function that gives the value of moisture at given time t can be given as follow.

$$w(t) \approx w(t_0) \cdot k \cdot t \tag{3.40}$$

where $w(t)$ is a function providing the time (first or the shortest time) needed to attain desired state of mass uptake. Determination of the exact form of equation (3.40) is difficult owing to complication brought by the inherent dynamical fluctuation and it would be better to find its scaling behaviour. Equation (3.34) can be simply given as

$$\frac{w(t)}{w(t_0)} \approx k \cdot t \tag{3.41}$$

Equation (3.41) is analogous to equation (2.7) if it is modified to the following form.

$$\left(\frac{w(t_\infty)}{w(t_0)}\right)^{-1} \approx k \cdot t^n \tag{3.42}$$

In Equation (3.42), if n takes a value of 0.5 then the diffusion is Fickian otherwise it is non-Fickian. Since k is only a dimensionless constant of proportionality, equation (3.42) is not dimensionally consistent as it is given. It is, therefore, necessary to multiply the left hand side of equation (3.42) by t^n.

$$\left(\frac{w(t_\infty)}{w(t_0)} \cdot t^{-n}\right)^{-1} \approx k \cdot t^n \tag{3.43}$$

Equation (3.43) is in agreement with the first time passage scaling behaviour of a random walk which can be applied in the network of wood and water vapour (Gallos *et al*., 2007; Havlin and Ben-Avraham, 2002). It can be experimentally proven that the following relation is valid.

$$p[w(t)]^{1-x} = \frac{w(t)}{[w(t) - x \cdot w(t_{0i})]^y} = \left(\frac{w(t)}{w(t_{0i})}\right)^{\frac{1}{1-x}} \approx t^{c_k} \tag{3.44}$$

where the value of c is close to two. Comparing equations (3.43) and (3.44) and by directly relating c to n, the following relation can be deduced.

$$\left(\left(\frac{w(t_\infty)}{w(t_{0i})} \right)^{\frac{4}{1-x}} \cdot t^{-8} \right)^{-\frac{1}{4}} \approx k \cdot t^{c_k} \tag{3.45}$$

which is the same as equation (3.46)

$$\left(\frac{w(t_\infty)}{w(t_{0i})} \right)^{\frac{1}{x-1}} \cdot t^2 \approx k \cdot t^{c_k} \tag{3.46}$$

Dividing both sides of equation (3.46) by the square of *t* gives equation

$$\left(\frac{w(t_\infty)}{w(t_{0i})} \right)^{\frac{1}{x-1}} \cdot t^2 \cdot \frac{1}{t^2} \approx k \cdot t^{c_k} \cdot \frac{1}{t^2} \tag{3.47}$$

that can further be rearranged to

$$\left(\frac{w(t_\infty)}{w(t_{0i})} \right)^{\frac{1}{x-1}} \approx k \cdot c_k \cdot t^{c_k - 2} \tag{3.48}$$

Equation (3.48) yields the following relation.

$$w(t_\infty) \approx \frac{1}{2} \cdot w(t_{0i}) \cdot k \cdot c_k^{x-1} \cdot t^{(1-x)\cdot(2-c_k)} \tag{3.49}$$

Equation (3.49) is valid should water sorption be dominated mainly by long range kinetics and merely predicts the equilibrium point. It does not describe the actual kinetics which makes its direct application for predication problematic. Even though the sorption is taking place below its glass transition point, the phenomenon involved at the onset of sorption is short range kinetics of Fickian diffusion type. The Fickian type kinetics has a quick decaying behaviour that soon vanishes leaving the long-range kinetics alone.

The method of determining parameter c in equation (3.49) and its relation to the short range kinetics should be established. The parameter c_k has two important aspects that require sufficient explanation which are namely its relation to the energy of sorption and the quantitative determination of its magnitude. Parameter c_k governs both the short and long range kinetics and two ways have been worked out in this study for its determination. The first one is based on analysis of the fluctuation of the variance that is due to the self-organizing critical behaviour while the latter is based on a relation derived in analogy with the Langmuirian theory of sorption. Through implementation of the first method, the kinetic data should be fitted into a function that empirically describes it well, preferably with kinetic equations. Then the fluctuations of the second moment are determined from the difference between the fitting empirical equation and experimental data. The obtained fluctuations are time series physical phenomena with already known long range interaction lengths. The moving ensemble interaction length can be obtained from the PDF of the left hand side of equation (3.41) based on experimental values and is numerically equivalent to $1/(1-x)$.

$$F_i^2\left(1/(1-x),i\right)=\left(\left(\frac{1}{n}\sum_{i=1}^{n}(K(t)_i\right)-k(t)_i\right)^2 \quad for\ i=1\ to\ r-n \tag{3.50}$$

$$p\left(F_i[1/(1-x),i]\right)\approx F_i\left[1/(1-x),i\right]^{c_k}\cdot F_i\left[1/(1-x),i\right]^{\frac{-1}{c_k+1}} \tag{3.51}$$

where F_i represents the fluctuation in the i^{th} moving interacting ensemble of wood-water mass. Equation (3.51) shows the two component nature of the fluctuation function that is the same as

$$p\left(F_i(1/(1-x),i)\right)\approx F_i\left[1/(1-x),i\right]^{\frac{c_k^2+c_k-1}{c_k+1}} \tag{3.52}$$

Equation (3.48) resembles the empirical Freundlich type Langmuir sorption equation. Since the Freundlich equation has been successful in fitting many chemisorption processes, many attempts were made to establish theoretical justifications for its parameters. Although many of the attempts remained futile, some recent progresses were achieved through the

application of statistical physics. It is now becoming clear that the empirical parameters can represent thermodynamic constants (Silva Da Rocha *et al.* 1996; Yang, 1998). Langmuir equation is good only for isotherms; however, its resemblance to equation (3.48) implies that the parameter c_k can be utilized to extract thermodynamic meaning based on statistical properties of the sorption kinetics.

Keeping the rigorous statistical physics assisted thermodynamic derivation on hold for the time being, a novel semi-empirical method of finding c_k and its analogous explanation as thermodynamic parameter is implemented. The latter option is more suitable for the purpose of this because the theoretical validation and the physical meanings that could be revealed may pretty well be confounded due to the observed dynamical phenomena shown in equations (3.36) to (3.39). Equation (3.53) which resembles equation (3.47) and takes into consideration effects of the long-range interactions is directly proposed. Equation (3.53) differs from equation (3.47) only by having the sigma notation that is helpful to establish a power law generating function. If the first passage time is assumed to directly scale with integral of weight uptake, then a relation in which c_k will represent the fractal dimension of wood can be established.

$$\sum_{i=1}^{n}\left(\frac{w(t)}{w(t_0)}\right)^{-\frac{1}{1-x}} \cdot t \approx k \cdot c_k \cdot t^{(c_k-1)} \tag{3.53}$$

The exponent c_k could be obtained by fitting the time dependent weight gain or loss data to equation (3.53).

In the beginning of section 3.0, the negative one (-1) power law scaling of the PDF from the renormalization exponent of equation (3.38) was obtained when its denominator had been raised to an increased power. This implies that negative one is one possible dimension based on which the different interaction lengths scale. Although this entails multifractality, negative one can be taken as generalized fractal dimension. In addition to the scaling exponent c_k that was obtained in equation (3.40) there is a need for a third parameter that equates the two component system as true and valid. In this section, the two components are identified as

long and short range kinetics. Details of the long range mechanism have been discussed in previous sections. The discussion will be concluded in this section by introducing a relation that creates a connection between the long and short range kinetics. The short range kinetics is a phenomenon which is scale dependent and defines specific sorption system. Equation (3.54) is defined in analogy with Einstein's scaling relation given in the literature review part of equation (2.15) ($d_w = \zeta + d_B$; *with* $\zeta = 2 - d + \bar{\mu}$) and the successfully tested conjecture of Alexander-Orbach (Condamin *et al*., 2007; Gallos *et al*., 2007; Havlin and Ben-Avraham, 2002).

$$\beta = c(H,T) + \gamma \tag{3.54}$$

where ζ is diffusion resistance exponent, $\bar{\mu}$ is average conductivity, d_w is the fractal dimension of the random walk, d_b is the fractal dimension of the substrate, c_k is the random walk exponent for wood which is a function of both temperature (T) and relative humidity (H), β is the fractal dimension of wood obtained from the fluctuation function based on relation (3.54) and is numerically equal to c_k+1, γ is the resistance exponent which is numerically equivalent to the exponent of self organizing criticality. If we assume γ to be related to surface emission coefficient then equation (3.54) becomes an analogy for effective diffusion coefficient in terms of surface emission and Fickian diffusion. The weight of wood is a linear length controlling the scaling dynamics along with the linear interaction length that can be obtained by scaling behaviour of equation (3.38). It can be shown that the scaling behaviour of the latter is invariant and close to -1. Therefore, γ in this case has a value of unity and represents the fractal scaling behaviour of equation (3.38) which is analogously known as self-organizing criticality.

Equation (3.48) predicts null moisture at the onset of sorption content but it also nullifies the initial weight which is absurd. Imposing an initial condition can give a second component or an intercept which can circumvent the absurdity. Moreover the equation should be corrected for short range interaction effects to make it consistent as sorption prediction model. Equation (3.48) is very similar to the Freundlich equation which has been considered as having difficulty in dealing with sorption on homogeneous surfaces. However, the two

equations are similar only in their expression and the Freundlich equation predicts an equilibrium state while the variable of concern here is dynamic or time dependent. The intercept or the second component should predict the initial weight at the initial time and at the same time should be the function of time, if it is to serve as a compensation term for short range kinetics. These two conditions can be met only by exponential function. The entropy of the system that is composed of two components can be regarded as separate, if the two components are assumed to be weakly coupled and in time dependent quasi-equilibrium state. Although it is not expected to have a similar turbulent phenomenon in this study, existence of a quasi-equilibrium state is usually assumed in direct numerical simulation (DNS) of fully developed turbulence using Fourier series to approximate the dissipation energy (Kaneda and Ishihara, 2009). Equation (3.53) can be regarded in this sense as an equation showing the proportions of states that are in power law dynamics.

The magnitude of parameter x in equation (3.37) can particularly be used to indicate the onset of power law dominating kinetics and its difference from unity shows the proportion of short range one. Considering the moment of maximum entropy, when the system can be fully described by the two components equally, the exponential decay equation can be established. Equation (3.55) can formally be established by direct use of equation (3.53), the entropy expression from Gibbs distribution, the exponent ($2\text{-}c_k$) from equation (3.49) for the contribution of the power laws behaviour and ($1\text{-}x$) for the short range kinetics.

$$\sum_{i=1}^{n}\left(\frac{w(t)}{w(t_0)}\right)^{-\frac{1}{1-x}}\cdot t\cdot \approx \int_0^t e^{\beta\cdot f(t)}\cdot dt \tag{3.55}$$

Differentiating equation (3.55) with respect to time yields the following

$$\frac{1}{1-x}\cdot\sum_{i=1}^{n}\left(\frac{w(t)}{w(t_0)}\right)^{-1}\cdot\left[\frac{1}{w(t_0)}\cdot\frac{d[w(t)]}{dt}\cdot dt\right]^{-\frac{1}{1-x}}\cdot t+\sum_{i=1}^{n}\left(\frac{w(t)}{w(t_0)}\right)^{\frac{1}{1-x}}=-\beta\cdot f(t)'\cdot e^{\beta\cdot f(t)} \tag{3.56}$$

Equation (3.56) can be rearranged based on equation (3.44) to give equation (3.51).

$$\left(\frac{w(t)}{w(t_0)}\right)^{-\frac{1}{1-x}} \cdot t + \sum_{i=1}^{n}\left(\frac{w(t)}{w(t_0)}\right)^{\frac{1}{1-x}} = -\beta \cdot f(t)' \cdot e^{\beta \cdot f(t)} \tag{3.57}$$

The second term of equation (3.57) can be approximated by equation (3.53) to give the following relation.

$$\left(\frac{w(t)}{w(t_0)}\right)^{-\frac{1}{1-x}} \cdot t = -k \cdot c_k \cdot t^{(c_k-1)} - \beta \cdot f(t)' \cdot e^{\beta \cdot f(t)} \tag{3.58}$$

During sorption, the time variable in the right-hand side of equation (3.58) plays differing roles at the onset and after a long duration. At the beginning of sorption when the prevailing kinetics is short range the initial weight has a controlling power and can be assumed to be independent of time. Therefore, it is more practical to use the weight description instead of the time variable in the right hand-side of equation (3.58). Furthermore since the long range kinetics is at its minimum at the onset of sorption, the value of x can be assumed to be close to zero and the right hand side of equation (3.58) can be closely approximated by the square of the ratio between $w(t)$ and $w(t_0)$. At large time limit the second term in the right hand side of equation (3.58) approaches zero and, being highly dependent on time, equation (3.58) will scale according to equation (3.48) displaying more dominant power law behaviour and the overall sorption description can, therefore, be given by the following relation.

$$\frac{w(t)}{w(t_0)} = k \cdot c_k^{x-1} \cdot t^{(1-x)\cdot(2-c_k)} + \beta^{-\frac{1}{2}} \cdot f(t)' \cdot e^{-\frac{1}{2}\cdot\beta \cdot f(t)} \tag{3.59}$$

The function $f(t)$ in equation (3.59) can be determined considering the critical exponents ($2-c_k$) and ($1-x$) for the purpose of scaling. Assuming the reciprocal of β to be the analog to the thermodynamic temperature that is given by the magnitude of the exponent c_k, the function

$f(t)$ can be determined as the time dependent free energy in quasi-equilibrium state that can be given by the following equation.

$$f(t) = \frac{t - t_c}{t_c} \tag{3.60}$$

where t_c is characteristic sorption time after which the long range kinetics starts to dominate. The characteristic sorption time t_c depends on c_k and x simultaneously which are parameters controlling the long and short range kinetics. Whitehead *et al*. (2009) have shown that $f(t)$ can be approximated by a power series expansion truncated at n^{th} order. However, the power series expansion can not yield a simple expression for t_c. Empirical tests in this study revealed that the product of $(2\text{-}c_k)$ and $(1\text{-}x)$ having a dimension of time can serve as an equivalent parameter for t_c that enables description of the short range kinetics. Therefore, the two component sorption can be explicitly given by the following scaling equation.

$$w(t) = w(t_0) \cdot k \cdot c_k^{x-1} \cdot t^{(1-x)\cdot(2-c_k)} + w(t_0) \cdot \beta^{-\frac{1}{2}} \cdot (2 - c_k) \cdot (1 - x) \cdot e^{-\frac{1}{2}\beta \cdot [((2-c_k)\cdot(1-x)\cdot t - 1)]} \tag{3.61}$$

where β is dependent on the level of sorption which correspond to low and high relative humidity ranges. Specifically, it is numerically equivalent to c_k+1 in the first level where the short range kinetics plays a dominant role while it takes the numerical magnitude of c_k in the second level that is dominated by long range kinetics.

The product of $(2\text{-}c_k)$ and $(1\text{-}x)$ controls the general dynamics of equation (3.61). When the product assumes a small value, the second term which is in the right hand side of equation (3.61) displays exponential decay and as it becomes larger it stretches more and ultimately attains a final profile approaching a straight line. This fact can be used to detect and determine the transition of sorption from level one to level two or from short range dominated to prevailingly long range kinetics. Equation (3.61) reveals not only the two components and two level behaviours of sorption, but also its dual nature. The sorption can

be described sufficiently by each of them separately at its end and onset, respectively while there is also an intermediate domain in which the two components are simultaneously active and should be considered for sufficient description. The new unified two-level and dual-mode sorption scaling can be generalized as follow.

$$w(t) = A_1 \cdot t^{(1-x)\cdot(c_k-2)} + A_2 \cdot e^{-\frac{1}{2}\cdot\beta\cdot[((2-c_k)\cdot(1-x)\cdot t-1)]} \tag{3.62}$$

$$A_1 = w(t_0)\cdot L_1 \cdot c_k^{x-1} \tag{3.63}$$

$$A_2 = w(t_0)\cdot L_2 \cdot \beta^{-\frac{1}{2}} \cdot (2-c_k)\cdot(1-x) \tag{3.64}$$

where L_1 a renaming of k and is a level parameter that determines the amplitude of mass uptake (it can be named as clustering or growth coefficient), L_2 is a parameter that is normally with a magnitude of unity, but can take some functional form in case of anomalous sorption with a sudden leap that was specially observed during this study.

It is clear that there is a general resemblance between the scaling model of kinetics and sorption that is traceable to the dynamical behaviour of both sorption properties that constantly evolve with time. Consequently, we are able to unify sorption kinetics and isotherms by describing sorption as a two-level and two-component physical system. The critical exponent c_k shows a power law dependence on temperature as follow.

$$\frac{\varepsilon}{c_k} = c_m + A \cdot \left(\frac{T}{T_0}\right)^d \tag{3.65}$$

where T_0 is a reference temperature (273.15K), T [K] is temperature, ε is a constant, c_m is a reference value for c_k and depends on the sorption system. Sorption isotherms at a given temperature have constant c_i while c_k (the kinetic constant) depends on relative humidity in a complicated way. Hence, in the case of sorption kinetics, all of the terms in equation (3.62)

depend on relative humidity. The following relation holds true for relative humidity dependence of the kinetic constant c_k.

$$\boldsymbol{h = \frac{w_\infty}{w_0} \cdot \frac{c_k}{\Delta h}} \tag{3.66}$$

Equation (3.66) can be rearranged and solved for infinitesimally small change of Δh to give equation (3.66).

$$\boldsymbol{\frac{h \cdot \Delta h \cdot w_0}{w_\infty} = c_k} \tag{3.67}$$

Equation (3.67) is the same as

$$\boldsymbol{\frac{h \cdot \Delta h}{c_k} = \frac{w_\infty}{w_0}} \tag{3.68}$$

where w_0 is the initial weight and h is the final vapour pressure at which the system is equilibrating and m_∞ is equilibrium mass uptake at given level of relative humidity. Equations (3.66) to (3.68) display various chaotic trajectories depending on complex interaction of mass uptake, vapour pressure and the kinetic scaling exponent c_k. Various shapes of chaotic trajectories can be obtained by rearranging parameters of equation (3.66). For the generalized theory of TLS, equation (3.66) is sufficient and agrees very well with the Boltzmann's sigmoid relation with elegant demonstration of the underlining mechanism of two levels of energy. Equations (3.62) to (3.68) are tested and validated using sorption data on earlywood, latewood and annual rings obtained as given in the experimental part of section 4.6.

All of the equations derived from (3.36) to (3.64) apply well to wood sorption isotherms also. Should the relative humidity be simply used in place of time variable t then two adjustments are needed to be performed. The first one is changing the sign of the exponent from negative to positive and vice versa. The second adjustment needed is changing the sorption dynamics controlling parameter. The product of $(2\text{-}c_k)$ and $(1\text{-}x)$ should be changed to the product of (1-

c_i) and another singularity behaviour describing parameter x, that can be obtained using equation (3.66). Equations (3.53) and (3.62) to (3.64) are valid and applicable for the description of sorption isotherms. They can be used for the prediction of parameters of sorption, specific internal surface area and fibre saturation point. Unlike the case of sorption kinetics, the scaling behaviours of isotherms are more dimensionally homogeneous and can be described by the mass fraction of moisture either in wood or in the air. Considering equation (3.58) when near equilibrium state is approached, the following relation is valid omitting the short range kinetics.

$$\left(\frac{w(t)}{w(t_0)}\right)^{-\frac{1}{1-x}} \cdot t = -k \cdot c \cdot t^{(c_i - 1)} \tag{3.69}$$

Notice that the subscript "*i*" in c_i is given to differentiate the scaling exponents for sorption isotherms from the previous scaling exponent of kinetics. When equilibrium is approached, equation (3.69) depends mainly on the level of relative humidity and, as the mechanism is independent of time then x can also be considered to be close to zero. If t is directly substituted by h then equation (3.69) transforms to a scaling relationship given by equation (3.70). This fact is experimentally verified to hold true in the exploratory phase of this study.

$$\frac{w(t)}{w(t_0)} = -k \cdot c \cdot h^{(c_i - 1)} \tag{3.70}$$

Let us consider the moisture content fraction in equation (4.2) that can be given as follows.

$$m_t = \frac{w_t - w_0}{w_0} \tag{3.71}$$

Rearranging equation (3.70) the following is valid under near equilibrium conditions

$$m_t = \frac{w_t}{w_0} - 1 \tag{3.72}$$

and by substituting equation (3.72) into (3.70) the following relation is obtained.

$$\boldsymbol{m_t = -k \cdot c \cdot h^{(c_i - 1)} - 1} \tag{3.73}$$

or in its identity form

$$\boldsymbol{k \cdot c \cdot h^{(c_i - 1)} - m_t = 1} \tag{3.74}$$

If m_t can be considered as an implicit power function then equation (3.74) may describe a two dimensional equilibrium phase space of relative humidity and moisture content. At the same time, the following mass transfer relation is valid.

$$\boldsymbol{\frac{dw}{dH} = -h_0(t) \cdot \left(w(t) - w_o\right)} \tag{3.75}$$

where the proportionality constant $h_0(t)$ is a function of both relative humidity and time. Equation (3.75) has a well known solution (see for example Krabbenhøft and Damkilde (2004), and Whitehead *et al.*, (2009)).

$$\boldsymbol{w(t) - w_0 = k \cdot e^{-h_0(t) \cdot H}} \tag{3.76}$$

which is the same as

$$\boldsymbol{\frac{w(t)}{w_o} - 1 = k \cdot e^{-h_0(t) \cdot H}} \tag{3.77}$$

Equation (3.73) is sufficient to describe the sorption isotherms when the diffusion is Fickian and the equilibrium moisture content is independent of time. However, when the diffusion is non-Fickian at higher relative humidity or at low temperature then the sorption isotherm is non-stationary and a function of time based on equation (3.70). Derivation of equation (3.77) with respect to time yields the non-stationary behaviour of isotherms as an identity and it is

directly related to the singularity parameter x and the scaling exponent c_i with similar functional form as it was applied to sorption kinetics. Therefore, the sorption isotherm is described by both equations (3.74) and time derivation of equation (3.77). The exponential term of equation (3.77) is determined rather heuristically as it is complex being a function of both time and relative humidity.

The consequence of equation (3.77) is that sorption isotherms are non-stationary as long as they are not describing the mean sorption isotherm. From this it follows that if the wood-water system is allowed to remain interacting for a very long time then the adsorption isotherms would be constantly shifted upward or attracted to the position of the mean sorption isotherms. The same conclusion could be drawn for desorption isotherms, namely, desorption isotherms would asymptotically be shifted downwards to the mean sorption isotherm provided the wood is kept constant at given temperature and relative humidity for a very long time after the relative humidity is very slowly lowered. The exponential term in equation (3.55) accounts for Fickian behaviour while in case of isotherms its role is compensating for non-stationary moisture content effect. Unlike the case of sorption kinetics, the second component diverges and scales with a factor of ¾, and not with scaling-exponent of ½ as it was earlier found for sorption kinetics. Equation (3.61) should, therefore, be modified by the superposition of equation (3.73) and (3.77) to

$$\boldsymbol{m(t) = k \cdot c_i \cdot h^{(c_i - 1)} + x \cdot \beta^{-\frac{1}{4}} \cdot e^{\frac{3}{4}\beta \cdot [((\frac{x}{\beta}) \cdot h - 1)]}} \tag{3.78}$$

in which h is vapour pressure, k is analogous to the L_1-parameter quantified for sorption kinetics. L_1 can be obtained from the intercept of the log-log plot of equation (3.69). The parameter β can be obtained based on equation (3.54) and numerically equals to c_i+1. The parameter x is numerically equivalent to the moisture content in fractions at the instance of phase transition from prevailing short range to long range kinetics. The nesting of the second component in equation (3.78) in a ¾ power law scaling can be readily noticed.

3.3. Derivation of two level systems model of physical properties and chemical composition of wood

A two-level system (TLS) analogy that has already been utilized in section 3.1 and 3.2 could also be applied to characterize wood physical properties and chemical composition as self-organizing or emergent system. Properties are defined as emergent if they arise by complex combination of many components and when they are not a lump-sum of properties of their components (Corning 2002). Wood displays this behaviour and can be described as TLS using its physical properties and chemical composition. In wood we can have many different TLS systems where each could represent a given species, physical or chemical state. This behaviour is especially well established in softwoods for which a model has already been developed in this study illustrating the case for earlywood and latewood in annual rings that show two distinct phases.

Regarding physical properties and chemical composition, the TLS behaviour that is being considered is not the direct product of nature. It arises when wood is separated into its components for the sake of determining its composition or its utilization. The state of wood after separation relates to the prior state of wood; however, this relationship is not a one-to-one matching and there is always information lost during separation. The practical aspect of this phenomenon becomes apparent if we consider density and shrinkage as physical properties with carbohydrate, lignin and extractives content as chemical composition.

Let density and shrinkage be identified as inactive or ground level energy state for the TLS. Presently, it is not possible to have full information about the cellulose, hemicelluloses and lignin composition of wood unless a wet chemical analysis is done. In the physical sense, the analysis provides information when the wood (system) is taken into a higher energy level and the components are separated receiving some amount of separation energy. The physical properties describe the wood before separation and the chemical components describe the altered state of wood. Hence, the chemical components and physical properties are descriptions of the wood properties at different points in time and for different states of wood. In chemical analysis the mass balance is normally performed based on weight of oven dried wood before and weight of chemical components after separation. However, the mass

balance is not exact as there is no specific and reliable method of separation for components such as hemicelluloses (Saka 2001). While complete knowledge of the mechanisms of chemical changes taking place during separation is still lacking, the following could be considered valid.

$$\textbf{\textit{physical property}} \approx f\left(\sum_i (\textbf{\textit{mass fraction}})_i\right) \tag{3.79}$$

The relationship in equation (3.79) as it is given is obvious and straight forward if complete description of the left and right hand side of the function are known. In that case the right hand side of the equation can be related to entropy through the general definition of entropy which is equivalent to Gibbs-Shannon entropy.

$$S = k \cdot \sum_i p_i \cdot ln(p_i) \tag{3.80}$$

Although the mass fraction of the i^{th} component is known, which can be an equivalence to its probability in the higher level energy, the integral energy of all the components in the after separation level cannot be exactly known, hence there is a difficulty in quantifying the right hand side of the equation. There is certain ignorance or missing information to completely trace-sum all the energy states that are accessible and to have a valid assumption of equal *a priori*. So, direct application of equations (3.79) and (3.80) appears to be troublesome. To circumvent this problem, a simple assumption can be made by stating the relationship in equation (3.79) to be scale invariant. Consequently, equation (3.80) could be equivalently described using power law instead of the usual lognormal distributions. Therefore, accounting for every accessible state of an ensemble as it is required by equation (3.79) will not be the concern of this study, but features that relate all to one, as components relates to the whole. This also helps to respect dimensional homogeneity by excluding the summation operation that is necessary to find the partition function so that ultimately the output can also be used for dimensional reduction. It is advantageous to start with the classic allometric equation that reads as follows.

$$Y = Y_0 \cdot M^{b} \tag{3.81}$$

in which Y is usually metabolic rate, Y_0 is a proportionality constant or amplitude, M is body mass and b is a scaling exponent. Equation (3.81) is a homogeneous scaling function and what is required for this study is a relation that can describe heterogeneous scaling involving multiple components. Therefore, in this study a new scaling equation that is equivalent to equation (3.81) is proposed. The new equation is of the same form to the conventional equation (3.81), but the dependent variable (metabolic rate) is the probability for the product of magnitude of two quantified wood properties to be scaled with a constant value across a wide range of diversity. The body mass term is still represented by similar terms, but in this case it will be a mass (weight) fraction that takes into consideration multiplicative effects of high dimensional interactions. The equation does not simply break the components down into weight fractions and then sum them so as to avoid non-homogeneous mathematical operation, which is not allowed in dimensional analysis. It also allows for variability and nesting. The derived equation is

$$\boldsymbol{p}\,(\boldsymbol{b}_2/\boldsymbol{b}_1) = \boldsymbol{A} \cdot \left(\left(\frac{\boldsymbol{C}_1}{\boldsymbol{C}_{0_1}} \right)^{\boldsymbol{b}_1} \cdot \left(\frac{\boldsymbol{C}_2}{\boldsymbol{C}_{0_2}} \right)^{\boldsymbol{b}_2} \right)^{\boldsymbol{b}} \tag{3.82}$$

in which $C_i^{b_i}$ are wood properties to be combined, b_1 describes the ground (inactive) state in conventional or fractal dimensions and b_2 the after separation (active) energy level exponents of high or low dimensions, A is the amplitude or proportionality constant and C_{0i} are system thresholds. The $C_i^{b_i}$ can by themselves be combinations of other properties. The exponent b being a result of self-organization is expected to transcend scale while the amplitude A may or may not be scale invariant.

The independent variable of equation (3.82) corresponds to the product of two dimensionless parameters of equation (3.81) that have separate exponents of their own. The exponent b remains usually as a fraction or small number which is close to one (1). However; in case of equation (3.82) there are nested exponents one of which is constant (b_1) and the other that

can vary (b_2) from zero to some large number. There is no limit placed on exponent b_1 and b_2 but b_1 is more useful if it is restricted in the range of zero to three which is the conventional limit of physical dimensions. An analogy taken from nuclear physics in which energy emission is expressed in terms of the product of two physical variables (the mass and speed of light) can give further perspective to the active and inactive state consideration. Although it is more relevant to the reverse dynamics, fertilization is another analogy that can bring clarity to the two component approach. A single egg which can represent the inactive (ground level) needs more than thirty million sperm cells for assured fertilization which is a process for the formation of an emergent property (see the appendix for detailed description of the metaphor). Both analogies show the high order differences in the magnitudes of the two states or components and underlie the biophysical basis of this study. Equation (3.82) can be generalized in a compact product notation that can be extended to *n*-level physical system as follows.

$$p(b_i/b_1) = A \cdot \left(\prod_{i=1}^{n} \frac{C_i^{b_i}}{C_{0_i}} \right)^b \tag{3.83}$$

Equation (3.83) states that the product of the magnitude of two or more wood properties that are in a relatively differing states or levels of energy which can be identified as active and inactive, if raised to some power b_i create a linear characteristic size which enters into a scale invariant relationship with its own joint statistical size distribution. Therefore, b is simply a fractal dimension of properties combination.

The following assumptions could be made about the two exponents of component C_1 and C_2: of equation (3.82) and (3.83) based on the general dynamics in the TLS:

- The inactive level can be defined by one physical property for any of the properties in the active level.
- There is a state of the inactive level in which the exponent b_1 remains constant for many corresponding exponents b_2 in the active level.

- If equations (3.82) and (3.83) hold true as power laws and if there is an exponent b for a product of $C_1^{b_1}$ and $C_2^{b_2}$ that remains constant while b_2 changes, then b is an emergent exponent transcending scale.
- If exponent b_2 is varied from zero to some higher value for some constant value of b_1 then the products of $C_1^{b_1}$ and $C_2^{b_2}$ will generate power law distributions having small exponents (b) with a value close to 1. Generally, higher values of b_2 can generate power law distributions while small values can result in other distributions, mainly lognormals.
- If for some changes in the higher b_2 values the change in the value of b remains infinitesimally small then the value of b can be considered scale invariant. This can be defined as equivalent to Liouville's theorem and the following equation (3.83) holds true,

$$\frac{db}{db_2} \approx 0 \tag{3.84}$$

This is equivalent to equation (3.85) where $f(b_1, b2)$ is a power function with b_1 being constant

$$\frac{df(b_1, b_2)}{db_2} \approx \text{Constant} \tag{3.85}$$

This analogy between the frozen structure in wood composition and Hamiltonian dynamics is created to anticipate conserved quantities in wood composition that can be traced back (reconstructed) and connected to a dynamic state that had existed while wood was being formed from living cells. The connection made can further impart a biophysical meaning to this study. It may be clear that from Hamiltonian dynamics point of view b_1 can imply location while b_2 may give a feeling for momentum in the wood composition phase space.

- If for continuous changes in the value of b_2 the change in the value of b remains infinitesimally small or changes very slowly then there is only a single fractal dimension governing the scaling relationships; however, if there are multiple and localized values of

b for which equation (3.83) to (3.85) are valid then the scaling relationship is governed by multifractal dimensions.

If b_2 is plotted against b then a curve similar to a multifractal spectrum that could be fitted with a power law obeying functional relationship can be obtained. It is preferable to call this functional relationship constant energy trajectory or a one dimensional mapping in a coordinate of (b_2, b) corresponding to equation (3.83), (3.84) and (3.85). This looks like skewing equation (3.82) so that it can generate power law distributions. However, the main purpose is accounting for multiplicative effects arising from interactions of the two levels. Selection of the constant value as exponent b_1 becomes trivial if it originates from dimensional analysis of physical properties. If dimensional analysis is difficult to apply then, it depends mainly on intuition and thus, it is beneficial to start from some frequently occurring dimensional values. The magnitude of exponent b_1 will be kept at some suitable value and exponent b_2 will be varied according to equation (3.83). The value of b_2 can be any number in the range from zero to infinity. Nonetheless, the real system cut-offs do not practically allow the b_2 dimension to become infinite.

The obtained exponents, that can synonymously be called fractal dimensions, are assumed to be scale invariant if they fulfilled the conditions given in equations (3.83) to (3.85) and are valid for any wood properties database. It is essential to test some of the long time tested and allometric exponents such as quarter (1/4), one third (1/3), two third (2/3) and three quarters (3/4) that frequently occur in nature as a value for b_1. One can speculate on the connection of these fractions to the three spatial dimensions or to the four space-time dimensions, even further to entropy of black body or cavity radiation. Linking self-organizing behaviour to scale invariant behaviour in wood composition can help to understand and explain hard to predict variations in wood properties and also to reconstruct their causal link to the dynamical history in wood formation. While mature wood in technological processes or under service may or may not be in self-organizing critical state, this dynamical phenomenon is being considered because wood formation is affected by sun light and rainfall parameters that show self-organizing criticality. A system which is in self-organizing critical state shows algebraic spatial and temporal correlations. Its power spectrum scales with the exponent of negative one, and this value can range from -0.5 to -1.5 (Bak *et al*., 1988). This indicates that

scale invariance that is accompanied by small exponents can also be the signature for self-organizing criticality. That is why the search for the critical fractal dimensions is preferred to be done around values of small numbers such as negative one (-1).

The variables integrated as two levels of one system will be used as dimensionally reduced inputs for the modeling of sorption using artificial neural networks. The scaling options that are applied in this study are elaborated as follow. Scaling exponents b_1 and b_2 can be considered as order parameters. The parameter b is a critical exponent that is obtainable from the power laws scaling behaviour of the probability distribution function of the integrated variables. Changing the magnitude of b_2 results in a change in the corresponding magnitude of b and this dependence can be expressed through a power law relation by introducing a new exponent d_b. Consideration of threshold magnitudes requires introduction of another scaling exponent that can be named as b_f, where f denotes the maximum fluctuation for given exponent of b_2. This scaling exponent is computable based on the probability distribution function obtained from the difference between value of each of the integrated magnitudes and the maximum value in the TLS. The following equation (3.86) that uses the TLS (integrated parameter) as predictor and that is valid for associated physical property can be proposed for dimensional reduction and scaling.

$$\textbf{\textit{Physical property}} = (\textbf{\textit{characterstic length}})^{\frac{b_n}{d_b-(b_2+1)}} \tag{3.86}$$

where b_n is the maximum (critical) value of b computed based on Equation (3.83). Equation (3.86) is related to equation (3.80) through the Einstein fluctuation dissipation function. Equation (3.86) diverges if the difference between d_b and b_2 numerically equals to positive one that makes it predict an infinite physical property. This critical behaviour may become very important with regard to shrinkage that can cause dangerous internal stress. Equations (3.83) and (3.86) are tested and validated using data obtained from chemical composition analysis of earlywood and latewood as given in the experimental part of section 4.9.

3.4 Development of the artificial neural networks sorption prediction model

The simplest multi-layer feed forward with error backpropagation ANN can be modeled with minimum transformation of inputs that mainly include operations such as standardization or division of each of the values by their respective observed maximum magnitude. It is also equally valid that transformation of each of the inputs using various nonlinear continuous functions, in addition to those that are usually applied on processing elements in hidden layers, helps to incorporate better the complex and nonlinear relationships between inputs and outputs with increased accuracy. However, the increased complexity may offset the gains since the resulting model becomes even more difficult for interpretation and problems with generalization may also occur due to over fitting. In many cases, it may become necessary to transform a single input using more than one nonlinear function that equally contribute to increased prediction accuracy. Omission of any of them can greatly affect the target output. The dimensional reduction models that have already been derived in the previous sections, therefore, become paramount in keeping the explosion in the number of inputs due to multiple nonlinear transformations at reasonable level.

The ANNs are used to develop three types of prediction models, namely, models that predict chemical composition of small specimens from physical properties, models that predict parameters of the TLS sorption prediction for the small specimens (earlywood, latewood and annual rings) and models that coarse-grain the small specimens' sorption properties to gross wood. The detailed list of variables used as inputs and outputs is given in Table 3.1. The categories are thirteen in number, and the variables in the twelve categories can be used as inputs while it is also possible to find interdependencies between them. The following seven categories are used as inputs to predict parameters of the TLS model of sorption.

i. Relative humidity and temperature.
ii. Basic ring parameters: wood type, width of wood type, ring number from pith, and basic density.
iii. Ring parameters derived from the TLS model of annual ring: Golden Ring Volume (GRV), Contracted Golden Ring Volume (GRV_c), integral of consecutive five contracted GRVc (5S-GRV_c).

iv. Basic chemical composition of annual ring: arabinose, galactose, glucose, xylose, mannose, acid insoluble lignin (AIL), acid soluble lignin (ASL).

v. Chemical composition parameters derived from the TLS model: the TLS description of chemical composition (Chem-TLS) and the i^{th} Chem-TLS description of chemical composition in a consecutive annual ring (C-TLS-T_1).

vi. Basic isotherm model parameters: slope for isotherms (c_i), wet weight based mass fraction (w_f/w_i).

vii. Derived or parameters calculated from the TLS models of sorption: BET internal surface area (BET-SA), surface area obtained from the TLS model of sorption isotherms (TLS-SA), relative humidity at the saturation of monolayer (H-Mono), moisture content of monolayer coverage (M-Mono), percentage of water vapour clusters in monolayer moisture content (M-Poly), the sum of mono layer moisture and poly-layer water vapour clusters content at the saturation of monolayer coverage (M-integ.), fibre saturation point (FSP).

Table 3.1 Inputs and outputs used in the development of the three categories of ANN sorption prediction models

Physical properties			Chemical composition		Parameters of the TLS models of sorption (kinetics and isotherms)							Gross wood sorption parameters
Relative humidity & Temperature	Ring parameters				Basic						Derived	
	Basic	Derived	Basic Chem. Comp.	TLS of Chem. Comp.	Kinetic				Isotherms			
H	Wood type	GRV	Arabinose	Chem-TLS	x-sing.	c_k	i-int	t-exp	L_1	c_i	BET-SA	M
T	Ring no	GRV_c	Galactose	C-TLS-T_1	x-NT_1	c_k-NT_1	i-NT_1	t-exp-NT_1	L_1-NT_1	w_f/w_i	TLS-SA	D
	Width	5S-GRV_c	Glucose	C-TLS-T_2	x-NT_2	c_k -NT_2	i-NT_2	t-exp-NT_2	L_1-NT_2		H-Mono	S
	Density		Xylose	C-TLS-T_3	x-NT_3	c_k -NT_3	i-NT_3	t-exp-NT_3	L_1-NT_3		M-Mono	
			Mannose	C-TLS-T_4	x-NT_4	c_k -NT_4	i-NT_4	t-exp-NT_4	L_1-NT_4		M-Poly	
			AIL	C-TLS-T_5	x-NT_5	c_k -NT_5	i-NT_5	t-exp-NT_5	L_1-NT_5		M-integ.	
			ASL	C-TLS-T_6	x-NT_6	c_k -NT_6	i-NT_6	t-exp-NT_6	L_1-NT_6		FSP	
				C-TLS-T_7	x-NT_7	c_k -NT_7	i-NT_7	t-exp-NT_7	L_1-NT_7			
				C-TLS-T_8	x-NT_8	c_k -NT_8	i-NT_8	t-exp-NT_8	L_1-NT_8			
					x-NT_9	c_k -NT_9	i-NT_9	t-exp-NT_9	L_1-NT_9			

Similarly the two categories of ring parameters can be used to predict the basic and derived chemical composition. The following parameters of the TLS models of sorption create five categories that are used in combination of the previous seven categories to predict gross wood sorption properties using ANN as a coarse-graining tool.

i. The singularity parameter of the TLS sorption kinetics (x) and the i^{th} neighbouring annual ring singularity parameter of the TLS sorption kinetics (x-NT_i).
ii. The slope of TLS sorption kinetics (c_k) and the slope of the i^{th} neighbouring annual ring TLS sorption kinetics (c_k-NT_i).
iii. The intercept of sorption kinetics (i-int) and the i^{th} neighbouring annual ring intercept of the TLS sorption kinetics (i-NT_i).
iv. The exponent of the time variable in the TLS (t-exp) and the time exponent of the i^{th} wood type in consecutive series of annual rings (t-exp-NT_i).
v. The growth parameter L_1 of the TLS sorption and the growth parameter of the TLS sorption kinetics of the i^{th} neighbouring annual ring (L_1-NT_i).

For each of the three types of prediction models, three categories of networks which contain a total of twenty four ANNs models were developed and trained as follows.

- Category I –Inputs and their transforms without being undergoing selection.
    a. Linear transformation of inputs with long range interactions (1.1.1).
    b. Linear and nonlinear transformation of inputs (comprehensive) (1.1.2).
    c. Linear transformation of inputs neglecting long range interactions (1.2.1).
    d. Linear and nonlinear transformation of inputs (comprehensive) neglecting long range interactions (1.2.2).
- Category II- All salient inputs and their transforms selected using genetic algorithms by considering long range interaction.
    a. Selection and inclusion of important inputs by putting all of them in one group only (2.1.1).
    b. Selection and inclusion of at least one important input from variables grouped and sub-grouped as anatomical, physical and chemical domain (2.1.2).
    c. Selection of at least one best fitting transform for each of the inputs by forcing each of the variables to be an input that contributes equally to the output (2.1.3).

- Category III- All salient inputs and their transforms selected using genetic algorithms by neglecting long range interaction.
    a. Selection and inclusion of important inputs by putting all of them in one group only (2.2.1).
    b. Selection and inclusion of at least one important input from variables grouped and sub-grouped as anatomical, physical and chemical domain (2.2.2).
    c. Selection of at least one best fitting transform for each of the inputs by forcing each of the variables to be an input that contributes to the output (2.2.3).

The comprehensive input transformation functions tested based on genetic algorithms include the following: Linear; Logarithmic functions: log(x), log(log(x)), ln(x/(1-x)); Exponential functions: exp(x), exp (exp(x)); Power functions: x^2, x^4, $x^{1/2}$, $x^{1/4}$, x^{-1}, x^{-2}, x^{-4},$x^{-1/2}$, $x^{-1/4}$; tanh function: tanh(x). ANNs sorption prediction model that uses only relative humidity and temperature as inputs was developed so that it can be used as a bench mark while evaluating the benefit obtained by incorporating anatomy, chemical composition and other physical properties. Attributes of the modeling process for the training of the ANNs in the three categories, with or without variable selection, using raw and dimensionally reduced inputs, are summarized in Table 3.2.

Table 3.2 Attributes of the modeling process for the training of ANN with or without variable selection using raw and dimensionally reduced inputs

Major attributes of the ANN modeling		Modeling of sorption with or without variables selection			
		ANN modeling without variable selection (Category-I)	Variable selection with genetic algorithms for ANN modeling with or without long-range interactions (Category II and III)		
			Grouping		
			All in one group (a)	Grouping based on domain of variable (b)	Grouping of transforms based on variable (c)
Inputs transformation		Linear and nonlinear	Comprehensive	Comprehensive	Comprehensive
Variable selection model		None	ANN	ANN	ANN
Best network search		Exhaustive	Exhaustive	Exhaustive	Exhaustive
Learning rule		Adaptive gradient	Adaptive gradient	Adaptive gradient	Adaptive gradient
Transfer function applied at layers	Hidden	tanh	tanh	tanh	tanh
	Output	sigmoid	sigmoid	sigmoid	sigmoid
Models evaluation criterion		Correlation function	Correlation function	Correlation function	Correlation function

3.4.1 Constructing the ANNs, training, testing and validation of models

The general procedure applied to build the ANNs models was similar for all of the three types of prediction models: models that predict chemical composition of small specimens from physical properties, models that predict parameters of the TLS sorption prediction for the small specimens and models that coarse-grain the small specimen's sorption property to gross wood. All the inputs were partitioned into training, testing and validation datasets based on round robin manner and allocation percentages of 75%, 10% and 15% to each of them, respectively. Each of the inputs were first analyzed by the NeuralWorks-Predict software so that numeric and categorical variables are internally identified and a work file that contained transformed data can automatically be created. The ANNs models were developed using all the inputs and also using only those inputs that are found to affect the outputs synergistically and significantly based on a genetic algorithm variables selection procedure.

The NeuralWorks-Predict software has four levels that can be chosen as no selection, superficial, moderate and comprehensive which correspond to the rigor of variable selection that automatically determines the number of cross validation sets as one, two, three and four, respectively. To increase the generalization capability of the developed ANNs models, the number of cross validation sets of this study was, however, increased to six. The variables selection was done using separately trained neural networks, for each of the variables and their transforms. The number of training records used was limited to a number equal to one hundred and sixty times the number of outputs. The quantization of variables was done in levels ranging from zero to hundred. Each of the quantization levels formed fitness-bins and variables fitness that fell within the same bin were considered equal with smaller and/or newer variable sets having precedence over larger and/or smaller ones. During the execution of the genetic algorithms new variable sets or individuals were obtained either from recombination of two parents or copied from a single parent with selection of the first parent based on fitness criterion that favours higher ranked parents according to a linear distribution while the second parent was selected randomly according to a uniform distribution. The genetic algorithm was allowed to be executed up to a maximum of one hundred generations

until the fitness was not able to improve below a tolerance of 0.001 for a maximum of ten consecutive generations. The selected synergistic inputs were then used to build the ANNs models.

The architecture of the ANNs was built using the cascade correlation (CC) learning method for determining a suitable number of hidden nodes. During the CC learning, one to three hidden processing elements were added at a time, both to already formed hidden processing elements and to the inputs, and constructing the ANNs architecture was stopped when performance of the network output was not able to show any improvement with the addition of the last hidden node. The network building and training parameters are given in Table 3.1.

During network training, the weights were initiated by uniform weight randomization and had a maximum limit of forty and a reduction factor of 0.5. The cascaded ANNs building was done first with direct connection of the input vectors to the outputs. The tanh transfer function that is given by equation (1.24) of section 2.11 was applied at the hidden processing elements while the sigmoid function, which is also given by equation (1.25), was used at the output so that the nonlinearities can sufficiently be captured. Adaptive gradient learning algorithm with line search iterations of one hundred having a tolerance of 0.00001 and a stochastic gradient factor of 0.1 was applied. Stochastic gradient factor is a random vector or a bias term that is added to the line search direction vector as given by equation (2.18) and (2.19) in section 2.11 and is obtained as a fraction of the length of the original direction vector.

The momentum term at both hidden and output processing elements was set at ten and the weights were allowed to decay with a factor of 0.0005 and 0.0001 for hidden and output nodes, respectively, to inhibit a tendency of favouring larger weight at any of the nodes. A learning rate, which is a multiplier of the gradient vector as given by equation (2.21) and (2.22) for weights to accelerate or decelerate the learning process at processing elements, was added with a magnitude of one hundred at the hidden processing elements and 0.01 at the output nodes. The tolerance for learning convergence was set close to 1 at exactly 0.999999 for both hidden and output nodes for the best prediction accuracy. The minimum and

maximum number of neural networks to be trained to get the best prediction of outputs was also set at one and ten, respectively. The algorithm was allowed to search for the best network up to ten different networks. If no improvement occurred for up to ten trained networks or if the tolerances on the objective function or the correlation remained 0.001 or lower then the search was terminated and the best performing network was retained and the rest discarded. The minimum epochs or the minimum number of passes of the complete line search was set at ten while training output weights and the epoch factors, (which give the maximum number of passes when it is multiplied by the number of output weights and added to the minimum epochs), was set at four and eight for the outputs and hidden nodes, respectively. The evaluation of network performance was done using correlation as the objective function.

3.4.2 Sensitivity and inputs contribution analysis

Sensitivity analysis quantifies the effect that a small change in an input value will have on the output values. The sensitivity analysis is a mathematical operation involving partial derivatives of output variables with respect to input variables as given by

$$\boldsymbol{O}_s(\boldsymbol{i},\boldsymbol{k}) = \frac{\partial[\boldsymbol{O}(\boldsymbol{i},\boldsymbol{k})]}{\partial[\boldsymbol{I}(\boldsymbol{i},\boldsymbol{j})]} \tag{3.87}$$

where $O_s(i,k)$ indicates the sensitivity of the k^{th} outputs for changes in the i^{th} inputs data set and for the j^{th} input data field, $O(i,k)$ indicates the k^{th} output for the i^{th} dataset and $I(i,j)$ indicates the input value in j^{th} data field for the i^{th} dataset. Sensitivity analysis can guide or give insight about which variable can be controlled with ease and the effect of increasing or decreasing the variables on the output. In the NeuralWare-Predict software, equation (3.87) was used to calculate the sensitivity of each of the modeled outputs to the change in every of the inputs using the active transforms of the input variables and outputs. The summary of sensitivity analysis statistics across all records of the inputs range was calculated and the average, variance and mean sum of squares of the sensitivity values were obtained for each input-output relationship. The average sensitivity value is important to indicate the

directionality of the sensitivity. A negative value for a given field means increasing the given input causes the corresponding output to decrease and vice versa. The average square sensitivity value is the best indicator for the relative magnitude of sensitivities regardless of directionality. The variance of the sensitivity shows the simple variance of each of calculated sensitivity values.

Contribution analysis is the ranking of the input variables or fields for a given input value based on the contribution they have made to the outcome. Computationally, it can be thought of as the additional information a field has brought to the prediction as compared to if it was missing. Each input variable is rated with a value ranging from 0 to 100 with higher values implying a more pronounced effect of the variable on the output. The inputs contribution analysis was done using the NeuralWare-Predict software by the following algorithmic steps.

i. The trained MLP neural network was run using the active inputs-outputs record.
ii. Simultaneously, the value of each of non-missing variables was replaced by the mid-range value and a modified output is calculated.
iii. The absolute difference between the neural net output of the original dataset and the modified dataset was calculated for each of the non-missing variables to obtain the "delta" for the non-missing fields.
iv. Each of the deltas was divided with the maximum delta over all non-missing variables so that the maximum delta is 100.

Negative contribution values can be obtained and their presence simply means that the neural network output calculated using the modified datasets is moving away from the output's extreme values, as compared to the outputs obtained using the unmodified datasets obtained in step *i*.

4.0. EXPERIMENTAL

4.1 Specimen sampling

Douglas-fir (*Pseudotsuga menziesii*) was selected as the wood species of investigation mainly for its visually distinct earlywood/latewood zones within the annual rings and the distinct sapwood/heartwood areas within a tree cross-section. Three trees of coastal Douglas-fir that were free of visible defects and growth anomalies were obtained from Malcolm Knapp Research Forest of the UBC-Faculty of Forestry. The forest stand was second growth and naturally regenerated from a forest fire in 1931. The three Douglas-fir trees that were felled had breast height diameters of 610mm, 705mm and 715mm, respectively. One 200mm thick disk located at breast height of each tree was obtained and marked to identify the north. Before the main experimental work was started, the experimental design given in Table 4.1 was developed based on pre-trials with the Dynamic Vapour System (DVS) to determine the optimum sample weight and amount of time needed to complete one sorption (full cycle) run. The number of successful DVS runs was a limiting factor for the number of annual rings for which densitometry and analysis of chemical composition could be done.

Table 4.1 Specimens sampling, preparation and experimental measurements performed on Douglas-fir

Type of measurement		Specimen specification	Method of sampling	Method of sample preparation	Specimens required	Total #	Days (Planned)
DVS - micro - sorption	T=25°C	Length=3mm Width= 1.7- 2.77mm Average wt.=1.5mg	Annual rings located at the beginning and end of mature heartwood, and sapwood	Separation of wood type and annual ring by sharp razor blade	2x (Extracted and non-extracted), 2x (Heartwood and sapwood), 3x (Earlywood, latewood and annual ring), 3x(Disks), 3x (Replications), Total number of specimens = 108	216+72	870 days 2.4 years
	T=50°C				2x2x3x3x3=108 (The detail is the same as the above)		
DVS –Sp. surface area					2x2x2x2x5=72 (The detail is the same as the above)		
PGC – Macro-Sorption	T=25°C	Thickness=5mm W=50mm L=100mm Wt.=13250mg (13.25g)		In radial direction cut strip boards matched to micro sorption specimens	2x (Sapwood and heartwood) 3x (Disks), 5x(Replications) Total number of specimens =30	60	320 days
	T=50°C				2x3x3=30 (The detail is the same as the 25°C above)		
Klason lignin –acid hydrolysis		1000 mg of 40 to 60 mesh number wood flour	Each of the wood types with 100mm length and 5mm width taken adjacent and matched to the micro-sorption specimens for earlywood and latewood	Microtome/razor blade slicing, milling to fines of 20 to 40 mesh numbers, extraction with acetone, acid hydrolysis and fractional extraction of holocellulose and purification of lignin residue	2x (Heartwood and sapwood), 2x (Earlywood and latewood), 3x(Disks), 3x (Replications), Total number of specimens = 36	36	30 days
HPLC-carbohydrate content					2x 2x3x3=36 (The detail is the same as the above)	36	
Density and widths of annual ring, earlywood and latewood		1.57 mm thick and 5mm wide Northern radial board strip	Two radial strips per disk	Cutting discs into strips and converting them into specimens using twin blade micro saws	3-extracted 3-unextracted Total number of strips=6	6	4 days

4.2 Douglas fir specimen preparation

Radial boards that were used for the preparation of meso-scale and gross-wood sorption measurement were cut according to the following scheme. The three disks were marked with two parallel lines running radialy from North to South so that the pith was included half-distance between them. Additionally, three lines spaced parallel and 10mm apart from each other were drawn on both sides of the pith-centered boards. The disks were then mounted on the bed of a portable horizontal band sawmill (Wood-Mizer). Each disk was set and fixed so that the saw line and the laid out lines are parallel to each other. The radial boards of each disk were cut along prescribed guidelines, adjusting the saw line as the cutting was progressed. In this way, seven radial boards, 10mm of uniform thickness were cut from each disk.

Halves of the radial boards located in the Southern-half of the disks were cut out and kept away. The top and bottom ends of the remaining half radial boards of the three disks that contained the pith (pith-boards) were trimmed by cutting-off 50mm wide end-strips. End-strips having a width of 25mm were removed from the top and bottom end of the remaining six boards that were cut from east and west side of the pith-boards. The boards were then ripped into two 100mm wide strips. The procedure of converting the disks into experimental samples is given in Figure 4.1 and the three dimensional cutting plan showing the sampled boards is shown in Figure 4.2. The pith-boards, both strips of the third radial boards and bottom halves of the second radial boards were planed to an accurate thickness of 5mm on a CNC-router (Precix, model: 3200). The remaining boards were stored in a -20^0C freezer until they were milled to wood fines of earlywood and latewood for chemical analysis.

4.3 Earlywood, latewood and annual rings of Douglas-fir's sample preparation for sorption and densitometry measurement

The pith boards that were trimmed to a width of 150mm were ripped into eighteen strips of 3mm and two strips of 1.57mm high in the longitudinal direction; both with a uniform tangential width of 5mm, using a special fixture made to hold samples (Figure 4.3). The

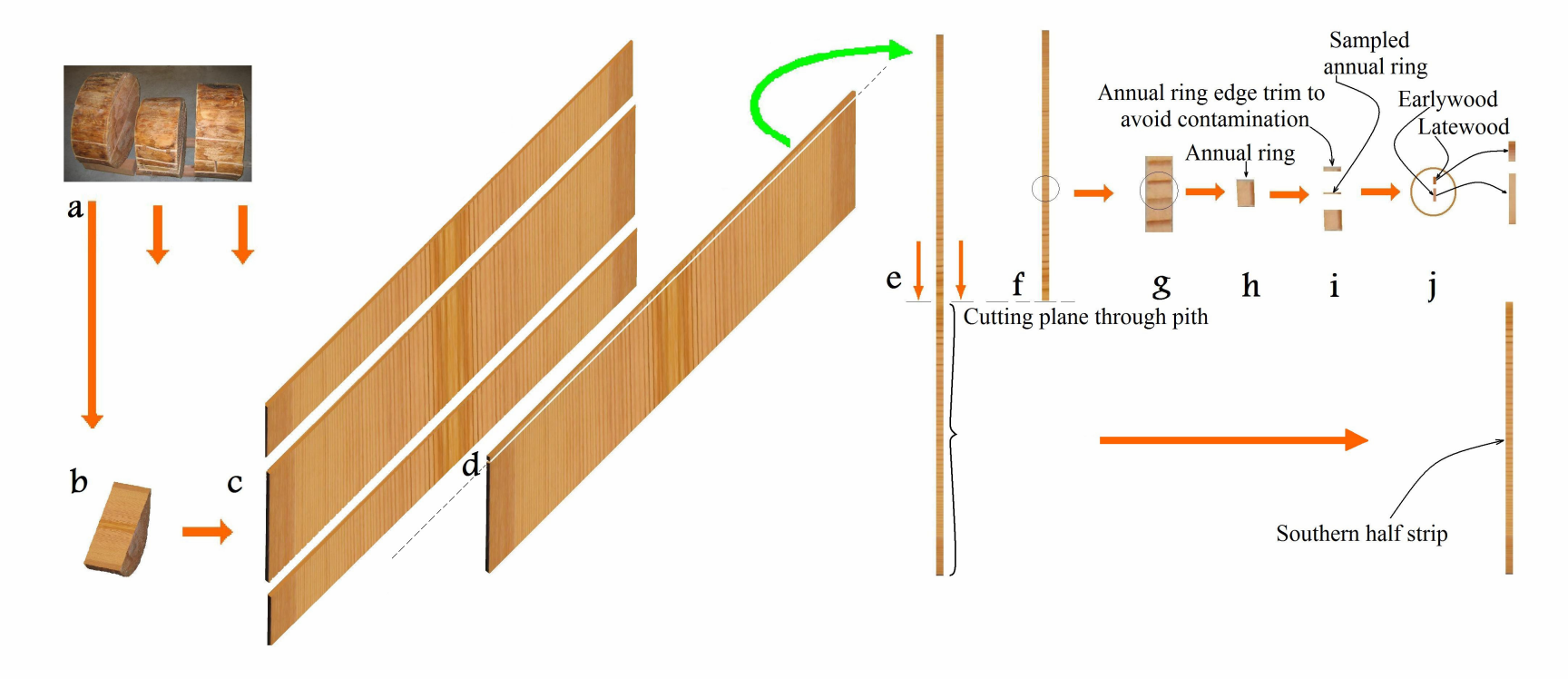

Figure 4.1 Specimen preparation procedures where in: a are shown the DBH disks, b-the half disk without the eastern part, c-shows how the radial boards are trimmed, d-the trimmed radial board, e-radial strip with cross section of 3mm by 5mm made from the trimmed radial board, f-the strip without the southern half, g-close up view on annual rings sampling location, h-annual ring cut out from the location shown by "g" and rotated 90^0 clockwise, i-sampled annual ring with a thickness of 0.2mm, j-cross-sectional view of separated earlywood and latewood of Douglas-fir with magnification (four times)

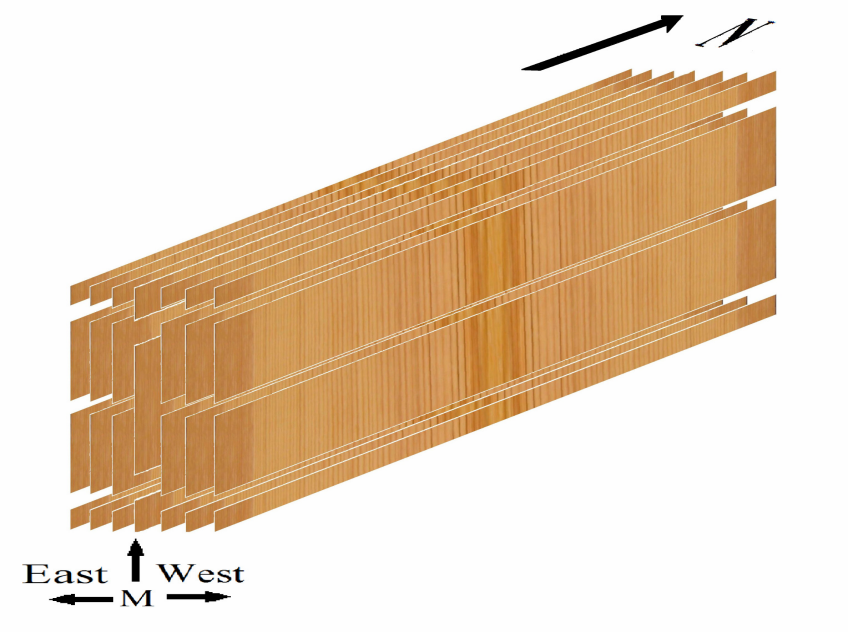

Figure 4.2 Three dimensional view of the cut made to obtain sampled radial boards; N and M represent North and middle

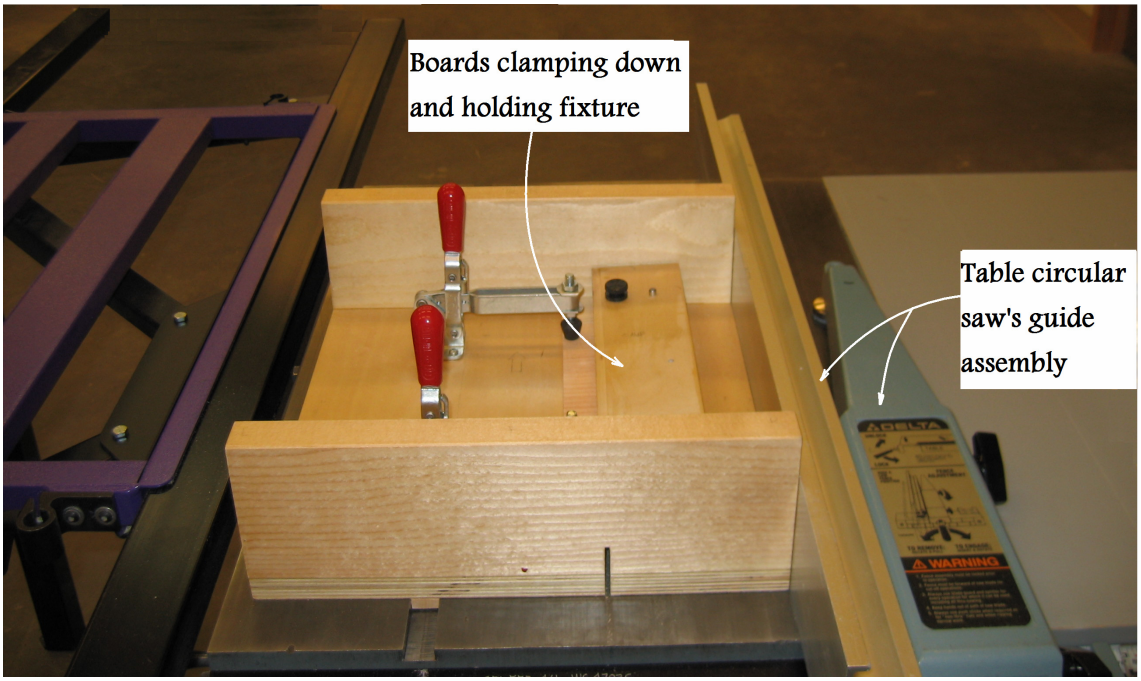

Figure 4.3 A fixture designed to prepare radial strips with a cross section of 3mm by 5mm

strips were numbered from 1 to 20 starting from the top. Strips numbered as 1 were used for inspection and control for occurrence of abnormal wood. These strips having a uniform longitudinal height of 3mm and width of 5mm were transversally inspected under a light microscope to assure absence of significantly detectable abnormal Douglas-fir wood.

The next two strips (number 2 and 3) that were used to measure density using x-ray diffraction densitometry were cut on a special bench mini-circular saw. The strips numbered from 4 to 20 were prepared by accurately ripping the remaining pith-board to a uniform longitudinal height of 3mm using the ripping fixture shown in Figure 4.3 and table circular saw. Every second radial strip that was cut on the bench mini-circular saw and every fourth strip that was cut on the table circular saw were passively extracted at ambient temperature (20 ± 1^0C) with a 9:1 ratio of acetone to water for 72 hours. Upon completion of the extraction, the acetone was drained off and the specimens were placed in a fume hood to allow the remnant acetone to evaporate. Following the extraction, both the extracted (strips numbered one and four) and un-extracted (strips numbered two and five) were dried at 50^oC in a vacuum-oven for 24 hrs. The densitometry samples were then left to equilibrate at a relative humidity of 63±1% and temperature of 20 ± 1^0C for ten days in a conditioning chamber (Parameter Generation and Control, Inc.) to attain an average moisture content of 8% before their density profile was measured. Strips that were numbered as 4 of each disk are then kept in a desiccator cabinet over anhydrous calcium sulphate until they were used for water sorption measurements.

Douglas-fir specimens for specific internal surface area measurements were prepared from earlywood and latewood of the radial strips by first splitting the annual rings into earlywood and latewood based on the density profile and then by manually slicing them into 0.2mm thickness using a sharp razor blade. The annual rings were sampled from alternative positions that started at the beginning of mature heartwood and sapwood based on a sampling design given in Table 4.2. A total of ninety (90) specimens with a replication of 10 were taken from each of the three sampling locations of the disks. The sampling plan given in Table 4.2 is also valid for specimens of annual ring, earlywood and latewood sampled for water vapour sorption measurements. The specimens were finally dried in a vacuum-oven at 50^0C for 24

hours and placed in a desiccator until the internal surface area measurements of un-extracted earlywood and latewood were carried-out.

Table 4.2 Transversal sampling plan of annual rings from heartwood and sapwood for sorption measurements inclusive of internal specific surface area

Disk Number	Number of rings in juvenile (JW), mature (MW) and mature sapwood (SW)				Ring numbers sampled for testing
	Total	JW	MW	SW	
1	67	15	38	14	16,18,20,54,56,58
2	69	15	35	19	16,18,20,50,52,54
3	63	15	29	19	16,18,20,44,46,48

4.4 Sampling and specimen preparation to determine Douglas-fir's gross wood sorption properties and chemical composition of its earlywood and latewood

Two strips of the third radial boards and bottom halves of the second radial boards shown in Figure 4.2 were used to prepare specimens for the measurement of gross wood diffusion coefficients and water vapour sorption isotherms after they were planed to a uniform thickness of 5mm using CNC-router (Precix, model: 3200). The three alternating annual rings for which sorption measurements were carried-out using the DVS apparatus and the other two annual rings located between them were included in the gross wood specimen. The specimens were composed of at least five annual rings. It was impossible to obtain sapwood sample widths that could be comparable to their corresponding matches in the heartwood due to narrow widths of the annual rings in the sapwood. Therefore, all of the sapwood annual rings were included as macro-sorption specimen. The sampling plan was similar to the one given in Table 4.1 in terms of location of transversal specimens in the radial boards and its detail is given in Table 4.3. The pictorial illustration of how the samples are cut is shown in Figure 4.1 and 4.4.

The two strips of the first radial boards and top halves of the second radial boards that were on both sides of the pith board of Figure 4.2 were used to prepare specimens for the analysis of chemical composition. Earlywood and latewood of the annual rings for which a matched

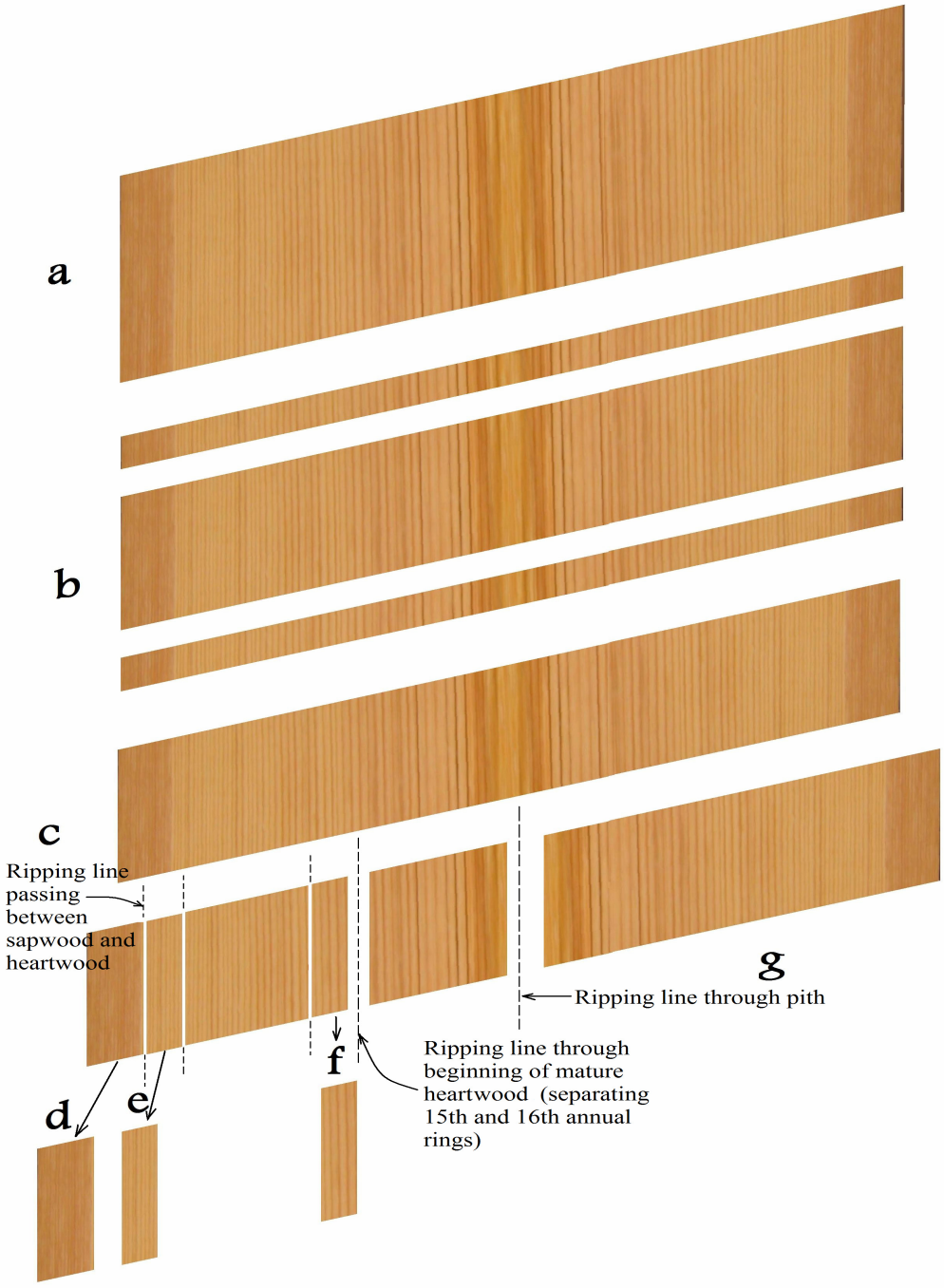

Figure 4.4 Procedure of Douglas-fir's gross wood sorption specimen preparation: a-radial boards, b-how radial boards are end trimmed, c-end trimmed radial board, d-sapwood gross wood sorption specimen, e-heartwood gross wood specimen sampled at the end of heartwood, f-heartwood specimen sampled from the beginning of mature heartwood

Table 4.3 Annual rings included in specimens for Douglas-fir's gross wood sorption measurements of heartwood and sapwood

Disk	Ring numbers sampled		
	Beginning of HW	End of HW	SW
1	16,17,18,19,20	49,50,51,52,53	54,55,56,…,65,66,67
2	16,17,18,19,20	45,46,47,48,49	50,51,52,…,67,68,69
3	16,17,18,19,20	39,40,41,42,43	44,45,46,…,61,62,63

sorption measurement was done as listed in Table 4.1 were manually separated into 18 all-earlywood and 18 all-latewood samples using a sharp razor blade, a pair of callipers, magnifying glass and densitometry profiles. The samples were coded, separately packed and reduced to match stick like splinters so that they could easily be fed into a Wiley mill. The splinters were pre-dried in a vacuum-oven at 50^{o}C for 24 hours to prevent the Wiley mill meshes from being clogged. Thereafter the splinters were ground and passed first through number 20 and then number 40 meshes.

The smallest weight for the milled earlywood of sapwood was 1.2216g and the average for all earlywood sapwood was 3.0893g. Therefore, for those earlywood and latewood samples which had a milled wood weight greater than three, a 3g milled wood was taken after a thorough mixing prior to sampling. The 3g sample was weighed, and the exact weight was recorded to four decimal places and thereafter placed in a coded capped 50mL corning tubes. The milled earlywood and latewood wood with a weight of less than 3g was recorded to four decimal places and similarly placed in coded and capped corning tubes. In each corning tube a 15mL of reagent grade acetone (RG ACS) was added for every gram of milled wood. The milled earlywood and latewood were then extracted passively for 72 hours. After the first 72 hours of extraction the acetone was drained and another equal amount of acetone was added for a second time. The procedure was repeated for a total of six times. At the end of the sixth step, the acetone was completely drained. The retained acetone residue was allowed to evaporate in a fume hood and the samples were finally dried at 101±1^{0}C.

4.5 Density profile measurement

The density profile of annual rings, earlywood and latewood was measured using an x-ray densitometer. The six extracted and un-extracted samples used for obtaining density profiles were allowed to equilibrate at a relative humidity of 63±1% and temperature of 20±1^{0}C for ten days to attain an average moisture content of 8%. Thereafter, they were mounted on a Quintek Measurement Systems (QMS-QTRS-01X) tree ring analyzer and the density profile was taken at 0.04mm increments. The tree ring analyzer measures density of a thin strip of material on the basis of mass attenuation coefficient (μ-probability of attenuation) of x-ray irradiation and detects the amount of light that is transmitted through the sample. It is a computerized measurement system in which few manually entered inputs are required regarding the thickness of the material, target density and threshold density of latewood. The target density (0.496 gm cm^{-3} based on Wood-handbook FPL-GTR-113 (1999)), latewood threshold density (0.540 gm cm^{-3}), thicknesses of the strips and the average *x*-ray coefficient of attenuation (2.90532) were variables that were manually entered to obtain the density profile from the measurements taken at each 0.04mm interval. The measurements were automatically translated into density and width of annual rings, earlywood and latewood.

4.6 Sorption kinetics and isotherm measurements for Douglas-fir

The water sorption measurements on earlywood, latewood and annual rings of Douglas-fir were done in the DVS apparatus. The picture and the schematic diagrams of the most important functional units of the DVS 1000 measurement system (SMS NA - Surface Measurement Systems, North America) is given in Figures 4.5 and 4.6, respectively. It has an accuracy of RH ±1%, T±0.1^{0}C and the microbalance is sensitive to 1ppm for a maximum weight capacity of 1.5g. The humidity generation is controlled by mixing of dry and saturated vapour gas flows using mass flow controllers and a look up RH (relative humidity) table that is part of the DVS application software. Humidity and temperature probes are separately used for the sample and reference areas. The apparatus performs a fully automated non-disturbed operation under control from a dedicated PC microcomputer that is interfaced to the balance control unit via RS-232 serial link.

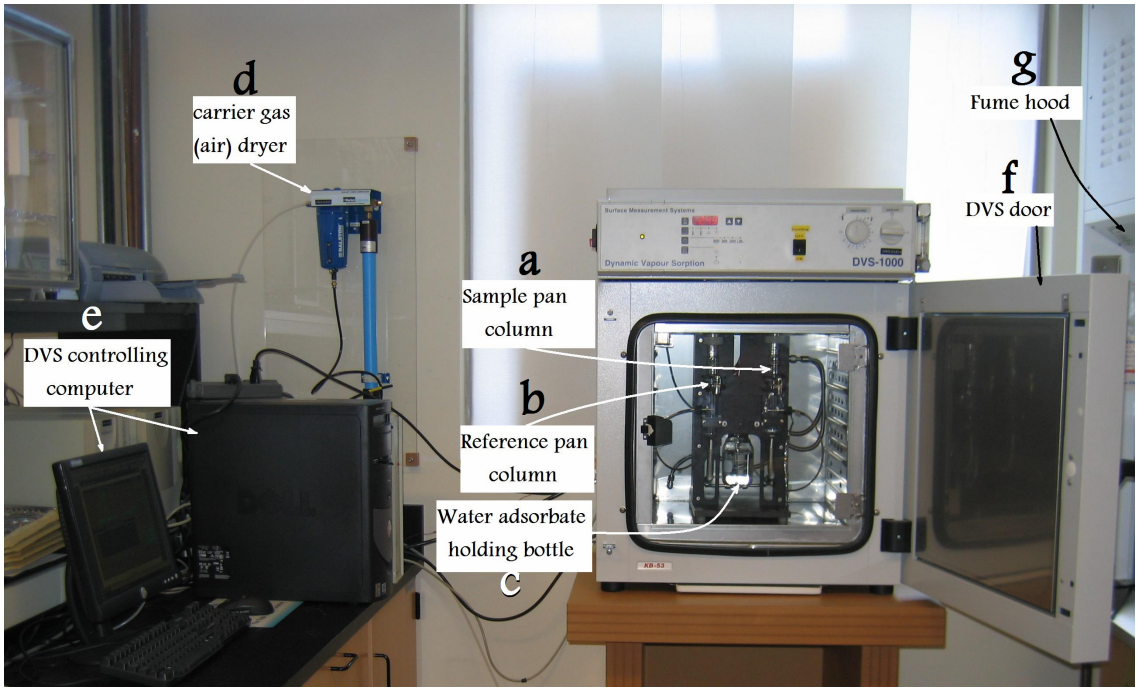

Figure 4.5 The DVS-1000 (SMS NA): a-sample pan with glassware housing, b-reference pan with glassware housing, c-adsorbate (water) bottle, d-compressed air drier, e-DVS- and the ultra microbalance controlling computer

The DVS takes gravimetric measurements. The time required per measurement is affected by the sample weight. Consequently, the optimum sample weight had to be determined before growth rings are separated and changed into final test specimens. The optimum weight was determined based on trial runs made on samples having weights in the range of 0.5 to 20mg. Based on equilibrium attainment criterion of 0.01% which is coupled with ten minutes of weight stability window (time length) for mass gain or loss in adsorption and desorption, respectively, less than 40 hours were required to complete a ten step, 0 to 95% relative humidity full cycle sorption measurement at 25^0C. By taking into consideration the minimum sample weight that can be reliably accommodated by DVS (which is 0.4mg) and the minimum number of runs required to get a statistically testable number of replications, the sample weight was chosen to be 3mg. As it was shown in the experimental design of Table 4.1, it required 29 months to complete 216 sorption runs as a result of slow sorption that was particularly encountered at 50^0C. This did not allow the possibility of multiple temperature treatments as additional higher temperature meant another very slow sorption process.

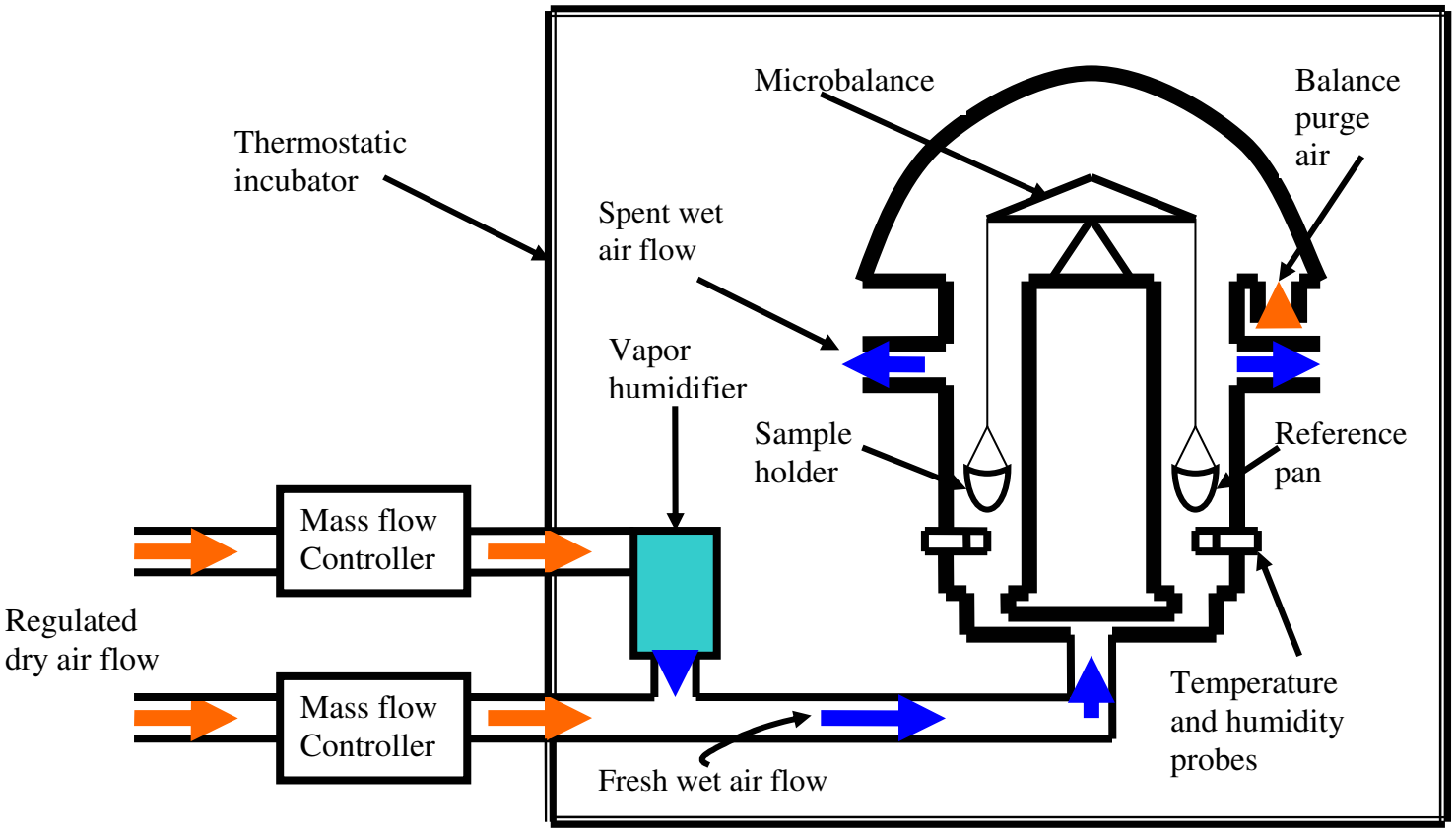

Figure 4.6 Schematic diagram of the dynamic vapour sorption (DVS-1000). The humidity (wet air flow) is generated by the humidifier using dry air coming through mass controller. The wet air flow is mixed with dry air coming through mass controller 2 to get a relative humidity within ±1%. The wet air having the required relative humidity is then passed through the sample and also the reference side symmetrically and exhausted through spent air outlet. The weight is measured by the ultra microbalance and can be recorded and saved every second. The whole unit is thermostated with accuracy of ±0.1^{0}C. Temperature and relative humidity are detected and registered by rotronic hygromer probes.

Three alternative heartwood and sapwood annual rings as given in Table 4.3 were manually separated and placed in a coded vial. The specimen preparation along with breakdown procedure is given in Figure 4.1. After the annual rings were manually separated with a sharp razor blade, they were weighed and the thickness that corresponds to a 3mg annual ring was proportionately calculated. The left side of the annual ring having a 2mm thickness was removed first to avoid any contamination, and then four 3mg weight slices that had a uniform average thickness of 0.2mm in radial direction were produced using a sharp razor blade, magnifying glass (10x), a pair of callipers and a densitometry profile. The four specimens were grouped into two pairs matched for DVS run at 25^0C and 50^0C. One from each pair is again separated into earlywood and latewood and kept in two separate and coded vials. Edges were not sealed due to possible significant contamination effect of sealants or edge coatings at small weights. The specimens were then stored in a desiccator cabinet over anhydrous calcium sulphate protected from UV rays until they were used for sorption measurement.

The sorption run started after the DVS measurement accuracy was assured to be within the range of T±0.1^{0}C, RH±1%, and drift of the microbalance below 0.01µm/min. The accuracy of relative humidity generation was tested and assured every month using a multiple point salt validation test with lithium chloride, potassium acetate, magnesium chloride, sodium bromide, sodium chloride, sodium nitrate and potassium sulphate (ACS AG). The DVS sorption measurement method was a full cycle adsorption/desorption run with relative humidity steps of 0, 20, 40, 60, 70, 75, 80, 85, 90, 95, 90, 85, 80, 75, 70, 60, 40, 20 and 0%. The change in weight was recorded and saved every twenty seconds. This method was set in such a way to closely trace and study the kinetics and equilibrium points that are complicated and difficult to predict.

The equilibrium criterion for the 25 and 50^0C was different for lower and higher relative humidity levels due to the very slow sorption that occurred at 50^0C. The sorption runs done at 25^0C were accomplished based on the criterion of the maximum rate of change in mass which was 0.001mg per minute for the entire range of 0 to 95% relative humidity. It was not possible to satisfy this criterion for sorption runs at 50^0C at higher relative humidity range

(greater than 75%) due to chaotic, very slow and linearly increasing and unbound kinetics. Therefore, it was necessary to set differing criteria for lower and higher relative humidity. The 0.001mg/min criterion was maintained for relative humidity steps from 0 to 75% while sorption runs at 80, 85, 90 and 95% were stepped up or down based on constant conditioning time of two hundred and forty (240) minutes which satisfied well the general criterion of ASTM (D 4933 2000) for attainment of equilibrium based on the number of weight change reversals. If in a sorption run far from the initial time, the change in weight crossed from gain (+) to loss (-) and vice versa three times then according to ASTM (D 4933 2000) it can be assumed as if the run has entered an equilibrium state. The DVS sorption run methods were the same for both extracted and un-extracted annual rings, earlywood and latewood.

The weight gains were recorded gravimetrically and moisture potential was calculated using the relations given in equations (4.1) and equilibrium moisture content using the relation given in equation (4.2).

$$E_i = \frac{w_i - w_0}{w_\infty - w_0} \tag{4.1}$$

$$M_{emc} = \frac{w_\infty - w_0}{w_0} \cdot 100 \quad [\%] \tag{4.2}$$

where w_0 is oven dry weight in grams or weight recorded as the average of measurements taken during the last minutes of sorption run at 0% (drying) relative humidity, w_i is the weight recorded in grams at the i^{th} minutes and w_∞ is the average of three weights recorded in grams during the last three minutes of sorption run at each relative humidity step. A total of 216 measurements consisting of 108 measurements of sorption at each temperature were accomplished. At each temperature, 36 specimens of annual rings, earlywood and latewood that included 12 samples of each of the wood type from every of the three disks were used for the sorption measurements.

4.7 Sorption measurement on gross wood (cluster of annual rings) of Douglas-fir

The ninety (90) specimens from each of the three disks that were prepared for the measurement of gross wood sorption properties of Douglas-fir were sorted into three groups: those taken at the beginning of mature heartwood, at the end of mature heartwood and all-sapwood. In each group there were thirty (30) specimens in total. No edge sealing was done so as to match conditions used for the DVS measurement of sorption. The thirty specimens are again randomly grouped into two for sorption runs at 25^0C and 50^0C. The specimens were first air dried in a fume-hood for ten days. After the tenth day, dimensions of the specimens were measured and recorded using the template shown on Figure 4.7, namely, thicknesses at six,

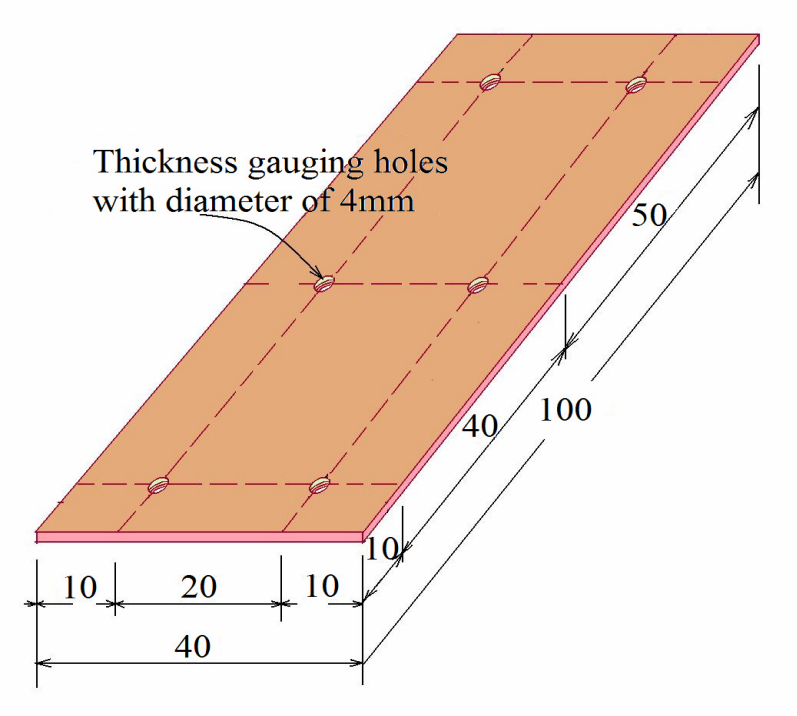

Figure 4.7 Template made to gauge thicknesses at six places shown by circular holes, width at three places and length at two places.

Table 4.4 Relative humidity stepping schedule for Douglas-fir's gross wood sorption measurement using the PGC (Parameter Generation and Control, Inc.) conditioning cabinet

25^0C air temperature		50^0C air temperature	
Relative humidity [%]	Water temp [^{0}C]	Relative humidity [%]	Water temp [^{0}C]
40	7.5	30	25
55	13	50	34
70	18	65	40
80	21	80	45
90	23	90	47
95	24	95	48.5

widths at three and lengths at two positions. The specimens were then dried at 101 ± 1^0C for twenty four hours. After 24 hours of drying, the specimens were taken out from the oven and immediately placed into a desiccator for cooling. Thereafter, they were weighed to the fourth decimal place and immediately placed into two PGC conditioning cabinets (Parameter Generation and Control, Inc.) that were set at temperatures of 25 and 50^0C. The conditioning cabinets could maintain air temperature within a tolerance of 0.2^0C and relative humidity in the range of ±0.5%. An air and water temperature controlling schedule that is shown in Table 4.4 was set so that the relative humidity can be stepped up or down based on desired levels.

The sorption measurements were performed first in adsorption by stepping up the water temperature at the end of each conditioning level after equilibrium was reached based on ASTM D 4933-2000. When equilibrium was confirmed, the samples were placed in a large Ziploc® bags and the water temperature was set up or down. The samples were left in the bags for two hours so that the cabinet was given enough time to reach T/RH equilibrium at the next step and immediately thereafter samples were removed from the bags and the next sorption step commenced. The sorption kinetics that is necessary to calculate the diffusion coefficient was obtained from the measurements taken at the 1^{st}, 2^{nd}, 4^{th}, 6^{th}, 8^{th}, 12^{th}, 16^{th}, 24^{th}, 36^{th}, 48^{th} and 72^{nd} hours from the moment the samples were removed from the plastic bags. The kinetic measurements were done only on samples taken from the beginning of mature heartwood and sapwood of Douglas-fir. The specimens that were taken from the end

of heartwood were used as a control for the effect of disturbance during kinetic measurement on final equilibrium moisture content and allowed to stay in the conditioning cabinet until equilibrium was achieved. The equilibrium moisture content computed based on equation (4.2) was then fitted to the Hailwood and Horrobin (1946) model given by the relation in equation (2.2). The coefficient of diffusion in tangential direction was calculated using the following relations and equation (4.1):

$$\boldsymbol{D = \frac{\overline{E}^2 \cdot L^2}{5.10 \cdot t}} \quad [\boldsymbol{m^2 s^{-1}}] \tag{4.3}$$

where M_{emc} is equilibrium moisture content in percent, w_0 is initial weight in grams, w_∞ is weight at equilibrium in grams, D coefficient of diffusion in m^2s^{-1}, L is the half thickness in meters, t is the half sorption time in seconds and $\bar{E}$ is the dimensionless moisture potential. The moisture content that corresponds to the diffusion coefficient was determined using equation (4.4) that was given by Siau (1995) for wood:

$$\overline{\boldsymbol{M}} = \boldsymbol{M}_1 + \frac{2}{3} \cdot (\boldsymbol{M}_2 - \boldsymbol{M}_1) \tag{4.4}$$

where $\overline{M}$ [%] is the average moisture content, M_1 [%] is the initial moisture content and M_2 [%] is the final moisture content. The tangential diffusion coefficient is then decomposed into the internal diffusion and surface emission coefficient based on equation (2.10).

4.8 Specific internal surface area measurement

The internal specific surface area measurement was carried out using AUTOSORB-1 MK3.0 (Quantachrome Instruments) specialized apparatus shown in Figure 4.8. Before sample measurements were initiated, its manifold volume was calibrated using its glass calibration tube fitted with a spring, a 12mm O-ring and a ferrule set by applying three sorption cycles and the calibration values were automatically saved. The internal surface area of un-extracted earlywood and latewood of Douglas-fir was measured with samples weighing 0.1g and

having a thickness of 0.2mm, length of 3mm and width of 5mm. The same sets of specimen were passively extracted with 9:1 ratio of acetone to water for 72 hours. Afterwards, the acetone was drained and the specimens were splashed with a 9:1 mixture of water to acetone. The residual acetone was allowed to evaporate by leaving the samples in an open vial inside a fume-hood overnight. The specimens were then dried in a vacuum oven at 50^0C for 24 hours after which they were placed in a desiccator over anhydrous calcium sulphate until the

Figure 4.8 Autosorb-1 sorption equipment used to measure internal surface area of earlywood and latewood of Douglas-fir: a-shows the sample set used to measure internal surface area, b-is cold trap that protects the sample from contaminating the system while being evacuated, c-is cold bath that keeps the adsorbate (Krypton) at its boiling point, d-samples in the process of outgassing, e-mantles in a canvas for heating the samples during outgassing

internal surface area measurement was done. Due to the low surface area of wood, liquid pressurized Krypton having a boiling temperature of 77.35^0K, a molecular cross sectional area 20.5 Å mol^{-1} and an effective diameter of 3.54Å was used as probe molecule. The equipment has a single sorption properties measurement and two outgassing ports. Sample cells having a diameter of 9mm with a bulge were washed; oven-dried over night and weighed on a digital balance with an accuracy of ±0.0001g. The earlywood and latewood samples of Douglas-fir were then placed in the cells and the combined weight was measured; after this, the samples were outgassed.

The outgassing was done based on 5μ min^{-1} pressure rise limit and using heating mantles set at 50^0C. Outgassing criterion was achieved by latewood quicker as it had lower surface area. The earlywood specimens were allowed to continue in an outgassing state while the measurement of internal specific surface area of latewood was made to proceed without a space filling rod. The internal specific surface area of earlywood samples was measured immediately next to the latewood ones on the same day. For both earlywood and latewood, eleven point measurements spanning from 0.05 to 0.3 vapour pressure in 0.025 increments with zero tolerance, and helium gas backfilling was applied. The internal surface area measurement was done first and then the cell containing the sample was backfilled with helium. The cell was then removed and immediately weighed while the sample was in it to obtain the dried and outgassed weight of the sample that was used to calculate specific surface area.

The internal specific surface area was calculated with the help of customized software of the instrument. The computation was performed using measured values that were automatically recorded during the krypton adsorption and oven dry weight of the sample (manually entered). The instrument used the BET equation that is embedded in its algorithm is given as

$$\frac{1}{V \cdot \left[(p_0 / p) - 1\right]} = \frac{1}{V_m C} + a \cdot \frac{C - 1}{V_m \cdot C} \quad [g\ Mol^{-1}] \tag{4.5}$$

where V [mL] is volume of gas adsorbed at pressure P [kPa], V_m [mL] is volume of gas required to form monolayer (monolayer capacity), C is BET constant and a is vapour pressure. Equation (4.5) is analogous to the straight line slope and intercept of a typical straight line equation of the form *Y*=a*X*+b. In equation (4.5) the slope and intercept are then

$$\textit{slope} = \frac{C-1}{V_m \cdot C}\,[g\ Mol^{-1}] \tag{4.6}$$

$$\textit{intercept} = \frac{1}{V_m \cdot C}\,[g\ Mol^{-1}] \tag{4.7}$$

$$V_m = \frac{1}{s+i} \quad [Mol\ g^{-1}] \tag{4.8}$$

$$\textit{Total surface area of the adsorbate} = \frac{V_m \cdot N}{22414} \cdot A_{ad} \quad [m^2] \tag{4.9}$$

$$\textit{Internal specific surface area} = \frac{\textit{Total surface area of the adsorbate}}{\textit{oven-dry weight of sample}}\,[m^2 g^{-1}] \tag{4.10}$$

where *N* is the Avogadro's number [6.022 141 793 X 10^{23} Mol g^{-1}], *s* is slope, *i* is intercept and A_{ad} is effective molecular cross sectional area of the adsorbate [Å^2].

4.9 Chemical components quantification

Klason analysis was performed on three (3) replications for a total of 36 samples of extractive-free Douglas-fir earlywood and latewood. Lignin content was determined using a modified Klason lignin method (TAPPI method T222 om-98). One litre (1000mL) of 72% (w/w) sulphuric acid was prepared by volumetric mixture of 665mL of its concentrate (Fisher Scientific ACS RG) with 335mL of distilled water. The 72% sulphuric acid was cooled down and kept at 4^0C. Approximately 0.2g of extractive-free, oven-dried wood samples were

weighed into a digestion vessel and 3mL of cold 72% H_2SO_4 were added and allowed to react and hydrolyzed at ambient conditions of temperature 20 ± 1^0C.
The milled wood specimens and H_2SO_4 were agitated every 10 minutes with mixing glass rods for 2 hours. The hydrolysis was terminated by the dilution of the digested mixture with 112mL of de-ionized water to a final acid concentration of 4% H_2SO_4 and the mixture was then transferred into serum bottles. The serum bottles were sealed with septa caps and autoclaved at 121^0C for one (1) hour in a Steris Amsco Century (SG-120 Scientific Gravity) sterilizer for 60 minutes. Thereafter they were cooled and filtered using vacuum suction through pre-weighed, oven-dried medium coarseness sintered-glass crucibles. After re-filtering, the filtrate was put away for analysis while the solids retained in the crucibles were further washed with 100mL of cold de-ionized water and oven-dried at $102\pm3\,^{\circ}$C for 12 hours. The acid-insoluble lignin was gravimetrically determined from the oven-dried weight of crucibles.

The acid soluble lignin was determined based on TAPPI Useful Method UM-250. A 4% (w/w) sulphuric acid was prepared by 5.55mL of the 72% sulphuric acid stock with 94.44mL of di-ionized water and cooled down. A 100µL of the filtered Klason lignin hydrolysates from each replication were added into micro tubes and further diluted with 900µL of the 4% H_2SO_4. The spectrophotometer (Milton Roy Spectronic 1001 Plus) was initially calibrated using the 4% sulphuric acid as a standard. After the solutions were thoroughly mixed with the help of shaker (vortex) and absorbance readings were assured to be within the range of 0.2 to 0.7 absorbance units (AU cm^{-1}) at 205 nm. Each of the diluted hydrolysates were injected into clean quartz cuvettes and placed in the spectrophotometer and absorbance readings were taken. The acid soluble lignin was calculated using the Beer's relation that reads as follow.

$$\textit{Acid soluble lignin} = \frac{B \cdot V}{1000 \cdot w_0} \cdot 100 \quad [\%] \tag{4.11}$$

$$B = \frac{Absorbance \cdot volume\ of\ diluted\ \ filtrate}{110 \cdot volume\ of\ \ original\ \ filtrate}\ [\,AU\ cm^{-1}\,] \tag{4.12}$$

where B is absorbance, V is total volume of filtrate in mL, w_0 is oven-dry weight of wood in grams.

Douglas-fir's earlywood and latewood carbohydrates content analysis was performed with replication of three for a total of 36 samples using the hydrolysates obtained from the Klason lignin digestion. Carbohydrate content was quantified using a Dionex DX-500 (Sunnyvale, CA USA) high performance anion exchange chromatography (HPAE) system controlled by Chromeleon (Version 6-80 SP2 Build 2284) software. The column (PA1) was equilibrated with 250mM NaOH. The Klason lignin hydrolysate was first filtered through Chromospec 4mm 0.45µ nylon (0.45UM P100) HV syringe filters (Chromatographic Specialties Brockville, Ontario, Canada), and then fucose (5mg/mL) was added as an internal standard. After injecting 20µl of filtered hydrolysate using AS 50 Dionex auto-sampler, the sugars were eluted using nanopure water at a flow rate of 1.0mL/min.

The monosaccharides were monitored using a Dionex E50 electrochemical detector (gold electrode), with parameters set for pulsed amperometric detection of sugars, as recommended by the manufacturer. NaOH (200mM) was added post column to the eluent (mobile phase) before the detector at a flow stream rate of 0.5mL/min for optimum baseline stability and to obtain the most sensitive detection. Arabinose, galactose, glucose, xylose and mannose standard curves were used to convert the electrical signals generated at the surface of gold electrodes by oxidation of eluted sugars into their concentrations. The total carbohydrate content was determined by calculating the total sum of all the monosaccharides present.

5.0 RESULTS AND DISCUSSIONS

The models are validated in the same order as they were derived in chapter 3. Briefly, this chapter will be presented in the following order: the GRV model of annual rings and their coarse-graining, the TLS model of sorption kinetics, the TLS model of sorption isotherms, the TLS model of chemical composition, annual ring level ANNs sorption models, and lastly the ANNs annual ring sorption properties coarse-graining model.

5.1. Testing and validation of the two-level systems model of annual rings and coarse-graining

The TLS model of annual rings which is developed on the basis of GRV (golden ring volume) obtained from the GRC (golden ring cube) in section 3.1 was validated using densitometry data and its statistical-physical parameters that are to be used in the coarse-graining of annual rings were computed and analyzed.

If the sorption prediction models being developed are assumed to have wider application then the first puzzle to be solved always is how the developed models will generalize at large. The simpler test for wider applicability probably would be detecting variations of model parameters used to describe timber species that display differing properties or species that widely differ in heterogeneity. The earlywood and latewood of Douglas-fir can be separated with greater relative ease than those of softwood species which usually have a prevailing narrow latewood spanning pith to bark. The width and density of earlywood and latewood may randomly fluctuate between two extremes and the fluctuations may also be either monofractals or multifractal. If the fluctuations are monofractals then the scaling functions are governed by a single scaling dimension which in turn simplifies the governing scaling functions. On the other hand, if the fluctuations are multifractal then the scaling functions should be described by multiple dimensions and this requires investigation at multiple scales to obtain the whole picture of scaling mechanisms. In short, there is an absolute need to know whether the scaling dimensions vary with change of characteristic length. It is, therefore, necessary to test fractality of annual ring series of Douglas-fir and another softwood species which display pronounced imbalance between earlywood and latewood properties.

Ring series fractal behaviours of two other softwood species namely, western hemlock (*Tsuga heterophyla*) and white spruce (*Picea glauca*), with distinct earlywood and latewood boundaries were preliminarily assessed. *X*-ray diffraction densitometry data that were compiled on the basis of basic density which was collected by FORINTEK in the 1980's for the purpose of describing basic wood properties of spruce hemlock and Douglas-fir were used for the exploratory purpose (Jozsa *et al*., 1998). The *x*-ray diffraction densitometry is a

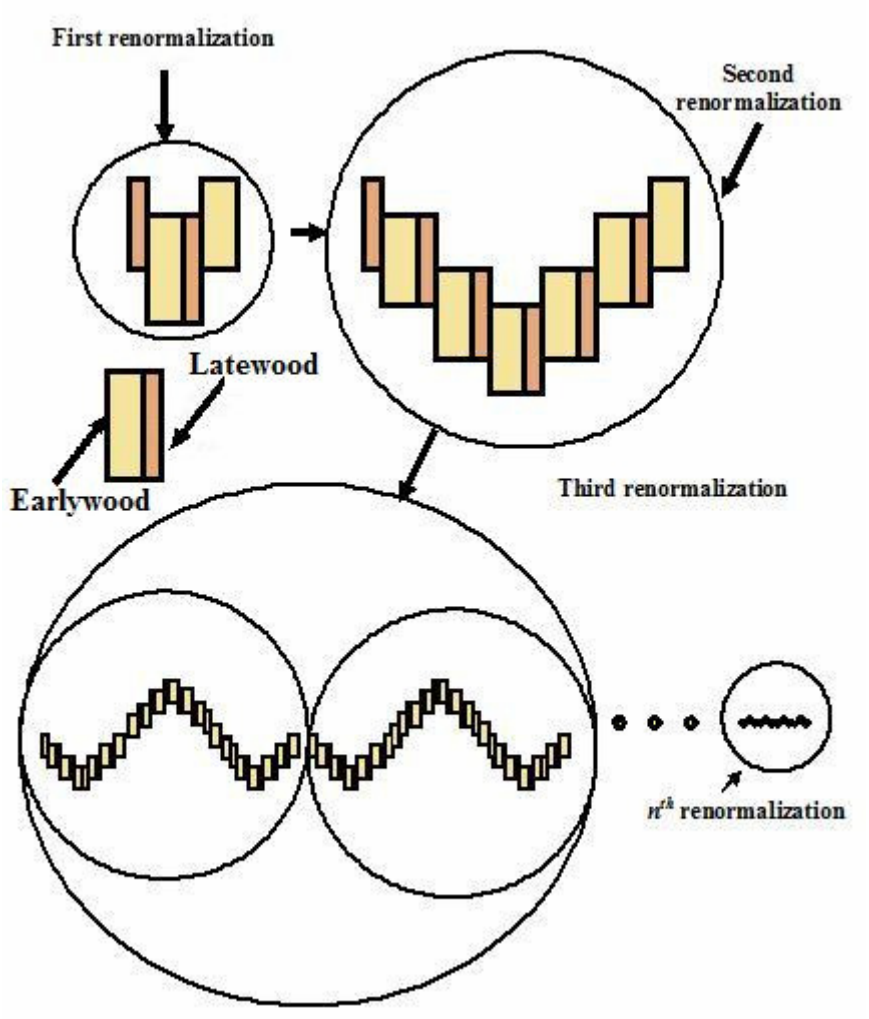

Figure 5.1 One-dimensional renormalization scheme based on the analogy of contraction of weakly interacting GRV with the lighter and wider rectangles representing earlywood while the darker and narrower are latewood

standard method and gives comparable results and it can safely be assumed that use of the published annual ring profiles will not introduce significant artefacts (Jozsa *et al,* 1987).

The multifractal behaviour was determined based on variability of the scaling exponent for the one dimensional renormalization of Douglas-fir, western hemlock and white spruce using the scheme given in Figure 5.1 and equations (3.6), (3.19) and (3.20). The one dimensional renormalization revealed that western hemlock displayed ring series scaling properties close to Douglas-fir, while white spruce was deviating. Douglas-fir and western hemlock exhibited mono-fractality with a dimension of 2.32 while white spruce displayed multifractality in which 2.32 occurred as one of the many possible dimensions. Hence, it was found that it is necessary to use spruce as a species of comparison and as a representative of the other relatively more heterogeneous end.

Any trajectory or series of annual rings can assume one of the infinite possible configurations. Figure 5.2 shows a general schematic representation of the GRV in relation to one instance of such growth trajectory and the spatial aspect of the subsequent coarse-graining. Equation (3.7) implies that the earlywood and latewood configuration in a GRV in terms of wood substance content, or the work done in wood creation in one growth year, is invariant for given equilibrium or quasi-equilibrium conditions of the inactive and active state which are alternatively earlywood and latewood. The parameter β was obtained by fitting equations (3.9) with densitometry data of Douglas-fir and white spruce. The

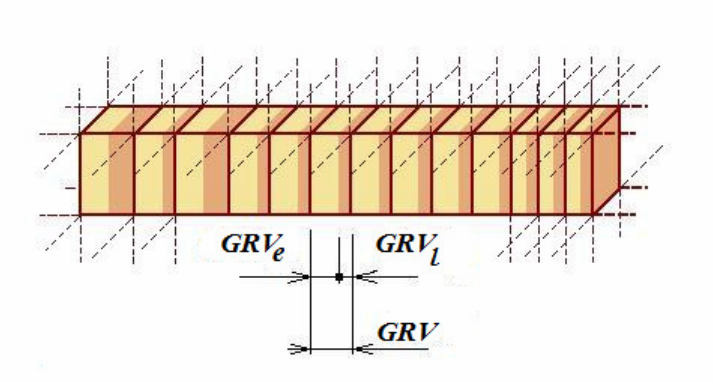

Figure 5.2 Schematic representation of the GRV in relation to growth trajectory or one instance of coarse-grained level complementing Figure 3.3

Table 5.1 Magnitudes of the parameter β for TLS (annual ring), earlywood and latewood of Douglas-fir based on description of the golden ring volume (GRV) and golden ring cube (GRC) and their comparison with that of white spruce

Level of self-organization	Unit	Douglas-fir		White spruce	
		β	r^2	β	r^2
GRV	TLS	16.1	0.9854	32.2	0.9954
	Earlywood	32.6	0.9756	42.6	0.9940
	Latewood	26.2	0.9903	119	0.9850
GRC	TLS	3.9	0.9862	6.5	0.9965
	Earlywood	7.8	0.9649	8.0	0.9935
	Latewood	6.3	0.9853	31.7	0.9781

Table 5.2 Dispersion of the magnitudes of width and density of earlywood and latewood of Douglas-fir around mean values (SEM is an abbreviation for standard error of the mean)

Property	Unit	Douglas-fir			White spruce		
		Value [mm]* [g cm^{-3}]**	Deviation		Value [mm] * [g cm^{-3}]**	Deviation	
			SEM	Percentage		SEM	Percentage
Width	Earlywood	3.1	±1.7	±54.8	1.4	±0.7	±50.3
	Latewood	2.0	±0.8	±38.5	0.4	±0.1	±40.6
Density	Earlywood	0.33	±0.04	±11.4	0.30	±0.03	±10.1
	Latewood	0.81	±0.06	±7.5	0.53	±0.06	±11.9

magnitudes of β for the GRV and GRC of TLS (GRV of annual ring), GRV of earlywood and latewood of Douglas-fir are given in Table 5.1 and they confirm the two-level system behaviour of the GRV as described in section 3.1.

Variability of the parameter β is noticeable from Table 5.1 and the numerical facts in Table 5.2 indicate the reason for doing so may not be a difference in the dispersion of the

* Unit of quantity for width
** Unit of quantity for density

magnitude of widths and densities, and neither do the differences in their absolute magnitudes explain the observed variability. Magnitude of the parameter β is hence species dependent. However, β scales with time invariantly and with a power of about negative one (~-1) according to equation (3.15). The scaling function was obtained based on the dependence of parameter β on the number of annual rings that are allowed to interact together based on the simple allometric form given in equation (5.1). The variable n represents the number of interacting annual rings which indirectly means the period of growth years and its reciprocal β_n is the frequency f that can assist to draw an analogy to self-organizing criticality.

$$\boldsymbol{\beta_n = \beta_1 \cdot n^{-1}} \tag{5.1}$$

Table 5.3 contains the magnitude of the interaction parameter for 0.5 (half) annual ring which is obtained through extrapolation based on equation (5.1). The half annual ring growth parameter exists if and only if the GRV is homogeneous, namely, when there is no distinction between earlywood and latewood. In the majority of softwood species, there is always a noticeable difference between earlywood and latewood, hence what is

Table 5.3 Magnitudes of the interaction parameter β based on number of annual rings obtained using derived equation (5.1) for Douglas-fir and white spruce

Number of annual rings	Interaction parameter β	
	Douglas-fir	White spruce
0.5	34.2	64.5
1	16.1	32.2
2	7.4	15.9
4	3.6	8.2
8	1.8	3.8

predicted by equation (5.1) may not agree with the value of β obtained using equations (3.12) and (3.13). The magnitude of this disagreement establishes conditions for the heterogeneity test criterion (HTC). Assuming that either earlywood or latewood could cause the maximum heterogeneity, the HTC criterion might be given by equation (5.2). HTC_{mm} is the minimum

or maximum heterogeneity index. The function $f^{1}(\beta_{e,l})$ is the inverse value of n obtained for earlywood (e) and latewood (l) using the parameter β. The parameter β is calculated based on equations (3.12) and (3.13) and the scaling equation (5.1). Equation (5.2) provides the equivalence of half GRV for earlywood and latewood while equation (5.3) calculates how far the GRV of earlywood and latewood deviate from the half TLS or ring GRV. Positive HTC indices mean that the half GRV calculated either for earlywood or latewood is greater than that of the half GRV predicted by the TLS allometric scaling, and negative values mean the converse. It is evident from Table 5.4 and Figure 5.3 that the heterogeneity of Douglas-fir is attributable more to its earlywood content and is generally less heterogeneous than spruce which is the comparative species.

$$\boldsymbol{HTC} = \left[\left[2 \cdot \boldsymbol{f}^{-1}(\boldsymbol{\beta}_{e,l})\right] - 1\right] \tag{5.2}$$

$$\boldsymbol{HTC}_{mm} = 2 \cdot \left[\left[\boldsymbol{f}^{-1}(\boldsymbol{\beta}_{e,l})\right]_{max} - \left[\boldsymbol{f}^{-1}(\boldsymbol{\beta}_{e,l})\right]_{min}\right] \tag{5.3}$$

Table 5.4 Indices of heterogeneity test criterion (HTC) for Douglas-fir and white spruce

Parameter	Douglas-fir		White spruce	
	Earlywood	Latewood	Earlywood	Latewood
β	26.2	32.4	68.4	119
n for half of a GRV	0.6	0.5	0.6	0.4
HTC	0.3	0.1	0.2	-0.3
HTC_{mm}	0.2		0.5	

The GRV could also be used to characterize the extent of chaos or complexity in annual ring trajectories. This requires using the properties of GRV shown in Table 5.4 and Figure 5.3 as a proxy for Lyapunov exponent to measure the divergence of ring trajectories that is caused by small difference in magnitudes of the GRV. The phenomenon can be discussed by comparing β values obtained based on the half GRV predictions of equation (5.1) and the corresponding earlywood and latewood GRV predictions in Tables 5.3 and 5.4. The β values of earlywood and latewood for Douglas-fir remain close to the β value obtained for the half GRV. However, white spruce differs from Douglas-fir in two aspects. For close values of

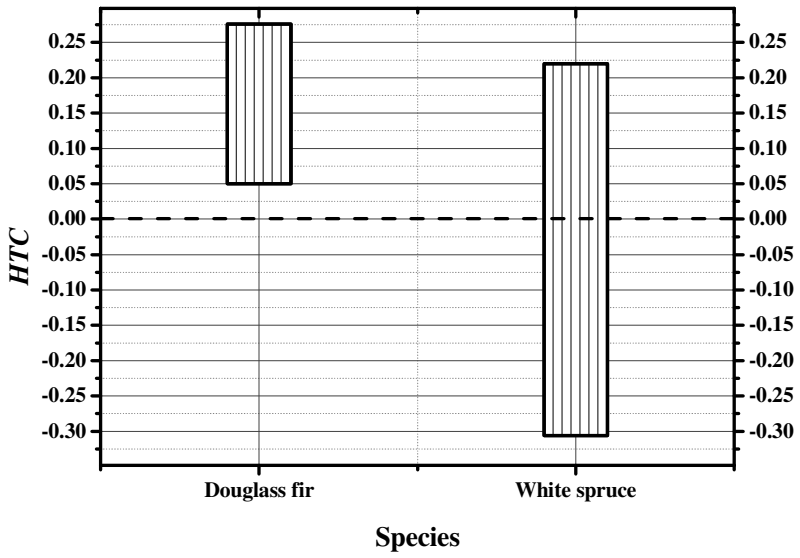

Figure 5.3 Magnitudes of HTC indices for earlywood and latewood of Douglas-fir and white spruce and the distance from zero heterogeneity or homogeneity

earlywood GRV (0.64 and 0.61 for Douglas-fir and white spruce, respectively) the corresponding β values differed by more than a factor of two and the situation is stronger in case of latewood. The β value differences for earlywood and latewood GRV of white spruce is more pronounced. The same explanation is evident when comparing the absolute magnitudes of HTC for earlywood and latewood of both species. Since β gives the magnitude of the long range effect of initial conditions (magnitude of GRV) the instability in it could mean the instability in the trajectory of given series of annual rings and hence can be utilized to detect the extent of chaos or complexity though the divergence is subtle as it obeys power laws rather than the usual exponential.

In addition to being a quantitative heterogeneity indicator, the HTC will serve in configuring the earlywood and latewood components once the GRV is determined thus, its use in the coarse-graining of annual rings is important. Evidently, investigating the behaviour of GRV across species may yield a classification framework for wood like the periodic table of chemical elements which would enable introduction of physical taxonomy as an emerging field in wood science.

The effective magnitude of wood substance, or work done due to growth in one year, can uniquely be obtained in the deterministic case if the magnitude of the width and weight of wood substance contained in earlywood and latewood is given. However, it has been described in section 3.1 that these magnitudes are chaotic and their occurrence is governed by mechanisms of self-organization. Given a GRV or GRC, the issue that shall be addressed to have a working coarse-graining model is the capability of reconstructing preceding annual rings and the ability to predict subsequent ones from infinite possibilities. Figures 5.4 and 5.5 show a discernible trend from left to right or pith to bark. Radial trends in the density profile of softwoods can be decreasing, increasing and a combination of both that usually approach a constant trend towards the bark (Zobel and Jett, 1995; Zobel, 1989; Panshin and De Zeeuw, 1980).

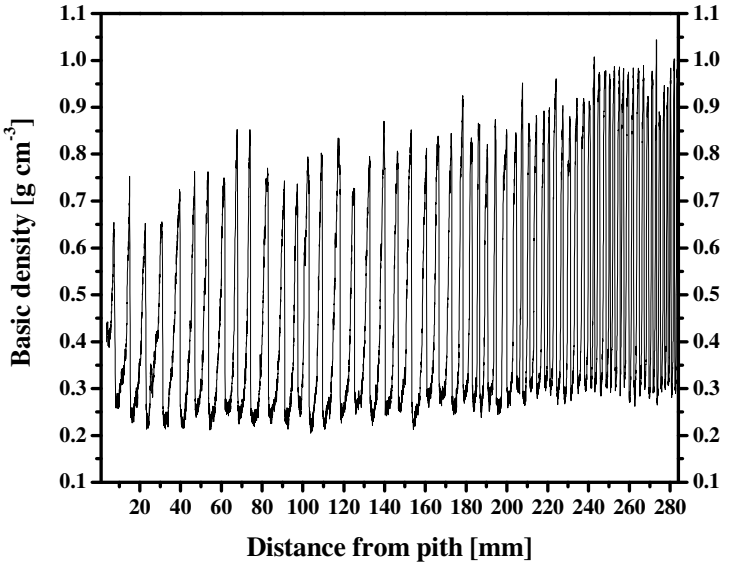

Figure 5.4 Breast height density profile of Douglas-fir showing basic density values measured at every 0.04 mm from pith to bark using x-ray diffraction technique

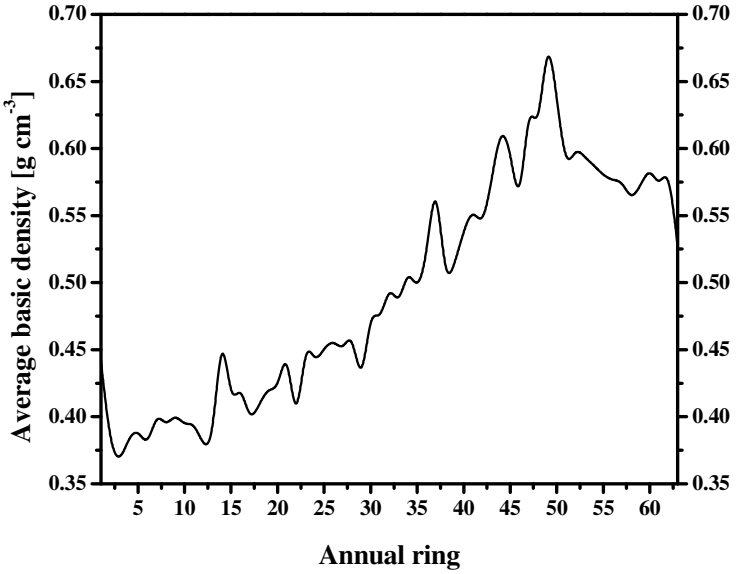

Figure 5.5 Breast height density profile of Douglas-fir from a single tree showing the magnitudes of average density from pith to bark

This trend is well known, but it is locally noisy as depicted by Figures 5.4 and 5.5. Equation (5.1) establishes the probable time length during which a threshold event decays and vanishes after its occurrence in the trajectory of consecutive annual rings. This in other words means that the magnitude of β provides the mean interaction length of annual rings. A number of threshold events take place within one growth trajectory which results in more than one characteristic interaction lengths β that cause complexity resulting in unpredictable threshold events both in terms of timing and magnitude. The good news in this complex mechanism is that the magnitude of threshold events follow power laws scaling behaviour when related to the number of times they occur in a given interaction length. The actual magnitude of β and the corresponding power laws scaling exponents are not constant and vary from trajectory to trajectory, but their variation, which is affected mainly by an increase or decrease in the magnitude of β, again follows power laws scaling. Therefore, the consequence of increased or decreased magnitude of β was analyzed by investigating the scaling behaviour associated with the number of threshold events and fluctuations based on equations (3.21) and (3.22). Equation (3.23) can be used to understand how the number of given threshold magnitudes (leaps or growth punctuations) scale when the value of β is varied above or below its

magnitude that was obtained based on equations (3.9) to (3.11). Similarly, equation (3.25) provides the scaling properties of fluctuations in consecutive series of annual rings depending on the magnitude of β. Values of the scaling parameters λ and α were calculated and the validity of equation (3.27) was tested for increasing and decreasing magnitudes of β. For values closer to the short range interaction length which is four, the magnitude of λ and α were having values close to -0.5, which is correct since it is approaching the random walk scaling exponent. And both have magnitudes close to -1 for values of the interaction length close to β_1 which proves the evidence of self organizing criticality. For very large value of β, the magnitudes of λ and α approached -1.5. The scaling behaviour of λ and α with respect to variation in β displayed invariance. However, λ showed a scaling exponent of one third ($1/3$) while α had an exponent close to a quarter ($1/4$). The variation of the magnitudes of λ and α in the range from -0.5 to -1.5 confirms the signature for self-organizing criticality. The same scaling behaviour was displayed for both Douglas-fir and white spruce implying species transcending property. The finding of ($1/3$) and ($1/4$) scaling exponents readily explains the thermodynamic origin of the observed behaviour in analogy with the second law of thermodynamics. When the scaling dimensions ($1/3$) and ($1/4$) are applied on equation (3.27) then the following relation was obtained:

$$\boldsymbol{F_i^q}\left[\boldsymbol{TLS}(\boldsymbol{\beta})\right] = \left[\boldsymbol{TLS}_{max}(\boldsymbol{\beta})\right]^{\frac{3}{4}} \tag{5.4}$$

In allometric scaling the left hand side of the equation usually represents basal metabolic rates such as heart beat while the right hand side stands for system size such as body mass (Brown and West, 2000). The second fluctuation moment is given as the magnitude of fluctuation per β number of annual rings and hence has a meaning of rate by itself. The immediate implication of equation (5.4) is that the fluctuation of the magnitude of contracted GRV_c is optimized based on the maximum threshold magnitudes and obeys the three quarter ($3/4$) allometric scaling. The scaling relation in equation (5.4) was equally valid for Douglas-fir and white spruce despite the wider difference in heterogeneity, a fact which can readily be used to justify the generalization of equation (5.4) at least to softwood species at large.

Demetrius, (2006) showed that the allometric scaling exponents generally may not be constant and deduced the scaling dimensions of green plants to vary in the range of ⅔ to 1, wider than that is assumed to be valid for animals. However the ¾ scaling obtained in this study for Douglas-fir is numerically equivalent to the largely reported magnitude even for animals. The remarkable aspect of equation (5.4) is that it relates the two fractal dimensions deterministically while they are established to describe a SOC mechanism existing in wood which is believed to be inherently unpredictable.

The scaling behaviour of the threshold magnitudes that is obtained based on equation (3.22) by using the densitometry data is shown in Figure 5.6 and the approximate scaling behaviour can be generalized as follows

$$\beta_n = -A \cdot \lambda^{-\frac{1}{3}} \tag{5.5}$$

Differentiating equation (5.5) based on λ and taking the logarithms of both sides yields

$$ln\left(\frac{d\beta}{d\lambda}\right) = -\frac{4}{3} ln\,\lambda + Constant \tag{5.6}$$

where the constant term is equivalent to the natural logarithm of the product of the parameter A and the scaling exponent (⅓). Equation (5.6) has a deep thermodynamic meaning in analogy to entropy of black body radiation. So, by assigning the left hand side of the derivative as the entropy of GRV avalanche or threshold events, the following general equation was obtained.

$$S(GRV) = -\frac{4}{3} \cdot ln\,\lambda + Constant \tag{5.7}$$

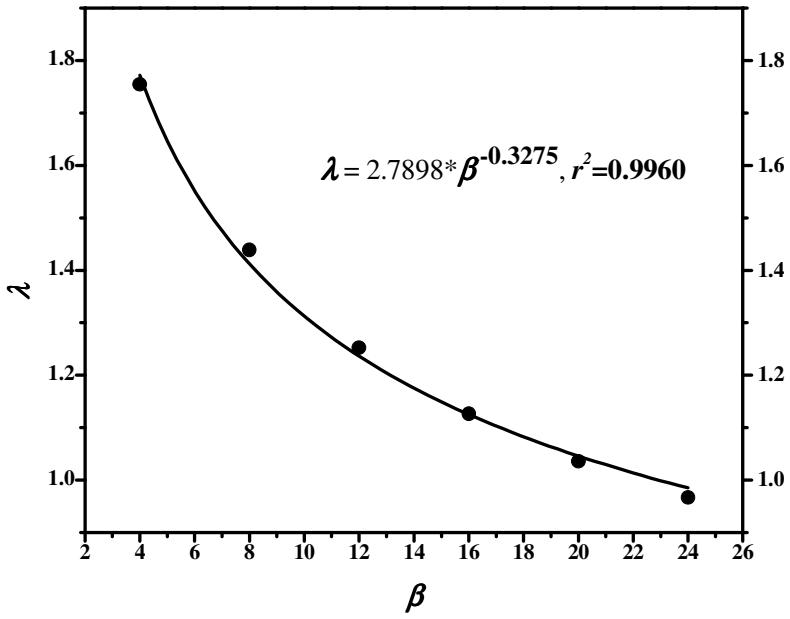

Figure 5.6 Scaling behaviour of the maximum amplitudes of avalanches that is obtained based on equation (3.22) using the densitometry data of Douglas-fir with the line representing the prediction of equation (5.5) and the filled dots indicating experimental points

where S represents entropy [J K^{-1}]. Equation (5.7) yields the entropy of growth rings or GRV TLS trajectory that linearly scales based on the constant term "Constant". It is apparent that equation (5.7) has a logical connection to the original equation for black body or cavity radiation as given in equation (5.8).

$$ln\,\lambda = \frac{u(\beta)}{\beta} \cdot V \tag{5.8}$$

where $u(\beta)$ is the analogous internal energy and V is the volume which in our case can readily be related to the GRV. Thus, the natural logarithm of λ is related to the interaction length (β). Entropy is additive and the entropy of ensemble of trajectories is therefore a result of the sum of the entropy of each trajectory as a consequence of which equation (5.7) generalizes for n number of weakly interacting series of annual rings as follow.

$$S(GRV_D) = -\frac{4}{3} \cdot (n-1) \cdot (\ln \lambda + constant) \tag{5.9}$$

where n is the number of trajectories. It is clear that equation (5.9) does not converge. However, the magnitude of n is always finite that can empirically be estimated. Equations (5.4) to (5.9) are all valid, both for Douglas-fir and white spruce. The entropy as a thermodynamic property provides for the invariance of equation (5.1) an energy dimension, which in other words, represents a conserved energy quantity. Equations (3.9) to (3.14) are therefore confirmed to be thermodynamic (energy) state representations for earlywood, latewood and annual rings.

Determination of the parameters for the dynamical partition function needs quantification of all possible values of β. Although it is possible to determine a spectrum of β values using equations (5.4) and (5.5) for a given species once the magnitude of β_1 is established based on equations (3.10) to (3.14), β varies from species to species depending on the magnitude of GRV. It is here that equations (5.4) and (5.5) as trajectories' memory of annual rings (history of GRV series) can be applied for thermodynamic utilization of the GRV at the softwood species level. They give integrated information for the dependence of the GRV on species, growth age factors, environmental interaction signals, growth punctuations caused by local endogenous and stand level exogenous disturbances and other random interactions.

It is shown that the coarse-graining for Douglas-fir turns less complicated if the number of interacting annual rings is restricted to sixteen (16), which is also justifiable based on equation (5.1) and Table 5.3. In this study, a macro-sorption measurement is performed on consecutive five annual rings in order to obtain coarse-scale sorption properties as described in section 4.4. This is a measurement done to match growth ring level sorption measurements performed based on section 4.6. Two issues were considered while coarse-graining. The first one is a reshuffled combination of properties of the three alternating growth rings that were taken from the five series of growth rings which were in compact radial sequence. In addition to the reshuffling in the five growth ring clusters, a ring series that is assumed to contain nine annual rings based on annual ring cluster combinations (five annual rings) are considered.

The second one is the generalization of the macro-sorption properties to any configuration of growth rings in wood regardless of the number of annual rings (in radial plane). It is only the former that has experimental validation data, whereas the latter one can only be cross inferred accordingly.

The oldest Douglas-fir trees of North America may be older than 800 years of age (Alden 1997). The oldest age of an individual Douglas-fir tree so far recorded is 1350 years on Vancouver Island. Old age or growth is defined from various aspects. One such definition gives old growth as the term defining old trees in forests of advanced age that is characterized by structural complexity and mix of species. The advanced age for Douglas-fir is in the range from 150 to 200 years. A second growth Douglas-fir ready for harvesting based on sustained yield forestry is about eighty years of age (Johnson and Swanson, 2009). One can, therefore, take a series of eighty annual rings for second growth or a series of two hundred annual rings for old growth to construct ring trajectories based on equations (3.10) to (3.18) and (5.1). The probability sampling generating function for earlywood and latewood composition can be obtained by using the GRV to GRC ratio based on equations (3.34) and

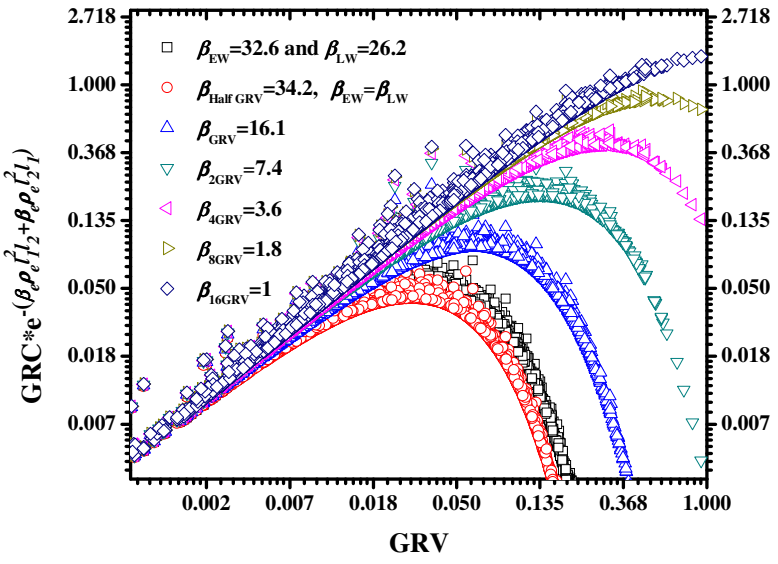

Figure 5.7 The scaling between the GRV and GRC of Douglas-fir showing good agreement with equation (3.35) when β was decreased from 32.6 to 1

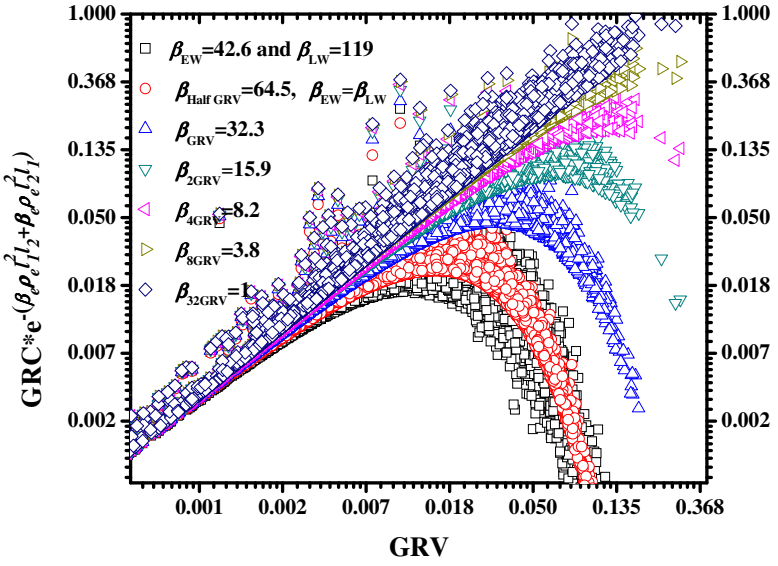

Figure 5.8 The scaling between the GRV and GRC of white spruce showing good agreement with equation (3.35) when β was decreased from 119 to 1

(3.35). While the occurrence of the ratio between the GRV and GRC is chaotic, Figure 5.7 and 5.8 show that the relation in equation (3.34) and (3.35) are valid both for Douglas-fir and white spruce which is good for predictability, although the physical meaning of the amplitude or normalization constant is not yet defined and its magnitude differed for the two species. Figures 5.7 and 5.8 further show that the relation given by equations 3.34 and 3.35 continuously change from lognormal (short-range) to power law (long-range) as the value of β continuously changes from the magnitude of interaction length (16 and 32 for Douglas-fir and white spruce, respectively) to unity. The spreading of HTC indices of white spruce on both sides of zero (negative and positive) and the positioning of the Douglas-fir HTC index only at the positive side, which was given in Figure 5.3, is apparent from Figures 5.7 and 5.8 since it can be explained by comparing corresponding spread of earlywood and latewood GRV magnitudes with that of half GRV for the respective species.

One interesting fact about the normalization constant of Douglas-fir and white spruce is that the power law relationship is preserved when the GRC is raised to some power above and below the magnitude of one. Figures 5.9 and 5.10 show that the GRV to GRC ratio for

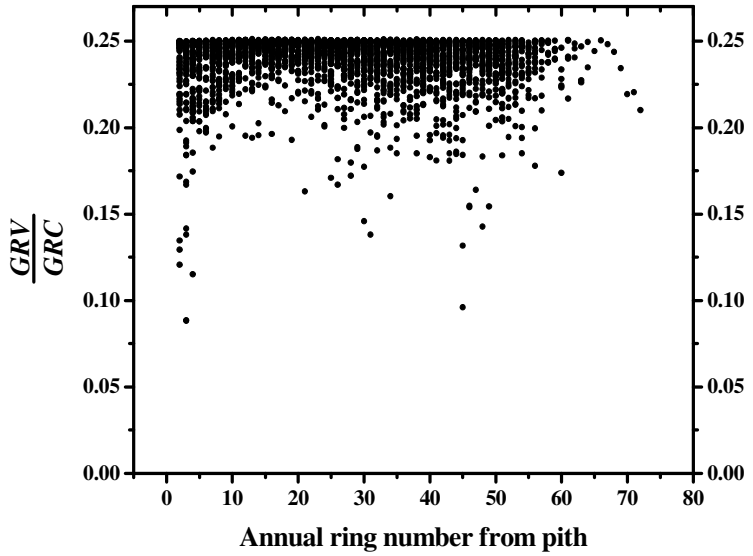

Figure 5.9 Spread of the GRV to GRC ratio of Douglas-fir that can be used as a proxy for the prediction of wood substance content of earlywood and latewood.

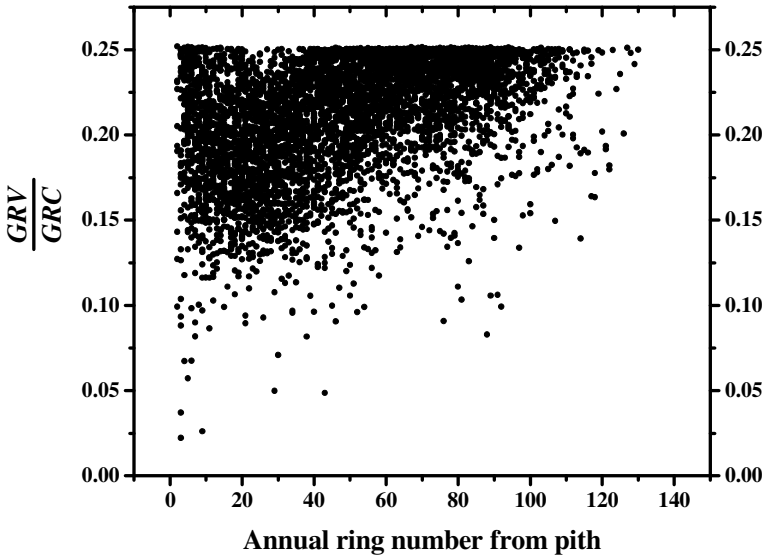

Figure 5.10 Spread of the GRV to GRC of white spruce that can be used as a proxy for the prediction of wood substance content of earlywood and latewood

Douglas-fir and white spruce attain the maximum value at 0.25 which is for a fifty-fifty probability of occurrence and this can outright be generalized to all species. However, dispersion of the product below the maximum is not the same for Douglas-fir and white spruce due to the multifractality exhibited by white spruce. The 0.25 or quarter ratio as a limiting asymptotic case and the consequence of optimized self-organization of a two component system can have some connections to the classical quarter allometric scaling that may prompt a need for further investigation in this direction.

Figure 5.9 shows the spread of the dispersion of the product for Douglas-fir and gives an imaginary picture of the percolation of water vapour through the end-grain of wood. Figure 5.10 also shows the same trend, but the spread is wider implying more heterogeneity while the percolation is biased with more momentum near the pith. In both cases the spreads get narrower towards the bark, though in case of Figure 5.9 the trend is not monotonous. The wider spread near the pith can be justified by the preference given to earlywood at early ages due to faster growth that declines towards the bark during maturity (Bond *et al.*, 2007; Curtis 1967). This remarkable trend may have a physical consequence that would enable explanation both to radial growth maxima and the span of growth trajectory. The trend further imparts the heterogeneity and wider scatter in the magnitude of the GRV to GRC ratio to be a signature for vigorous growth and expansion. However, generally the observed difference in the spread of the products of probabilities in the two species calls for an extensive pattern typology study for other species, too. It is only then that a generic probability density of states generating function and algorithm can be proposed. Havlin *et al*. (2002) have analytically shown that *n*-dimensional diffusion on Sierpinski gasket can exactly be given by

$$\boldsymbol{d}_{w} = \frac{\boldsymbol{ln}(\boldsymbol{n}+3)}{\boldsymbol{ln}(2)} \tag{5.10}$$

The Sierpinski gasket is a lattice with fractal scaling dimension and is constructed by subdividing an equilateral triangle into four and by taking out the middle one, and by repeating this process infinitely in each of subdivided triangles (Figure A.1). If the number of dimensions *n* is taken to represent the number of interacting components which, in the case

of earlywood and latewood in an annual ring assumes a magnitude of two then, the anomalous diffusion coefficient will scale with a magnitude of 2.32. Earlier in this study, the probability of occurrence of the magnitude of collapsed GRV given in equation (3.21) was also found to scale with the same fractal dimension of 2.32 for Douglas-fir, strongly supporting the correctness of the analogous TLS interaction given in Figure A.1 and the chaotic occurrence of the GRV in a ring series. The other interesting scaling property of Douglas-fir is the scaling behaviour for the TLS magnitude of collapsed GRV obtained according to equations (3.20) to (3.25) that displayed a close to quarter scaling exponent (λ). The observed general trend of scaling is given in Figure 5.11 displaying a sudden leap in the amplitude of the scaling equation from 1.77 to 2.59 as the number of interacting rings is decreased. The same scaling trend, but with a reduced scaling exponent of about -0.20 was obtained for white spruce. However, the scaling exponent for white spruce might be close to 0.25; because it is reported that *x*-ray diffraction measurement has a problem in accurately detecting latewood which may have few rows of tracheids (Vahey *et al*., 2007). White spruce

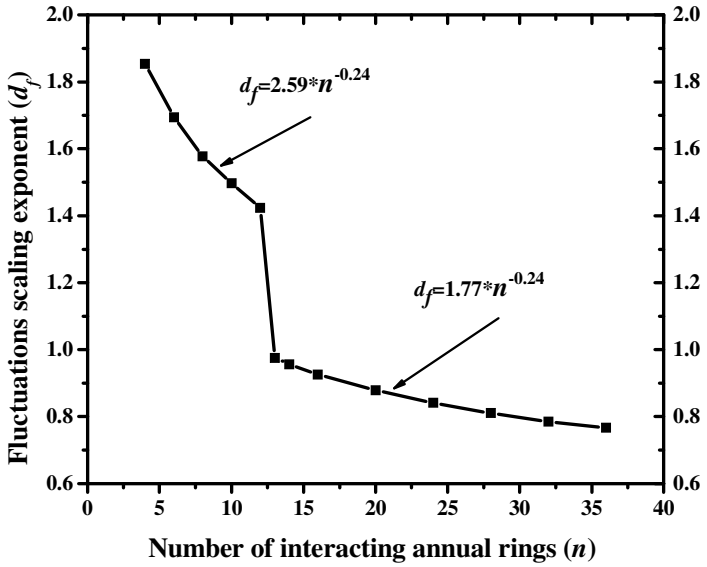

Figure 5.11 Scaling behaviour of the probability of magnitudes of fluctuations of the collapsed GRV in a ring trajectory of Douglas-fir showing a close to quarter scaling with a leaping transition after the 12th annual ring

has narrow latewood which is also implied in the wider scatter of the GRV to GRC ratio and as shown in Figure 5.10. Although it may require further investigation, this phenomenon can be connected to differing properties of juvenile and mature wood as the obtained numbers are close to the number of annual rings in juvenile wood (Koubaa, *et al*., 2005; Abdel-gadir and Krahmer, 1993). The twelve year leap found in this study is intriguing as it remarkably coincides with the 11-years mean solar cycle making tree rings good indicators of peak sun spots or solar activity hypothesized by Andrew Douglas a century back (Robinson, 1990; Deslauriers *et al.*, 2007). The leap occurs for white spruce after the tenth annual ring and the difference from Douglas-fir is not as wide as the difference between the β values which were found to be of sixteen in magnitude. If this is the case and if the leaps in other species are found to be in the range of nine to fourteen then it can be concluded that the GRV will have significant contribution in dendroclimatology also.

This study has found fundamental differences between the fractal behaviour of Douglas-fir and white spruce which is well supported by the findings given in Table 5.2 and Figures 5.9 and 5.10, in addition to the observed spread of the GRV to GRC ratio which was more chaotic for white spruce. The spread for Douglas-fir shown in Figure 5.9 is relatively narrow. However, the chaotic nature may not allow generating random probabilities. Therefore, the SOC behaviour should be given sufficient consideration, while proposing coarse-graining algorithms. This means that the earlywood and latewood composition ratio should be complexly generated using equations (5.4) and (5.5) in which multiple component interaction should be duly considered. Generally, the observed two extremes of complexity need further investigation. While the remarkable simplification of the heterogeneous interactions in Douglas-fir into a two-component or two-level system makes it an ideal experimental species for further investigation, the persistence of multi-component interaction in white spruce is still a puzzle to be solved along with conditions of transition from two-component to multi-component or conditions of simplifications from multi-component to two-component.

The monofractality and multifractality that are concluded to exist in softwood species may further be used as an alternative method of HTC or classification of heterogeneity based on the suggested pattern typology study on the GRV to GRC ratio. The detailed components of

earlywood and latewood, which are conceived in this study as their chemical composition, should also be allowed to come into play in the trajectory formation and reconstruction. Of course, the two-component or TLS model of chemical composition is validated at the end of this chapter. It is suggested that while applying the neural networks or any other computation procedures involving annual rings for coarse-graining, the following algorithmic steps should be followed.

- Identifying structures and levels of components and their properties (Earlywood, latewood, physical properties and chemical composition).
- Identifying and quantifying the GRV.
- Identifying and quantifying the interaction parameter β.
- Identifying and quantifying the transformed (dimensionally contracted) GRV.
- Identifying and quantifying the Markovian (short range) transition probabilities between consecutive GRV.
- Determining the fractality of ring series or trajectory (mono or multifractality).
- Computing the scaling parameters λ and α and confirming the one third ($1/3$) and quarter ($1/4$) scaling and quantifying the dynamical partition function.
- Prediction and/or reconstruction of short range trajectory (GRV_1 to GRV_5).
- Computing and predicting/reconstructing growth trajectories (long range) or series of annual rings that may span from pith to bark.
- Computing trajectory thermodynamic quantities: Entropy and work-energy.

5.2. Testing and validation of the two-level systems models of sorption for Douglas-fir wood

The two-component or two-level models derived in section 3.2 for the prediction of sorption properties of annual rings were validated with experimental data of Douglas-fir obtained as described in section 4.6. For annual rings sorption prediction models to be used either for the purpose of generating inputs and outputs for neural networks model development or as independent sorption prediction models after coarse-graining, it was necessary to obtain experimental data for gross wood (compact consecutive annual rings) of Douglas-fir.

Therefore, this part of models testing and validation contains three parts: testing and validation of models for sorption kinetics, sorption isotherms of annual rings and fitting of gross wood diffusion and isotherm model for the purpose of interpolation. The fitting of gross wood tangential diffusion coefficient and isotherms was done in two ways.

The sorption isotherm points collected at 25 and 50^0C were fitted to a one hydrate H-H model, so that matching isotherm points are available for isotherms predicted by sorption models of annual rings. The curve fitting and interpolation with regard to diffusion was more complicated because it involved separation of the diffusion coefficient into internal and surface emission coefficients. This was preceded by finding an interpolation polynomial for experimentally obtained diffusion coefficients that are assumed to match kinetic parameters predicted by annual ring level sorption models. The experimental data were statistically analyzed for significant differences in the mean values of sorption properties of earlywood, latewood, annual ring, heartwood and sapwood of Douglas-fir before they were used for testing and validation of the novel TLS models of sorption. Two-level and two-component models of chemical composition were also developed in a similar analogy to the modeling of sorption and with the same intent of using the generated parameters for ANNs modeling of sorption. They also went through the same statistical analysis.

5.2.1. Testing and validation of the two-level systems model of sorption kinetics

The validation of sorption kinetics is focused mainly on equations (3.61) to (3.64). Equation (3.61) requires estimation of two parameters that are used in the model in a complex way so as to describe the two components of sorption. Equilibrium moisture content and moisture potential are computed using equation (4.2) utilizing experimental data obtained from measurements of mass uptake or loss. The procedure did not differ for very small weight (milligram of weight) or large one as far as the same criterion for the attainment of equilibrium was imposed. In case of kinetics however, the two required different approaches. For data obtained on large surfaced specimens, the one dimensional (tangential direction) Fickian diffusion coefficient is calculated using equations (4.1) to (4.4) and the half thickness perpendicular to the largest face of the specimen. On the other hand, measurements on small

specimens are constrained by the inability to impose one dimensional flow. One dimensional flow can be assumed if very thin microtomed specimens are used, but there is still a problem with the sensitivity in detecting moisture gain or loss resulting from the very small weight which is a result of very small thickness. Therefore, statistical analysis of the kinetics obtained from small specimen was limited to the parameters obtained by the fitting of time dependent moisture potential from the newly derived equations (3.61) to (3.64). In this study earlywood, latewood and annual rings of Douglas-fir are used as small specimens and their coarse-graining was done based on the HTC and GRV TLS models developed and validated in section (5.1) and the ANNs computation. The statistical analysis is presented in the following section, first for BET-surface area (specific internal surface area), isotherms and kinetics of small specimens (earlywood, latewood, annual ring, heartwood, sapwood). Statistical analysis of isotherms and diffusion coefficients of sapwood and heartwood of the large specimens is also done.

5.2.1.1. Statistical summary for the results of the BET-internal specific surface area of Douglas-fir

The BET-surface area measurement was obtained from extracted and un-extracted Douglas-fir earlywood and latewood separately taken both from sapwood and heartwood. The mean BET-surface area measured for annual rings was 0.33 $m^2\ g^{-1}$ with a wide one standard deviation of 0.15 $m^2 g^{-1}$. This value is higher than 0.21 $m^2\ g^{-1}$ which is the only available reference for wood (Stamm, 1964). Stamm's (1964) internal specific surface area was obtained from mercury porosimetry. Generally, earlywood of Douglas-fir had a higher and significantly differing (p<0.05) value than its latewood. This is a fact that can directly be related to density differences. Similarly, the mean value of heartwood was higher than the corresponding sapwood value for both earlywood and latewood. The eight wood types yielded twenty eight combinations of means for comparisons of differences. Twenty four of the combinations were found to have significant (p<0.05) differences while the differences between un-extracted late heartwood and extracted late sapwood, un-extracted late sapwood and extracted late sapwood, extracted early heartwood and un-extracted early sapwood, and extracted early heartwood and un-extracted early heartwood were not significant. If the concern is only the internal surface area of cell-wall substance then the effect of extractive

substances should be accounted for and only the result obtained from extracted specimens should be considered. In this case, then the average BET-surface area of cell-wall was 0.35 m^2g^{-1} for extracted specimens, without a significant difference in the standard deviation. Stamm's (1964) value was close to the specific internal surface area obtained for latewood (0.21 m^2g^{-1}) with basic density 0.72 $g\ cm^{-3}$, which falls at the upper limit for most species and cannot represent a mean density. It seems, therefore, there is a difference between the value reported by Stamm (1964) and the result of current study. If there is a disagreement between the absolute magnitudes of internal surface areas reported by various authors, then the issue is not easy for resolution even if the measurement is performed under similar

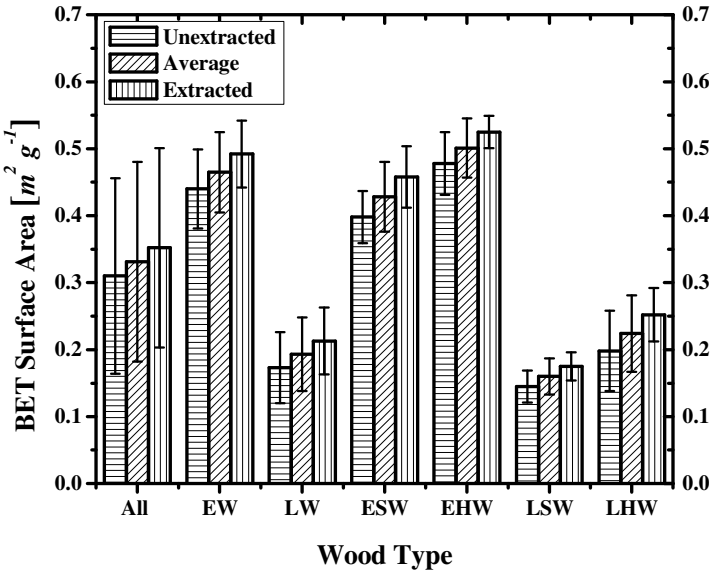

Figure 5.12 BET-surface area of early- and latewood of Douglas-fir obtained using Krypton as a probe molecule with the abbreviations denoting: EW-earlywood, LW-latewood, EHW-early heartwood, LSW-late sapwood, LHW-late heartwood (Error bars indicate standard error of the mean - SEM)

experimental conditions (IUPAC, 1972). The measurement is indirect with an assumption of monolayer coverage that can be affected by internal structure of the material which is variable and unpredictable in most instances. The BET-surface area obtained in the current study will be further discussed in connection with the value predicted by the newly derived two-component and two-level sorption prediction model that is validated following the

Table 5.5 BET-surface area of earlywood and latewood of Douglas-fir obtained using Krypton as a probe molecule with the abbreviation denoting: EW-earlywood, LW-latewood, ESW-early sapwood, EHW-early heartwood, LSW-late sapwood, LHW-late heartwood, SEM-standard error of the mean

Wood type	Un-extracted				Extracted				Average			
	Basic density [$g\ cm^{-3}$]		Surface area [$m^2\ g^{-1}$]		Basic density [$g\ cm^{-3}$]		Surface area [$m^2\ g^{-1}$]		Basic density [$g\ cm^{-3}$]		Surface area [$m^2\ g^{-1}$]	
	Average	SEM	Average	SEM	Average	SEM	Average	SEM	Average	SEM	Average	SEM
EW	0.31	0.02	0.44	0.06	0.30	0.03	0.49	0.05	0.31	0.03	0.47	0.06
LW	0.75	0.07	0.17	0.05	0.72	0.13	0.21	0.05	0.74	0.10	0.19	0.06
ESW	0.32	0.02	0.40	0.04	0.31	0.03	0.46	0.07	0.32	0.03	0.43	0.05
EHW	0.31	0.02	0.48	0.05	0.28	0.01	0.53	0.02	0.30	0.02	0.50	0.04
LSW	0.81	0.04	0.15	0.02	0.76	0.17	0.18	0.02	0.79	0.12	0.16	0.03
LHW	0.70	0.03	0.20	0.06	0.67	0.75	0.25	0.04	0.69	0.04	0.22	0.06
ALL	0.55	0.23	0.31	0.15	0.52	0.24	0.35	0.15	0.52	0.23	0.33	0.15

presentation of experimental measurements. Detailed summary of results of the internal surface area measurements are given on Figure 5.12 and Table 5.5.

5.2.1.2. Statistical summary for results of small specimens' sorption isotherms measurements

Sorption isotherm points were obtained at 25 and 50^0C at 20, 40, 60, 70, 75, 80, 85, 90 and 95% relative humidity. Due to the long storage time required for most of the specimens before use, they were first dried and stored. When the sorption measurement was performed it was not suitable to use green specimens as there is a high risk of contamination that could invalidate the experiment at one to three milligrams of weight. Therefore, it was decided to do first an adsorption run. That was immediately and automatically followed by desorption by keeping the same relative humidity levels as used for adsorption. Desorption isotherms obtained in this way could not be used as predictors for the boundary desorption curve and so they can be used only as scanning curves. Therefore, the experimental results of the sorption isotherms that are summarized in this section were made to include only adsorption isotherms. However, desorption experiments for annual rings were done both for un-extracted and extracted specimens using a relatively greater weight of five milligrams and with replications of three, so that the effect of sorption hysteresis could be taken into consideration in the developed models.

The mean adsorption points for Douglas-fir obtained at 25^0C were greater than those obtained at 50^0C and the difference was significant (p<0.05) in the relative humidity range 60 to 85%. The observed adsorption property agreed with the common behaviour of a decrease in equilibrium moisture content with increasing temperature. The obtained shape of sorption isotherms also agreed very well with the generally reported sigmoid or IUPAC type-II sorption curve for wood and lignocellulosic materials (Skaar, 1988; Siau 1995). Figure 5.13 shows that the two isotherms lie close to each other with the 50^0C isotherms having wider dispersion which is caused by increase in chaotic behaviour with increasing temperature.

The difference between sorption isotherm points of earlywood, latewood and annual ring obtained at 25^0C was significant (p<0.05) in the entire range of relative humidity. Earlywood had higher equilibrium moisture content than latewood while the annual ring had an intermediate value that was biased towards latewood as shown by the summaries given in

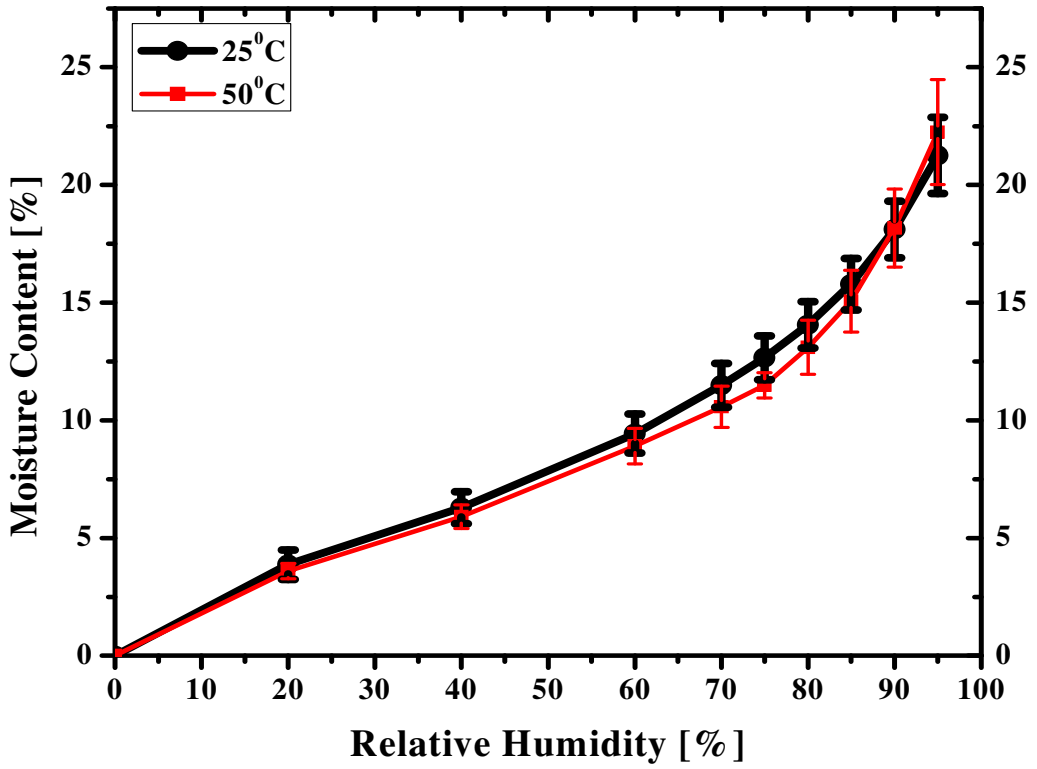

Figure 5.13 Mean adsorption points of Douglas-fir obtained from sorption measurements at earlywood, latewood and annual ring level at 25 and 50^0C (Error bars indicate SEM)

Table 5.6 and Figure 5.14. Earlywood had higher EMC than latewood corresponding to higher hemicelluloses content obtained for earlywood as shown in the summary of chemical composition given in Table 5.15. The differences between the mean equilibrium moisture content of heartwood and sapwood obtained both for un-extracted and extracted earlywood, latewood and annual rings were also significant (p<0.05). The same trend was observed for

Table 5.6 Mean adsorption isotherm points of earlywood, latewood and annual rings of Douglas-fir obtained from sorption measurements at 25^0C

H [%]	Earlywood		Latewood		Annual Ring	
	M [%]	SEM [%]	M [%]	SEM [%]	M [%]	SEM [%]
20	4.3	0.4	3.5	0.6	3.9	0.4
40	6.8	0.5	6.0	0.7	6.2	0.5
60	9.8	0.6	9.2	0.8	9.4	0.7
70	11.7	1.0	11.3	0.9	11.6	1.2
75	13.0	0.9	12.4	1.0	12.6	0.8
80	14.4	1.0	13.8	1.1	14.0	0.8
85	16.2	1.1	15.5	1.2	15.7	0.9
90	18.6	1.1	17.8	1.4	18.0	1.0
95	21.7	1.6	20.8	1.9	21.3	1.3

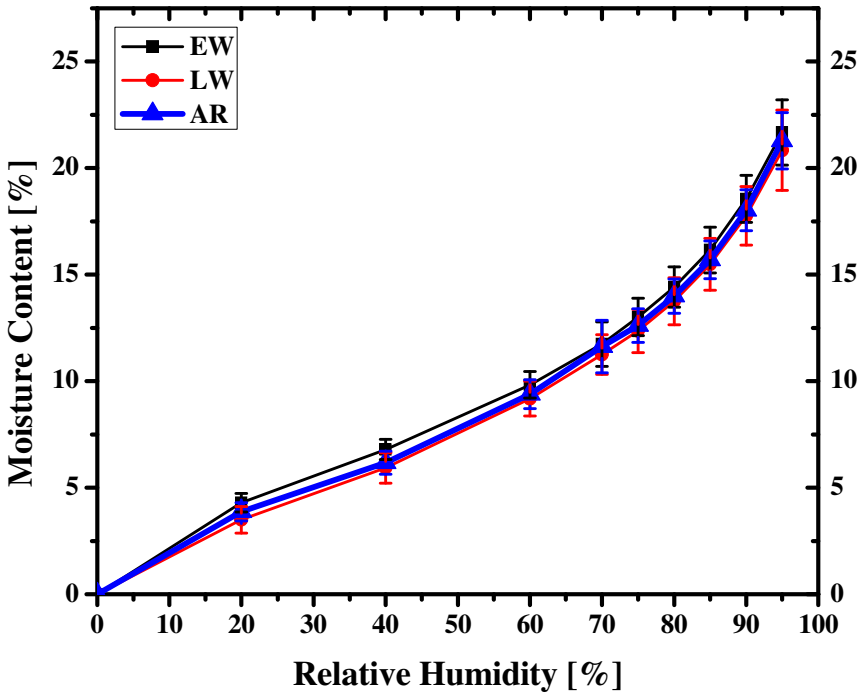

Figure 5.14 Mean adsorption points of earlywood, latewood and annual ring of Douglas-fir obtained from sorption measurements at 25^0C with the abbreviations denoting EW-earlywood, LW-latewood and AR-annual ring (Error bars indicate SEM)

Table 5.7 Mean adsorption points of earlywood, latewood and annual rings of Douglas-fir obtained from sorption measurements at 50^{0}C

H [%]	Earlywood		Latewood		Annual Ring	
	M [%]	SEM [%]	M [%]	SEM [%]	M [%]	SEM [%]
20	3.6	0.2	3.6	0.2	3.6	0.2
40	5.9	0.4	6.0	0.5	5.9	0.3
60	8.8	0.5	8.5	0.6	9.0	0.4
70	10.5	0.6	10.6	0.5	10.7	0.4
75	11.4	0.6	11.5	0.5	11.6	0.4
80	13.0	0.7	13.0	0.7	13.3	1.1
85	15.1	0.9	14.9	0.8	15.2	0.6
90	18.3	1.2	17.9	1.2	18.4	0.9
95	22.4	1.9	21.8	1.9	22.6	1.5

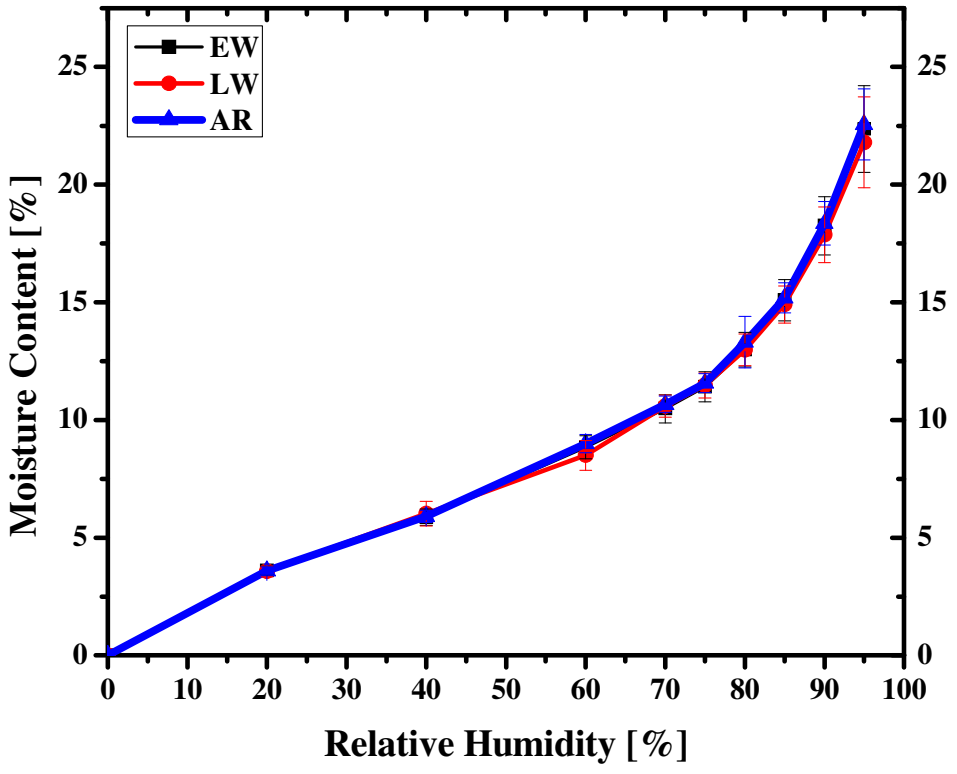

Figure 5.15 Mean adsorption points of earlywood, latewood and annual ring of Douglas-fir obtained from sorption measurements at 50^{0}C (Error bars indicate SEM)

Table 5.8 Mean absolute hysteresis and hysteresis ratio for annual ring of Douglas-fir obtained at 25 and 50^{0}C

H [%]	Absolute Hysteresis [%]				Hysteresis Ratio			
	25^{0}C		50^{0}C		25^{0}C		50^{0}C	
	Mean	SEM	Mean	SEM	Mean	SEM	Mean	SEM
20	2.0	0.3	1.1	0.2	0.7	0.0	0.8	0.0
40	3.5	0.4	2.1	0.3	0.6	0.0	0.7	0.0
60	4.4	0.7	2.7	0.4	0.7	0.0	0.8	0.0
70	4.9	0.8	3.1	0.4	0.7	0.0	0.8	0.0
75	5.2	0.9	3.4	0.5	0.7	0.0	0.8	0.0
80	5.3	1.1	3.6	0.5	0.7	0.1	0.8	0.0
85	5.6	1.0	3.8	0.7	0.7	0.0	0.8	0.0
90	6.0	1.4	4.0	1.2	0.8	0.1	0.8	0.1
95	5.9	1.9	3.3	2.0	0.8	0.1	0.9	0.1

adsorption points measured for earlywood, latewood and annual ring of Douglas-fir at 50^{0}C. The mean values of un-extracted and extracted sapwood and heartwood of earlywood, latewood and annual rings significantly (p<0.05) differed from each other. However, the difference between the mean equilibrium moisture content values of earlywood, latewood and annual rings were found to be statistically insignificant. Summary of the experimental results for the latter are given in Table 5.7 and Figure 5.15.

The experimental evidences showed that the major source of significant variations in sorption properties arise owing to hysteresis. The mean absolute hysteresis ratio ranged from 2 to 6% at 25^{0}C and from 1 to 4% at 50^{0}C showing up to two times differences between the values at the two temperatures. Detailed summary of the mean magnitudes of sorption hysteresis at 25 and 50^{0}C in the relative humidity range of 0 to 95% are given in Table 5.8 and in Figures 5.16 and 5.17. The differences both in the absolute magnitudes of hysteresis and hysteresis ratio were significant (p<0.05) in the relative humidity range 60 to 75% where the hysteresis attains maximum values. According to Skaar (1972), average hysteresis ratios can range 0.8 to 0.9 which agrees to values obtained at 50^{0}C, but were larger than those values obtained at 25^{0}C. The disparity is apparent because the results obtained at 25^{0}C should be in the lower range of the hysteresis while the 50^{0}C one should be close to the mean values given earlier. A closer observation of Figure 5.16 generally gives an important clue regarding the behaviour of sorption hysteresis. The dependence of mean absolute values of sorption hysteresis on

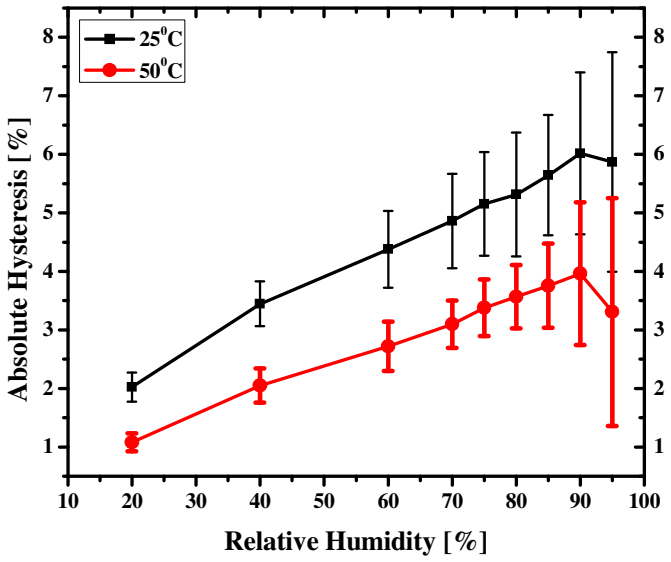

Figure 5.16 Mean absolute magnitudes of hysteresis for annual ring of Douglas-fir at 25 and 50^{0}C in the relative humidity range of 0 to 95% (Error bars indicate SEM

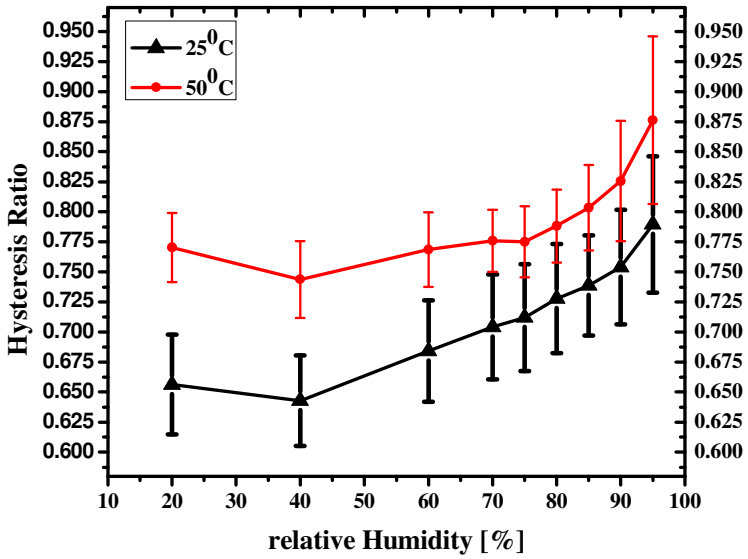

Figure 5.17 Mean magnitudes of hysteresis ratio for annual ring of Douglas-fir at 25 and 50^{0}C in the relative humidity range of 0 to 95% (Error bars indicate SEM)

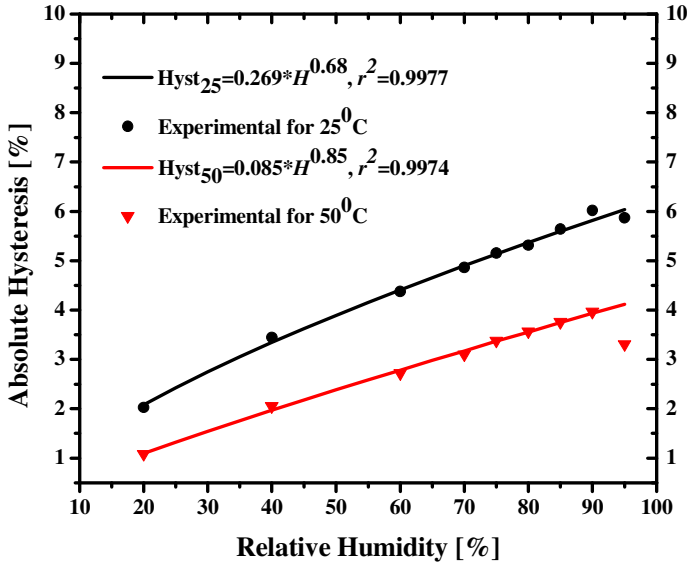

Figure 5.18 Dependence of the average absolute magnitudes of sorption hysteresis of Douglas-fir on relative humidity in the range of 0 to 95% at 25 and 50^{0}C

relative humidity obeys power law at both temperatures as shown in Figure 5.18. The chaotic nature of the sorption hysteresis is revealed in the exponential increase of the magnitude of the standard deviation when relative humidity was increases from 0 to 95%. Exponential divergence of trajectories is a signature for chaotic physical process which helps to readily categorize sorption hysteresis as a chaotic phenomenon. The exponential increase of the standard deviation of Douglas-fir annual ring sorption hysteresis is given in Figure 5.19. Figure 5.16 further depicts that with an increase in temperature the magnitude of sorption hysteresis decreases which then translates into the major decrease in mean value of equilibrium moisture content. However, Figure 5.19 at the same time shows the chaotic nature of increase in magnitudes of hysteresis with increasing temperature and relative humidity making sorption boundary curves more unstable.

Un-extracted sapwood annual ring (USAR) of Douglas-fir had the highest mean absolute magnitude of sorption hysteresis both at 25 and 50^{0}C as shown in Figures 5.20 and 5.21. The difference between the mean absolute magnitude of hysteresis of un-extracted and extracted

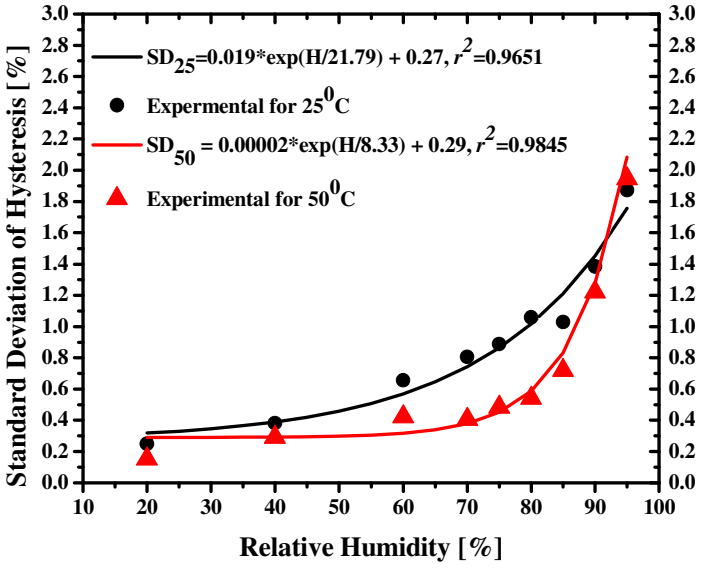

Figure 5.19 Exponential dependence of the standard deviations of the average absolute magnitudes of sorption hysteresis of Douglas-fir on relative humidity in the range of 0 to 95% at 25 and 50^0C

heartwood, and un-extracted and extracted sapwood was narrowing when the relative humidity was decreasing below 85%, but the differences were significant (p<0.05) above 60% relative humidity. There was insignificant difference between extracted and un-heartwood as shown on both Figures 5.20 and 5.21. Extraction of annual ring significantly (p<0.05) decreased hysteresis in sapwood annual ring. The chaotic behaviour of sorption hysteresis that was revealed by the exponential divergence in Figure 5.19 and the power law dependence of the absolute magnitude of hysteresis on relative humidity shown in Figures 5.16, 5.20 and 5.21 strengthened the prior assumption of criticality in sorption. Hence it is necessary to follow a different approach than equilibrium thermodynamics. In Figures 5.20 and 5.21 USAR denotes un-extracted sap annual ring, ESAR-extracted sap annual ring, UHAR- un-extracted heart annual ring and EHAR denotes extracted heart annual ring.

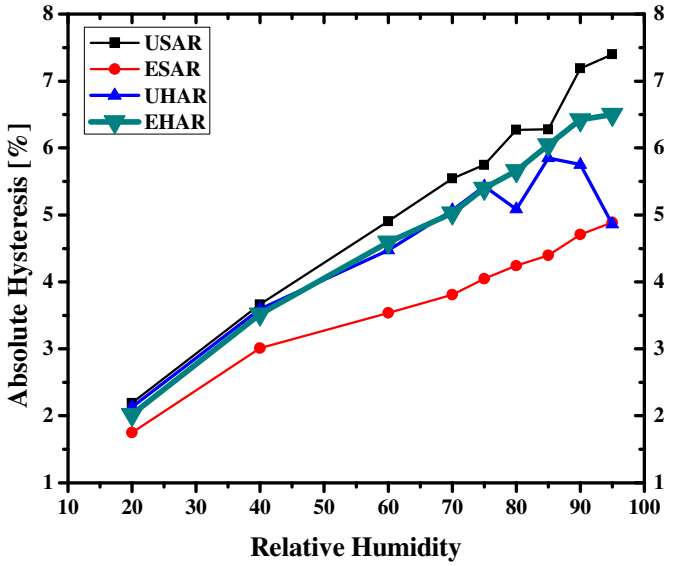

Figure 5.20 Mean absolute magnitudes of hysteresis for un-extracted and extracted sapwood and heartwood annual ring of Douglas-fir at 25^0C and 0 to 95% relative humidity

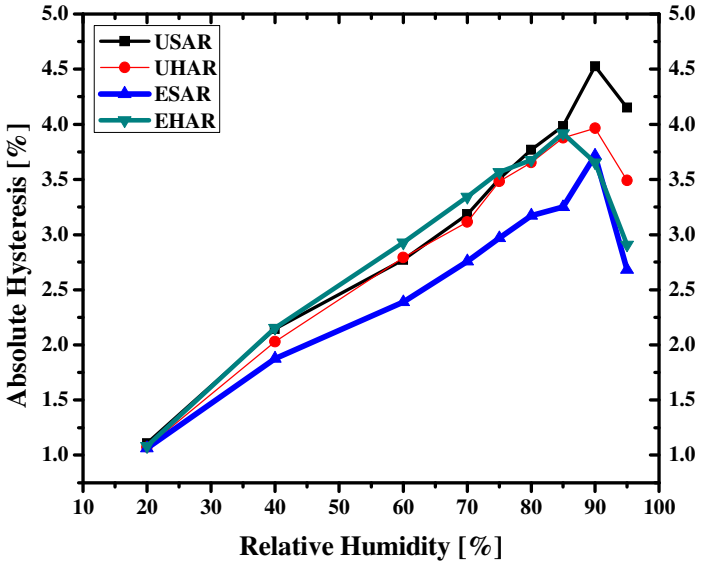

Figure 5.21 Mean absolute magnitudes of hysteresis for un-extracted and extracted sapwood and heartwood annual ring of Douglas-fir at 50^0C in the relative humidity range of 0 to 95%

5.2.1.3. Statistical summary for results of large specimen sorption isotherms measurements

Weight gains of each of the specimens measured at the five relative humidity steps chosen for 25 and 50^0C were computed into equilibrium moisture content based on equation (4.2). Thereafter, the isotherm points were fitted in to a one hydrate sorption isotherms model of Hailwood-Horrobin (H-H) that was given by equation (2.3). The dynamic moisture potential obtained based on equation (4.1) was further processed according to equations (4.3) and (4.4) to obtain the diffusion coefficients. Sapwood had significantly ($p<0.05$) higher equilibrium moisture content than heartwood which agrees with earlier reports for Douglas-fir (Fan *et. al.*, 1999). The experimental isotherms were able to be fitted very well with the H-H model having coefficients of the determinants (r^2) for sapwood at 25 and 50^0C ranging from 0.9822 to 0.9858 and 0.8505 to 0.9083, respectively. The r^2 for heartwood at 25 and 50^0C were 0.9698 to 0.9778 and 0.8101 to 0.8940, respectively. Summary of the H-H parameters are given in Table 5.20 and Figure 5.22. The hydrated water parameter K_1 and *W* (molecular weight of dry cell-wall per sorption site [kg mol^{-1}]) differed significantly ($p<0.05$) for sap and heartwood at both temperatures, while the difference in the parameters of dissolved water (K_2) values were found to be insignificant. This can lead to a conclusion that the K_2 parameter may be scale invariant. Table 5.9 reveals that sapwood has more sorption site per kilogram of dry wood based on the magnitudes of K_1. The magnitudes of K_1 and K_2 decreased by about 20% when the temperature was increased from 25 to 50^0C for both sapwood and heartwood while there was an increase in the magnitudes of W. The obtained K_2 values are close to the one reported for redwood, basswood and white spruce. On the other hand the K_1 values of sapwood and heartwood differed widely like the variations observed in earlier reports for redwood, basswood and white spruce (Skaar, 1988).

Table 5.9 Summary of the Hailwood-Horrobin (H-H) parameters obtained from sorption experiments done on the large specimens

Parameter	25^0C				50^0C			
	SW	SEM	HW	SEM	SW	SEM	HW	SEM
K_1	27.2	0.6	23.2	0.9	21.7	1.9	18.1	0.8
K_2	0.9	0.0	0.8	0.0	0.7	0.0	0.7	0.0
W	266.0	3.1	290.9	5.7	331.8	1.1	358.2	21.2

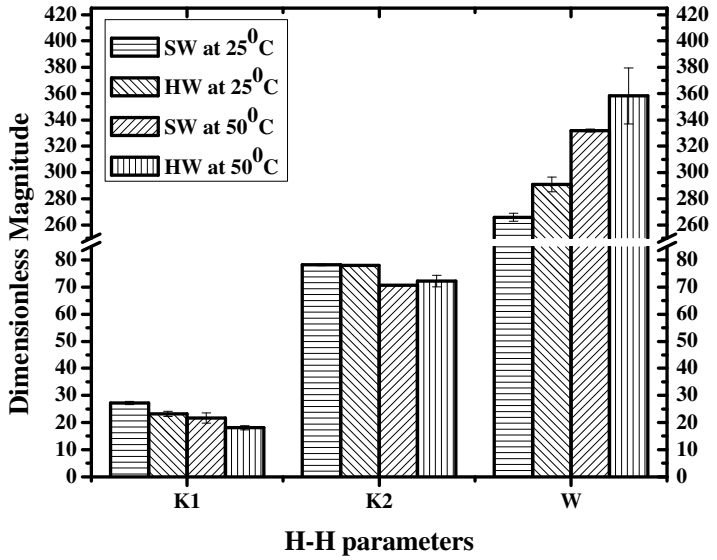

Figure 5.22 H-H model parameters for sapwood (SW) and heartwood (HW) specimens of Douglas-fir at 25 and 50^{0}C. K_2 was multiplied by hundred (100) to make the graphical representation easy for comparison in one plot (Error bars indicate SEM)

At 25^{0}C the tangential diffusion coefficients of sapwood were greater than that of heartwood up to one and half times, while the difference was up to two times at 50^{0}C. The increase in temperature from 25 to 50^{0}C caused a six times increase in diffusion coefficient in both sapwood and heartwood. Generally, the diffusion coefficient decreased with increasing relative humidity as can be seen from the linear interpolation plots in Figures 5.23 and 5.24 and also from Table 5.10. This trend has not been well noticed by many, and the prevailing assumption has been that the diffusion coefficient increases with increasing relative humidity. However, recent numerical simulations have shown that, in the case of prevailing non-Fickian diffusion conditions, it is preferable to assume a decrease in diffusion coefficient with an increase in relative humidity that agrees with the results of this sorption study on large and small specimens (Krabbenhoft and Damkilde, 2004; Olek and *et al*. 2005). Lastly, the surface emission coefficients were calculated according to equation (2.13) based on the half sorption time that showed the same trend and the details are summarized in Table 5.11.

Table 5.10 Summary of diffusion coefficients of the large specimens for sapwood (SW) and heartwood (HW) of Douglas-fir at 25 and 50^{0}C

25^{0}C				50^{0}C			
SW		HW		SW		HW	
M [%]	D [m^{2}s^{-1}]	M [%]	D [m^{2}s^{-1}]	M [%]	D [m^{2}s^{-1}]	M [%]	D [m^{2}s^{-1}]
3.3	2.5×10^{-11}	4.5	1.7×10^{-11}	3.0	9.2×10^{-11}	2.7	6.0×10^{-11}
7.6	1.5×10^{-11}	8.1	9.4×10^{-12}	5.8	4.5×10^{-11}	5.3	2.7×10^{-11}
11.1	1.8×10^{-11}	11.1	1.2×10^{-11}	7.9	4.1×10^{-11}	7.2	2.7×10^{-11}
14.5	8.8×10^{-12}	14.4	5.8×10^{-12}	10.6	4.7×10^{-11}	9.8	3.1×10^{-11}
18.5	1.2×10^{-11}	18.2	7.0×10^{-12}	12.8	10×10^{-12}	11.8	1.0×10^{-11}
22.3	2.9×10^{-12}	21.5	2.6×10^{-12}	14.8	1.7×10^{-11}	13.7	8.8×10^{-12}

The experimental results obtained for magnitudes of tangential diffusion coefficient and the surface emission coefficient are close to values reported by earlier studies for various wood species (Skaar, 1958; Stamm, 1960; Comstock, 1963; Rosen, 1978; Avramidis and Siau, 1987; Hunter, 1993; Wadsö, 1993, Olek and Weres, 2007, Neimsuwan *et al*., 2008).

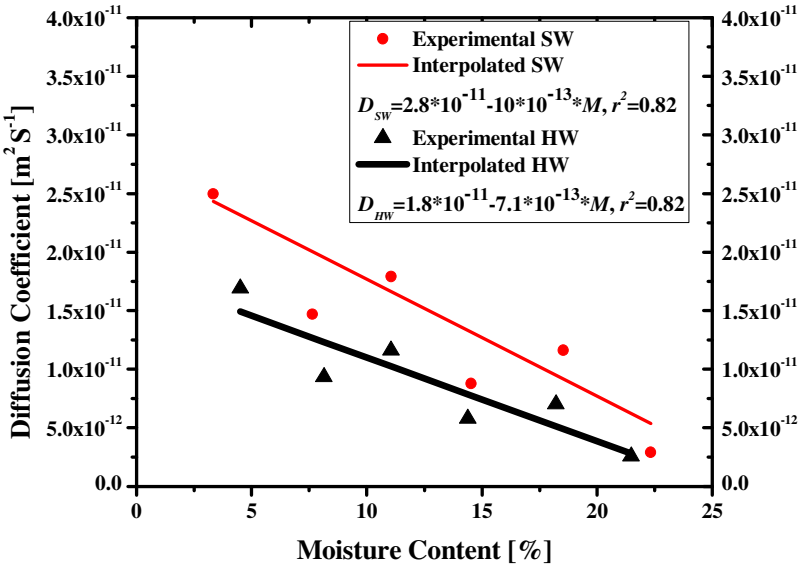

Figure 5.23 Linear interpolations of the tangential diffusion coefficient of sapwood (SW) and heartwood (HW) of Douglas-fir on relative humidity at 25^{0}C

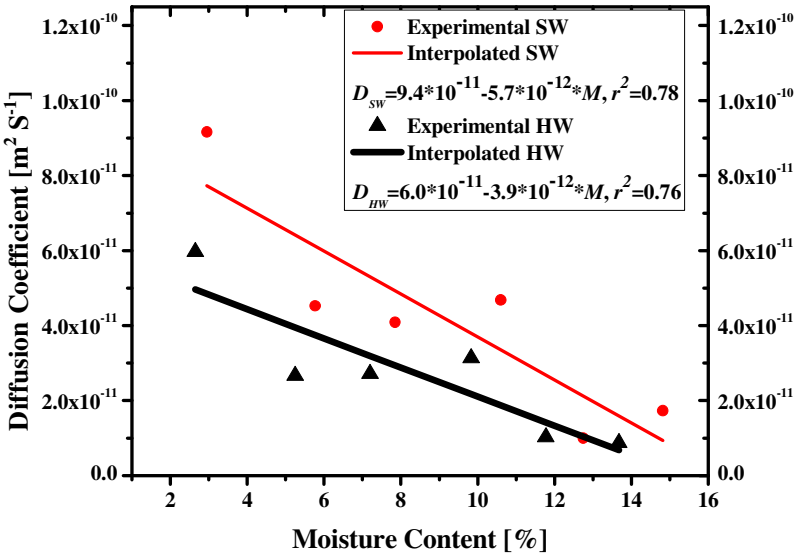

Figure 5.24 Linear interpolations of the tangential diffusion coefficient of sapwood (SW) and heartwood (HW) of Douglas-fir on relative humidity at 50^{0}C

Table 5.11 Summary of surface emission coefficient of sapwood (SW) and heartwood (HW) of Douglas-fir at 25 and 50^{0}C computed from diffusion coefficients obtained at the five experimental steps of relative humidity

25^{0}C				50^{0}C			
SW		HW		SW		HW	
M [%]	S [m s^{-1}]	M [%]	S [m s^{-1}]	M [%]	S [m s^{-1}]	M [%]	S [m s^{-1}]
3.3	4.0x10^{-08}	4.5	2.5x10^{-08}	3.0	1.5x10^{-07}	2.7	9.0x10^{-08}
7.6	2.4x10^{-08}	8.1	1.4x10^{-08}	5.8	7.3x10^{-08}	5.3	4.0x10^{-08}
11.1	2.9x10^{-08}	11.1	1.7x10^{-08}	7.9	6.6x10^{-08}	7.2	4.1x10^{-08}
14.5	1.4x10^{-08}	14.4	8.5x10^{-09}	10.6	7.6x10^{-08}	9.8	4.8x10^{-08}
18.5	1.9x10^{-08}	18.2	1.0x10^{-08}	12.8	1.6x10^{-08}	11.8	1.6x10^{-08}
22.3	4.6x10^{-09}	21.5	3.8x10^{-09}	14.8	2.8x10^{-08}	13.7	1.3x10^{-08}

5.2.2. Testing and validation of the two-level systems model of sorption kinetics

In this section the derived two-component and two-level equations (3.62) to (3.64) were validated as models describing kinetics of sorption. The sorption isotherms analog of the same two-level and two-component model was also fitted and tuned with corresponding model parameters, and validated. Equations (3.62) to (3.64) require quantification of three parameters c_k, L_1 and x. Parameter β is numerically equal to c_k or c_k+1 depending on temperature and level of relative humidity and does not require extra computation. Parameter c_k was obtained by fitting equation (3.53) with experimental data. The parameter x is found to be numerically equal to the fraction of moisture content at which the kinetics crosses over from prevailing short-range to prevailingly long-range kinetics. The cross over is equivalent to phase transition and may be characterized by a discontinuity in the differential heat of sorption. This in other words means that the differential heat of sorption approaches zero that can be deduced from a minimal moisture gain in the region of transition. This phenomenon is usually observed when the vapour pressure approaches unity. When the vapour pressure approaches unity then the mass uptake approaches zero. Assuming an insignificant moisture uptake makes the weight ratio in equation (5.11) equivalent to unity which, in other words, means when the sorption becomes independent of specimens weight or when the sorption phenomenon becomes chaotic (in phase transition), integration of the same equation (3.66) gives the following relation

$$\boldsymbol{h} = \frac{\boldsymbol{c}_k}{\boldsymbol{h}+\mathbf{1}} \tag{5.11}$$

The threshold magnitude of c_k is numerically equivalent to two and the maximum value that is experimentally obtained was 1.98. Let us assume that the left hand side of the equation is equal to unity and with a 1.98 value of c_k equation (5.11) holds true for vapour pressure of 0.98 which would also be true for practical fibre saturation point without significant risk of capillary condensation. However, the paradox is that equation (5.11) holds true in lower relative regions, at least once. This is experimentally observed in this study to be in the region from approximately 0.75 to 0.80 of vapour pressure, probably closer to 0.80 at 50^0C.

Equation (5.11) can be approximated by unity if and only if its right hand side of equation (5.11) is raised to some power x which is less or equal to 0.1. It has been easy to find a straightforward solution for the parameter x. States in phase transition exhibit a number of scaling behaviours. A close look at equations (3.36) to (3.39) reveals that equation (3.36) may in some form serve as characteristic length that can possess the required scaling behaviour. Hence, it was found that the moisture content fraction at the phase transition can serve as a scaling exponent very well. Equation (5.11) is therefore transformed to

$$\boldsymbol{h} = \left(\frac{\boldsymbol{c}_k}{\boldsymbol{h}+\mathbf{1}} \right)^{x} \tag{5.12}$$

and x is equivalent to

$$\boldsymbol{x} = \frac{\boldsymbol{m}_t - \boldsymbol{m}_0}{\boldsymbol{m}_t} \tag{5.13}$$

where m_t [gm or kg] is the specimens weight at phase transition and m_0 [gm or kg] is oven dry or weight at zero vapour pressure. Equation (5.13) circumvents computational difficulties that could have arisen from the multifractal behaviour of equations (3.36) to (3.39). It also presents a major scaling behaviour in sorption that can have applications in wood drying and hydrothermal modification in addition to its utility in this research.

The parameter L_1 of equation (3.63) obviously represents amplitude or a constant for the fastness of the long range sorption. Every increase in relative humidity involves first a short-range kinetics that is immediately superseded by a long-range one and every such event is characterized by a transition from short-range to long-range kinetics. The transition point determines the magnitude of L_1 and as parameter of long-range kinetics, it too, posses power law scaling behaviour. The reciprocal of x was found to be the best scaling exponent for L_1 as given in equation (5.14), where m_{tl} [gm or kg] is weight at the crossing instance to long-range kinetics and m_{0i} [gm or kg] is initial weight at the onset of sorption which can be different from oven dry weight. L_2 of equation (3.64) is satisfied by a value of unity. Summaries of

$$L_1 = \left(\frac{m_{tl}}{m_{oi}} \right)^{\frac{1}{x}} \tag{5.14}$$

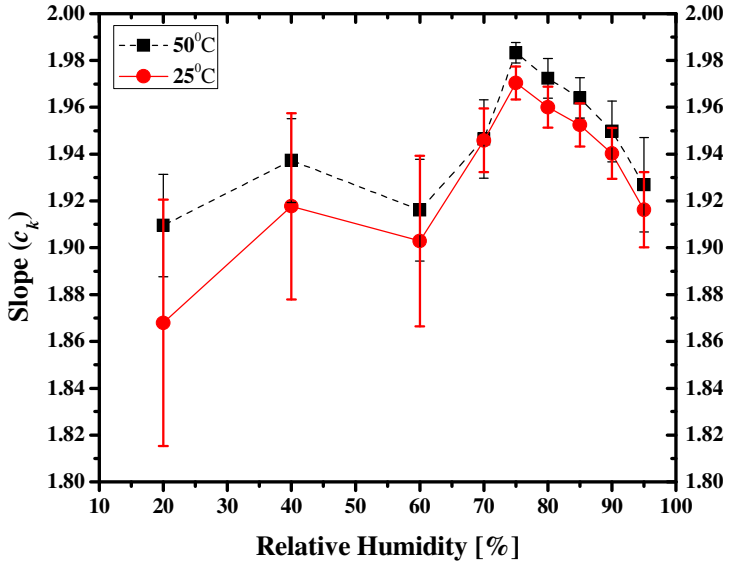

Figure 5.25 Dependence of parameter c_k of Douglas-fir on relative humidity at 25 and 50^{0}C (Error bars indicate SEM)

the parameters obtained based on equations (3.53), (3.62) to (3.64) and (5.12) to (5.14) are presented in Tables (5.12) and (5.13). The dependence of parameter c_k on relative humidity at 25 and 50^{0}C is shown in Figures 5.25, 5.26 and 5.27 in which the essence of equation (5.11) can be easily visualized. Equation (5.11) can be best elaborated if the dependence of c_k both on relative humidity and moisture content is shown simultaneously as it is elegantly demonstrated in Figure 5.26 and 5.27 at 25 and 50^{0}C, respectively. The three dimensional trajectory shown in the Figures render explanation as to how sorption accelerates and

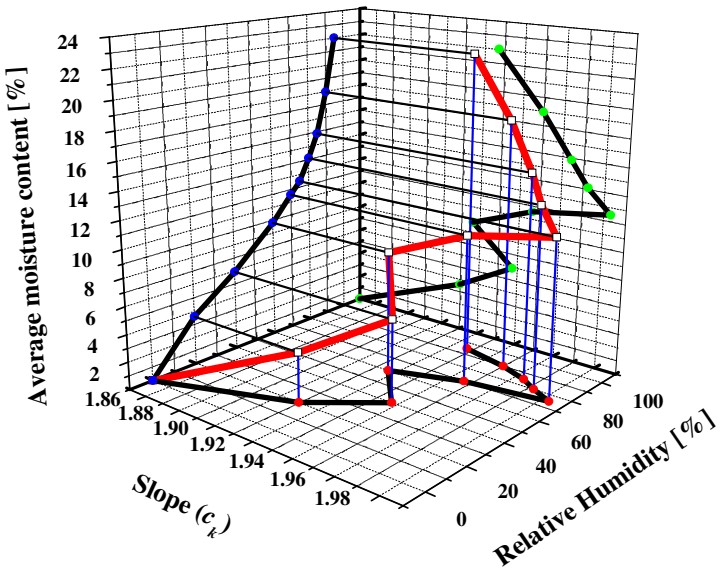

Figure 5.26 Three-dimensional reverse ε-trajectory of the dependence of c_k of Douglas-fir on moisture content and relative humidity at 25^0C

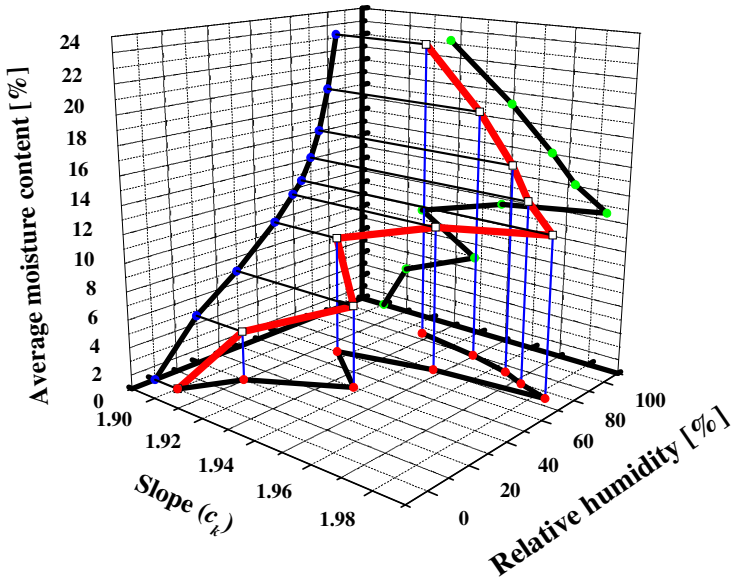

Figure 5.27 Three-dimensional reversed ε-trajectory of the dependence of c_k of Douglas-fir on moisture content and relative humidity at 50^0C

Table 5.12 Detailed magnitudes of major parameters for kinetics of Douglas-fir at 25^0C for the small specimens

H [%]	Parameter	Sap EW		Heart EW		Sap LW		Heart LW		Sap AR		Heart AR	
		Mean	SEM	Mean	SEM	Mean	SEM	Mean	SEM	Mean	SEM	Mean	SEM
20	**i**	0.740	0.324	0.665	0.355	0.534	0.361	0.359	0.433	0.587	0.330	0.544	0.316
	c_k	1.826	0.051	1.839	0.063	1.908	0.012	1.884	0.048	1.888	0.051	1.850	0.050
	t-exp	1.091	0.122	1.063	0.091	1.045	0.021	1.055	0.032	1.025	0.059	1.022	0.078
	$\mathbf{L_1}$	1.024	0.021	1.028	0.023	1.050	0.014	1.039	0.018	1.046	0.024	1.027	0.023
40	**i**	0.637	0.341	0.593	0.367	0.499	0.360	0.303	0.443	0.537	0.330	0.499	0.332
	c_k	1.915	0.042	1.913	0.044	1.934	0.013	1.919	0.021	1.936	0.025	1.892	0.049
	t-exp	1.130	0.104	1.104	0.107	1.051	0.029	1.064	0.031	1.044	0.043	1.036	0.069
	$\mathbf{L_1}$	1.045	0.019	1.041	0.019	1.054	0.007	1.041	0.011	1.054	0.015	1.030	0.023
60	**i**	0.617	0.314	0.576	0.415	0.522	0.364	0.315	0.463	0.575	0.338	0.482	0.359
	c_k	1.907	0.041	1.905	0.044	1.911	0.013	1.902	0.031	1.908	0.033	1.893	0.037
	t-exp	1.103	0.094	1.076	0.066	1.045	0.031	1.057	0.045	1.043	0.040	1.040	0.057
	$\mathbf{L_1}$	1.046	0.019	1.041	0.021	1.050	0.007	1.040	0.015	1.048	0.019	1.034	0.016
70	**i**	0.536	0.349	0.447	0.408	0.476	0.363	0.244	0.475	0.568	0.282	0.420	0.380
	c_k	1.945	0.024	1.959	0.012	1.944	0.013	1.949	0.013	1.950	0.011	1.953	0.013
	t-exp	1.098	0.069	1.106	0.080	1.045	0.024	1.071	0.030	1.045	0.026	1.069	0.046
	$\mathbf{L_1}$	1.055	0.014	1.058	0.007	1.052	0.005	1.052	0.005	1.054	0.009	1.049	0.007
75	**i**	0.506	0.355	0.443	0.423	0.462	0.373	0.214	0.502	0.490	0.340	0.382	0.409
	c_k	1.969	0.006	1.969	0.008	1.965	0.009	1.970	0.007	1.970	0.006	1.972	0.007
	t-exp	1.109	0.083	1.090	0.064	1.052	0.026	1.078	0.034	1.050	0.026	1.071	0.039
	$\mathbf{L_1}$	1.063	0.007	1.058	0.005	1.055	0.006	1.055	0.004	1.060	0.007	1.056	0.004
80	**i**	0.509	0.356	0.482	0.425	0.464	0.377	0.213	0.502	0.496	0.339	0.376	0.404
	c_k	1.960	0.008	1.960	0.011	1.955	0.008	1.959	0.010	1.961	0.007	1.961	0.006
	t-exp	1.099	0.077	1.091	0.065	1.046	0.027	1.065	0.031	1.043	0.028	1.058	0.043
	$\mathbf{L_1}$	1.060	0.007	1.056	0.007	1.053	0.005	1.052	0.004	1.058	0.008	1.053	0.003
85	**i**	0.513	0.354	0.454	0.425	0.463	0.374	0.232	0.489	0.502	0.336	0.385	0.400
	c_k	1.951	0.009	1.953	0.011	1.948	0.009	1.950	0.008	1.954	0.008	1.954	0.007
	t-exp	1.093	0.070	1.081	0.067	1.043	0.025	1.065	0.035	1.041	0.025	1.055	0.040
	$\mathbf{L_1}$	1.059	0.007	1.056	0.006	1.052	0.005	1.050	0.005	1.057	0.008	1.052	0.003
90	**i**	0.517	0.360	0.469	0.416	0.477	0.366	0.237	0.491	0.521	0.342	0.406	0.415
	c_k	1.937	0.013	1.938	0.010	1.932	0.014	1.938	0.013	1.941	0.010	1.941	0.011
	t-exp	1.081	0.058	1.072	0.063	1.071	0.135	1.055	0.027	1.038	0.025	1.049	0.035
	$\mathbf{L_1}$	1.056	0.008	1.052	0.004	1.048	0.007	1.049	0.005	1.055	0.007	1.050	0.005
95	**i**	0.488	0.371	0.422	0.406	0.487	0.396	0.170	0.475	0.515	0.373	0.380	0.427
	c_k	1.917	0.016	1.919	0.015	1.910	0.019	1.916	0.014	1.916	0.016	1.918	0.016
	t-exp	1.075	0.058	1.062	0.051	1.038	0.021	1.047	0.020	1.029	0.025	1.044	0.037
	$\mathbf{L_1}$	1.051	0.009	1.049	0.006	1.046	0.007	1.043	0.004	1.050	0.011	1.045	0.006

Table 5.13 Detailed magnitudes of major parameters for kinetics of Douglas-fir at 50^0C for the small specimens

H [%]	Parameter	Sap EW		Heart EW		Sap LW		Heart LW		Sap AR		Heart AR	
		Mean	SEM	Mean	SEM	Mean	SEM	Mean	SEM	Mean	SEM	Mean	SEM
20	**i**	0.763	0.088	0.766	0.217	0.634	0.197	0.684	0.171	0.675	0.140	0.666	0.198
	c_k	1.922	0.023	1.910	0.024	1.899	0.015	1.910	0.019	1.906	0.015	1.910	0.028
	t-exp	1.017	0.030	1.035	0.060	1.009	0.017	1.034	0.031	1.026	0.034	1.112	0.364
	$\mathbf{L_1}$	1.031	0.013	1.023	0.012	1.036	0.010	0.986	0.222	1.035	0.007	1.083	0.208
40	**i**	0.682	0.055	0.652	0.193	0.591	0.209	0.599	0.191	0.644	0.145	0.634	0.208
	c_k	1.939	0.014	1.945	0.016	1.926	0.024	1.937	0.017	1.935	0.015	1.940	0.018
	t-exp	1.017	0.018	1.035	0.036	1.013	0.030	1.034	0.036	1.035	0.026	1.037	0.028
	$\mathbf{L_1}$	1.038	0.009	1.040	0.009	1.040	0.014	1.043	0.008	1.043	0.010	1.043	0.011
60	**i**	0.690	0.058	0.645	0.179	0.601	0.207	0.592	0.208	0.641	0.147	0.649	0.185
	c_k	1.920	0.028	1.918	0.023	1.909	0.020	1.915	0.023	1.917	0.017	1.918	0.020
	t-exp	1.012	0.031	1.014	0.034	1.006	0.026	1.017	0.039	1.025	0.033	1.030	0.021
	$\mathbf{L_1}$	1.047	0.014	1.043	0.016	1.036	0.011	1.036	0.011	1.040	0.011	1.036	0.012
70	**i**	0.670	0.060	0.622	0.188	0.556	0.217	0.779	0.895	0.592	0.151	0.584	0.207
	c_k	1.941	0.024	1.948	0.009	1.941	0.010	1.956	0.012	1.945	0.014	1.949	0.022
	t-exp	1.021	0.019	1.030	0.033	1.010	0.016	1.027	0.024	1.022	0.038	1.024	0.019
	$\mathbf{L_1}$	1.044	0.015	1.044	0.005	1.045	0.006	1.050	0.007	1.047	0.009	1.047	0.013
75	**i**	0.642	0.050	0.596	0.188	0.520	0.225	0.549	0.190	0.572	0.147	0.557	0.228
	c_k	1.983	0.003	1.984	0.003	1.982	0.009	1.985	0.003	1.982	0.003	1.983	0.003
	t-exp	1.052	0.017	1.053	0.035	1.036	0.016	1.044	0.029	1.047	0.034	1.044	0.023
	$\mathbf{L_1}$	1.068	0.006	1.066	0.004	1.069	0.005	1.065	0.005	1.068	0.003	1.065	0.004
80	**i**	0.649	0.057	0.602	0.187	0.506	0.235	0.542	0.216	0.547	0.174	0.533	0.225
	c_k	1.966	0.011	1.970	0.008	1.976	0.006	1.974	0.007	1.972	0.007	1.976	0.006
	t-exp	1.044	0.019	1.049	0.034	1.029	0.012	1.034	0.021	1.034	0.025	1.032	0.014
	$\mathbf{L_1}$	1.060	0.007	1.061	0.005	1.069	0.005	1.063	0.005	1.065	0.006	1.065	0.005
85	**i**	0.659	0.055	0.617	0.184	0.517	0.232	0.542	0.205	0.553	0.170	0.552	0.224
	c_k	1.959	0.011	1.963	0.009	1.968	0.008	1.965	0.008	1.963	0.007	1.966	0.006
	t-exp	1.048	0.019	1.052	0.035	1.027	0.014	1.028	0.015	1.031	0.022	1.030	0.014
	$\mathbf{L_1}$	1.060	0.006	1.061	0.005	1.065	0.006	1.060	0.005	1.062	0.005	1.062	0.005
90	**i**	0.680	0.055	0.641	0.180	0.540	0.219	0.569	0.200	0.573	0.167	0.577	0.222
	c_k	1.943	0.013	1.948	0.014	1.952	0.016	1.954	0.009	1.951	0.011	1.951	0.013
	t-exp	1.051	0.015	1.057	0.034	1.031	0.017	1.034	0.013	1.039	0.026	1.035	0.013
	$\mathbf{L_1}$	1.058	0.008	1.060	0.006	1.063	0.008	1.061	0.005	1.064	0.007	1.061	0.007
95	**i**	0.708	0.065	0.661	0.186	0.577	0.209	0.605	0.193	0.626	0.173	0.613	0.227
	c_k	1.922	0.023	1.928	0.023	1.932	0.025	1.934	0.015	1.923	0.017	1.925	0.017
	t-exp	1.052	0.013	1.056	0.030	1.031	0.018	1.034	0.010	1.038	0.026	1.027	0.014
	$\mathbf{L_1}$	1.058	0.011	1.057	0.007	1.060	0.011	1.057	0.007	1.058	0.009	1.054	0.007

decelerates at various levels of relative humidity. Accordingly, it is easy to imagine the mechanism of sorption in analogy with an automobile climbing up the hill. At the start of an uphill journey, the road can be imagined bumpy, where the automobile has to overcome both an uneven road as well as the gradient. As it climbs up, the road becomes increasingly smooth but slippery. The road zigzags to reduce the steepness of the gradient. The zigzagging is named in Figures 5.26 and 5.27 as reversed ε-trajectory as it looks like a mirror reflection of the Greek letter ε and hence the name reversed ε-trajectory for the sake of easier visualization. The parameter c_k of Douglas-fir can, therefore, be regarded as a gradient of sorption in which, when it becomes less, the gradient gets smaller and the rate of sorption hence becomes faster. When c_k gets larger it implies steep gradient of sorption that involves many unpredictable number of slip backs and it also implies the prevailing critical state of the sorption in general. Therefore, the long range sorption takes infinite time to meet the criterion of sorption that holds true for equilibrium systems due to the dissipative nature of the process demonstrated.

In addition to its dependence on relative humidity and moisture content, the parameter c_k is not constant at given relative humidity, moisture content and temperature. The c_k fluctuations are governed by similar relation to the entropy of black body radiation as shown to be valid for the GRV given in equation (5.6). Generally, the following relation is found to be valid for the fluctuation of c_k of Douglas-fir that is dependent on a variable obtained as intercept along with it during its quantification from experimental values.

$$\frac{c_k}{e^i} = 3 \cdot \sigma + 2 \cdot \sigma \cdot i^{\sigma} \tag{5.15}$$

where i is the intercept and σ is a scaling exponent. The magnitude of σ ranges approximately 0.61 to 0.68. Equation (5.15) reads as given in equation (5.16) in the special case when σ attains a magnitude close to ⅔ and when the relative humidity approaches 98 to 100%.

$$\frac{c_k}{e^i} = 2 + \frac{4}{3} \cdot i^{\frac{2}{3}} \tag{5.16}$$

The constant term with the magnitude of two is equivalent to the maximum magnitude of c_k. This term attains a magnitude of two when the value of the intercept is zero in which case the sorption can be assumed in a super critical state where it becomes difficult to externally control the sorption as a physical system. If equation (5.16) is equivalent to the entropy of black body radiation then the term $i^{2/3}$ represents the internal energy of unit volume of the sorption system. The right hand side of equation (5.16) becomes equal to two in magnitude if and only if either the internal energy is zero ($i^{2/3}=0$) or if the volume of the system collapses to zero. It is probably in this condition that the sorption system displays a discontinuity in one of its thermodynamic parameters (internal energy or volume) hence a phase transition occurs. Equation (5.16) consequently makes the sorption (mass transfer) that takes place infinitely closer to 100% relative humidity, or at lower level of relative humidity at which phase transition occurs, analogous to the cavity (black body) radiation. A black body radiation is a radiation coming from a perfect black body which is assumed to be in thermal equilibrium but which is also at the same time dissipative. It is well known that it is difficult to keep experimental conditions at exactly 100% relative humidity and this finding explains the reason to be the inherent dissipative fluctuation.

Another interesting relation can be found when values of the intercept and the growth parameter of Douglas-fir sorption kinetics are computed with a similar relation to equation (5.16). Let the value of c_k be substituted by the magnitude of L_1 then the following relation holds true if tested experimentally.

$$\frac{L_1}{e^i} \approx 1.07 + \frac{2}{3} \cdot i^{\frac{2}{3}} \tag{5.17}$$

where the constant value 1.07 is the magnitude of the long range sorption around which the growth parameter L_1 fluctuates. The right hand side of equations (5.16) and (5.17) are in an approximate proportionality ratio of 2:1. Equations (5.16) and (5.17) can thus be used to obtain a direct relation between the growth parameter L_1 and the intercept which can also show a linkage to scaling exponent c_k and to the state of phase transition based on equation (5.14). The magnitude of parameters c_k, i, L_1, and t-exp in Tables 5.12 and 5.13 in addition to

their dependence on relative humidity and temperature are found to differ for earlywood, latewood and annual rings of Douglas-fir. Figure 5.27 shows that at 25^0C and in the range of lower relative humidity, latewood has a significantly (p<0.05) higher value of c_k than earlywood and the position is switched over in the higher relative humidity levels where the long range kinetics prevails. Similar trend is observed at 50^0C as it is shown in Figure 5.30 although the difference between earlywood and latewood is found to be insignificant.

At the same temperature of 25^0C, earlywood has a higher value of the time exponent of the sorption kinetics than latewood that is computed based on relative humidity for earlywood, latewood and annual ring using equation (3.47). The trend is the same for the 50^0C sorption, but the difference becomes significant (p<0.05) at higher relative humidity levels and it is also in that range where earlywood takes higher values of the time exponent than latewood. Furthermore, latewood had higher value of the magnitude of L_1 in the lower relative humidity ranges that showed a cross over in the long range sorption or higher humidity levels. Earlywood and latewood had significantly differing magnitudes of L_1 at 25^0C. At 50^0C earlywood and latewood were rather showing indistinguishable trends in the lower relative humidity ranges, but they also displayed a trend similar to the 25^0C one with a significant difference (p<0.05) between earlywood and latewood in the higher relative humidity levels.

Temperature dependence of the time exponent and the growth parameter L_1 are shown in Figures 5.34 and 5.35, respectively. Generally, at lower temperature the mechanism of sorption was more non-Fickian and hence as the temperature decreases the dimensionless time exponent increases as shown in Figure 5.33. The denser the wood, the higher the value of the time exponent and this is apparent by a significantly (p<0.05) higher value of the time exponent for latewood than earlywood which is detailed in Tables 5.12 and 5.13. Figure 5.34 shows that generally the growth parameter L_1 had higher magnitude in the lower humidity range for 25 than 50^0C that again switched over in the higher relative humidity where the kinetics is prevailingly long range. All of the parameters, namely c_k, the time exponent and the growth parameter L_1 displayed a similar wavy trend both at 25 and 50^0C. Generally, the

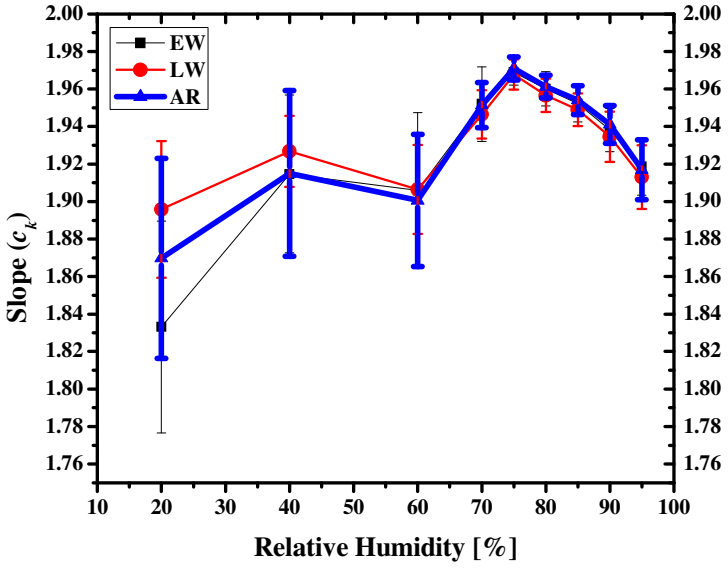

Figure 5.28 Dependence of the scaling parameter c_k on relative humidity for earlywood, latewood and annual ring of Douglas-fir at 25^0C (Error bars indicate SEM)

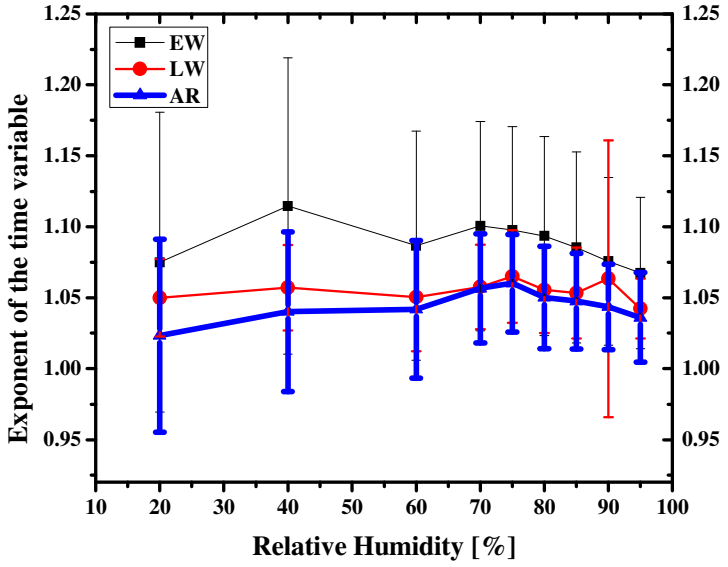

Figure 5.29 Dependence of the time exponent of the sorption kinetics on relative humidity for earlywood, latewood and annual ring of Douglas-fir at 25^0C based on of equation (3.47) (Error bars indicate SEM)

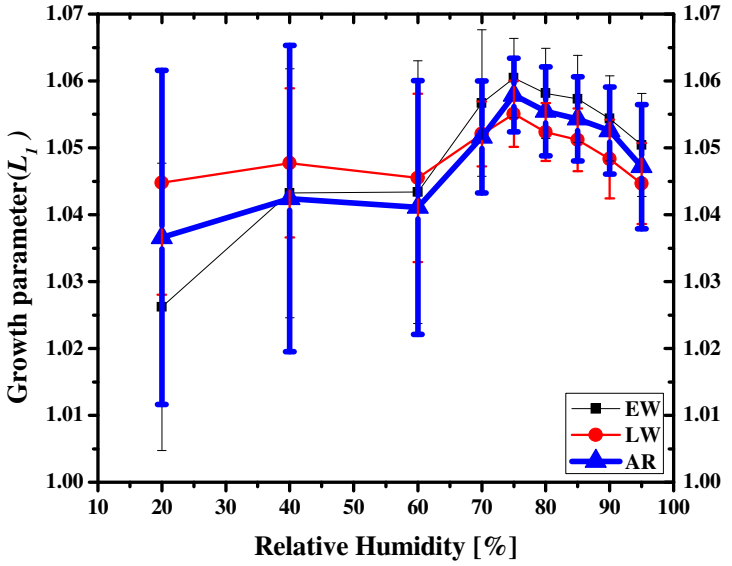

Figure 5.30 Dependence of the growth parameter L_1 of the sorption kinetics on relative humidity for earlywood, latewood and annual ring of Douglas-fir at 25^0C (Error bars indicate SEM)

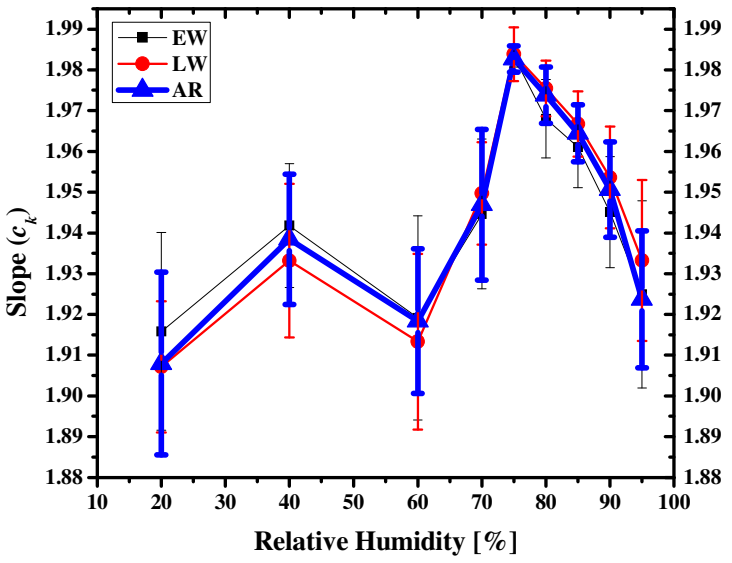

Figure 5.31 Dependence of the scaling parameter c_k on relative humidity for earlywood, latewood and annual ring of Douglas-fir at 50^0C (Error bars indicate SEM)

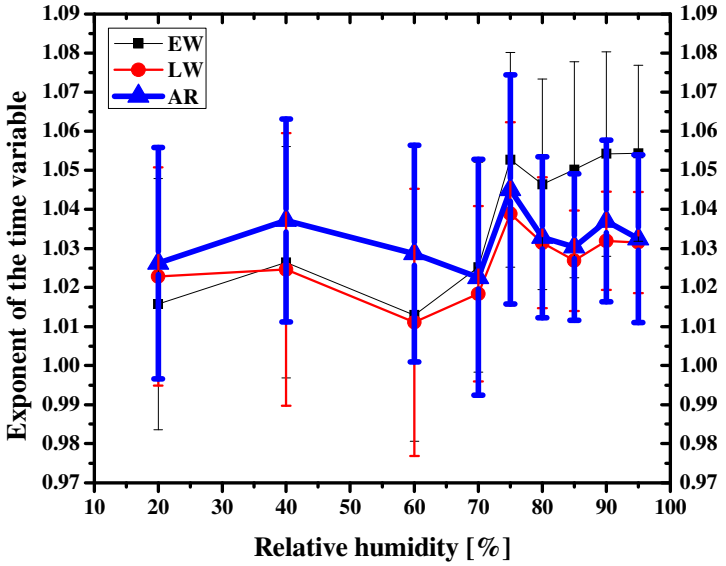

Figure 5.32 Dependence of the time exponent of the sorption kinetics on relative humidity for earlywood, latewood and annual ring of Douglas-fir at 50^0C based on of equation (3.47) (Error bars indicate SEM)

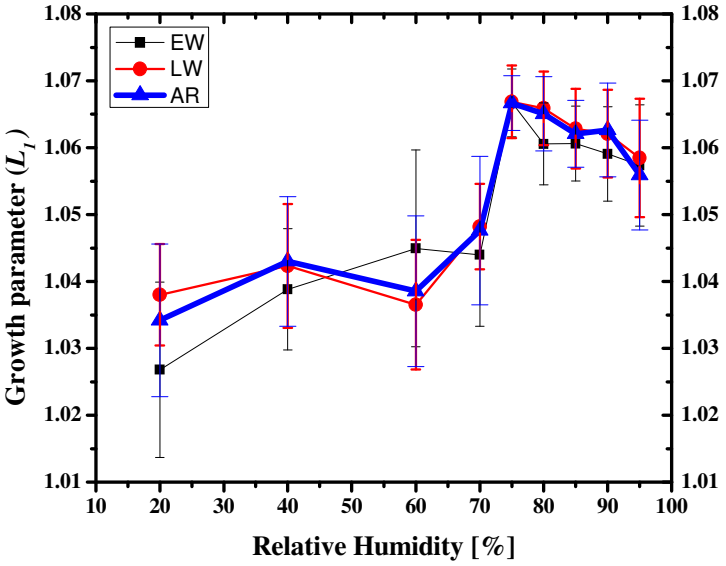

Figure 5.33 Dependence of the growth parameter L_1 of the sorption kinetics on relative humidity for earlywood, latewood and annual ring of Douglas-fir at 50^0C (Error bars indicate SEM)

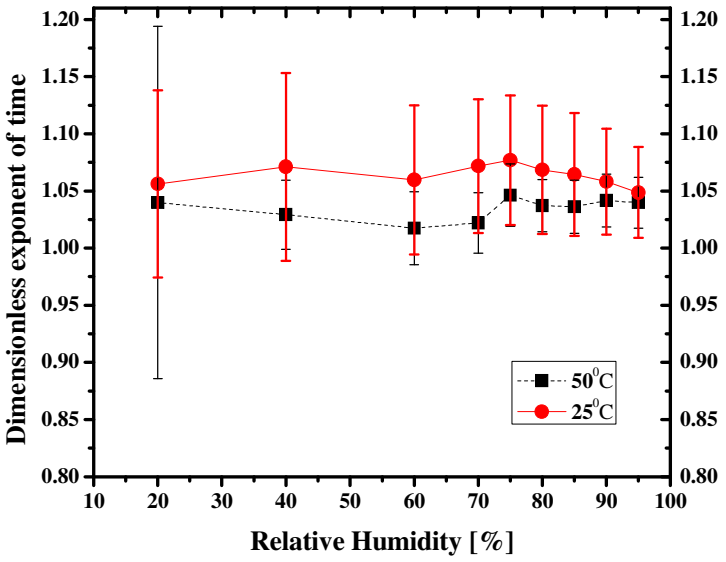

Figure 5.34 Dependence of the time exponent in the left hand side of equation (3.47) on temperature and relative humidity for Douglas-fir wood (Error bars indicate SEM)

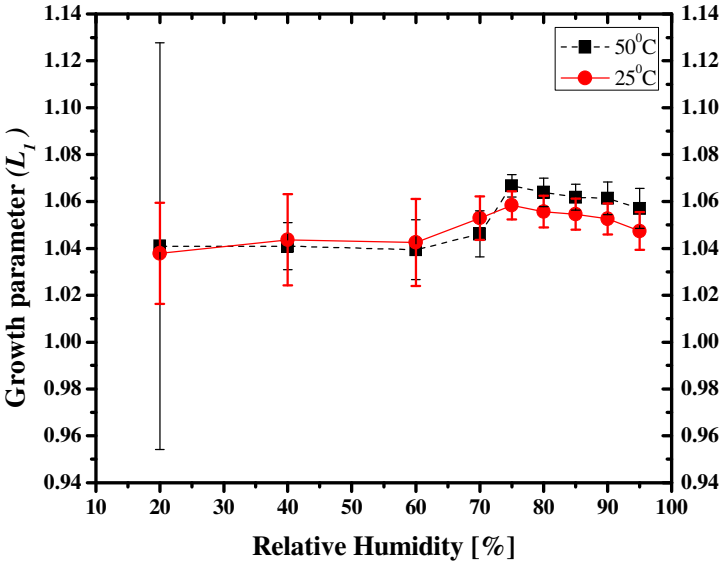

Figure 5.35 Dependence of the growth parameter L_1 on temperature and relative humidity for Douglas-fir wood (Error bars indicate SEM)

parameters at 50^0C had narrower standard deviation than at 25^0C except at 20% relative humidity at which they displayed a relatively wider scatter.

Equations (3.61) to (3.64) describe both the transport of water vapour or kinetics in the cell-wall and lumens. The parameters describe transport of water vapour in wood as an emergent property resulting from the complex interaction of water vapour and cell-wall components in heterogeneous network of wood porous structures. The network of porous structures is considered as rather fractal than simple assumptions of conductive structures connected in series or in parallel. In this regard, this work introduces a new direction in tackling the complex wood-water vapour interaction and complements the recent report of Frandsen and Svensson (2007) which treated transport of water vapour in wood as "multi-Fickian". The diffusion at lower relative humidity was considered as Fickian that is dominated by diffusion of water vapour in the cell-lumen. On the other hand, diffusion that takes place at higher relative humidity was considered as non-Fickian and is dominated by diffusion of water vapour in the cell-wall. It is very important to point out here the fact that in this study it was shown that non-Fickian behaviour is not only due to sorption at higher relative humidity, but also due to low temperature as demonstrated on Douglas-fir .

5.2.3 Testing and validation of the two-level systems model of sorption isotherms for Douglas-fir

Equation (3.78) is the isotherm version of the TLS prediction model that was validated in section 5.2.2. The isotherm has been justified during its derivation on the basis of empirical evidences of non-Fickian and non-stationary or quasi-equilibrium state at 25 and 50^0C that are illustrated in Figures 5.36 to 5.39. The Figures demonstrate that the sorption kinetics of Douglas-fir's annual ring is predominantly non-Fickian with slowly and constantly shifting saturation points. Adsorption saturation point at a given level of relative humidity moves up while the corresponding desorption saturation point moves downward being asymptotic to a mean sorption isotherm at large time limit, towards which each of the boundary sorption curves gradually move. The observation in other words means that if the Douglas-fir wood-water system is allowed to remain interacting for a very long time, then the adsorption isotherms would be constantly shifted upward or attracted to the position of the mean

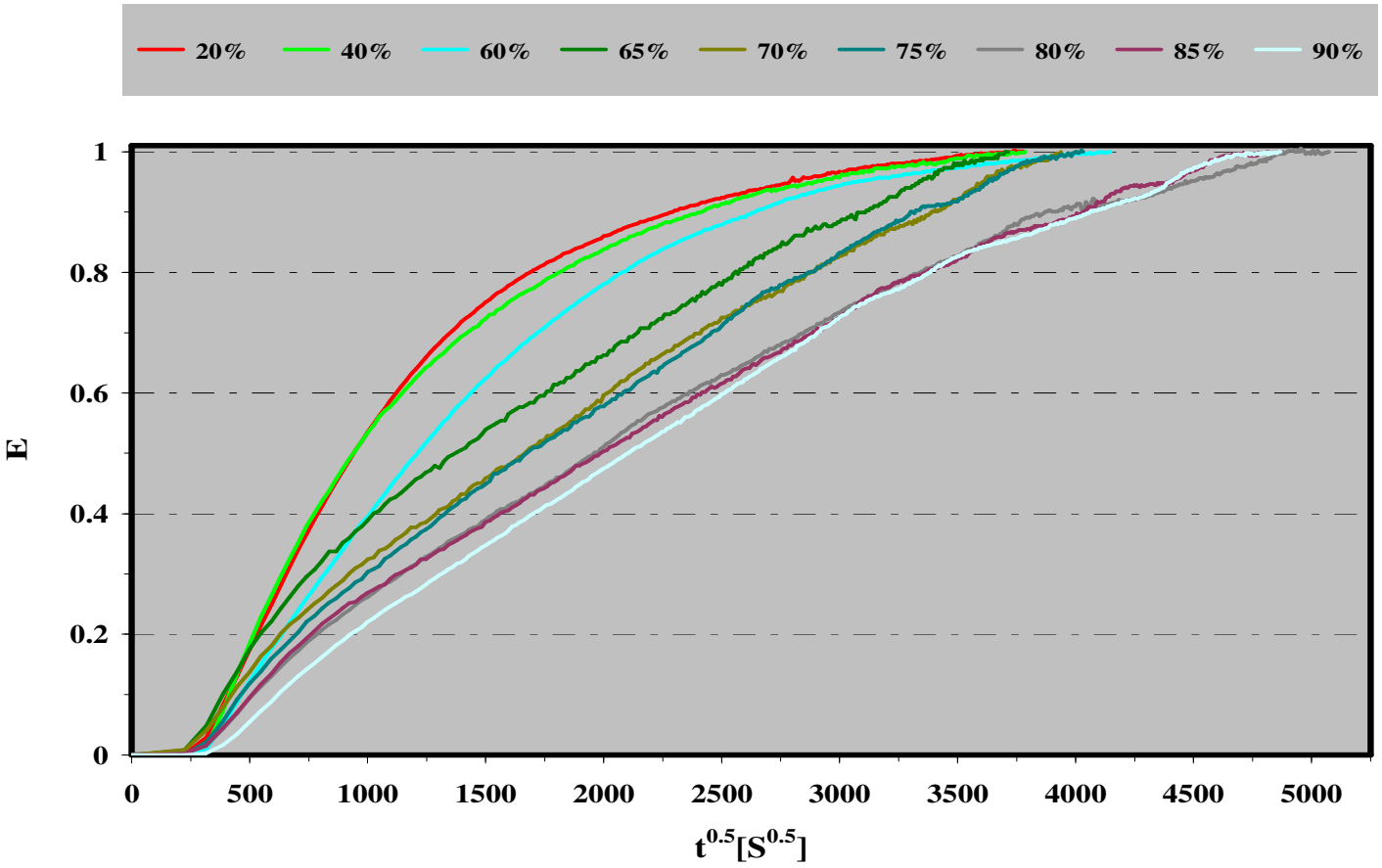

Figure 5.36 Adsorption kinetics of Douglas-fir's annual ring at 25^0C showing dominance of non-Fickian behaviour in the entire range of relative humidity that becomes increasingly stronger with increasing relative humidity

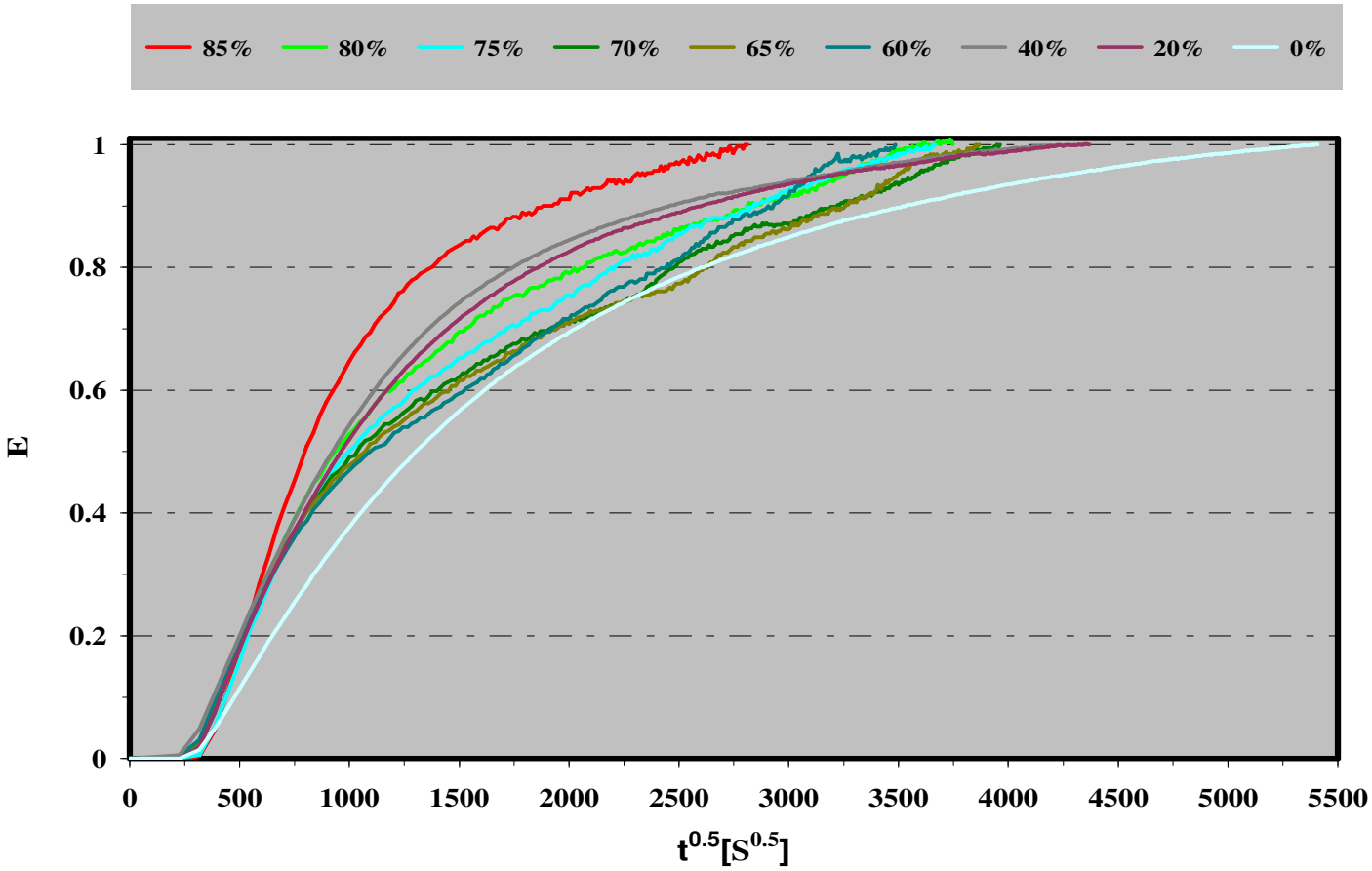

Figure 5.37 Desorption kinetics of Douglas-fir's annual ring at 25^0C showing dominance of non-Fickian behaviour in the entire range of relative humidity that becomes increasingly stronger with increasing in relative humidity

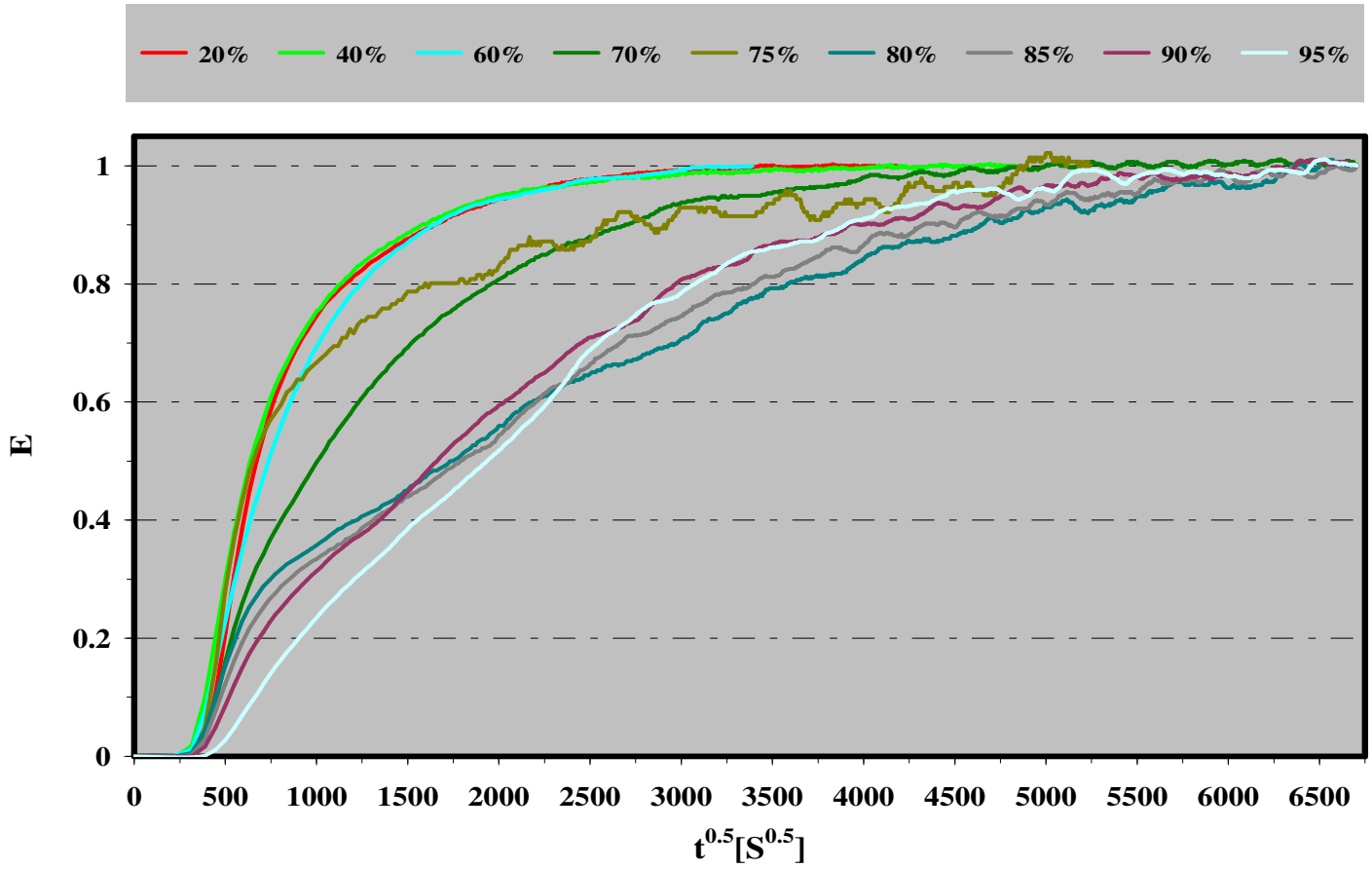

Figure 5.38 Adsorption kinetics of Douglas-fir's annual ring at 50^0C showing dominance of non-Fickian behaviour in the entire range of relative humidity that becomes increasingly stronger with increasing relative humidity

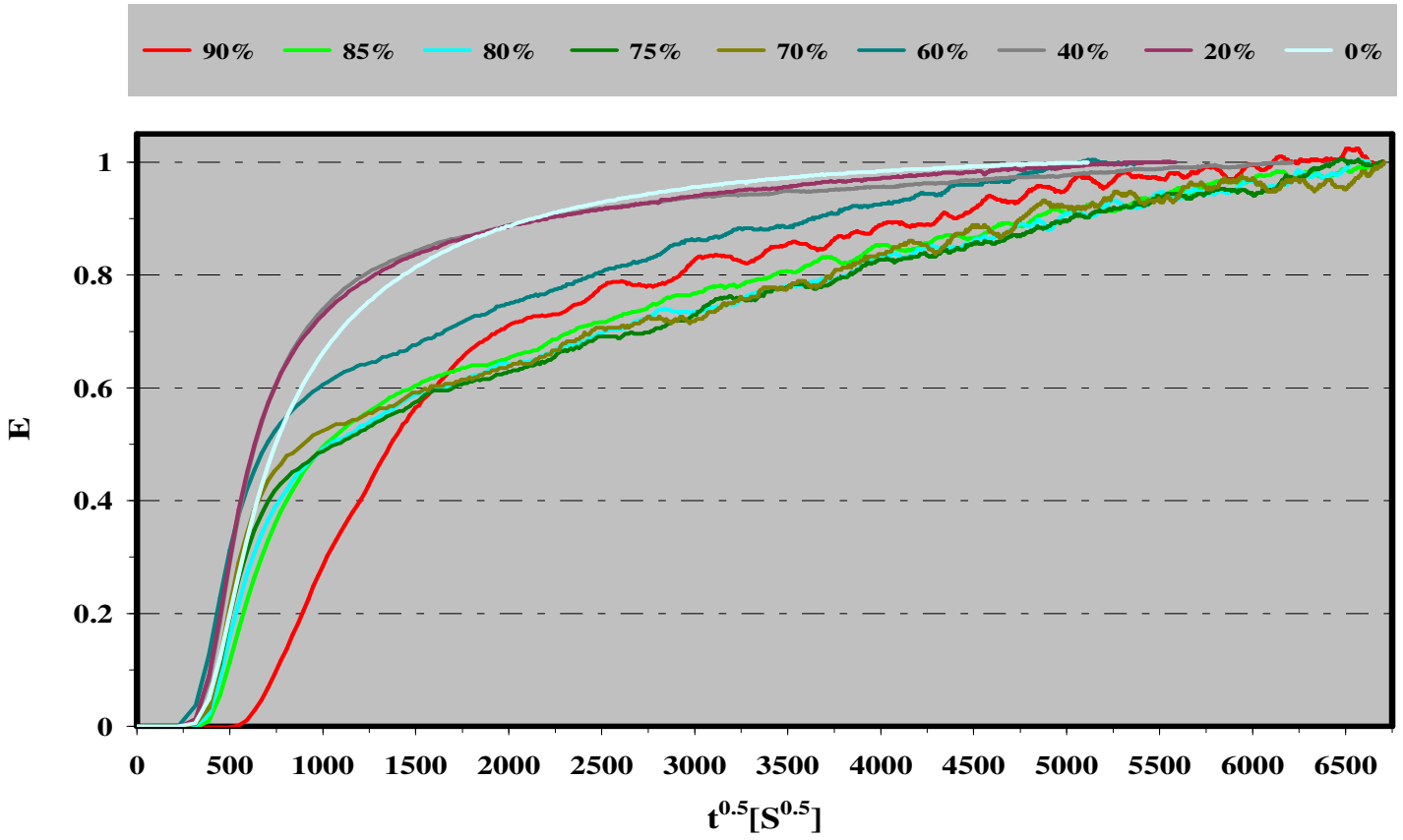

Figure 5.39 Desorption kinetics of Douglas-fir's annual ring at 50^0C showing dominance of non-Fickian behaviour in the entire range of relative humidity that becomes increasingly stronger with increasing relative humidity

sorption isotherms. In a similar way, the desorption isotherms would asymptotically be shifted down towards the mean sorption isotherm provided the wood is allowed to remain at constant temperature and relative humidity for a very large time after the relative humidity is perturbed (lowered or increased) by a small amount. Therefore, it can be concluded that hysteresis in Douglas-fir wood is significant if the wood is made to adsorb and desorb water vapour relatively quickly and if it is allowed to go the sorption process very slowly then the hysteresis would vanish to zero. However, under real conditions changes in ambient conditions are fast from which follows that hysteresis is a common observation that becomes an irreversible process due to permanent modification of the structure of wood. The more the rate of change in ambient conditions becomes faster, the more severe becomes the criticality in the wood-water vapour interaction. The consequence of this phenomenon is that models that use shrinkage as a major predictor for internal stresses should take into consideration the

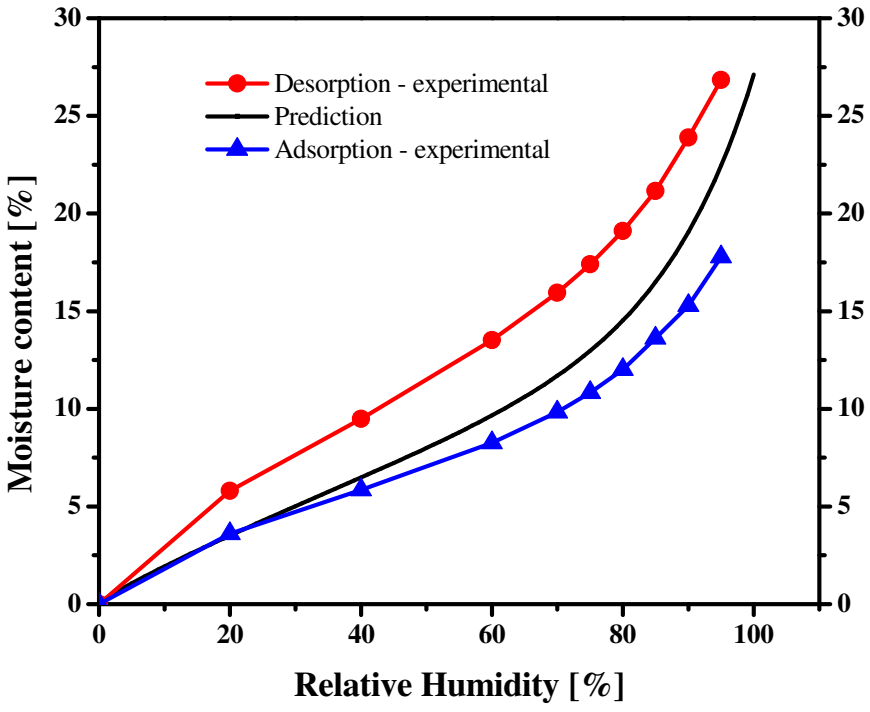

Figure 5.40 Prediction of sorption isotherm at 25^{0}C based on the TLS model of isotherms and the concept of SOC due to long range and slowly driven fluctuation of the second component moisture content

magnitudes of change in ambient conditions, the rate of change and mainly the magnitudes of hysteresis to capture the long-range and non-linear behaviour that may give rise to failures such as collapse of cell-walls or honeycomb.

Equation (3.78) is dynamical which implies that it gives a non-stationary moisture content that evolves with time in addition to its variation with the change of relative humidity due to hysteretic phenomena. Equation (3.78) is based on the premise that at large time limit the adsorption and desorption isotherms will be attracted to a single sorption isotherm predicted by it and sorption equilibrium is a quasi-static physical phenomenon. Summary of the validation tests of the TLS and SOC based prediction of equation (3.78) at 25 and 50^0C are given in Figure 5.40 and 5.41. Except the dynamical behaviour of the kinetics and non-

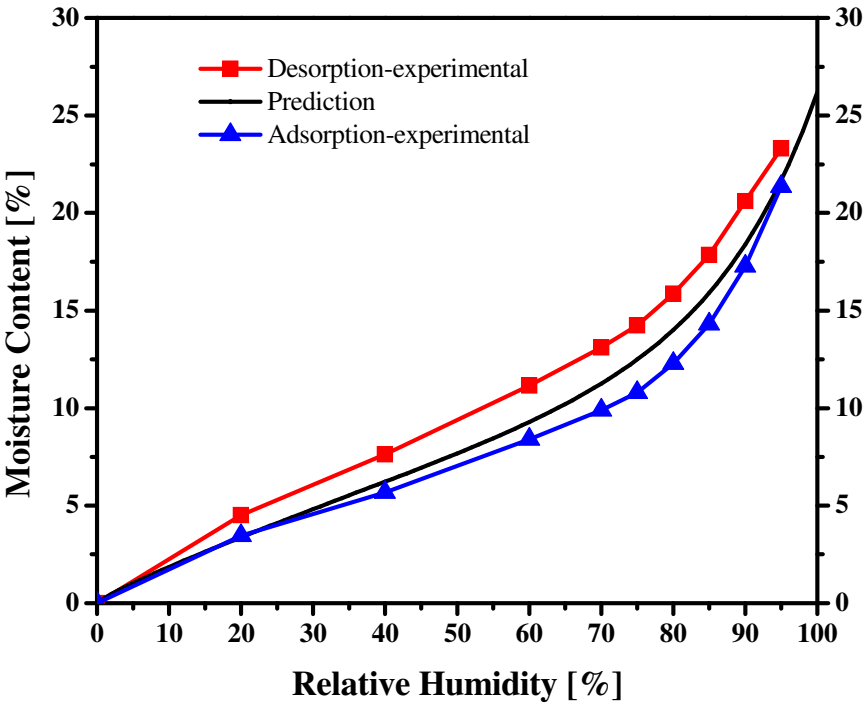

Figure 5.41 Prediction of sorption isotherms of Douglas-fir at 50^0C based on the TLS model of isotherms and the concept of SOC due to long range and slowly driven fluctuation of the second component moisture content

stationary nature of the boundary adsorption and desorption curves, the basic shape of sorption isotherm is type-II (sigmoid) both at 25 and 50^0C, in agreement with the IUPAC (1972) classification.

It is apparent that the mean sorption isotherm predicted by equation (3.78) resembles a scanning curve that started at equilibrium moisture content corresponding to 100% relative humidity and overlapped with the adsorption boundary curve at about 20% of relative humidity. The similarity and domain independent models of sorption hysteresis also predict that desorption scanning curves overlap with adsorption boundary curves if the wood is allowed to undergo a desorption to a moisture content corresponding to a relative humidity difference of more than 40% (Perlata, 1995; Peralta and Bangi, 1998). The conclusion of Peralta and Bangi (1998) was made from experimental evidence obtained with an assumption of stationary adsorption and desorption boundary curves. When the non-stationary behaviour is taken into consideration then the 40% relative humidity difference can be assumed to get larger and larger which ultimately will lead to reconciliation with the experimental evidence obtained in this study. Therefore, it is natural that the predicted mean sorption isotherm is close to the adsorption boundary curve at lower relative humidity ranges.

The parameter c_i of sorption isotherms depends on temperature and its general temperature dependence is given in Figure 5.42 for Douglas-fir. At lower temperature (25^0C) it displays wider dispersion while it becomes narrower as the temperature was increased to (50^0C). The dependence of parameter c_i on temperature can be described both by exponential and power law relation as our exploratory assessments made using FPL data with temperatures ranging from -1 to 127^0C show (Simpson and TenWolde, 1999). Latewood had significantly (p<0.05) higher value of c_i than earlywood and annual ring had an intermediate magnitude. Although exploratory modeling of the dependence of c_i on temperature obtained using FPL data show a strong correlation (r^2=0.9928) in the range 1.1 to 126.7^0C, this study did not found a significant difference in the magnitudes of c_i of Douglas-fir's annual ring when the temperature was changed from 25 to 50^0C as it is shown in Figure 5.43. When the temperature was increased from 25^0C to 50^0C, the dispersion in the mean magnitudes of c_i became narrower.

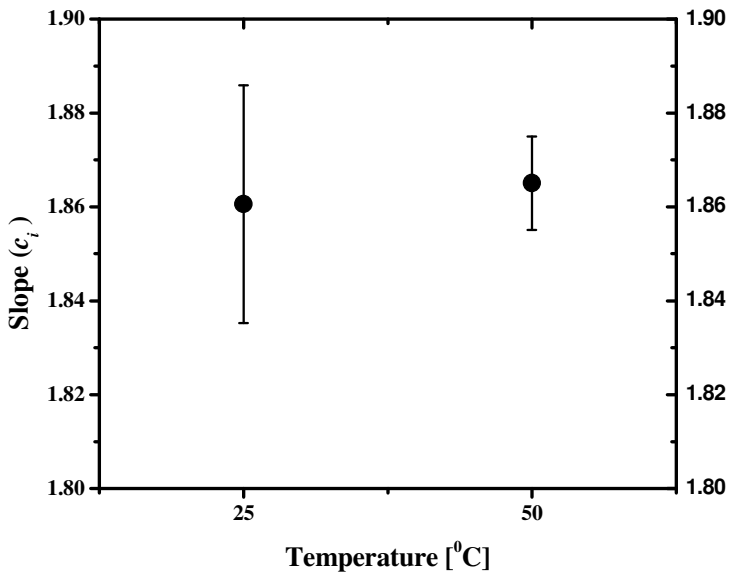

Figure 5.42 Dependence of parameter c_i of isotherms on temperature for Douglas-fir at 25 and 50^{0}C (Error bars indicate SEM)

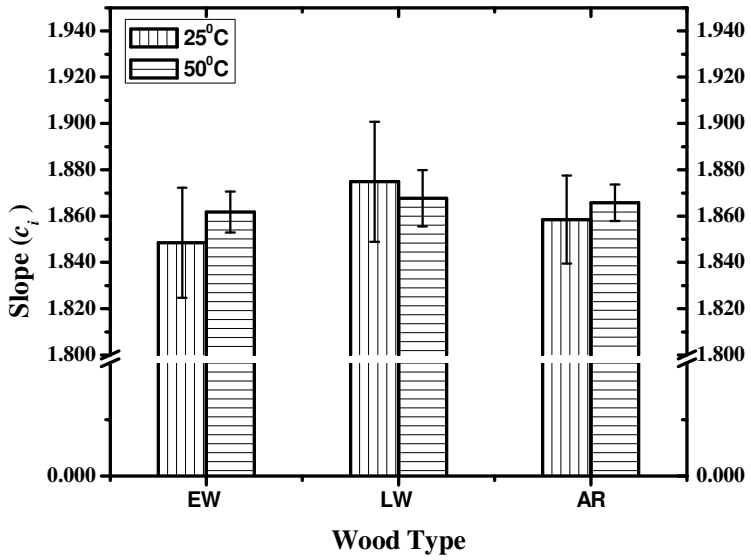

Figure 5.43 Dependence of parameter c_i of isotherms on temperature for earlywood, latewood and annual ring of Douglas-fir (Error bars indicate SEM)

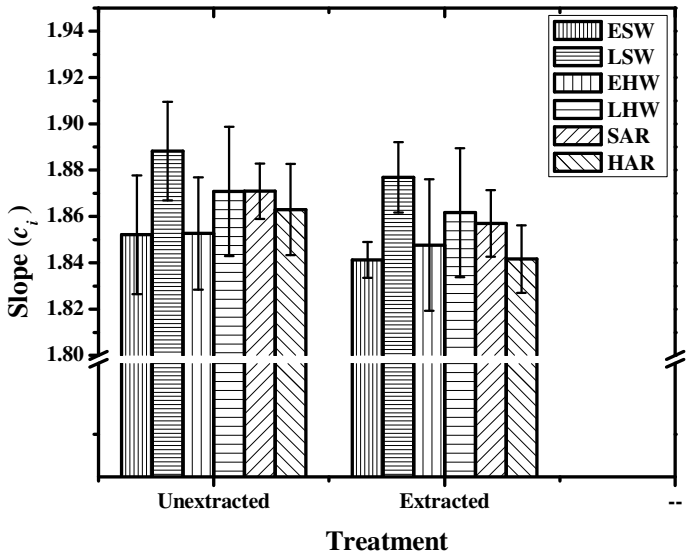

Figure 5.44 Dependence of parameter c_i of isotherms of earlywood, latewood and annual ring of Douglas-fir on extractive content removal at 25^0C (Error bars indicate SEM)

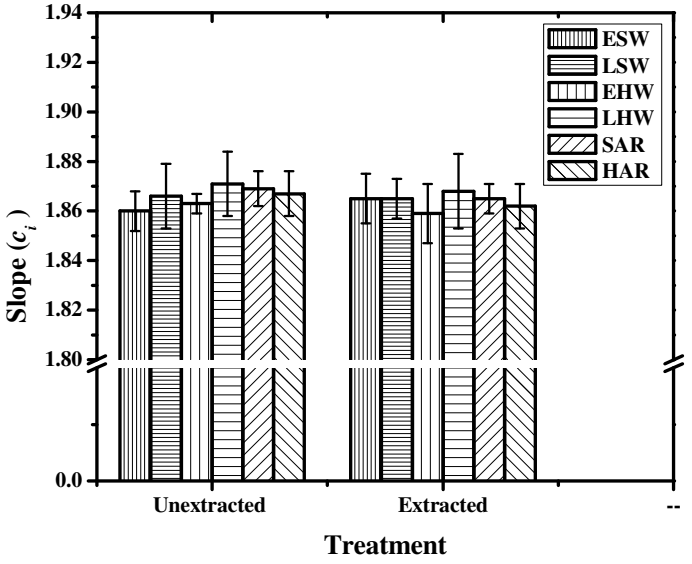

Figure 5.45 Dependence of parameter c_i of isotherms of earlywood, latewood and annual ring of Douglas-fir on extractive content removal at 50^0C (Error bars indicate SEM)

This can be linked to a decrease in magnitudes of sorption hysteresis. This implies that an increase in temperature may also cause sorption isotherms to converge to a single sorption isotherm. Therefore, at some higher temperature hysteresis may practically vanish. Figure 5.44 shows that extraction significantly (p<0.05) decreased the magnitude of sapwood c_i at 25^0C. However extraction affected the parameter c_i little at 50^0C and the general trend is shown in Figure 5.45.

Equation (3.78) can be used to compute surface area and fibre saturation points. It is well known that surface area is directly related to primary sorption sites that can be linked to hydroxyl groups which in turn can be related to chemical composition. First-component, second-component, fibre saturation point and internal specific surface area prediction for extracted and un-extracted Douglas-fir earlywood, latewood and annual rings were analyzed at 25 and 50^0C. Although the magnitudes of the first and second components increase as the relative humidity increases, the amount of moisture content that characterize wood as hygroscopic material with definite amount of sorption potential (sorption sites) should be constant. It is from this physical premise that the sorption parameters characterizing the specific internal surface area can be computed. The parameters are obtained when the terms in the exponent of equation (3.78) are minimized which is essentially equivalent to

$$\frac{\mathbf{1}}{\boldsymbol{\beta}} \cdot \boldsymbol{x} \cdot \boldsymbol{h} - \mathbf{1} = \mathbf{0} \tag{5.18}$$

From equation (5.18), the relative humidity at which the second-component becomes constant is obtained. Once the relative humidity is determined then it is substituted back into equation (3.78) to calculate moisture content. Computation of the specific surface area is finally performed according to the standard procedure of calculating surface area using the oven dry weight of wood and molecular weight of water (Sing 1985). In this research, there was no assumption how the water would bind to sorption sites. The developed model is heterogeneous that allows interaction of all length scale according to equations (3.61) to (3.64), but unlike the surface layering theories of sorption, it considers existence of two-

levels or components that are weakly interacting in all directions but are at the same time separable.

Generally, adsorption based computation of internal specific surface area is problematic since it is temperature dependent. This newly developed method is not tested for temperature dependent adsorption since the experimental data are obtained only at 25 and 50^0C. However, the internal specific surface area predictions obtained at 25^0C are close to the BET-based experimental measurements except in the case of earlywood values. The BET-based measurement showed that earlywood had up to two times internal specific surface area than latewood which on the basis of adsorption based argument becomes problematic since we do not have a twofold adsorption in earlywood than in latewood throughout the sorption isotherms. The BET-method and the measurement techniques, that use super-cooled liquid inert gas as surface probe molecules, are developed for high internal specific surface area ($>1 m^2g^{-1}$) materials which have higher importance in catalysis and the specimens are also made to undergo size reduction to the smallest size as possible. In the case of earlywood, the amount of probe molecules that are adsorbed on internal surfaces and those that are trapped in the pores may be comparable to cause inflated specific internal surface area. Table 5.14 shows that the new model prediction is not far from the one reported by Stamm (1964) which is $0.21 m^2g^{-1}$.

What is remarkable about the new model is that BET-based internal specific surface area measurements usually give a very high value due to the clustering effect of water molecules that causes high adsorption values. However, this is not the case for the new model. The internal specific surface area prediction of the new model should further be investigated for the optimum adsorption temperature that will give comparable results with the standard method. It is also commendable to investigate the applicability of high surface area methods for wood. Having in mind all the unfinished jobs with the internal specific surface area prediction of the new method, it is proper to discuss the values predicted at 25 and 50^0C. The model's predictions for earlywood and latewood of Douglas-fir are given in Table 5.14 and for extracted and un-extracted heartwood and sapwood of Douglas-fir in Figures 5.46 and 5.47, both at 25 and 50^0C.

Table 5.14 Internal specific surface area of Douglas-fir's earlywood and latewood based on the new model from water vapour adsorption and BET-internal surface from adsorption measurement using krypton as probe molecule

Wood type	Internal specific surface area [m^2g^{-1}]			
	The new model prediction		BET	
	Mean	SEM	Mean	SEM
Earlywood	0.19	0.02	0.60	0.05
Latewood	0.17	0.02	0.21	0.05

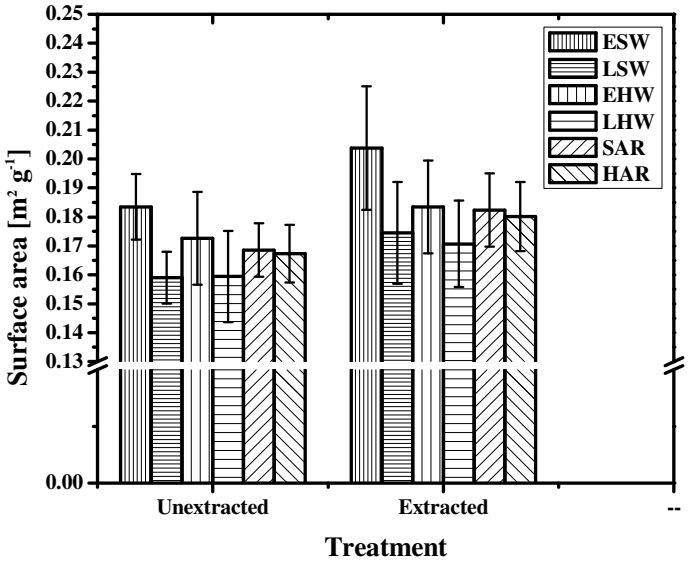

Figure 5.46 Dependence of Douglas-fir's internal specific surface area on un-extracted and extracted earlywood, latewood and annual ring of sapwood and heartwood based on adsorption at 25^0C (Error bars indicate SEM)

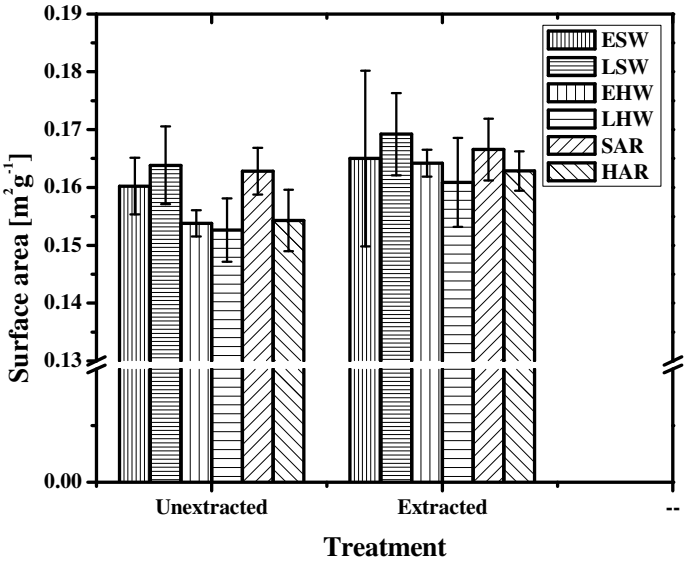

Figure 5.47 Dependence of Douglas-fir's internal specific surface area on un-extracted and extracted earlywood, latewood and annual ring of sapwood and heartwood based on adsorption 50^{0}C (Error bars indicate SEM)

Earlywood and sapwood had higher values for the internal specific surface area than latewood and heartwood. Extraction caused a significant (p<0.05) increase in the value of internal specific surface area both for sapwood and heartwood. The measurement at 50^{0}C may not be suitable for the purpose of internal specific surface area as the results are more chaotic.

Figures 5.48 and 5.49 show the dependence of the fractional moisture content at phase transition on wood type and extraction. Neither the differences between wood types nor the differences between un-extracted and extracted Douglas-fir were significant, and neither do the differences show a distinct regular pattern. This is perhaps due to the chaotic nature of physical properties at phase transition. Phenomena at phase transition are characterized by critical exponents and scaling behaviour, but it is rare to find single characteristic correlation length and properties are correlated at all length scales. Figure 5.49 shows at 25^{0}C

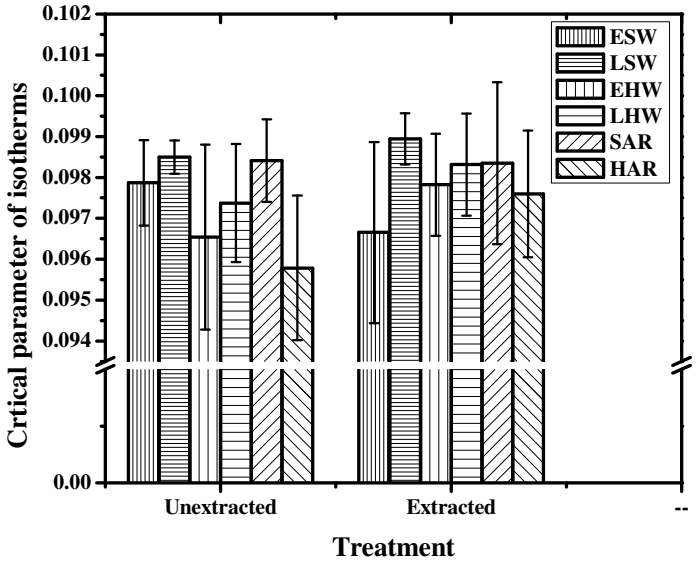

Figure 5.48 Dependence Douglas-fir's phase transition moisture weight fraction on un-extracted and extracted earlywood, latewood and annual ring of sapwood and heartwood at 25^0C (Error bars indicate SEM)

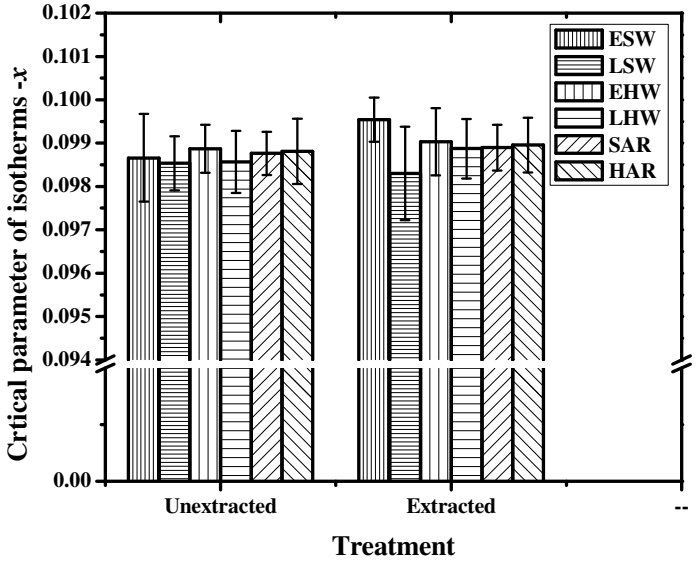

Figure 5.49 Dependence Douglas-fir's phase transition moisture weight fraction on un-extracted and extracted earlywood, latewood and annual ring of sapwood and heartwood at 50^0C (Error bars indicate SEM)

latewood revealed higher critical moisture weight fraction than earlywood and annual rings had intermediate magnitude; however, the differences remained statistically insignificant. Figure 5.50 shows that when the temperature was increased to 50^0C the differences almost vanished and the spread around mean values also narrowed. Generally, the experimental evidences imply that the critical moisture content can be a constant value that mainly depends on temperature. The dependence of the first component moisture on wood type, extraction and temperature are given in Figures 5.51 and 5.52. At 25^0C earlywood had higher first component moisture content than latewood with annual ring in the intermediate position. Sapwood also had higher first component than heartwood and the differences were significant (p<0.05) in all cases. While an increase in temperature caused a significant (p<0.05) decrease in the magnitude of the first component moisture content, extraction of the Douglas-fir specimens resulted in an increase at both 25 and 50^0C. Extraction of the specimens with acetone caused an increase in the dispersion of the mean values of first

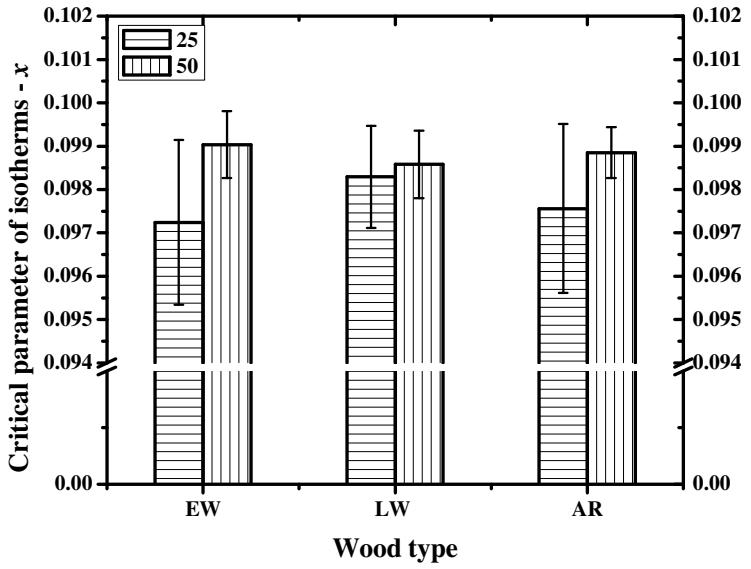

Figure 5.50 Dependence of Douglas-fir's phase transition moisture weight fraction on temperature for earlywood, latewood and annual ring (Error bars indicate SEM)

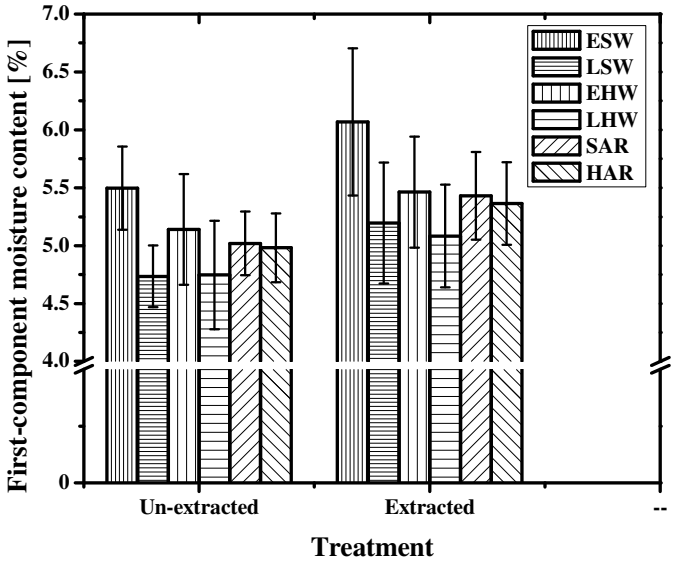

Figure 5.51 Dependence of Douglas-fir's first component moisture content on un-extracted and extracted earlywood, latewood and annual ring of sapwood and heartwood at 25^0C (Error bars indicate SEM)

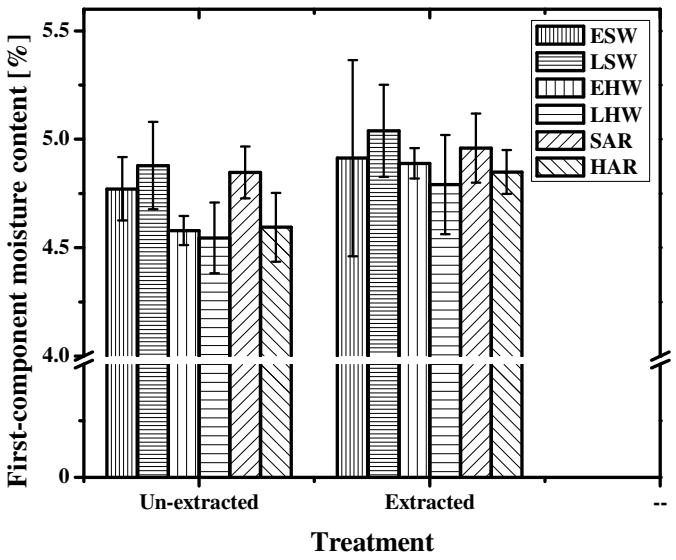

Figure 5.52 Dependence of Douglas-fir's first component moisture content on un-extracted and extracted earlywood, latewood and annual ring of sapwood and heartwood at 50^0C (Error bars indicate SEM)

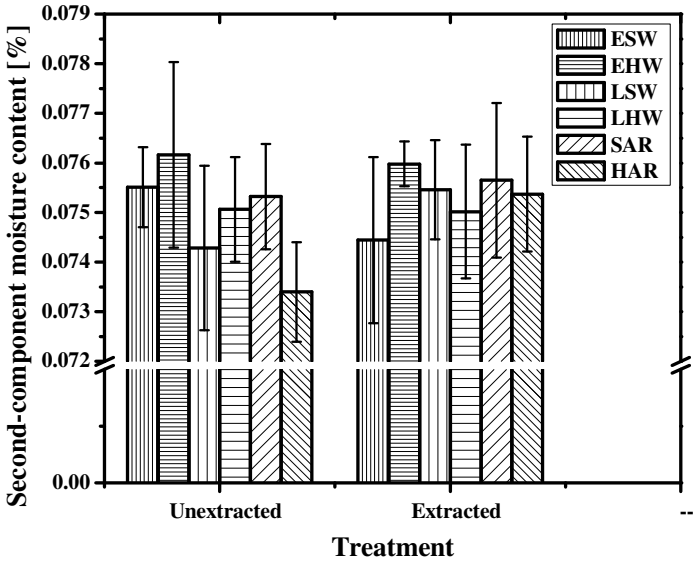

Figure 5.53 Dependence of Douglas-fir's second-component moisture content on un-extracted and extracted earlywood, latewood and annual ring of sapwood and heartwood at 25^0C (Error bars indicate SEM)

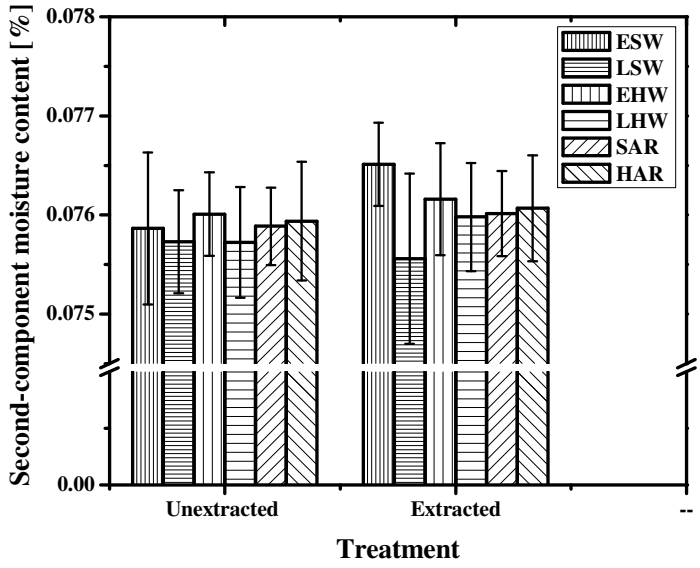

Figure 5.54 Dependence of Douglas-fir's second-component moisture content on un-extracted and extracted earlywood, latewood and annual ring of sapwood and heartwood at 50^0C (Error bars indicate SEM)

component moisture content and that is strongly displayed by sapwood. Although the differences were found to be statistically insignificant at 50^0C, late sapwood had higher first component moisture content than early sapwood.

The amount of second component moisture weight fraction when equation (3.78) becomes valid was also analyzed. The second component moisture content is actually a moisture content that becomes significant when the slippery road dominates as it was metaphorically discussed based on Figures 5.26 and 5.27. Statistical tests may not yield a reliable conclusion in this chaotic regime where there is correlation at all length scales, the variables can mutually depend on each other and the physical process is governed by power laws. Figures 5.53 and 5.54 show that, although the differences were statistically insignificant, earlywood had higher second component moisture content than latewood at 25^0C and early heartwood and late heartwood had higher second component moisture content than early sapwood and late sapwood, respectively. Extraction generally caused a minor increase in the magnitude of second component moisture content of Douglas-fir both at 25 and 50^0C. The same pattern in differences between wood types is observed at 50^0C as the one discussed for 25^0C, but the differences were narrower in the latter case.

Equation (3.78) predicts a fibre saturation point at 25^0C close to the values reported for Douglas-fir at 20^0C which was 28% (Alden 1997). The new model predicted mean fibre saturation point of Douglas-fir to be 28.49% at 25^0C, with minimum value of 25.53% for un-extracted heart annual ring and maximum value of 30.04% for extracted late sapwood, with extracted early sapwood closely following with a value of 29.64%. The half percent difference of the current mean fibre saturation point from earlier reports corresponds just to the equilibrium moisture content that is a result of a 5^0C difference in temperature (Simpson and TenWolde, 1999). Figures 5.55 and 5.56 show that extraction increased the fibre saturation point of Douglas-fir while an increase in temperature resulted in a decrease. The temperature dependence of sorption can be used to compute the heat of water vapour sorption in wood using equation (2.1) which gives the isosteric heat of sorption from isotherms measured at two temperatures at constant moisture content.

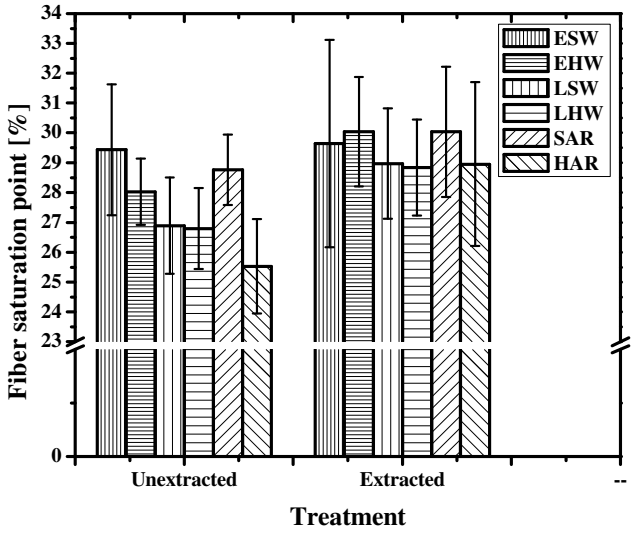

Figure 5.55 Dependence Douglas-fir's fibre saturation point on un-extracted and extracted earlywood, latewood and annual ring of sapwood and heartwood based on adsorption at 25^0C (Error bars indicate SEM)

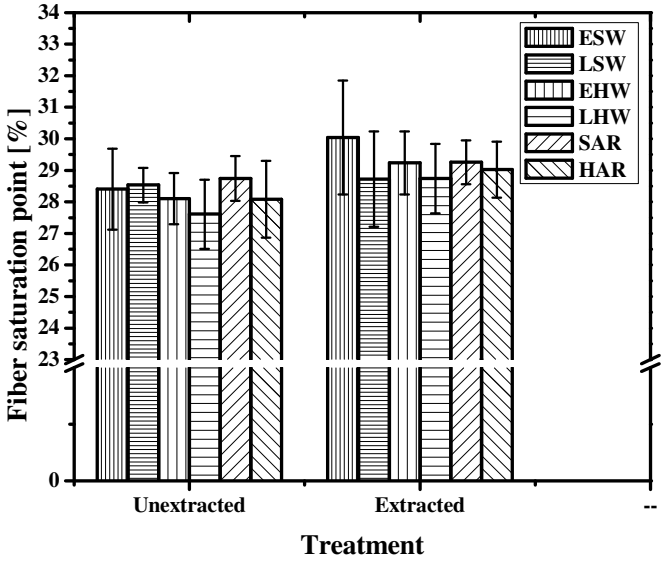

Figure 5.56 Dependence Douglas-fir's fibre saturation point on un-extracted and extracted earlywood, latewood and annual ring of sapwood and heartwood based on adsorption at 50^0C (Error bars indicate SEM)

The findings obtained so far in this study validate the two-level systems models of sorption kinetics and isotherms to be novel and sufficient that consider both the long and short range sorption mechanisms shown to be intrinsic to wood-water vapour interaction. The successful separation of components into two helps to better incorporate the effect of wood anatomical structure and chemical composition in complex sorption properties prediction models. Generally, the transversal anatomical diversity in Douglas-fir is found to be sufficient enough to render high resolution and sensitive experimental data that can be used to model and predict gross wood sorption properties. The experimental data and predicted parameters of the two-level models of sorption properties are used as input and outputs in the complex and unified modeling of sorption kinetics and isotherms for Douglas-fir.

Equation (3.78) describes sorption isotherms as non-stationary or quasi-equilibrium states of wood-water vapour interaction. It does not assume sorption to be dominated by only primary and secondary sorption site as do the majority of models of sorption isotherms and considers existence of interactions of all length scales in the complex wood-water vapour system. Therefore, it can be concluded that this study introduced a new direction in tackling the complex wood-water vapour interaction and presents an alternative approach that is based on states of criticality and phase transitions (Peralta, 1995 and 1996; Perlata and Bangi, 1998; Frandsen and Svensson, 2007, Frandsen *et al*, 2007).

5.3. Testing and validation of the two-level systems model of physical properties and chemical composition for Douglas-fir

The summary of results for the chemical composition of earlywood and latewood of sapwood and heartwood of Douglas-fir is presented first and followed by validation of the developed two-component and two-level self-organization model for the chemical composition and physical properties.

5.3.1. Statistical summary of chemical composition of Douglas-fir earlywood and latewood

The statistical summaries of the experimental measurements of chemical composition are given in Table 5.15 for cell-wall components and in Table 5.16 for extractive substances.

Sapwood latewood had significantly (p>0.05) higher mean glucose content and early heartwood the least. Xylose and galactose showed the reverse pattern as early heartwood had significantly (p>0.05) higher value and late sapwood the least. Significantly (p>0.05) higher amount of arabinose was found in early sapwood and the least in late heartwood. Considering an approximate estimation of cellulose content based on the relation given by Easty and Malcolm (1982) the mean cellulose content of Douglas-fir was 45.2%, slightly higher than the mean value of 42% given for softwood species. However, the mean values of cellulose content of earlywood and latewood obtained in this study are lower than those of earlier reports as summarized by Kennedy and Warren (1970).

The differences between earlywood and latewood are generally consistent with earlier reports given by Squire (1967) that concluded the difference between them to range from 1.7 to 5.4%. Early heartwood had the highest lignin content while late sapwood had the least. The mean values for lignin content of early sapwood and late heartwood were close to the mean value given for softwood species. Early heartwood had the highest extractive content while late sapwood had the least. Findings of earlier reports about the content of extractives in earlywood and latewood were not consistent. However, Douglas-fir latewood and heartwood had the highest extractive content in this study (Hale and Clermont, 1963; Campbell *et al*., 1965). The graphical summaries of measurement of the chemical composition are given in Figures 5.57 to 5.59

Table 5.15 Chemical composition of earlywood and latewood of sapwood and heartwood of Douglas-fir based on extractive free oven dry weight

Wood type	Arabinose [%]		Galactose [%]		Xylose [%]		Mannose [%]		Glucose [%]		AIL [%]		ASL [%]	
	Mean	SEM	Mean	SEM	Mean	SEM	Mean	SEM	Mean	SEM	Mean	SEM	Mean	SEM
ESW	1.6	0.6	2.1	0.8	2.9	1.0	11.8	2.2	50.0	4.9	29.8	3.1	0.3	0.1
LSW	1.4	0.6	1.6	0.2	1.9	1.0	13.8	0.8	54.8	4.6	25.5	4.2	0.3	0.1
EHW	1.2	0.4	3.4	0.8	3.3	1.5	12.7	2.5	43.2	2.3	34.2	1.4	0.3	0.0
LHW	0.9	0.1	2.3	0.3	2.7	1.1	12.8	1.9	48.0	2.7	31.6	2.8	0.3	0.0

Table 5.16 Extractives content of earlywood and latewood of sap-and heartwood of Douglas-fir obtained gravimetrically from passive extraction of specimens with 9:1 ratio of acetone and water for specific surface area measurement

Wood type	Extractives [%]	
	Mean	SEM
ESW	4.5	1.8
LSW	1.8	1.1
EHW	6.1	1.8
LHW	3.5	2.1

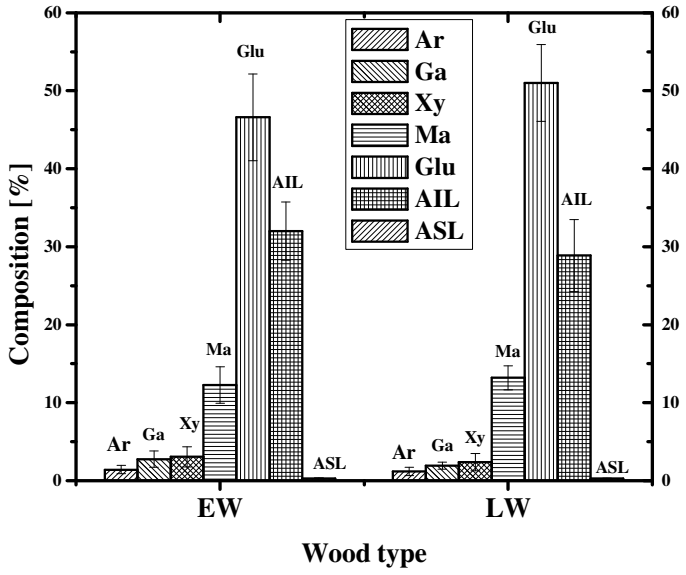

Figure 5.57 Cell-wall chemical composition of earlywood and latewood of Douglas-fir (Ar-Arabinose, Ga-galactose, Xy-Xylose, Ma-Mannose, Glu-Glucose, AIL-Acid insoluble lignin, ASL-Acid soluble lignin (Error bars indicate SEM)

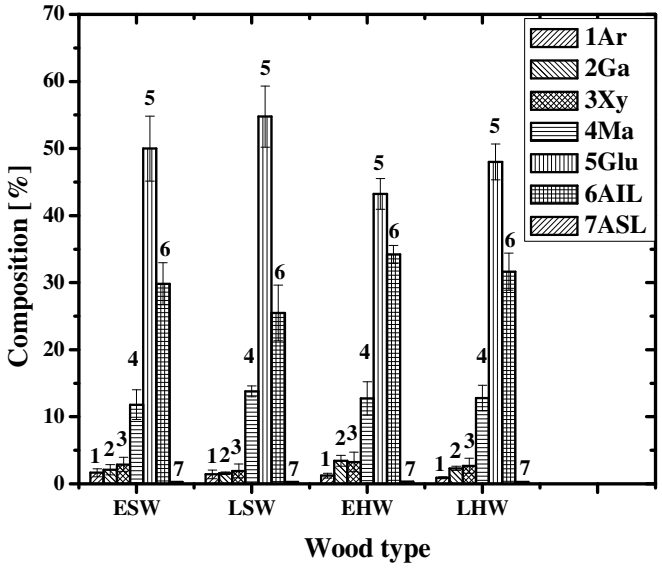

Figure 5.58 Cell-wall chemical composition of earlywood and latewood of sapwood and heartwood of Douglas-fir (Error bars indicate SEM)

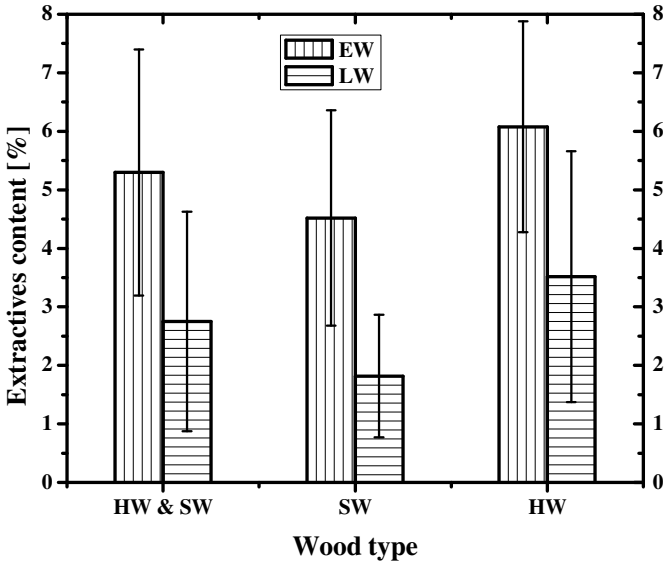

Figure 5.59 Extractives content of earlywood and latewood of sapwood and heartwood of Douglas-fir (Error bars indicate SEM)

5.3.2. Testing and validation of the two-level systems model of physical properties and chemical composition of Douglas-fir

The two-component and two-level self-organizing model of chemical composition that was derived and given by equation (3.82) and that utilizes equation (3.86) is tested and validated using data obtained from the experimental measurements presented in section 4.9. Chemical composition represents a state which had been a result of self-organizing criticality although as a frozen glassy state it may not undergo any further dynamic (time) evolution in composition. Therefore, the modeling is an attempt to reconstruct the dynamic mechanism that led to the formation of the final state of wood based on equation (3.82) and the allometric scaling properties that existed during wood formation assuming the phenomenon had been taking place in critical state or had been involving phase transitions. The concept is simple in a sense that the complex network of chemical components follows a simple renormalization scheme which can follow volume dependent scaling behaviour similar to the mechanism described by equations (2.14) and (2.15) as given by Gallos *et al.* (2007). Equations (2.14) and (2.15) describe a scaling behaviour that involves transport phenomena and their application to chemical composition is not direct. However, volume dependency of the mechanism is the footprint that transcends the state that can either be evolving or static. The concept attempted to be intuitive with metaphorical discourse to biological reproduction in the appendix.

It is perhaps the simplest to consider density and weight which are used to quantify physical properties and chemical composition. Hence, basic density (weight of oven dried wood per its green volume) was used to describe the inactive (ground or first) level and the first component in equations (3.82) and (3.86). The second component was chemical composition which was either evolving based on equation (3.82) or was describing the critical state with a scaling behaviour given by equation (3.86). All sets of exponents for both equations were computed based on experimentally obtained densitometry and chemical composition data. It is well known that there are three major cell-wall components, namely, cellulose, hemicelluloses and lignin. Hemicelluloses are diverse and there are many random possibilities according to which they would renormalize or coarse-grain as one component if they are wanted to form the second or active component of the model. As it was discussed

during derivation of equation (3.82) or (3.86) nesting of components is allowed provided that the two-component concept is preserved. The two component renormalization was done by adding glucose and mannose together to form one of the two-components of carbohydrates while the rest of hemicelluloses are made to form the second component. Since mannose mainly exists as glucomanan it was decided that its weight fraction be added to glucan. The product of glucan and mannose with the rest of hemicelluloses then formed one of the components that were allowed to interact with lignin in the two component concept of the cell-wall. The final carbohydrate-lignin component then formed the active level or state while basic density was assumed to represent the inactive or ground state of equation (3.86).

The TLS of basic density and chemical composition, exponents named as b, b_1 and b_2 were generated based on the two-component coarse-graining from which were then obtained other exponents named as b_n and d_f. The values of $-b$, b_1 and b_2 generated for TLS combinations discussed are given in Table 5.17, and the plots of b_2 versus $-b$ is given in Figure 5.60. Table 5.18 and Figure 5.60 show the scaling behaviour of the deviation or fluctuations from the maximum magnitude (b_f) and it is apparent that the b_f exponents generated for b_1 values

Table 5.17 Magnitude of Douglas-fir's self-organizing criticality exponent $-b$ for b_1=3 and changing value of b_2

b_2	Value of $-b$ for b_1=3		
	$-b$	amplitude	r^2
1	0.66	6.75	0.9688
2	0.79	4.61	0.9699
3	0.94	2.92	0.9886
4	1.10	2.12	0.9929
5	1.15	1.54	0.9884
6	1.59	1.23	0.9906
7	1.59	1.23	0.9910
8	1.52	1.44	0.9875
9	1.58	1.26	0.9843
10	1.55	1.34	0.9839
11	1.52	1.45	0.9817
12	1.85	3.69	0.9972
13	1.84	3.73	0.9972
14	1.82	3.87	0.9964

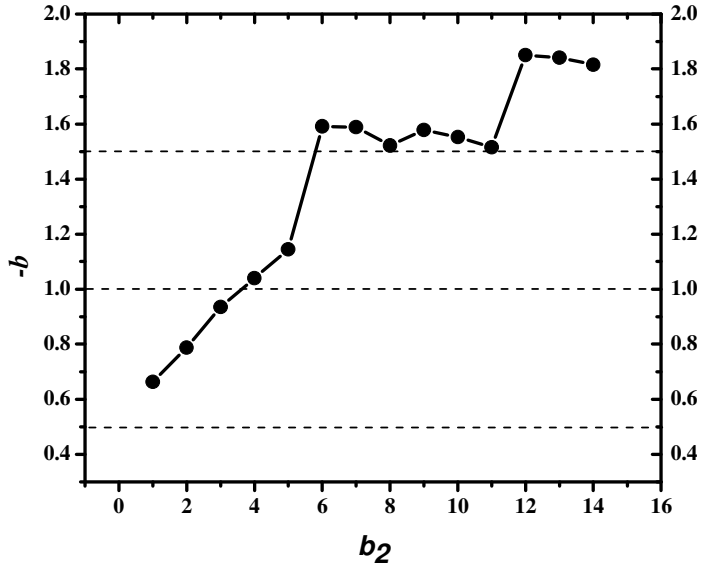

Figure 5.60 Dependence of the TLS exponent on b_2 for Douglas-fir. It is noticeable that the TLS system is limited with a maximum magnitude of b_2 around six that readily makes the SOC range to be -0.5 to -1.5 that well agrees with pink noise

Table 5.18 Scaling exponent of the probability distribution of the maximum deviation or fluctuation depending on the magnitude of b_1 and b_2 of Douglas-fir

b_2	b_f values for b_1=2 to 5							
	b_1=2		b_1=3		b_1=4		b_1=5	
	b_f	r^2	b_f	r^2	b_f	r^2	b_f	r^2
1	1.82	0.9683	2.22	0.9768	2.85	0.9778	3.70	0.9787
2	2.84	0.9773	3.77	0.9613	4.31	0.9722	4.66	0.9673
3	4.88	0.9817	5.28	0.9679	5.47	0.9797	5.97	0.9773
4	6.33	0.9964	6.16	0.9893	5.99	0.9795	5.99	0.9834
5	7.63	0.9950	7.63	0.9950	7.62	0.9916	7.47	0.9832
6	9.78	0.9971	9.67	0.9941	9.67	0.9941	8.51	0.9911
7	9.78	0.9971	11.41	0.9970	11.3	0.9939	9.67	0.9941
8	9.78	0.9971	11.41	0.9970	11.41	0.9970	11.3	0.9939
9	11.41	0.9970	11.41	0.9970	11.41	0.9970	11.41	0.9970
10	11.41	0.9970	14.18	0.9970	11.41	0.9970	11.41	0.9970
11	11.41	0.9970	14.18	0.9970	14.18	0.9970	11.41	0.9970
12	11.41	0.9970	14.18	0.9970	14.18	0.9970	14.18	0.9970
13	11.41	0.9970	14.18	0.9970	14.18	0.9970	14.18	0.9970
14	11.41	0.9970	14.18	0.9970	14.18	0.9970	14.18	0.9970

ranging from one to four collapsed to a single power law curve for the b_2 value of up to seven. A dashed line with inwardly pointing arrows is given to guide the eyes parallel to an imaginary line to which all of the b_f curves are assumed to collapse in the narrow b_2 range of one to seven. The sameness of the intermediate gradient or the slope of the trajectory curves can be visualized better in Figure 5.62 on which the magnitudes of b_2 and b_f are normalized by their respective maximum values. It can be noticed that that for b_1 values greater than four the slope changes dramatically if the b_2 values are also greater than four while the initial gradients of all trajectories collapse to the same curve. The self-organizing criticality exponents plotted in Figure 5.60, and which are also given in Table 5.17, were obtained by using a b_1 value of three. The choice of this value is justified further by physically motivated phenomena (entropy of cavity radiation) based on the plots given in Figures 5.63 and 5.64.

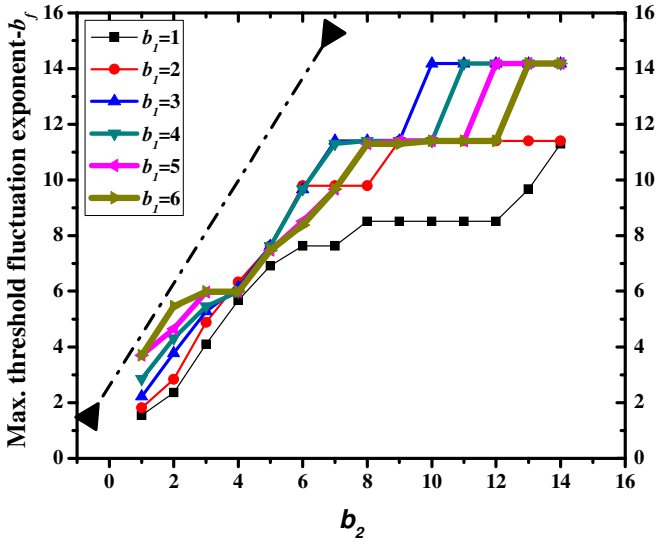

Figure 5.61 Dependence of the scaling exponent of the probability distribution of the maximum deviation or fluctuation (b_f) for Douglas-fir depending on the magnitude of b_2 for b_1 values ranging from 1 to 6

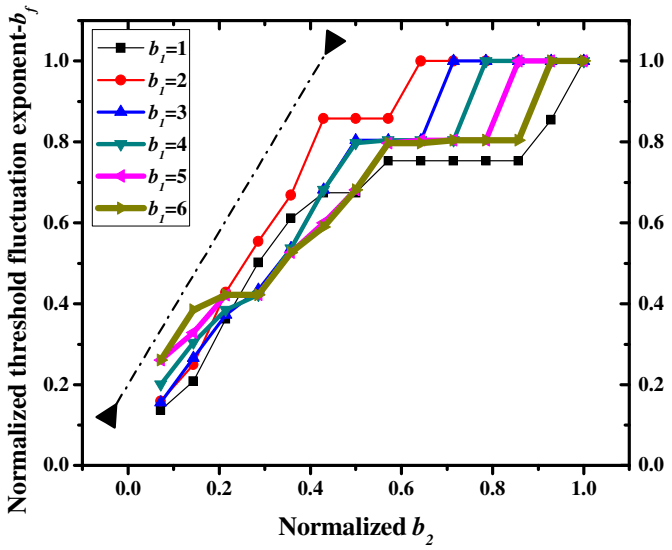

Figure 5.62 Dependence of the normalized scaling exponent of the probability distribution of the maximum deviation or fluctuation (b_f) for Douglas-fir depending on the normalized magnitude of b_2 for b_1 values ranging from 1 to 6

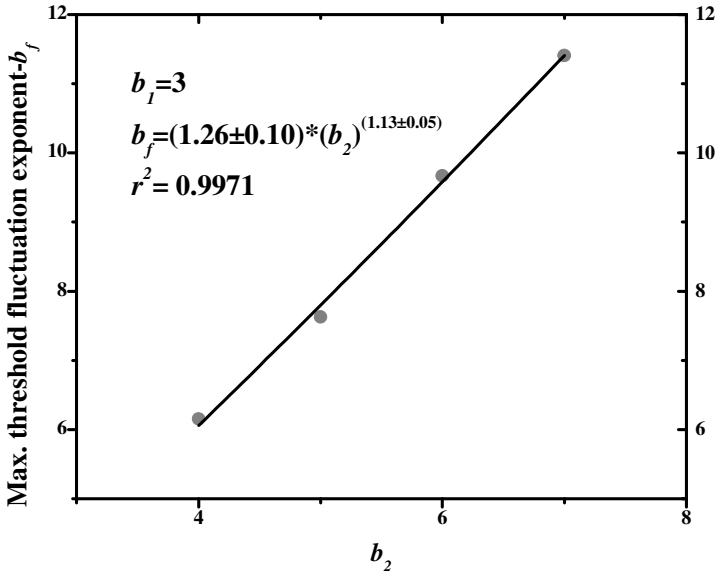

Figure 5.63 Dependence of the scaling exponent of the probability distribution of the maximum deviation or fluctuation (b_f) for Douglas-fir on the magnitude of b_2 for values ranging from 4 to 7 and constant b_1 value of 3

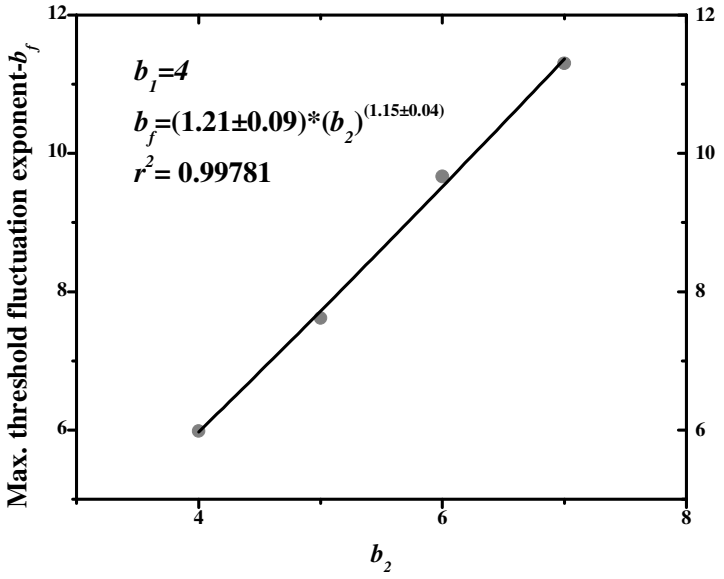

Figure 5.64 Dependence of the scaling exponent of the probability distribution of the maximum deviation or fluctuation (b_f) for Douglas-fir on the magnitude of b_2 for values ranging from 4 to 7 and constant b_1 value of 4

The equation of the plot given in Figure 5.63 can be generalized for Douglas-fir to the form given in equation (5.19) which has also been utilized in the two-component modeling of sorption in equation (5.16) as an entropy analog that can globally be used to impart thermodynamic based physical meaning to the scaling behaviour.

$$b_f = \frac{4}{3} b_2^{b_n} \tag{5.19}$$

It can be seen that the exponent for the scaling function with b_1 having a magnitude of three is more close to one as b_n value than the scaling exponent given for b_f in Figure 5.64, which is a scaling function with an exponent b_n for corresponding magnitude of four for b_1. The more the exponent approaches one the more the value of the amplitude approaches the value of $4/3$. If this is the case, then b_2 is a physical parameter that gives the internal energy content per unit of cubic volume. In equation (5.19) the integration constant (the intercept) is zero and hence the scaling function is homogeneous resulting in a rare and simple allometric scaling model. Tekleyohannes and Avramidis (2009) have shown that in most of the

considered cases of TLS combination of physical properties and chemical composition, the suitable values of b_2 were found to be not much beyond a value of ten. This is also shown to hold true in this study in Figure 5.61 where it appears to be a system cut off for values far greater than ten.

The obtained TLS scaling behaviour is related to the classical biological allometry. Therefore, it was applied in the subsequent part by utilizing the TLS modeling of chemical composition and physical properties of Douglas-fir to predict the first component of the two-level sorption model from chemical composition and basic density. The concept is implemented with an assumption that a TLS of chemical composition and physical properties which have prevailing behaviours that obey power law dependence can have an integrated and simple scaling property given by equation (3.86). This can be shown by demonstrating the prediction capability of equation (3.86) against some dependence between percentage composition of one of the carbohydrates, preferably glucose, and physical properties such as basic density or the first component of the two-level sorption. Figure 5.65 presents the linear regression interpolation/prediction of glucose content from basic density of earlywood and latewood of Douglas-fir. From Figure 5.65 it is evident that most of the strength in the already weak correlation may have come from the difference between the glucose content of earlywood and latewood, and if for example the dependence of earlywood glucose content is considered separately, then basic density alone becomes a very weak predictor for glucose. However, when the percentage chemical composition was used to construct a TLS based on equations (3.83) and (3.86) then the plot given in Figure 5.66 was obtained. Use of equation (3.78) for the prediction of the first component moisture content revealed a remarkable result when b_f was obtained through power law dependence between b_1 and changing the value of b_2 as the integrated scaling exponent of equation (3.86). The exponent was found to be equal in magnitude to 0.27 which is very close to 0.25 ($1/4$). The $1/4$ value is the quarter allometric scaling exponent that relates body mass or biomass to metabolic basal activities of living things (West *et al*., 1999; Brown and West, 2000). With a remarkable agreement to the Sierpinski gasket analogy given to demonstrate the physical process that ranges from unification to invariance (identity), the self-organizing criticality exponent at the

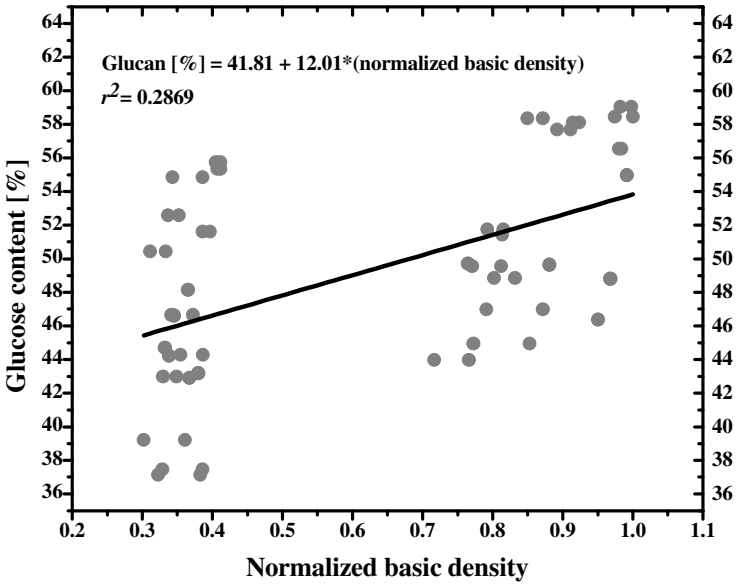

Figure 5.65 Possible linear empirical prediction of glucan from basic density of early and latewood of Douglas-fir

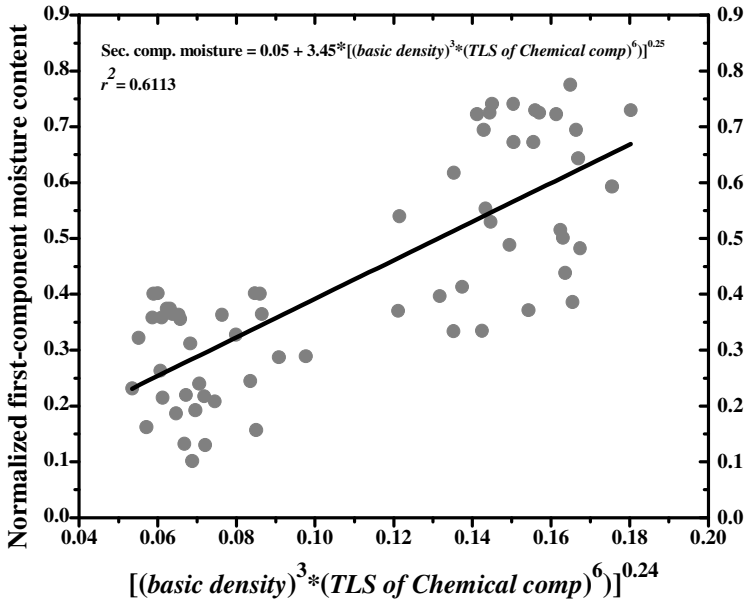

Figure 5.66 Prediction of the first component moisture content based on TLS model of chemical composition and basic density with the regression equation being as follow:

$$Sec.\ comp.\ moisture = 0.05 + 3.45 \cdot [(basic\ density)^3 \cdot (TLS\ of\ chem\ comp)^6]^{0.25}$$

highest order of dimensionality b_n of the two component and two-levels scaling relation given by equation (3.86) is found to be identical to the fractal dimensionality of the Sierpinski gasket in two dimensions $\{ln(3)/ln(2)=1.59\}$. The order dimensionality of the two-component and two-level scaling can be obtained from the plot in Figure 5.60 that shows the dependence of $-b$ on b_2. When the b_2 value attained a magnitude of six, the $-b$ value was 1.59 and further increments in the magnitude of b_2 were not able to show any significant difference from 1.59. Hence, the value of $-b$ for Douglas-fir was 1.59 which is exactly the same as the fractal dimensionality of the Sierpinski gasket in two-dimensions that can readily enable the generalization of the two-component and two-level systems to n-components and n-level systems.

$$\boldsymbol{b_n = -\frac{ln(n+1)}{ln(2)}} \tag{5.20}$$

where b_n becomes the self-organizing criticality exponent of the n-level or n-component system. However, the self-organizing exponents of various systems quantified so far do not go far beyond a magnitude of three. In that case, it is not practical to consider the value of n beyond seven for which b_n exactly equals to three. Accepting the maximum magnitude of n to be seven agrees well with the data of Douglas-fir shown in Figures 5.61 and 5.62. It is noticeable that there is a system cut-off for n beyond the magnitude of six which is a value not much far from seven and the system itself remains practically constant for n greater than six. It may also be useful to point out that the number of self-avoiding walks (SAW) rooted at similarity or diversity and directed to identity is ten, provided the walk is performed by excluding the similarity vertex when the walk was originating from the diversity one and vice versa, then the number of SAW becomes seven. These coincidental numerical values are quite intriguing as they are also close to system limiting (cut-off) magnitudes and consequently the TLS interaction coarse-graining framework of the Sierpinski gasket becomes more relevant. The Sierpinski gasket analogy of Figure A.1 elegantly illustrates the dynamics of interaction in a two-level and two-component system. However, one of the physical significance of describing a physical mechanism on the Sierpinski gasket is the self-similarity resulting from repeated division of sides of the equilateral triangles into two and

connecting the midpoints to each other. Geometrically, the result is obvious and the scaling dimension is already discussed. But what come as intermediates between similarity and unity, similarity and complexity, complexity and diversity, diversity and integrity, integrity and identity, unity and identity? Or are they the smallest fundamental units of interaction defined by the Sierpinski gasket? Can the walk from vertices of similarity and diversity to unity be random or even anomalous? These are legitimate scientific questions that would be born in mind, but for this study, the walk is assumed to be rooted and directed and the triangles are the smallest fundamental frameworks of interaction. As it is shown in Figure A.1, the Sierpinski gasket laterally gives the interacting components while a vertical placement on it gives levels as emergent properties of laterally interacting components.

If equation (5.20) is to be restricted to pink noise as a form of self-organizing criticality as described by Bak *et al*. (1987 and 1988) then it is clear that it shall be modified to the form given in equation (5.21) which converges to a magnitude of one for larger values of *n* while at the same time satisfying equation (5.20) for *n* with a value of two.

$$\boldsymbol{b} = -\frac{\boldsymbol{ln(n+1)}}{\boldsymbol{ln(n)}} \tag{5.21}$$

Equation (5.21) makes the extension of equation (5.20) to *n* components more complete and for *n* equal to one equation (5.21) predicts an infinite dimension making the two-component system the smallest to be valid. Self-organizing criticality is the property of many component complex systems and consideration of large *n* is a necessary condition for the sake of generality. Based on validation results obtained from Douglas-fir, equation (5.21) could be taken as a new definition for self-organizing criticality in general and particularly for wood properties and chemical composition which could also be similarly applied to any physical, chemical or biological systems.

Tekleyohannes and Avramidis (2009) have shown that the scaling between shrinkage in softwoods and TLS combination of basic density with carbohydrates and lignin is governed by a scaling exponent close to $1/3$ (a value different from $1/4$). The first component moisture

content can be seen in light of a physical phenomenon resulting from mass transport in vascular plant tissues as given by West *et al*. (1999) and hence the correctness of the close to quarter scaling exponent obtained in this study can implicitly be accepted as if it is equivalent to biological allometry. On the other hand, the ⅓ scaling exponent obtained by Tekleyohannes and Avramidis (2009) can have a lot to do with volumetric dependence of shrinkage on the TLS combinations of wood constituents. If the mean magnitude of shrinkage is considered as a physical phenomenon equivalent to swelling of wood in which a sorption site is randomly occupied by water vapour molecules from which follows consideration of a shrinkage as a process of proportionately and randomly vacating occupied sorption sites then, the one third (⅓) scaling exponent becomes equivalent to the first time scaling exponent obtained for a random walker to return to his origin as described by Havlin and Ben-Avraham (2002) based on a spherical diffusion front. Therefore, the TLS modeling of chemical composition and physical properties of wood can generally be regarded as an allometric scaling which has arisen from the dynamical physical mechanism of self-organization. The direct consequence of this study is the capability to describe the physical properties and chemical composition of Douglas-fir wood with simple scaling laws while the global consequence is an explanation for the mechanism that gives rise to the allometric scaling behaviour in timber species (biomaterials to biological systems) which would contribute to rendering explanation to the lacking theoretical foundation.

5.4. Development, testing and validation of the ANNs sorption properties models for Douglas fir

5.4.1. Input and output transformation and selection

A total of fifteen nonlinear and one linear function were allowed to be selected by the genetic algorithm as input and output transformation functions. The maximum number of best transfer functions selected from the pool was a maximum of six per input and one for each output. Depending on the category of inputs given in section 3.4, they were selected at least once or rejected as a whole due to low fitness. Inputs were rejected when any of their transforms were not able to fulfill the fitness criterion. Based on the category of modeling to which the inputs belonged to and their type, up to six transforms were selected mainly for

Table 5.19 Inputs and outputs linear and nonlinear transforms used in the development of ANNs models for prediction of carbohydrates and lignin content from anatomical and physical properties of Douglas-fir wood

Inputs transformation						Outputs transformations		
Anatomical and physical properties			TLS of chemical composition			Outputs		
Input		Inputs transforms	Input	Number	Inputs transform	Input	Number	Transforms
Wood type	6	String	Chem-TLS	3	Linear, fourth power, tanh	Arabinose	1	Log
m_f/m_i	5	Linear, tanh, squared, fuzzy left, fuzzy right	C-TLS-NT1	3	Linear, inv. of square root, inv	Galactose	1	Fourth power
H	3	Linear, log, inverse	C-TLS-NT2	3	Linear, log, square root	Glucose	1	Squared power
T	1	Logical	C-TLS-NT3	3	square root, linear, ln(x/(1-x))	Xylose	1	Squared power
Ring no.	3	Linear, square root, ln(x/(1-x))	C-TLS-NT4	3	Linear, inv. of square root, inv.	Mannose	1	Squared power
Width	4	Linear, exponential, tanh, fuzzy left	C-TLS-NT5	3	Linear, log, square root	AIL	1	Squared power
Density	4	Linear, square root, ln(x/(1-x)),fuzzy left	C-TLS-NT6	3	Linear, inv. of square root, inv.	ASL	1	Linear
GRV	4	Linear, log log,log fuzzy right	C-TLS-NT7	3	square root, linear, ln(x/(1-x))			
GRV_c	4	Linear, log log, inverse of fourth root, fuzzy right	C-TLS-NT8	3	Linear, square root, ln(x/(1-x))			
5S-GRV_c	3	Linear, log log, inverse of the fourth root						

Table 5.20 Inputs and outputs linear and nonlinear transforms used in the development of ANNs models for prediction of parameters of the TLS sorption prediction models for Douglas-fir earlywood, latewood and annual rings

Inputs transformation						Outputs transformations		
Anatomical and physical properties			Chemical composition and TLS			Outputs		
Input	Number	Inputs transforms	Input	Number	Inputs transform	Input	Number	Inputs transforms
m_f/m_i	5	Linear, tanh, squared power, fuzzy left, fuzzy right	Chem-TLS	3	Linear, fourth power, tanh	BET-area	1	Squared power
H	3	Linear, log, inv.	C-TLS-TN_1	3	Linear, inv. of square root, inv.	x	1	Fourth root
T	1	Logical	C-TLS-TN_2	3	Linear, log, square root	c_k	1	Exponential
Wood type	6	String	C-TLS-TN_3	3	Square root, linear, ln(x/(1-x))	M	1	Squared power
Ring number	3	Linear, square root, ln(x/(1-x))	C-TLS-TN_4	3	Linear, inv. of square root			
Width	4	Linear, exponential, tanh, fuzzy left	C-TLS-TN_5	3	Linear, log, square root			
Density	4	Linear, square root, ln(x/(1-x)), fuzzy left	C-TLS-TN_6	3	Linear, inv. of square root, inv.			
GRV	4	Linear, log log, log, fuzzy right	C-TLS-TN_7	3	Square root, linear, ln(x/(1-x))			
GRV_c	4	Linear, log log, inv. of the fourth root, fuzzy right	C-TLS-TN_8	3	Linear, square root, ln(x/(1-x))			
5S-GRV_c	3	Linear, log log, inv. of the fourth root	Arabinose	3	Linear, inv., log			
			Galactose	3	Linear, tanh, fourth power			
			Glucose	3	Linear, squared, tanh			
			Xylose	3	Linear, squared, tanh			
			Mannose	3	Linear, squared, tanh			
			AIL	3	Linear, log, squared power			
			ASL	3	Log, squared power, linear			

Table 5.21 Inputs and outputs linear and nonlinear transforms used in the development of ANNs models for prediction of sorption isotherms points, diffusion coefficient and surface emission coefficient Douglas-fir

The comprehensive inputs transformation obtained						Outputs transformations		
Anatomical, physical and chemical composition			Small specimens sorption			Outputs		
Input	Number	Inputs transforms	Input	Number	Inputs transform	outputs	Number	Inputs transforms
m_f/m_i	4	Linear, squared, fuzzy left, fuzzy right	BET-area	3	Linear, squared, fuzzy left	M	1	Squared power
H	2	Linear, inverse	Surface area	4	Linear, tanh, fuzzy left, fuzzy right	D	1	Exponential
T	1	Logical	H-Mono	4	Linear, tanh, fuzzy left, fuzzy right	S	1	Exponential
Wood type	6	Logical 1 to 6	M-Mono	4	Linear, tanh, fuzzy left, fuzzy right			
Ring no	2	Linear, ln x/(1-x)	M-poly	3	Linear, tanh, fuzzy right			
Width	3	Linear, tanh, fuzzy left	M-Integrated	4	Linear, tanh, fuzzy left, fuzzy right			
Density	3	Linear, ln x/(1-x), fuzzy left	FSP	3	Linear, tanh, fuzzy right			
GRV	3	Linear, log, fuzzy right	*x*	3	Linear, log, fuzzy right			
GRV_c	3	Linear, log log, fuzzy right	*x*-NT_2 to NT_6	3x5	Linear, log, fuzzy right			
5S-GRV_c	3	Linear, log, log, fuzzy right	*x*-NT_7 to NT_8	2x2	Linear, log			
Chem-TLS	2	Linear, tanh	*x*-NT_9	3	Linear, log, fuzzy right			
C-TLS-T1	2	Linear, inverse	i	3	Linear, tanh, fuzzy right			
C-TLS-T2	2	Linear, square root	i-NT_1 to NT_3	3x3	Linear, tanh, fuzzy right			
C-TLS-T3	2	Linear, ln x/(1-x)	i-NT_4	2	Linear, tanh			
C-TLS-T4	2	Linear, inverse	i-NT_5	4	Linear, tanh, fuzzy right, fuzzy left			
C-TLS-T5	2	Linear, square root	i-NT_6	3	Linear, inverse squared, fuzzy right			
C-TLS-T6	2	Linear, inverse	i-NT_7	2	Linear, tanh			
C-TLS-T7	2	Linear, ln x/(1-x)	i-NT_8	3x2	Linear, tanh, fuzzy right			
C-TLS-T8	2	Linear, ln x/(1-x)	c_k	3	Linear, tanh, fuzzy right			
Arabinose	2	Linear, log	c_k -NT_1	2	Linear, tanh			
Galactose	2	Linear, tanh	c_k -NT_2	3	Linear, squared, fuzzy left			
Glucose	2	Linear, tanh	c_{k-}-NT_3	4	Linear, tanh, fuzzy left, fuzzy right			
Xylose	2	Linear, tanh	c_k -NT_4	3	Linear, tanh, fuzzy right			
Mannose	2	Linear, tanh	c_k -NT_5	4x4	Linear, squared, fuzzy right, fuzzy left			
AIL	2	Linear, squared	c_k -NT_9	3	Linear, tanh fuzzy left			
ASL	2	Linear, squared	t-exp	4	Linear, squared, fuzzy right, fuzzy left			
			t-exp-NT_1 to NT_2	4x2	Linear, squared, fuzzy right, fuzzy left			
			t-exp-NT_3	3	Linear, tanh fuzzy left			
			t-exp-NT4	4	Linear, squared, fuzzy right, fuzzy left			
			t-exp-NT_5 to NT_9	3x4	Linear, tanh, fuzzy left			
			L_1	4	Linear, tanh, fuzzy right, fuzzy left			
			L_1-NT_1	3	Linear, tanh, fuzzy right			
			L_1-NT_2 to NT_4	2x3	Linear, tanh			
			L_1-NT_5	4	Linear, tanh, fuzzy right, fuzzy left			
			L_1-NT_6	2	Linear, tanh			
			L_1-NT_7 to NT_9	3x3	Linear, tanh, fuzzy right			
			c_i	3	Linear, squared, tanh			

wood type, since it had to be comprised of at least earlywood and latewood both for heartwood and sapwood. This means that, in some cases it was necessary to use multiple linear and nonlinear transforms of one and the same input in order to obtain best fitness. This unfortunately increased the network size in many cases making models prone to over-fitting. The transforms applied at the three levels of modeling, namely, prediction of carbohydrates and lignin, prediction of small specimen sorption and Douglas-fir gross wood sorption are summarized in Tables 5.19 to 5.21.

Different transforms were found to be efficient in incorporating nonlinearity in one and the same input based on the initial conditions of the variable selection genetic algorithm. This can be easily seen in Tables 5.19, 5.20 and 5.21 from the transforms applied on GRV, GRV_c and 5S-GRV_c. The same fact can be observed for neighbouring TLS of chemical composition that were taken to be clusters representing Douglas-fir gross wood or series of annual rings in long range interaction. In transforming the GRV and its derivatives, one up to four of the transforms (linear, log log, inverse of fourth root, fuzzy right) were selected and applied. For transforming inputs of the TLS of chemical composition three transfer functions were able to perform the transformation well from a pool of seven linear and nonlinear functions (linear, x^4, tanh, x^{-1}, $x^{0.5}$, log, ln(x/(1-x))). The outputs were best satisfied by linear, square root, power, logarithmic and exponential transform functions.

5.4.2. Training testing and validation of ANNs models for carbohydrates and lignin composition of Douglas-fir's earlywood and latewood

The highest number of inputs and their transforms selected was from category 1.1.2 and the least from category 2.1.1 and 2.2.1 that correspond to the ones with comprehensive input transformation with no variable selection and a category with exhaustive variables selection, respectively. Generally, increased parameterization did not either significantly increase the training correlation coefficient or improve the generalization capability of trained networks. The networks with nine inputs were able to perform better than that of having sixty four inputs although they were equally parameterized with thirty weights of hidden nodes. Use of networks did not drastically improve the correlation coefficient of the TLS modeling of chemical composition and physical properties obtained in section 5.2 and in Tekleyohannes

Table 5.22 Major Douglas-fir's cell-wall carbohydrates and lignin content prediction performance of the ANNs developed based on linearly and nonlinearly transformed inputs without selection using genetic algorithms

Models category	Output	Architecture	Model's performance					
			Correlation			Accuracy (20%)		
			Train	Test	Valid	Train	Test	Valid
1.1.1	Arabinose	24-29-7	0.9065	0.7869	0.6454	0.8550	0.7055	0.7710
	Galactose		0.9037	0.4773	0.4836	0.9398	0.7815	0.8384
	Glucose		0.9568	0.7669	0.2994	0.9857	0.9786	0.8653
	Xylose		0.9144	0.6454	0.5853	0.9120	0.8456	0.8081
	Mannose		0.9140	0.7396	0.4736	0.9334	0.9145	0.8350
	AIL		0.9623	0.7630	0.6511	1.0000	0.9786	0.8788
	ASL		0.8502	0.6055	0.4019	0.9065	0.8480	0.6061
1.1.2	Arabinose	64-30-7	0.9830	0.9018	0.7736	0.9937	0.9216	0.6970
	Galactose		0.9486	0.4184	0.6842	0.9635	0.6247	0.8687
	Glucose		0.9850	0.8432	0.2316	1.0000	0.8931	0.8788
	Xylose		0.9482	0.8208	0.6637	0.9984	0.9786	0.6835
	Mannose		0.9683	0.5884	0.2792	0.9929	0.8076	0.9057
	AIL		0.9844	0.8754	0.7160	1.0000	0.9786	0.8754
	ASL		0.9182	0.3055	0.4715	0.9414	0.6793	0.7980

and Avramidis (2009). Consequently, it appears that to keep the high correlation coefficient obtained in the training of the neural nets there is a need to use more training datasets.

Detailed results of the training, testing and validation of the neural networks for all eight categories for prediction of carbohydrates and lignin content from the physical properties of Douglas-fir wood are shown in Tables 5.22 and 5.23. The GRV and GRV_c contributed more to the prediction of carbohydrate and lignin than the rest of inputs. Figure 5.67 shows that the magnitudes of physical properties and TLS of chemical composition at phase transition (at about 65% relative humidity) contributed more to the prediction of chemical composition, a physical situation in which properties cease to be governed by unique characteristic lengths and they scale according to allometric exponents. However, their contribution is not predictable based on their effect on the output in relative humidity ranges which are out of the criticality state location. Figure 5.68 shows that at 50^0C, there was no significant difference in the contribution of various properties in the prediction of chemical composition in the entire range of relative humidity. This leads to the assertion that the effect of chemical composition is restricted to low temperature sorption. Carbohydrate and lignin content

Table 5.23 Major Douglas-fir's cell-wall carbohydrates and lignin content prediction performance of the ANN developed based on linearly and nonlinearly transformed inputs and inputs selected by applying genetic algorithms

Models category	Output	Architecture	Model's performance					
			Correlation			Accuracy (20%)		
			Train	Test	Valid	Train	Test	Valid
2.1.1	Arabinose	09-30-7	0.9721	0.9136	0.7901	0.9929	0.8931	0.9091
	Galactose		0.9606	0.6970	0.7533	1.0000	0.7435	0.9091
	Glucose		0.9758	0.8642	0.1783	1.0000	0.9786	0.9091
	Xylose		0.9750	0.7353	0.8547	1.0000	0.9572	0.9394
	Mannose		0.9397	0.7155	0.3533	0.9802	0.8290	0.9024
	AIL		0.9656	0.7418	0.7659	0.9881	0.9715	0.9091
	ASL		0.8717	0.7373	0.5269	0.8891	0.8575	0.7946
2.1.2	Arabinose	15-30-7	0.9721	0.9559	0.8168	0.9857	1.0000	0.9091
	Galactose		0.9283	0.5538	0.8074	0.9485	0.6437	0.8889
	Glucose		0.9362	0.7659	0.3303	0.9572	0.9525	0.8721
	Xylose		0.9142	0.7778	0.8033	0.9334	0.9620	0.8586
	Mannose		0.9094	0.4385	0.5699	0.9136	0.6152	0.8384
	AIL		0.9400	0.7936	0.5839	0.9929	1.0000	0.8788
	ASL		0.8423	0.7657	0.5826	0.9089	0.8575	0.7441
2.1.3	Arabinose	40-30-7	0.9883	0.9361	0.7423	1.0000	0.9762	0.8855
	Galactose		0.9755	0.5571	0.8430	0.9992	0.7435	0.9091
	Glucose		0.9818	0.8615	0.2371	1.0000	0.9145	0.9091
	Xylose		0.9668	0.8888	0.8727	0.9984	1.0000	0.9091
	Mannose		0.9758	0.7374	0.4393	0.9960	0.8575	0.8956
	AIL		0.9732	0.8323	0.7338	0.9992	0.9834	0.9091
	ASL		0.9562	0.5517	0.6915	0.9968	0.9074	0.8923
2.2.1	Arabinose	09-28-7	0.9375	0.8662	0.7520	0.9255	0.8765	0.8788
	Galactose		0.8231	0.4553	0.6902	0.8217	0.7197	0.7778
	Glucose		0.8091	0.5100	0.3408	0.7409	0.8147	0.5185
	Xylose		0.8249	0.4872	0.7444	0.7773	0.6675	0.6633
	Mannose		0.7960	0.4851	0.0745	0.7742	0.7173	0.5185
	AIL		0.8033	0.3753	0.5826	0.7290	0.6841	0.5724
	ASL		0.7713	0.3462	0.5873	0.7837	0.6960	0.4545
2.2.2	Arabinose	18-25-7	0.9592	0.9663	0.8106	0.9540	0.9952	0.8990
	Galactose		0.9358	0.6254	0.7988	0.9746	0.8266	0.8990
	Glucose		0.9436	0.8103	0.3042	0.9429	0.9572	0.8822
	Xylose		0.9429	0.6686	0.8238	0.9469	0.8575	0.8687
	Mannose		0.9319	0.4600	0.5790	0.9628	0.7435	0.8855
	AIL		0.9392	0.7395	0.5910	0.9683	0.9026	0.8653
	ASL		0.8456	0.7616	0.5622	0.8962	0.8456	0.8013
2.2.3	Arabinose	19-30-7	0.9730	0.9620	0.8003	0.9754	0.9976	0.9057
	Galactose		0.9699	0.6925	0.7479	0.9913	0.6912	0.9057
	Glucose		0.9571	0.8123	0.3998	0.9707	0.9881	0.9024
	Xylose		0.9540	0.8104	0.8085	0.9929	0.9952	0.9024
	Mannose		0.9282	0.5047	0.5085	0.9770	0.7387	0.8990
	AIL		0.9512	0.7362	0.5937	0.9857	0.9026	0.8990
	ASL		0.8785	0.6756	0.5736	0.9350	0.8242	0.8047

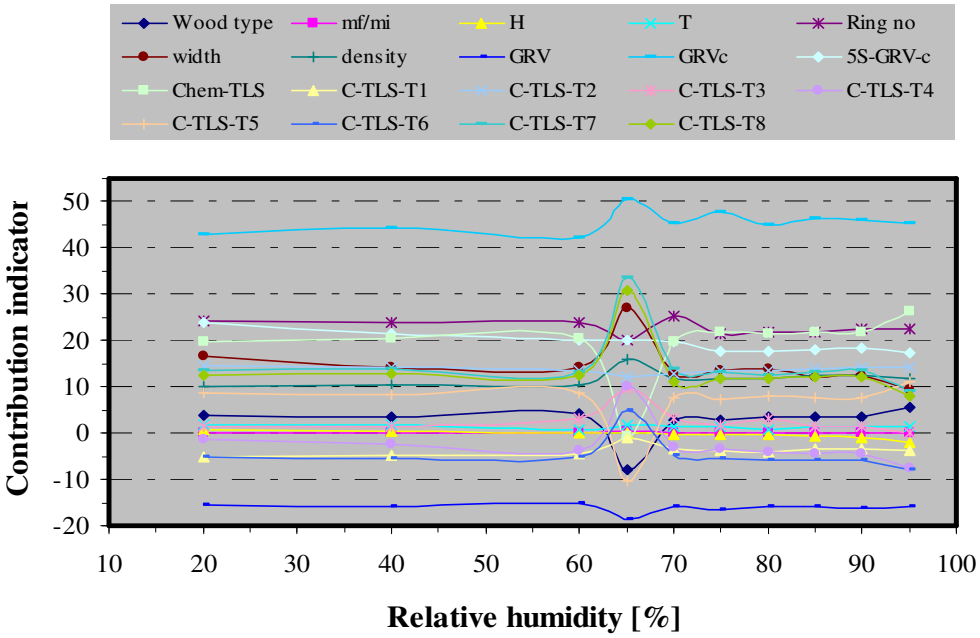

Figure 5.67 Contribution of physical properties and TLS of chemical composition to carbohydrates and lignin content of Douglass-fir at 25^0C and in the range 0 to 95% relative humidity

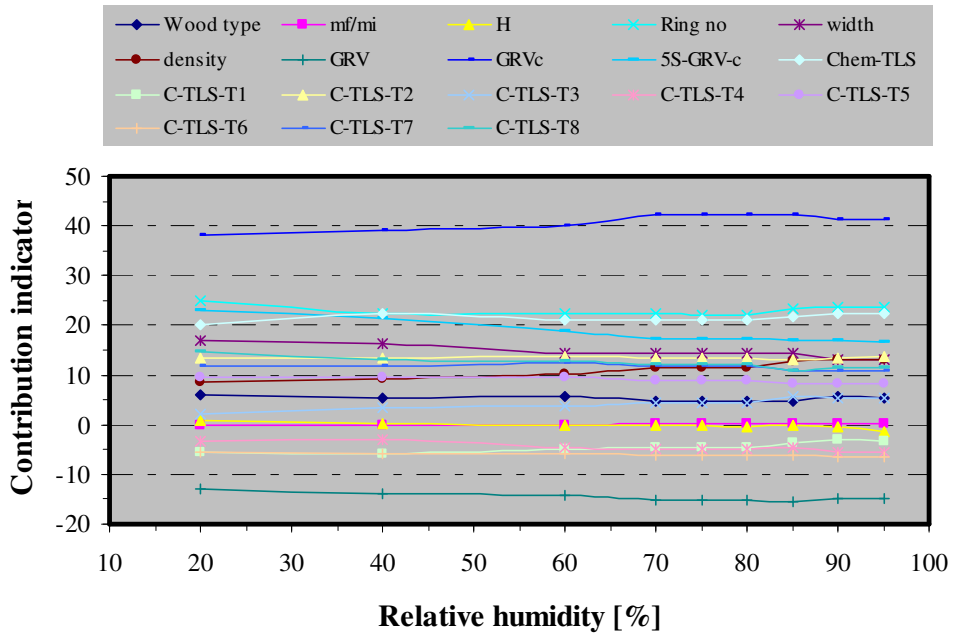

Figure 5.68 Contribution of physical properties and TLS of chemical composition to carbohydrates and lignin content of Douglass-fir at 50^0C and in the range 0 to 95% relative humidity

prediction was found to be extremely sensitive (up to an order of three) to cluster of collapsed 5S-GRV_c. It was also highly sensitive to GRV and GRV_c with exponential increase in sensitivities from GRV to GRV_c and then to 5S-GRV_c. The outputs are also found to be moderately sensitive to TLS of chemical composition.

5.4.3. Training testing and validation of ANNs models for the prediction of Douglas-fir's small specimens sorption properties

The highest number of inputs and transforms obtained was for category 1.1.2 and the least was for network category 2.2.1. The first attempt to predict all model parameters of the TLS sorption that were derived and given in equations (3.61) to (3.64) was largely unsatisfactory as given in Table 5.24. All of the parameters of the TLS sorption attempted to be estimated by neural networks are critical exponents except one which is the amplitude or growth parameter L_1. The twenty percent accuracy band was good for most of network predictions implying that the reason for the unsatisfactory prediction being fluctuation of the parameters in a very narrow band. The major reason probably is the fact that equation (3.61) is too complex to have its parameters directly estimated by the trained networks. Table 5.24 shows performance of the ANNs in predicting the BET-surface area and equilibrium moisture content which are actually magnitudes of physical properties. In the same table, the 20%

Table 5.24 Performance of the ANNs in predicting parameters of the TLS sorption prediction models for Douglas-fir

Models category	Output	Architecture	Model's performance					
			Correlation			Accuracy (20%)		
			Train	Test	Valid	Train	Test	Valid
2.1.2	BET-area	30-29-9	0.8603	0.8826	0.8422	0.9810	0.9881	0.9764
	Surface area		0.4128	0.2836	0.1788	0.9334	0.9691	0.8519
	x		0.7339	0.6647	0.6092	0.6292	0.8741	0.3670
	i		0.3248	0.2750	0.4701	0.9952	1.0000	0.9966
	c_k		0.3843	0.7531	-0.0238	0.9643	0.9952	0.7946
	t-exp		0.3334	0.2474	0.2692	0.9810	0.9976	0.9259
	L_1		0.2484	0.2108	-0.0960	0.9992	1.0000	0.9360
	c_i		0.0548	0.3596	-0.1777	0.8510	0.8884	0.7643
	M		0.9822	0.8978	0.8151	1.0000	0.9976	0.9529

Table 5.25 TLS sorption model's parameters prediction performance of the ANNs developed in the six categories for Douglas-fir

Models category	Output	Architecture	Models performance					
			Correlation			Accuracy (20%)		
			Train	Test	Valid	Train	Test	Valid
1.1.1	BET-area	31-26-4	0.9247	0.9041	0.9384	0.9723	0.9715	0.9663
	x		0.9751	0.8404	0.9063	0.9612	0.9810	0.9428
	c_k		0.3962	0.7848	0.0526	0.9532	0.9976	0.8384
	M		0.9648	0.9269	0.8859	0.9976	1.0000	0.9764
1.1.2	BET-area	85-26-4	0.8059	0.8308	0.8198	0.9794	0.9905	0.9798
	x		0.9323	0.9107	0.8240	0.8407	0.9857	0.8114
	c_k		0.5011	0.8145	0.1134	0.9556	0.9976	0.8552
	M		0.9368	0.9464	0.8526	0.9945	1.0000	0.9663
2.1.1	BET-area	10-27-4	0.8407	0.8507	0.8840	0.9596	0.9691	0.9596
	x		0.7547	0.7239	0.6004	0.6165	0.9715	0.4310
	c_k		0.1477	0.5234	-0.0328	0.9192	0.9976	0.7845
	M		0.9471	0.9115	0.8748	0.9952	1.0000	0.9697
2.1.2	BET-area	25-29-4	0.8354	0.8527	0.8675	0.9770	0.9905	0.9764
	x		0.9202	0.9104	0.8063	0.7575	0.9857	0.6195
	c_k		0.1723	0.6872	-0.0666	0.9525	0.9952	0.8418
	M		0.9542	0.9273	0.8838	0.9952	1.0000	0.9697
2.1.3	BET-area	43-21-4	0.8210	0.8270	0.8440	0.9786	0.9905	0.9798
	x		0.8192	0.7345	0.6743	0.6070	0.9739	0.4141
	c_k		0.1755	0.5684	-0.0796	0.9326	0.9976	0.7845
	M		0.9519	0.9334	0.8916	0.9952	1.0000	0.9697
2.2.1	BET-area	08-25-4	0.8463	0.8595	0.8942	0.9723	0.9905	0.9663
	x		0.8919	0.7990	0.8283	0.7750	0.9739	0.7710
	c_k		0.1025	0.5542	-0.1013	0.9271	0.9952	0.8081
	M		0.9535	0.9273	0.8953	0.9952	1.0000	0.9697
2.2.2	BET-area	17-26-4	0.8486	0.8676	0.9046	0.9683	0.9905	0.9596
	x		0.4344	0.1441	0.2240	0.3811	0.8646	0.1313
	c_k		0.1852	0.6787	-0.0821	0.9509	0.9929	0.8316
	M		0.1618	0.1698	0.1096	0.8605	0.9454	0.7946
2.2.3	BET-area	21-28-4	0.8606	0.8558	0.9013	0.9659	0.9786	0.9596
	x		0.9321	0.9121	0.8296	0.8590	0.9881	0.8788
	c_k		0.1885	0.7022	-0.1007	0.9556	0.9976	0.8586
	M		0.9502	0.9159	0.8811	0.9952	1.0000	0.9697

accuracy estimations obtained for badly estimated parameters of equation (3.61) are fairly good. This may imply that the parameters are prevailingly critical exponents and describe complex magnitudes by themselves and the attempt to have them all estimated in one neural net is indirectly an attempt to estimate the even more complex equation (3.61) which was

prone to failure. Therefore, it is better to investigate performance of ANNs in predicting BET-surface area and equilibrium moisture content which are relatively simple and directly measurable physical quantities. The singularity parameter x was predicted well by the ANNs and it is also necessary to see how the same neural nets perform in predicting the kinetics scaling exponent c_k which is the major scaling parameter in the TLS model of sorption. The detailed results of ANNs modeling of sorption properties of the small specimens are given in Table 5.25.

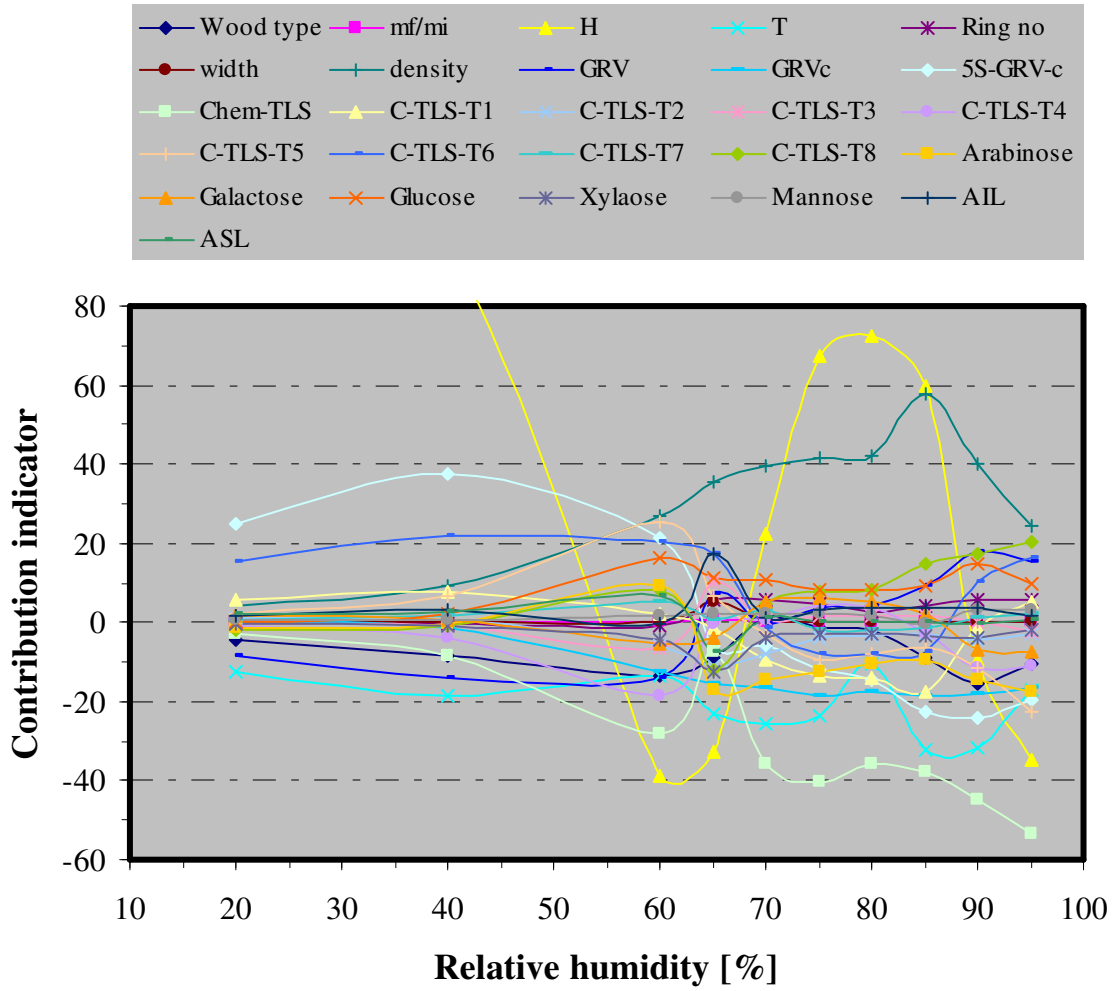

Figure 5.69 Contribution of physical properties and chemical composition inputs with individual inputs and long range clusters on the prediction of BET-surface area, the singularity parameter, the kinetic slope and equilibrium moisture content of earlywood, latewood and annual rings of Douglas-fir at 25^0C

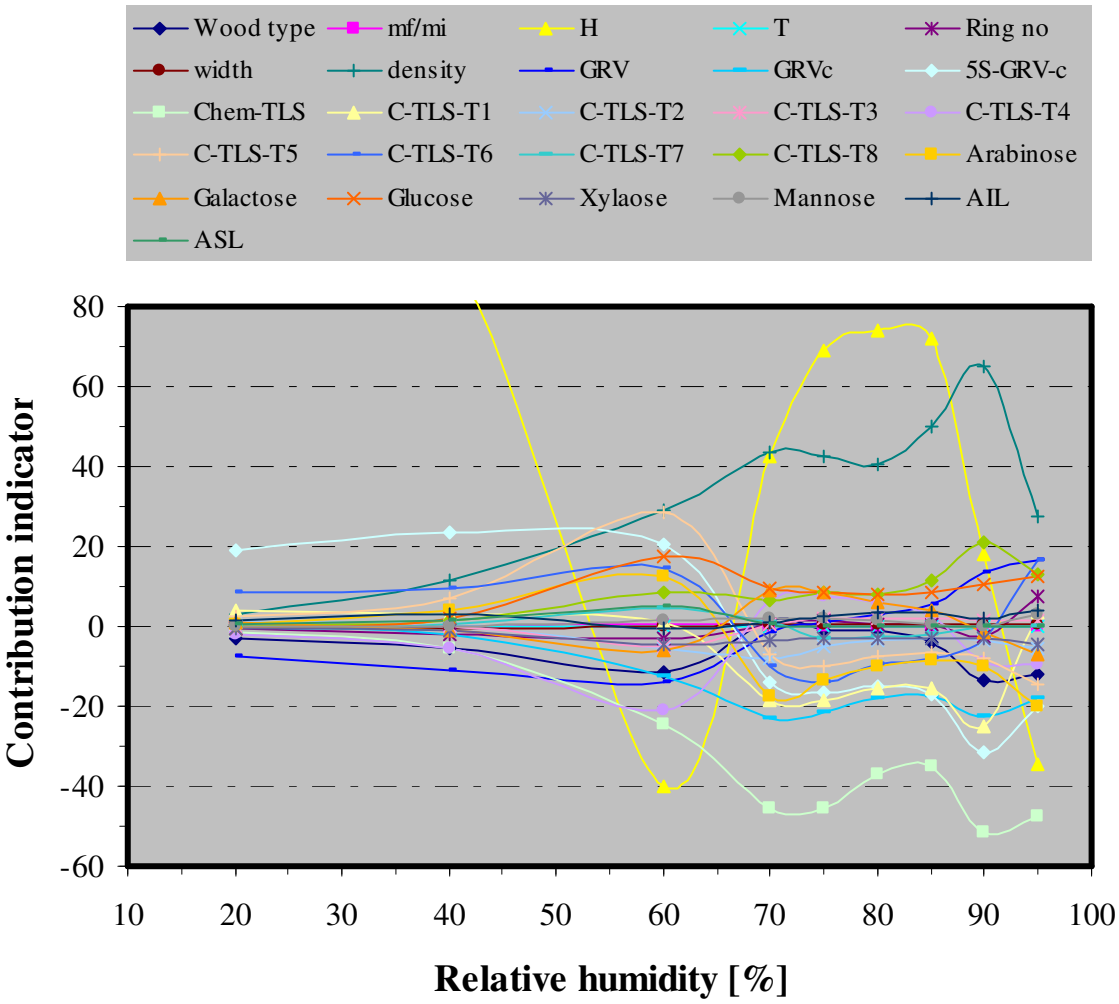

Figure 5.70 Contribution of physical properties and chemical composition inputs with individual inputs and long range clusters on the prediction of BET-surface area, the singularity parameter, the kinetic slope and equilibrium moisture content of earlywood, latewood and annual rings of Douglas-fir at 50^0C

It is usually useful to scrutinize the performance improvement obtained using more inputs and neural weights or hidden processing elements over the smallest size network. Use of more inputs and one more hidden processing element did improve the performance of the neural nets while at the same time they had a better generalization capability. The BET-surface area and equilibrium moisture content prediction were close to each other for networks developed using individual inputs with long range clusters and for networks that

require use of inputs (parameters) obtained based on TLS modeling of physical properties and chemical compositions. Since the inputs obtained from TLS modeling of growth rings and chemical composition can have wider validity, the networks developed using them will have a better generalization capability. Categories 1.1.1 and 1.1.2 represent linear and nonlinear transformations of inputs, respectively. It can be seen from Table 5.24 that non-linearization of the inputs slightly improved the ANNs prediction performance. The contribution of inputs in the neural development categories of 2.1.3 and 2.2.3 is presented in Figures 5.69 to 5.70. The contributions are point estimates but were connected with continuous lines to show the changing trend with change of relative humidity. Figures 5.69 and 5.70 reveal that the contribution of inputs to the network model category 2.1.3 is dominated by relative humidity, 5S-GRV$_c$ and TLS of chemical composition in the relative

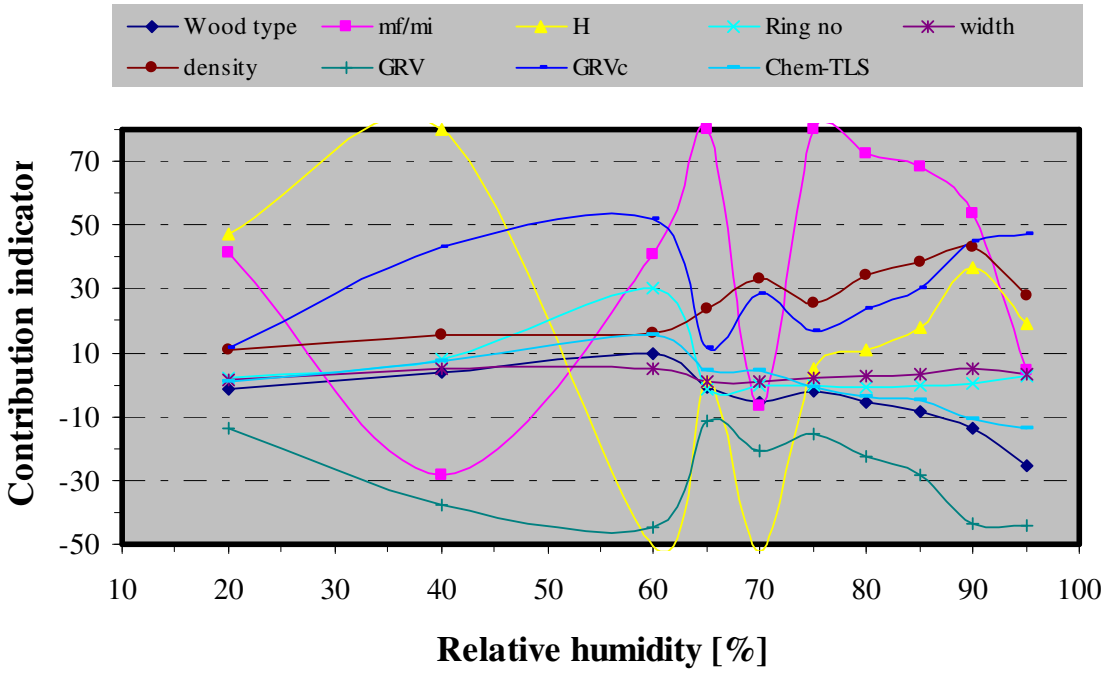

Figure 5.71 Contribution of physical properties and chemical composition inputs with individual inputs and TLS parameters on the ANNs category 2.2.3 prediction of BET-surface area, the singularity parameter, the kinetic slope and equilibrium moisture content of earlywood, latewood and annual rings of Douglas-fir at 25^{0}C

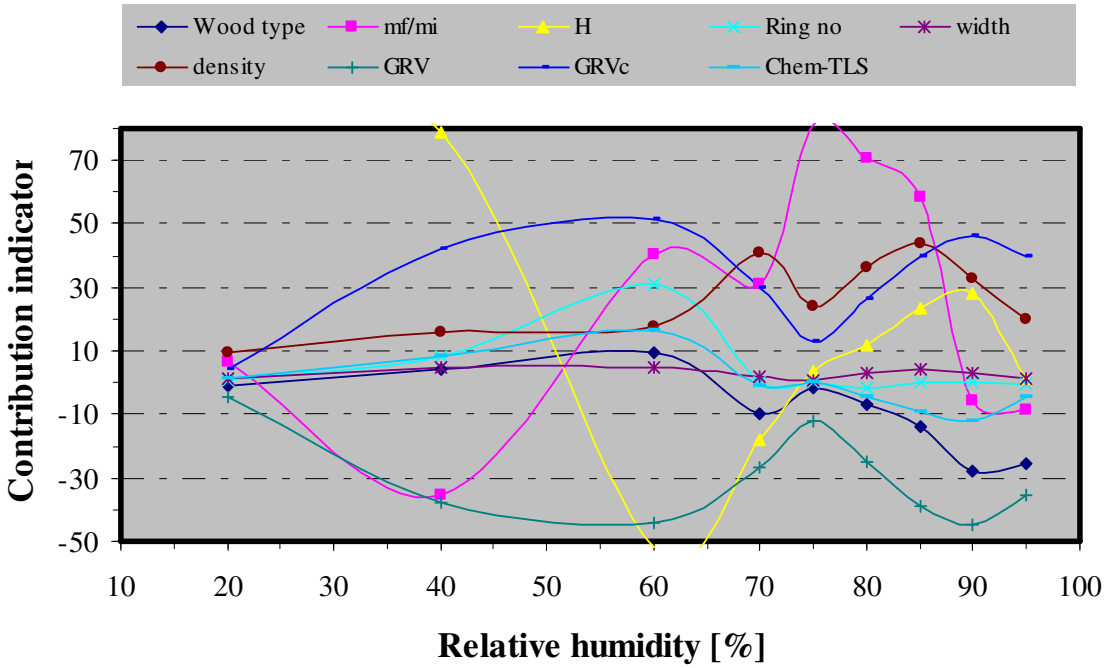

Figure 5.72 Contribution of physical properties and chemical composition inputs with individual inputs and TLS parameters on the ANNs category 2.2.3 prediction of BET-surface area, the singularity parameter, the kinetic slope and equilibrium moisture content of earlywood, latewood and annual rings of Douglas-fir at 50^0C

humidity range below 65%. Density of Douglas-fir, TLS of chemical composition, 5S-GRV_c and relative humidity played a major contribution above 65% of relative humidity both at 25 and 50^0C. The rest of inputs had lesser contributions that were close to each other in magnitude with an increasing trend towards 60% relative humidity that abruptly dropped down at about 65% relative humidity and remained constant up to 80% of relative humidity and then again showed a slight increase.

Contributions of inputs for neural nets category 2.2.3 displayed a distinct pattern that can be described as a laying vase. Relative humidity, GRV, and GRV_c displayed an increase in contribution towards 60% relative humidity that slightly increased at 70% with another decrease at 75% and then increased up to 95%. The contribution of GRV_c was positively correlated with the outputs while GRV was negatively correlated. Density had a reduced

Table 5.26 Sensitivities of the category 2.2.3 neural nets outputs for BET-surface area, the singularity parameter *x*, the kinetic slope, and equilibrium moisture content on the inputs of parameters and variables for sorption properties of the Douglas-fir at 25^0C

Outputs		Input parameters and variables								
		Wood type	**mf/mi**	**H**	**Ring no**	**width**	**density**	**GRV**	**GRV_c**	**Chem-TLS**
Average	BET-area	-0.018	0.026	0.053	0.353	-0.032	-1.190	-1.510	-0.119	0.058
	x	-0.001	-0.388	0.460	0.086	0.033	0.122	-0.741	135.610	0.014
	c_k	0.003	-0.377	-0.001	-0.014	-0.062	0.000	0.676	23.800	0.051
	M	-0.005	0.075	1.132	0.119	0.048	-0.064	-0.163	-5.406	0.002
Average Square	BET-area	0.003	0.004	0.015	0.843	0.002	1.925	7.531	446.470	0.031
	x	0.000	0.289	1.304	0.016	0.003	0.076	2.432	69348.039	0.007
	c_k	0.000	0.147	0.016	0.002	0.006	0.003	1.166	1553.508	0.006
	M	0.000	0.021	1.945	0.036	0.004	0.011	0.087	731.706	0.001
Variance	BET-area	0.003	0.004	0.012	0.719	0.001	0.509	5.253	446.681	0.028
	x	0.000	0.139	1.093	0.008	0.002	0.061	1.885	50983.844	0.007
	c_k	0.000	0.005	0.016	0.002	0.002	0.003	0.710	987.546	0.003
	M	0.000	0.015	0.664	0.022	0.002	0.006	0.060	702.837	0.001

contribution from the case in category 2.1.3, but showed the same trend with an over all increase towards higher relative humidity and displayed a negative correlation with wood type. The coupled symmetrical trend displayed by density and wood type is similar to that of GRV and GRV_c.

The sensitivities of BET-surface area, the singularity parameter *x*, the kinetic slope and equilibrium moisture content to small changes in the inputs are shown in Tables 5.26 and 5.27 at 25 and 50^0C, respectively. The sensitivities are presented as average, square of the average and variance. The square of the average helps to compare sensitivities which can have opposite signs and also to magnify the differences. The outputs were found to be extremely sensitive to small changes in the GRV and GRV_c of Douglas-fir. The outputs were also sensitive to small changes in relative humidity and density, but they were found to be the least sensitive to wood type of Douglas-fir. The overall trend held true for sensitivities of outputs for category 2.1.3 neural nets, also. Generally, the input contributions shown in Figures 5.71 and 5.72 confirm the evidence that at phase transition, the sorption mechanism is governed by complex factors and is rather difficult to attribute the physical process to individual inputs.

5.4.4. Training testing and validation of ANNs models for the prediction of Douglas-fir gross wood sorption properties

The prediction performance of MLP ANNs based on the classical variables, namely relative humidity and temperature, was the reference to start with and shall be discussed first. Summary of the transforms used for the inputs and outputs of two neural nets is given in Table 5.27. Temperature and relative humidity changes had only two levels and hence were considered as logical inputs. Diffusion and surface emission coefficients were transformed using exponential function while the squared power function better suited equilibrium moisture content. The total number of inputs therefore was expanded from four to nine which can give the maximum prediction accuracy that is obtainable while using classical sorption variables as inputs. Table 5.28 shows the performance of MLP AANs while predicting diffusion coefficient and surface emission coefficient, and equilibrium moisture content from the classical variables. Inclusion of the change in relative humidity as input slightly increased

the correlation coefficient both for diffusion and surface emission coefficient. Generally, the ANNs prediction was better than that of the classical ones except in moisture content prediction at 25^0C in which the sorption is less chaotic and can be described by smooth function.

Table 5.27 Inputs' and outputs' linear and nonlinear transforms used in the development of ANNs models for prediction of sorption isotherms points, diffusion coefficient and surface emission coefficient of Douglas-fir

Inputs			Outputs		
variable	**number**	**Transforms**	**Parameter**	**number**	**transforms**
H	3	Linear, logarithmic, inverse	D	1	Exponential
dH	1	Logical	S	1	Exponential
T	1	Logical	M	1	Sq. power
M	4	Linear, squared power, tanh, fuzzy right			

Table 5.28 The ANNs models performance while using only relative humidity, temperature, equilibrium moisture content and the change in relative humidity to predict diffusion coefficient and surface emission coefficient of Douglas-fir

Major inputs	Outputs	Architecture	Correlation			Accuracy (20%)		
			Train	**Test**	**Valid**	**Train**	**Test**	**Valid**
H-T-M	D	08-24-02	0.8295	0.7404	0.8411	0.9942	0.9076	0.9682
	S		0.7990	0.7030	0.8237	0.9942	0.8975	0.9652
H-dH-T-M	D	09-09-02	0.8311	0.7548	0.8500	0.9957	0.9076	0.9692
	S		0.8041	0.7315	0.8335	0.9942	0.8958	0.9646
H-dH-T	M	05-02-01	0.9427	0.9612	0.9482	0.9921	0.9933	0.9924

The ANNs models of category 1.1.1, 1.1.2, 1.2.1, 1.2.2, 2.1.2, 2.1.3 and 2.2.3 performed well and were close to each other in prediction performance. Category 2.2.3 was able to yield the best performing ANNs model followed by category 1.2.1 and 1.1.1. Category 1.2.1 had the smaller size networks and its inputs were transformed only linearly which can be a reason to be at the top of best performing models. Category 1.1.1 also scored the highest in the prediction of sorption isotherms although it uses more inputs and has more hidden processing

elements. The models validation revealed that grouping of variables into thermodynamic, anatomy and chemical composition increased prediction performance in terms of accuracy.

Table 5.29 Performance of the MLP ANNs in predicting diffusion coefficient, surface emission coefficient and equilibrium moisture content of Douglas-fir using various categories of inputs and neural architecture

Models category	Output	Architecture	Model's performance					
			Correlation			Accuracy (20%)		
			Train	Test	Valid	Train	Test	Valid
1.1.1	M	089-29-3	0.9799	0.9830	0.9910	0.9992	1.0000	1.000
	D		0.9503	0.9426	0.9164	0.9921	0.9976	0.9663
	S		0.9452	0.9463	0.9030	0.9913	0.9976	0.9663
1.1.2	M	240-02-3	0.9112	0.9500	0.9175	0.9863	1.0000	0.9904
	D		0.9209	0.8476	0.9070	0.9805	0.9899	0.9833
	S		0.9106	0.8605	0.9012	0.9791	0.9882	0.9818
1.2.1	M	030-24-3	0.9638	0.9890	0.9741	0.9952	1.0000	0.9933
	D		0.9346	0.9246	0.9118	0.9945	0.9952	0.9764
	S		0.9318	0.9295	0.9108	0.9913	0.9834	0.9731
1.2.2	M	092-28-3	0.9360	0.9863	0.8738	0.9921	1.0000	0.9731
	D		0.9322	0.9413	0.8504	0.9889	0.9857	0.9764
	S		0.9251	0.9290	0.8470	0.9842	0.9715	0.9697
2.1.1	M	002-20-3	0.9491	0.9900	0.9266	0.9929	1.0000	0.9798
	D		0.7210	0.6093	0.7609	0.9651	0.9169	0.9461
	S		0.7056	0.5865	0.7485	0.9596	0.9169	0.9428
2.1.2	M	053-24-3	0.9475	0.9839	0.9336	0.9921	1.0000	0.9731
	D		0.9466	0.9430	0.9078	0.9905	0.9952	0.9798
	S		0.9486	0.9431	0.9002	0.9929	0.9952	0.9798
2.1.3	M	172-24-3	0.9349	0.9829	0.9167	0.9913	1.0000	0.9731
	D		0.9506	0.9477	0.9047	0.9889	0.9857	0.9798
	S		0.9368	0.9339	0.8952	0.9857	0.9810	0.9764
2.2.1	M	002-27-3	0.9493	0.9889	0.9270	0.9929	1.0000	0.9798
	D		0.7384	0.6180	0.7687	0.9659	0.9169	0.9461
	S		0.7185	0.5795	0.7518	0.9604	0.9074	0.9360
2.2.2	M	014-26-3	0.9489	0.9899	0.9282	0.9929	1.0000	0.9798
	D		0.8029	0.7143	0.7936	0.9731	0.9264	0.9428
	S		0.7977	0.7042	0.7775	0.9667	0.9121	0.9327
2.2.3	M	041-28-3	0.9494	0.9874	0.9302	0.9929	1.0000	0.9798
	D		0.9464	0.9401	0.9278	0.9881	0.9786	0.9798
	S		0.9467	0.9407	0.9232	0.9865	0.9786	0.9764

Figures 5.73 and 5.74 show the contribution of inputs of category 1.1.1 to the prediction of equilibrium moisture content, diffusion and surface emission coefficient and also revealed that the singularity parameter *x* and its clusters had a dominant effect on the output. This brings to light the direct relation of the singularity parameter to the outputs that did not require a nonlinear transformation of inputs for good prediction performance. However, observing the comprehensive performance of ANNs of category 2.1.3 and 2.2.3 can give a better aspect of comparison between large and small size networks, and also can show the benefit gained by the use of TLS models of sorption and properties of annual rings in the heterogeneous and unified modeling of water vapour sorption in Douglas-fir wood. It is clear from Table 5.29 that the category 2.2.3 ANNs had been superior in performance and they were developed using TLS models of sorption and properties of annual ring, regardless of the properties of neighbouring annual rings. Category 2.2.3 ANNs were as accurate in prediction as category 2.1.3 based on the twenty percent accuracy band with additional benefit of having higher correlation coefficient. The ANNs sorption models that incorporated the comprehensive set of anatomical, physical and chemical composition inputs generally performed well above those that were developed using relative humidity and temperature alone. The contribution of inputs to the prediction of diffusion coefficient, surface emission coefficient and equilibrium moisture content are give in Figures 5.75 to 5.78.

The general trend of inputs contribution in category 2.1.3 displayed an interesting pattern in which the contributions of most variables were enveloped by a well defined profile, from the above by the GRV_c, and from the bottom by the GRV. The relative humidity and the singularity parameter contributed much to the outputs in the entire experimental relative humidity range. However, their contribution drastically fell near the phase transition range at about 65% relative humidity for 25^0C and at about 75% relative humidity for 50^0C. It can be deduced that the GRV_c-GRV envelope is formed to compensate for this drastic fall. The singularity parameter *x* and relative humidity gradually regained their dominant contribution to the outputs after the phase transition. The input that was not much in harmony with the GRV_c-GRV envelope was the slope of sorption kinetics. Its contribution was dominant just after the phase transition that abruptly peaked at 80% relative humidity.

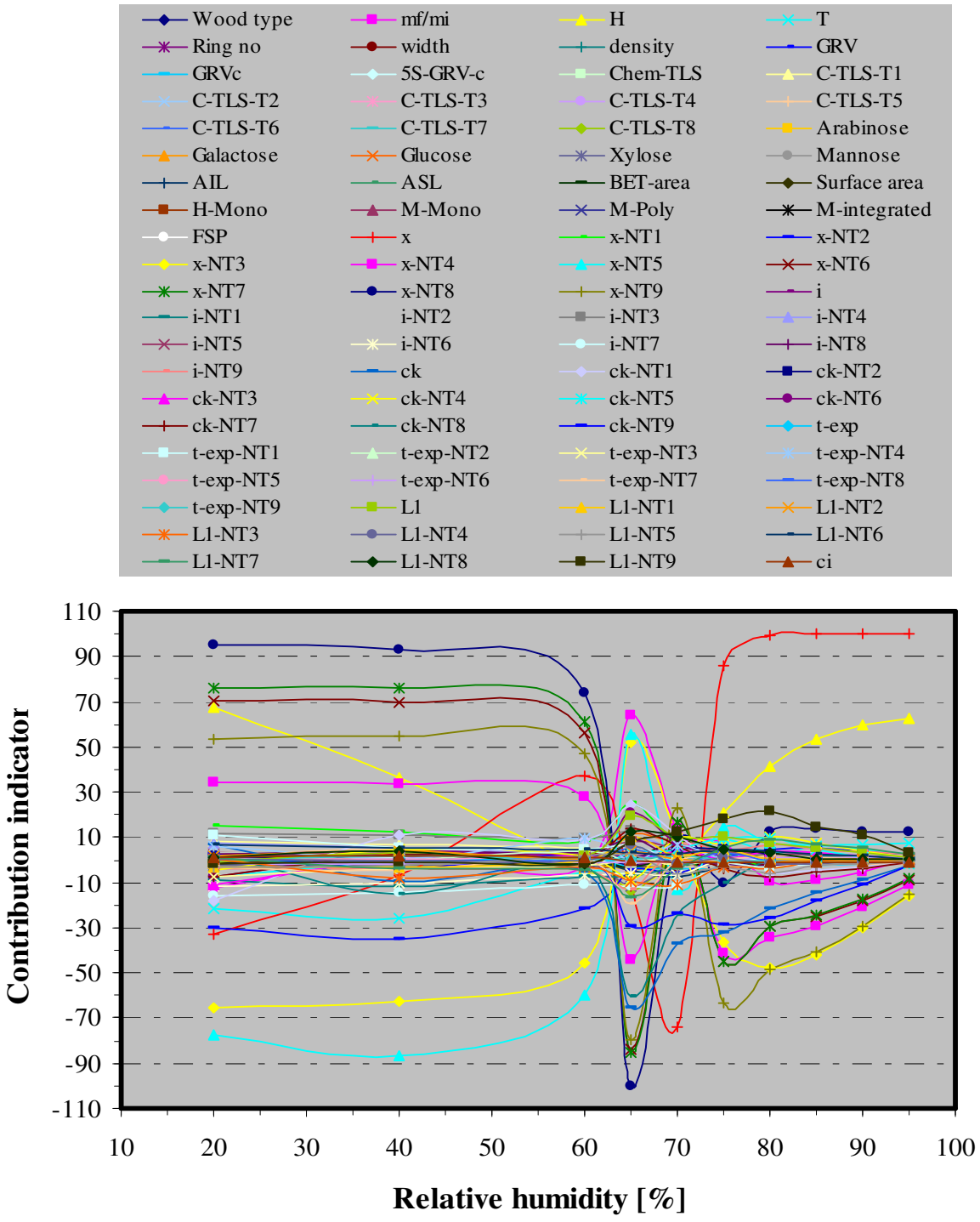

Figure 5.73 Contribution of physical properties, chemical composition and parameters of the TLS models of sorption as individual inputs and long range clusters (Category 1.1.1) on the prediction of diffusion coefficient, surface emission coefficient and equilibrium moisture content of Douglas-fir gross wood at 25^0C after a linear inputs transformation

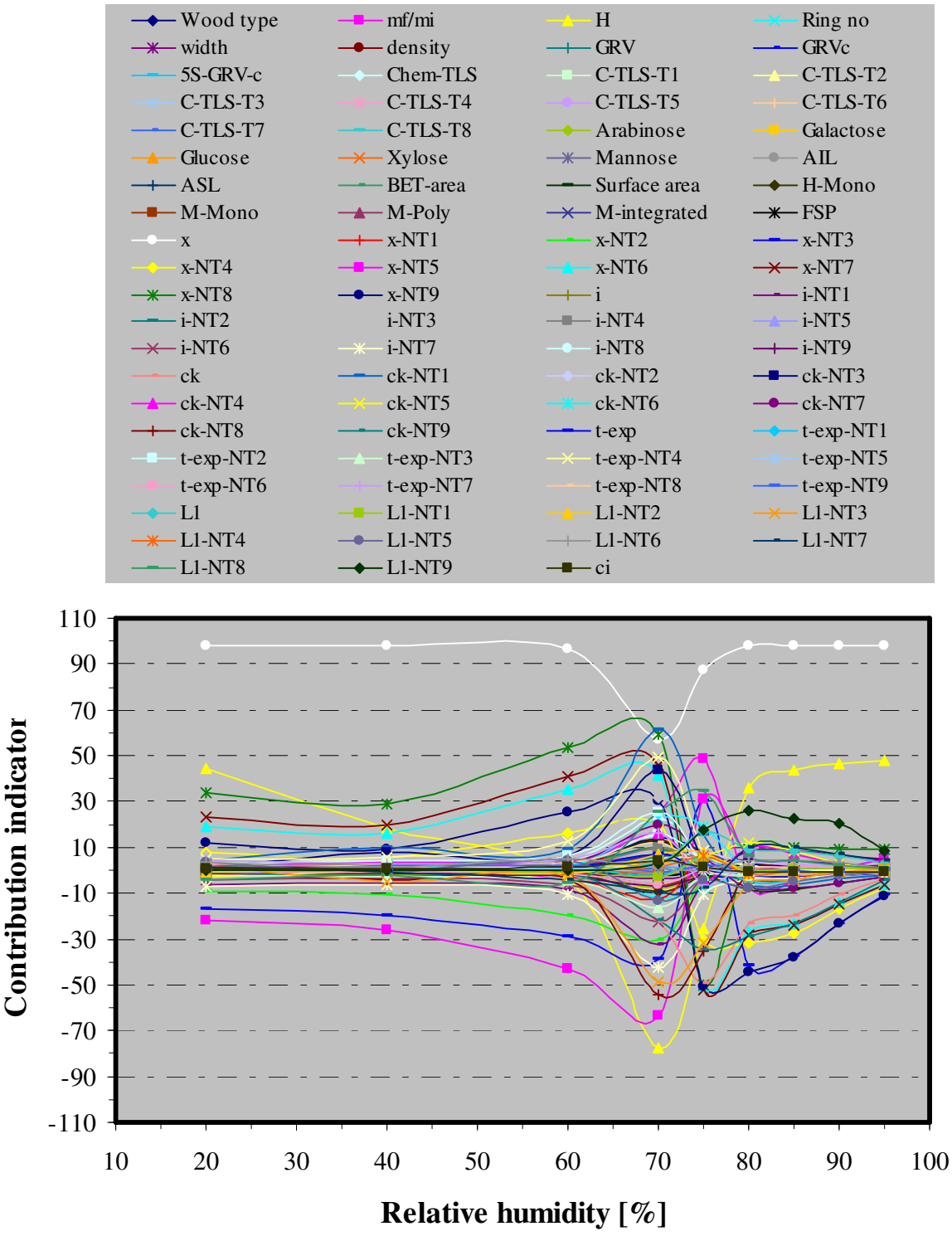

Figure 5.74 Contribution of physical properties, chemical composition and parameters of the TLS models of sorption as individual inputs and long range clusters (Category 1.1.1) on the prediction of diffusion coefficient, surface emission coefficient and equilibrium moisture content of Douglas-fir gross wood at 50^0C after a linear inputs transformation

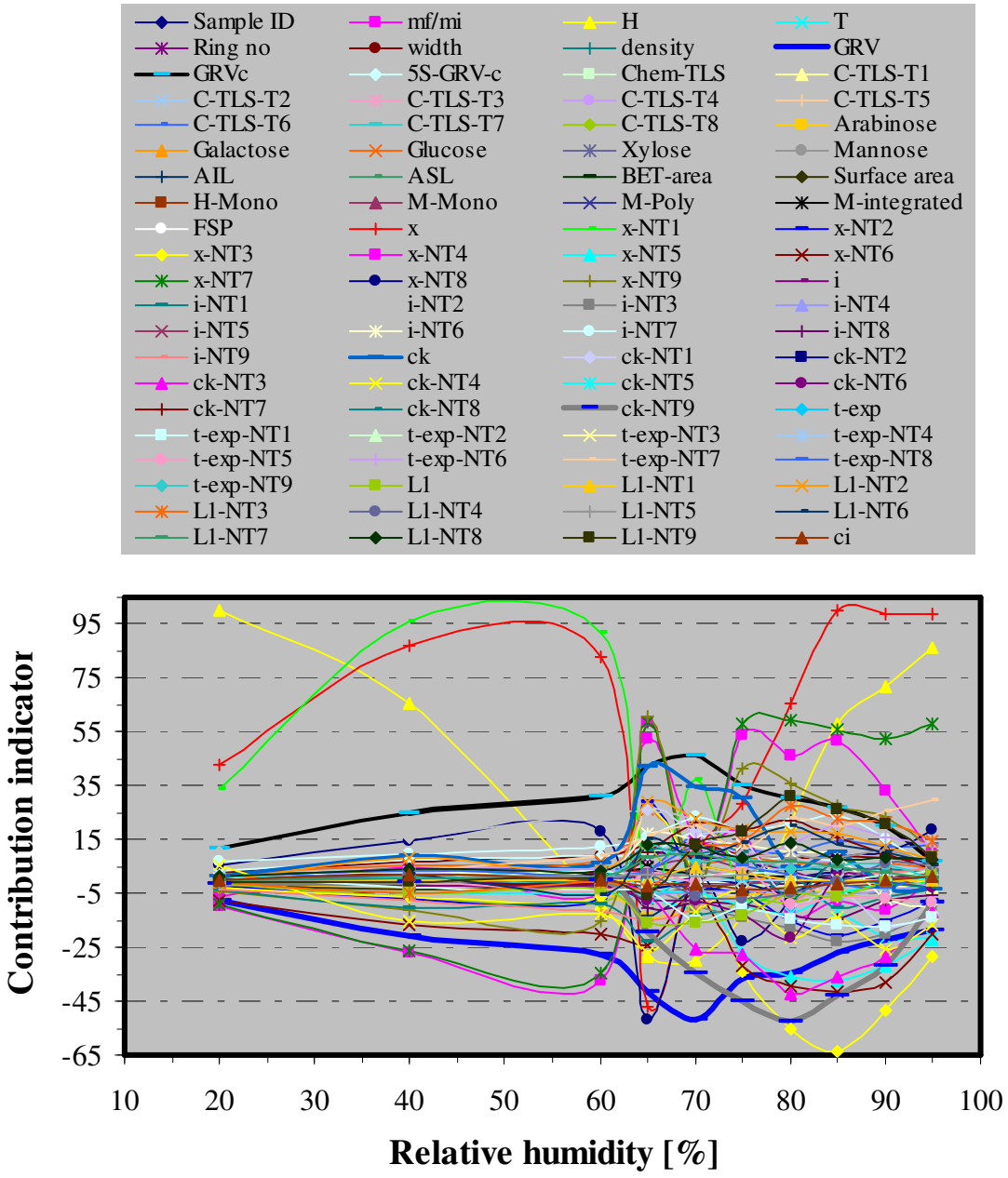

Figure 5.75 Contribution of physical properties, chemical composition and parameters of the TLS models of sorption as individual inputs and long range clusters (Category 2.1.3) on the prediction of diffusion coefficient, surface emission coefficient and equilibrium moisture content of Douglas-fir gross wood at 25^0C

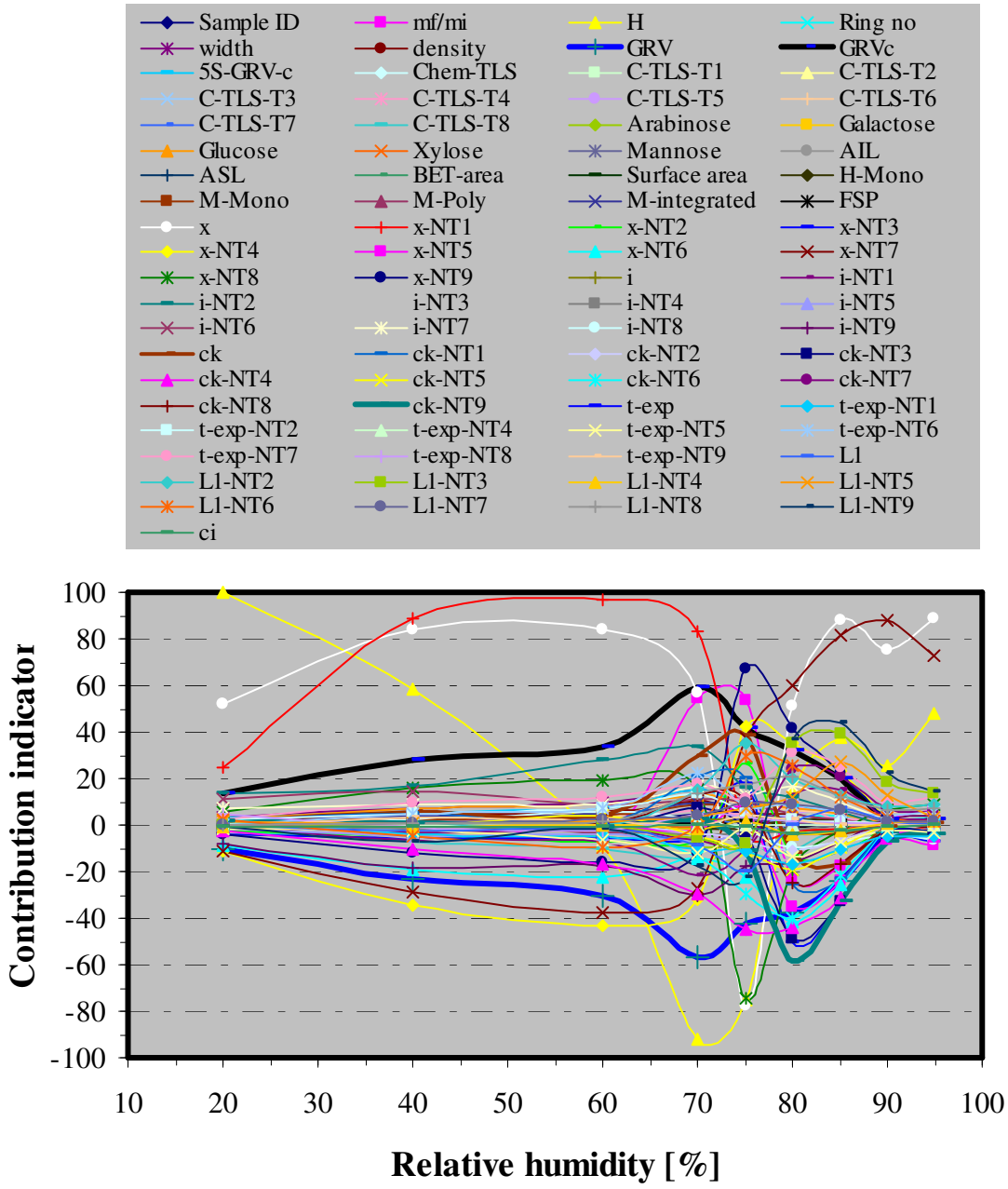

Figure 5.76 Contribution of physical properties, chemical composition and parameters of the TLS models of sorption as individual inputs and long range clusters (category 2.1.3) on the prediction of diffusion coefficient, surface emission coefficient and equilibrium moisture content of Douglas-fir gross wood at 50^0C

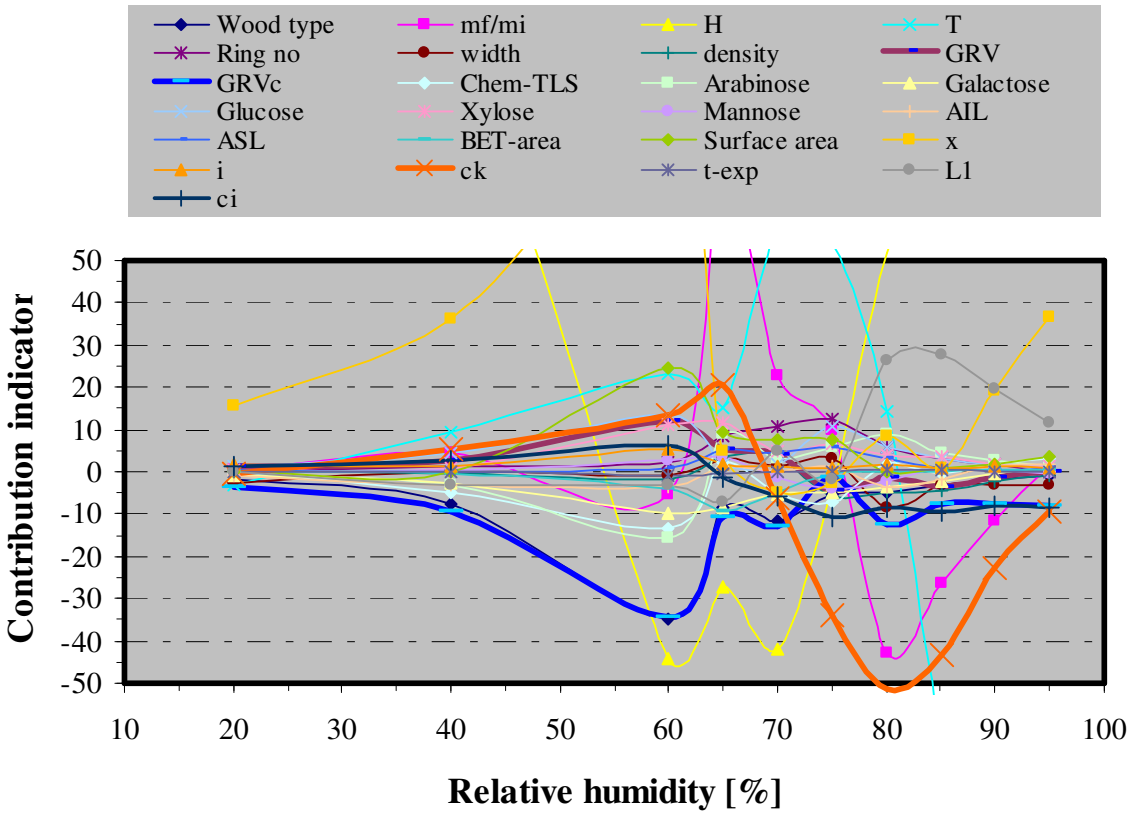

Figure 5.77 Contribution of physical properties, chemical composition and parameters of the TLS models of sorption as individual inputs and parameters of TLS models of sorption on the prediction of diffusion coefficient, surface emission coefficient and equilibrium moisture content of Douglas-fir gross wood at 25^0C

The trend in the contribution of inputs for the ANNs model of category 2.2.3 was not the same as observed with category 2.1.3. Figures 5.77 and 5.78 show that the GRV_c contribution was halved while that of the GRV was reduced to one sixth. On the other hand, contribution of density and widths of earlywood, latewood and annual rings of Douglas-fir remained very low. However, the trend in the kinetics slope remained the same and this can probably imply that the slope that has served as scaling exponent in the TLS modeling of sorption is an emergent property by itself that is little affected by other interacting inputs. The slope of sorption kinetics and GRV_c had the largest contribution to the prediction of

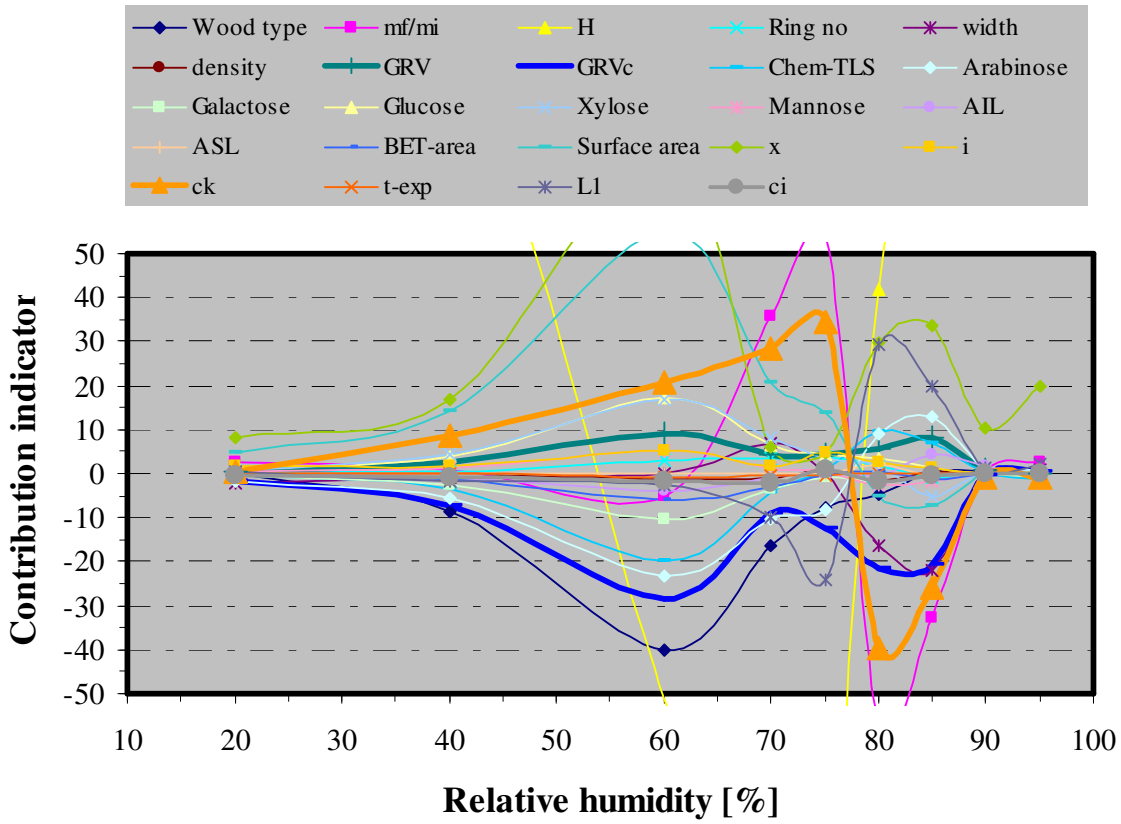

Figure 5.78 Contribution of physical properties, chemical composition and parameters of the TLS models of sorption as individual inputs and parameters of TLS models of sorption on the prediction of diffusion coefficient, surface emission coefficient and equilibrium moisture content of Douglas-fir gross wood at 50^0C

moisture content, diffusion and surface emission coefficient. The trend in the contributions of relative humidity and the singularity parameter *x* is almost similar. The contributions of the growth parameter L_1 were also found to remain the same which leads to the obvious conclusion that the TLS model of sorption yields an independent set of information to predict the outputs. Table 5.30 lists sensitivities of diffusion coefficient, surface emission coefficient and the equilibrium moisture content. The GRV_c contributed much for the prediction of the outputs and they were also found to be relatively very sensitive to small changes in its magnitude as Table 5.30 reveals. The outputs were also sensitive to small changes in the magnitudes of the singularity parameter *x*, relative humidity and temperature. They were relatively less sensitive for small changes in both the TLS of chemical composition and

Table 5.30 Sensitivities of the diffusion coefficient, surface emission coefficient and equilibrium moisture content prediction of Douglas-fir on small changes of the corresponding general inputs

Input	Outputs sensitivities								
	Average			Average Square			Variance		
	M	D	S	M	D	S	M	D	S
Wood type	-0.010	-0.004	-0.002	0.000	0.000	0.000	0.000	0.000	0.000
m_f/m_i	0.169	-0.066	-0.044	0.070	0.059	0.045	0.041	0.055	0.043
H	0.765	-0.330	-0.327	0.724	0.200	0.186	0.139	0.091	0.079
T	-0.033	-0.373	-0.313	0.033	0.262	0.194	0.032	0.124	0.096
Ring no	0.062	0.165	0.159	0.020	0.070	0.065	0.016	0.043	0.040
Width	0.003	-0.018	-0.005	0.004	0.011	0.008	0.004	0.011	0.008
Density	-0.023	-0.035	-0.037	0.002	0.005	0.006	0.001	0.004	0.005
GRV	0.014	-0.012	-0.001	0.001	0.001	0.001	0.000	0.001	0.001
GRV_c	-19.611	-8.277	-14.190	1845.773	3864.136	3564.991	1461.935	3797.541	3365.337
Chem-TLS	-0.012	-0.024	-0.029	0.001	0.004	0.004	0.001	0.004	0.004
Arabinose	-0.029	0.080	0.069	0.005	0.022	0.016	0.004	0.016	0.011
Galactose	-0.031	-0.044	-0.048	0.001	0.005	0.005	0.000	0.003	0.003
Glucose	-0.052	0.025	0.021	0.005	0.004	0.004	0.003	0.003	0.003
Xylose	0.011	-0.012	0.000	0.002	0.002	0.002	0.002	0.002	0.002
Mannose	-0.018	-0.048	-0.052	0.003	0.008	0.008	0.002	0.005	0.005
AIL	-0.015	0.002	-0.002	0.007	0.019	0.015	0.007	0.019	0.015
ASL	0.008	-0.036	-0.042	0.001	0.004	0.005	0.001	0.003	0.003
BET-area	-0.021	-0.040	-0.042	0.002	0.006	0.006	0.001	0.004	0.004
Surface area	0.122	-0.059	-0.057	0.017	0.006	0.005	0.002	0.002	0.002
x	0.113	0.131	0.028	2.671	1.869	0.890	2.659	1.853	0.890
i	-0.014	-0.003	-0.004	0.001	0.001	0.001	0.001	0.001	0.001
c_k	-0.083	0.196	0.185	0.010	0.057	0.053	0.003	0.019	0.019
t-exp	-0.000	-0.000	0.000	0.000	0.000	0.000	0.000	0.000	0.000
L_l	0.071	-0.153	-0.143	0.007	0.035	0.032	0.002	0.012	0.012
c_i	0.019	-0.033	-0.028	0.003	0.004	0.003	0.002	0.002	0.002

individual monosaccharide and lignin content. Thus, it can be concluded that GRV and GRV_c modeling of annual rings created an emergent parameter that was able to successfully replace the role of thickness in sorption or generally in mass transfer in the hygroscopic range.

This study advances the exploratory work done by Avramidis and Iliadis (2005) and Avramidis and Wu (2007) to a new edge in breadth and depth. The unified and heterogeneous model of water vapour sorption in Douglas-fir which was developed and validated in this study is the first of its type on the basis of dealing with sorption at earlywood and latewood level in combination with basic density and chemical composition by considering critical behaviours and mechanisms of self-organization. Recently Frandsen and Svensson (2007) and Frandsen *et al*., (2007) described water sorption in wood by considering both the Fickian and non-Fickian behaviour under an umbrella of "multi-Fickian model" and they also described on the same principle sorption hysteresis. The current study; however, investigated causes of non-Fickian behaviour such as criticality in Douglas-fir wood-water vapour system, heterogeneity in density and chemical composition, and self-organization which were not part of the multi-Fickian modeling. The benefit of this unified and heterogeneous modeling is that it opens up opportunity to identify components and properties that contribute to the overall sorption property in nonlinear and complex way and enables devising ways of controlling certain components to obtain desired sorption behaviour.

6.0 CONCLUSIONS

The study was driven by an ambition to sufficiently explain water vapour sorption in wood which has been displaying non-Fickian behaviour and also to develop a model which is unified in describing the dynamic as well as the static state of water vapour sorption. During the theoretical exploration of the Douglas-fir wood-water vapour interaction it was also identified that not only was the diffusion non-Fickian, it was also coupled with a non stationary or quasi-equilibrium state which made the task formidable. The non-Fickian and dynamical behaviour led to the strengthening of the justification that water vapour sorption in wood is dominated by critical phenomena that involve phase transitions. Based on a single basic premise of two-level and two-component self organization, four novel physical prediction models were derived and validated as integral part of this graduate research. The physical models were used to synergistically enable a unified and heterogeneous modeling of water vapour sorption in Douglas-fir using artificial neural networks computational tools. Extensive experimental data were collected on density and widths of annual rings, carbohydrates and lignin composition. Sorption isotherm points, diffusion and surface emission coefficient of Douglas-fir gross wood were also collected coupled with experimental measurements of dynamic water vapour sorption in earlywood, latewood and annual rings of Douglas-fir. The following findings are delivered by this research

- The TLS modeling of annual rings yielded optimized physical quantities named as GRV/GRC, GRV_c and HTC for which validations performed on Douglas-fir and white spruce densitometry data showed the following physical consequences:

  - The scaling parameters obtained from the statistical mechanics of the GRV are related to the magnitude of sapwood as optimized quantity.
  - The scaling parameters obtained from statistical mechanics of the GRV_c are related to the magnitude of juvenile wood (the leaping phenomenon).
  - The stat-physics of the new quantities explains the link between SOC and the allometric scaling behaviours.
  - Energetic characterization of growth rings.

- In the TLS modeling of chemical composition and physical properties a number of critical exponents were determined that are shown to have application in the prediction of physical properties.
- The TLS modeling of sorption isotherms resulted in a novel method for determining the internal specific surface area of wood from water vapour adsorption isotherms and the method is validated on the isotherms data of Douglas-fir.
- Validation of the isotherms model on Douglas-fir experimental data shows that sorption hysteresis is a quasi-static dynamical phenomenon from which follows that if wood and water vapour are allowed to interact for a very long time accompanied with very small change in thermodynamic parameters, then the sorption and desorption isotherms will asymptotically approach a narrow region and may converge to one another or to a single sorption isotherm.
- The TLS modeling yielded physical quantities that were directly used in the modeling of sorption properties of annual rings of Douglas-fir and in the coarse-graining of annual ring level sorption properties to gross wood using ANNs.
- Analysis of the ANNs models prediction of sorption properties at annual rings level shows that there is more correlation between TLS of physical properties and chemical composition in the narrow range where there is an apparent phase transition, which is at about 65% relative humidity at 25^0C.
- The ANNs carbohydrate and lignin content prediction for Douglas-fir was found to be extremely sensitive to cluster of GRV_c, single GRV_c and GRV which implies existence of potential butterfly-effect (small changes in chemical composition can bring about a drastic change in the wood substance content/ density or sorption properties and vice versa).
- This graduate work delivered ten categories of synergistic MLP ANNs models that predict equilibrium moisture content, diffusion coefficient and surface emission coefficient of Douglas-fir using input variables obtained from annual rings anatomical, physical, chemical composition data and parameters of TLS models.
- Based on results obtained from the prediction of equilibrium moisture content, diffusion coefficient and surface emission coefficient of Douglas-fir it can be concluded that the

dimensional analysis and use of the genetic algorithms for variables selection increased the ANNs performance and reduced the problem of over fitting in the majority of cases.

- The TLS models enabled a simplified and hierarchical ANNs coarse-graining framework that resulted in an improved accuracy and prediction performance of equilibrium moisture content, diffusion coefficient and surface emission coefficient of Douglas-fir over exclusive use of T/H.

The unique attribute of this study is that it was able to build an ANN sorption prediction model from chemical composition and densitometry data up to gross wood level of Douglas-fir by revealing and explaining the inherent physical mechanisms at each level along with the linear and nonlinear relationships between interacting components.

The four novel physical models were primarily implemented to assure wider applicability of the developed ANNs models. Nonetheless, ANNs models like any other data driven models are dependent on the type, quality and representativeness of the database used for training, testing and validation. The sorption database used in this dissertation is experimentally generated from three breast height disks of Douglas-fir. It is well known that the highest variability exists transversally at breast height in a given tree than between trees within a species or across species. Therefore, it can be assumed that the transversal sorption studies may have simulated and captured within species variability in Douglas-fir and the developed models may also have species wide applicability. However, it is necessary to validate and revalidate the developed models on a new dataset that are obtained from a different ecosystem than the origin of the three disks. It is also necessary to test validity of the models for other softwood species. The same validation procedure should be followed if the models are required to be used for hardwood species. If the models are found to be performing poorly in the prediction of sorption properties on new dataset then the ANN models should be retrained, retested and revalidated until an acceptable performance is obtained so that they can incorporate lacking properties/ interactions.

7.0. RECOMMENDATIONS FOR FURTHER WORK

On the basis of the results of this study two domains are clearly visible for further work, namely, research still needed to be carried out at the level of annual ring and those that should be advanced to nano up to molecular level. The introduction of the four novel TLS models revealed a row of challenges that require further investigation for satisfactory solutions. The heterogeneity in annual rings which displayed fractal and multifractal behaviour in Douglas-fir and white spruce, respectively, is probably the urgent challenge that requires an in-depth understanding of physical mechanisms in wood and shall rigorously be solved in the future in similar studies. The TLS modeling of annual rings has a potential to be utilized as a tool in energetic characterization of growth increments which in essence can be utilized as a new frame work for the classification of wood. The benefit of this type of energetic classification of wood is that it enables prediction of modified wood sorption and other properties in a given energy class. The allometric scaling properties and chaotic behaviours shall therefore be investigated across species.

The current increasing accuracy in automated measurement instruments in combination with the ability of a close to continuous data collection and retrieval is enabling the opportunity to study the physical phenomena exhibited due to the interaction of water with wood at various anatomical levels. The fine-scale validity of the TLS modeling can, therefore, be investigated down to nano or molecular level. However, the amount of data generated during studies at fine-scale is so large and complex that conventional analytical tools are not good enough to investigate, discover and reveal the complex governing physical mechanisms and properties hidden in the generated data. Luckily, tools of artificial intelligence such as ANNs and machine learning are bringing forth constantly newer and newer opportunities and solutions to utilize the knowledge and natural laws hidden deep in any data structure. Genetic algorithm for example has recently been applied in the automatic discovery of governing differential equations of natural laws with the respective initial and boundary conditions in the description of nonlinear systems. It is, therefore, commendable that in addition to their applications as a variable selection and modeling tools which is well utilized in this study, ANNs and genetic algorithm are suggested to be used in finding simple conservation laws

and corresponding governing equations that can complement the developed complex ANN modeling of water vapour sorption in wood and further demystify the black box notion in their use at large.

Since models derived from data generally depend on database size, it is always recommended that the neural networks developed should be updated as new datasets that are unseen by them during training are available. The datasets that require further incorporation are Douglas-fir itself, other softwood and hardwood species.

REFERENCES

Abdel-gadir, A. Y. and R. L. Krahmer. 1993a. Estimating the age of demarcation of juvenile and mature wood in Douglas-fir. *Wood and Fiber Science*, 25(3):243–249.

Abe, S. and N. Suzuki.. Complex Earthquake Networks. In: Encyclopaedia of complexity. Ed- Meyers, R.A. Part-19 (S) Springer–Verlag (2009).

Adkins, J.C. *Equilibrium Thermodynamics*. McGraw-Hill, London (1968).

Aguerre, J.R., Suarez, C. and P.E. Viollaz. 1989. New BET Type Multilayer Sorption Isotherms. Part I: Theoretical Derivation of the Model. *Journal of Food Science and Technology (Lebensmittel Wissenschaft und Technologie)*, 22(4):188-191

Aguerre, J.R., Suarez, C. and P.E. Viollaz. 1989. New BET Type Multilayer Sorption Isotherms. Part I: Modeling Water Sorption in Foods. *Journal of Food Science and Technology (Lebensmittel Wissenschaft und Technologie)*, 22(4):192-195

Ahlgren, P.A., Wood, J. R. and D.A.I. Goring. 1972. The fibre Saturation Point of Various Morphological Subdivisions of Douglas-Fir and Aspen Wood. *Wood Science and Technology*, 6:81-84

Alden, H. 1997. Softwoods of North America. United States Department of Agriculture, Forest Service. *Forest Products Laboratory. General Technical Report,* FPL-GTR-102

Alfrey, T., Guerenee, E.F. and W.G. Lloyd. 1966. Liquid sorption in polymers. *Journal of Polymer Science,* C12:249

American Standard for Testing and Materials (ASTM). *Standard guide for moisture conditioning of wood and wood-based materials*, ASTM committee D-7, PA, USA (2000).

Aminabhavi, T.M. and U.S. Aithal. 1988. An overview of the Theoretical Models to Predict Transport of Small Molecules through Polymer Membranes. *JMS-Review of Macromolecular Chemistry and Physics, C28:* 421-474

Anderson, N.T and J.L. McCarthy. 1963. Two Parameter Isotherm Equation for fibre-water systems. *Industrial Engineering and Chemical Process Design and Development*, 2:103-105

Anderson, P. W. 1972. More Is Different. *Science*, 177 (4047): 393-396.

Anderson, R.B. 1946. Modification of the Branauer, Emmett and Teller equation. *Journal of the American Chemical Society*, 68:686-691

Arianos, S. and A. Carbone. 2007. Detrending moving average algorithm: A closed-form approximation of the scaling law. *Physica A*. 382:9-15

Assis, K.T.A. 2004. The principle of physical Proportions. *Annales de la Fondation Louis de Brogile*, 29(1-2):149-171

Auriault, L.J. 1991. Heterogeneous Medium. Is an Equivalent Macroscopic Description Possible? *Applied and Engineering Science*. 29(7):785-795

Auriault, L.J. 2002. Upscaling Heterogeneous Media by Asymptotic Expansions. *Journal of Engineering Mechanics*, 128(8):817-822

Avramidis, S., Englezos, P. and T. Papathanasiou. 1992. Dynamic Nonisothermal Transport in Hygroscopic Porous Media: Moisture Diffusion in Wood. *AIChE Journal, 38* (8): 1992

Avramidis, S., Hatzikiriakos, G.S. and J.F. Siau. 1994. An Irreversible Thermodynamics Model for Unsteady-State Nonisothermal Moisture Diffusion in Wood. *Wood Science and Technology,* 28(3):349-358

Avramidis, S. and Iliadis, L. 2005. Wood-water sorption isotherm prediction with artificial neural networks: A preliminary study. *Holzforschung*, 59:336-341

Avramidis, S. and L. Iliadis. 2005. Predicting wood thermal conductivity using artificial neural networks. *Wood and Fiber Science*, 37:682-690

Avramidis, S. and Siau, F.J. 1987. An Investigation of the External and Internal Resistance to Moisture Diffusion in Wood. *Wood Science and Technology, 21*:249-256

Avramidis, S. and H. Wu. 2007. Artificial neural network and mathematical modeling comparative analysis of nonisothermal diffusion of moisture in wood. *Holz als Roh und Werkstoff*, 65: 89-93

Babiak, M. and J. Kúdela. 1995. A contribution to the definition of fibre saturation point. *Wood Science and Technology*, 29: 217-226

Bahadishia, H. K. D. H. 1999. Neural Networks in Material Science. Review. *ISIJ International,* 39(10):966-979

Baeza, J. and J. Freer. Chemical characterization of wood and its components. In *Wood and Cellulosic Chemistry*. Eds: Hon, N. S. D. and N. Shiraishi.. Marcel Dekker Inc. New York (2001)

Bagley, E. and F.A. Long. 1955. Two Stage Sorption and Desorption of Organic Vapour in Cellulose Acetate. *Journal of American Chemical Society,* 77:2172-2178

Bailer-Jones, M.D. and C.A.L. Bailer-Jones. Modeling data; analogies in neural networks, simulated annealing and genetic algorithms. In *Model based reasoning: Science, Technology,*

values, Eds. Magnani, L. and N. Nersessian. Kluwer Academic/Plenum Publishers, New York (2002)

Bak, P. Tang, C. and K. Wiesenfeld. 1987. Self-organized criticality: an explanation of 1/*f* noise. *Physical Review Letters*, 59: 381-384
Bak, P. Tang, C. and K. Wiesenfeld. 1988. Self-organized criticality. *Physical Review A*, 38: 364

Bakshi, R.B. and R. Chatterjee. 1998. Unification of neural and statistical methods as applied to materials structure-property mapping. *Journal of Alloys and Compounds*. 279:39-46

Barbero, G. and L.R. Evangelista. 2004. Two-level system description for the adsorption phenomenon: the meaning of the adsorption energy. *Physical Letters A*, 324:224–226

Barenblatt, I.G. Scaling. Cambridge University Press (2003).

Basher, I.A. and M. Hajmeer. 2000. Artificial neural networks: fundamentals, computing, design, and application. *Journal of Microbiology,* 43:3-31

Bellamine, F.H. and A. Elkamel. 2008. Model order Reduction Using Neural Network Principal Component Analysis and Generalized dimensional Analysis. *Engineering Computation*. 25(5):443-463

Belli, M. Conti, M., Crippa, p. and C. Turchetti. 1999. Artificial neural networks as approximates of stochastic processes. *Neural Networks,* 12:647-658.

Bertaud, F. and B. Holmbob. 2004. Chemical composition of earlywood and latewood in Norway spruce heartwood, sapwood and transition zone wood. *Wood Science and Technology,* 38:245-256

Bhadeshia, H.K.D.H. 1999. Neural Networks in Material Science. *ISIJ International*, 39(10): 966-979

Bhuiyan, M. T. R., Hirai, N., and N. Sobue. 2000. Changes of Crystallinity Wood Cellulose by Heat Treatment Under Dried and Moist Conditions. *Journal of Wood Science*, 46: 431-436

Blanco, M., Coello, J., Iturriaga, H., Maspoch, S. and J. Pagés. 2000. NIR. Calibration in non-linear systems: different PLS approaches and artificial neural networks. *Chemometrics and Intelligent Laboratory Systems,*50:75-82

Blank, B.T and D.S. Brown. 1993. Nonlinear Multivariate Mapping of Chemical Data Using Feedforward Neural Networks. *Analytical Chemistry,* 65:3081-3089

Bond, B.J, Czarnomski, N.M., Cooper, C. Day, M.E. and M.S. Greenwood. 2007. Developmental decline in height growth in Douglas-fir. *Tree Physiology* 27: 441–453

Bongard, J. and H. Lipson. 2007. Automated reverse engineering of nonlinear dynamical systems, *Proceedings of the North American Academy of Science*, 104(24): 9943–9948

Boquet, R., Chirife, J. and H.A. Igelesias. 1980. Technical note: On the equivalence of isotherm equations. *Journal of Food Technology*. 15: 345-349

Breuckner, S and S. Rudolph. 2000. Neural Control and System Identification Using a Similarity Approach. In: *Smart Structures and materials 2000: Mathematics and Control in Smart Structures*. Ed: Varadan, V.V, Proceedings of SPIE, 3984:244-255

Brown, J.H. and G.B. West .*Scaling in Biology*. A volume in Santa Fe Institute Studies in the Science of Complexity. Oxford University Press, New York (2000)

Brunauer, S., Deming, S. L., Deming, W.E. and E. Teller. 1940. On a theory of the van der Waals Adsorption of Gases. *Journal of American Chemical Society*, 62:1723

Brunauer, S., Emmett, P.H. and E. Teller. 1938. Adsorption of gases in multimolecular layers. *Journal of American Chemical Society*. 60:309-318

Buckingham, E. 1914. On Physical Similar Systems; Illustrations of the Use of Dimensional Equations. *Physical Review*, 4(4):345-376

Campbel, J.R., Swan, E.P. and J.W. Wilson. 1965. Comparison of wood growth zone resinous extracts in Douglas-fir. *Pulp and Paper Magazine of Canada*, 66:248-252

Cardy, J. Scaling and Renormalization in Statistical Physics. *Cambridge lecture notes in physics*. Cambridge University Press (1996).

Cerofolini, F.G and L. Meda. 1998. A theory of multilayer adsorption on rough surfaces in terms of clustering and melting BET piles. *Surface Science*. 416: 403–422

Cerveny, S., Colmenero, J. and A. Alegria. 2007. Dynamics of confined water in different environments. Eds: Koza, M. Frick,B. and R. Zorn. In: 3rd International Workshop on Dynamics in Confinement. *The European Physical Journal*. EPJ ST Special Topics. 141: 49-52

Chen, C.L.P., Cao, Y. and R. LeClair. 1998. Materials structure-property prediction using a self-architecturing neural network. *Journal of Alloys and Compounds,* 279:30-38

Christensen, G.N. 1965. The rate of sorption of Water Vapour by Thin Materials. In*: Humidity and Moisture*, (Ed) Wexler, A., New York, Reinhold Publishers, pp 279-293

Christenensen, G.N. and E.K. Kelsey. 1958. The sorption of Water Vapour by the Constituents of Wood: Determination of Sorption Isotherms. *Australian Journal of Applied Science*, 9:265-282

Christensen, K. and N.R. Moloney. Complexity and criticality. *Imperial College Press Advanced Physics Texts*, Vol 1. Imperial College Press (2005).

Chvosta. P. 2007. Probability distribution of work done on a two-level system during a nonequilibrium isothermal process. *Physical Review E*, 75:041124-1-10

Comstock, L.G. 1963. Moisture Diffusion Coefficient in Wood as Calculated from Adsorption, Desorption, and Steady State Data. *Forest Products Journal,* 13(3):97-103

Condamin, S., Bénichou,O., V. Tejedor1,V., Voituriez, R. and J. Klafter. 2007. First-passage time in complex scale-invariant media. *Nature*, 450(1):77-80

Cook, R.E. and K. Briffa. Data analysis. In *Methods of Dendrochronology*, Applications in the Environmental Sciences. Eds: Cook, R.E. and A. Kairiukstis. Kluwer Academic Publishers (1990).

Crank, J. and G.S. Park. 1951. Diffusion in High Polymers: Some Anomalies and Their Significance. *Transactions of the Faradays Society*, 47:1072-1084

Crank, J. and S.G. Park. *Diffusion in polymers*. Academic Press London (1968).

Crank, J. *The Mathematics of Diffusion*. Clarendon Press, Oxford (1975).

Crooks, E.G. 2000. Path-ensemble averages in systems driven far from equilibrium. *Physical Review E*, 61(3):2361-2366

Cunningham, M.J. 1994. A Model to Explain "Anomalous" moisture Sorption in Wood under Step Function Driving Forces. *Wood and Fiber Science,* 27 (3): 265-277

Curtis, R.O. 1967. Height-Diameter and Height-Diameter-Age Equation for Second Growth Douglas-fir. *Forest Science*. 13(4):365:375

Dahmen, A.K., Sethna, P.J., Kuntz,C.M. and O. Perković. 2001. Hysteresis and avalanches: phase transitions and critical phenomena in driven disordered systems. *Journal of Magnetism and Magnetic Materials*. 226-230: 1287-1292

De Boer, J.H. *The Dynamical Character of Adsorption*. Oxford: Clarendon Press (1953). pp 200-219

De La Barra, L.B and B. Günter. 1965. Thermal Similarity Principle, Dimensional Analysis and Homeothermy. *Acta Physiologica Latino America*, 15(4):378-385

Demetrius, L. 2006. The origin of allometric scaling laws in biology. *Journal of Theoretical Biology,* 243:455–467

Denbigh, G.K. and J.S. Denbigh. *Entropy in relation to incomplete knowledge.* Cambridge University Press, Cambridge, London, New York, New Rochelle, Melbourne, Sydney (1985).

Dent, R.W. 1977. A multilayer theory for gas adsorption. I. Sorption of a single gas. *Textile Research Journal*. 47:145-152

Deslauriers, A. Rossi, S. and A. Tommaso. 2007. Dendrometer and interannual tree growth. What kind of information can be inferred? *Dendrochronologia*, 25: 113–124

Donald, F.S. 1992. Enhancement to probabilistic neural networks. *IEEE,* 0-7803-0559:761-768

Donohue, M.D. and G.L. Aranovich. 1998. Classification of Gibbs adsorption isotherms. *Advances in Colloid and Interface science*. 76-77:137-152

Donohue, M.D. and G.L. Aranovich.1999. A new classification of isotherms for Gibbs adsorption of gases on solids. *Fluid Phase Equilibra,* 158–160:557–563

Downes, G. M., Wimmer, R. and R. Evans. 2002. Understanding wood formation: gains to commercial forestry through tree-ring research. *Dendrochronologia,* 20 (1-2): 37-51

Dwianto, W., Tanaka, F., and M. Inoue. 1996. Crystallinity changes of wood by heat or steam treatment. *Wood Research*. 83: 47-49

Easty, D.B. and E.W. Malcolm. 1982. Estimation of pulping yield in continuous digesters from carbohydrate and lignin determinations. *TAPPI Journal*, 65(12):78–80

Fahlman, S.E. and C. Labiere. 1990. The cascade-Correlation learning architecture, *Carniege Mellen Report,* CMU-CS-88162

Fahlman, S. The Cascade –Correlation Learning Architecture. In *Advances in Neural Information Processing Systems 2*, ed: David S. Touretzky, San Mateo, California: Morgan Kaufmann Publishers(1990).

Fan, K., Hatzikiriakos, S. G. and S. Avramidis. 1999. Determination of the surface fractal dimension from sorption isotherms of five softwoods. *Wood Science and Technology* 33:139-149

Farmer, L.C. 2002. Upscaling: a review. *International Journal for Numerical Methods in Fluids*, 40:63-78

Favre, E., Nguyen, T.Q., Clément, R. and J. Néel. 1995. The engaged species induced clustering (ENSIC) model: a unified mechanistic approach of sorption phenomena in polymers. *Journal of Membrane Science*. 117:227-236

Fernandes, F. and L. Lona. 2005. Neural Network application in polymerization processes. *Brazilian Journal of Chemical Engineering,* 22(03):401-418

Forest, S. 1993. Genetic Algorithms of Natural Selection. *Science, New series*, 261(5123):872-878

Francis, W.M., Schwarze, R., Spycher, M. and S. Fink. 2008. Superior wood for violins-wood decay fungi as a substitute for cold climate. *New Phytologist,*179:1095-1104

Frandsen, L.H. Modeling of Moisture Transport in Wood –State of the Art and Analytic Discussion. *Wood Science and Timber Engineering, Paper no. 1*, 2nd edition. Department of Building Technology and Structural Engineering (2005).

Frandsen, L.H. and S. Svensson. 2007. A revised multi-Fickian moisture transport to describe non-Fickian effects in wood. *Holzforschung*, 61:563–572

Frandsen, L.H. and S. Svensson. 2007. Implementation of sorption hysteresis in multi-Fickian moisture transport. *Holzforschung,* 61:693–701

Frandsen, H.L., Svensson, S. and L. Damkilde. 2007. A hysteresis model suitable for numerical simulation of MC in wood. *Holzforschung*, 61:175–181

Gallos, K.L., Song, C., Havlin, S. and H.A. Makse. 2007. Scaling theory of transport in complex biological networks. *Proceedings of the National Academy of Sciences*. 104(19): 7746–7751

Garrahan, J. P., Jack, R. L., Lecomte, V., Pitard, E. van Duijvendijk, K. and F. van Wijland. 2007. Dynamical First-Order Phase Transition in Kinetically Constrained Models of Glasses. *Physical Review Letters*, 98-195702:1-4

Garrahan, J. P., Jack, R. L., Lecomte, V., Pitard, E., van Duijvendijk, K. and F. van Wijland. 2009. First-order dynamical phase transition in models of glasses: an approach based on ensembles of histories. *Journal of Physics A: Mathematical and Theoretical,* 42 -075007:1-34

Geoffrey, M.D., Wimmer R. and R. Evans. 2002. Understanding wood formation: gains to commercial forestry through tree-ring research. *Dendrochronologia*, 21(1-2):37-51

Geszti, T. Physical Models of neural Networks. World Scientific. Singapore (1990)

Greaves, N.G., Wilding, M.C., Fearn, S., Langstaff, D., Kargel, F., Cox, S., Van, Q.V. Majérus,O., Benmore, J.C. Weber, R. Martin, M.C. and L. Hennert. 2008. Detection of First-Order Liquid/Liquid Phase Transitions in Yttrium Oxide-Aluminum Oxide Melts. *Science*. 322:566-570

Gregg, J.S. and K.S.W. Sing. *Adsorption, Surface Area and Porosity*. Academic Press (1982).

Groen, C.J., Peffer, A.A.L. and J. Pérez-Ramírez. 2003. Pore size determination in modified micro- and mesoporous materials. Pitfalls and limitations in gas adsorption data analysis. *Microporous and Mesoporous Materials*, 60:1-17

Gugenheim, E.A. *Application of Statistical Mechanics*. Oxford: Clarendon Press (1966).

Gukhman, A.A. 1965. *Vedeniye v Toriyu Podobiya "Introduction to the theory of similarity"*. Translated by Scripta Technica, Inc. Academic Press New York and London

Günter, B., Morgado, E. and R.F. Jiménez. 2003. Homeostasis and Heterostasis: from Invariant to Dimensionless Numbers. *Biological Research*, 36:211-221

Hale, J.D. and L.P. Clement. 1963. Influence of prosenchyma cell-wall morphology on basic physical and chemical characteristics of wood. *Journal of Polymer Science Part C: Polymer Symposia.* 2:253-261

Hartley, D.I. and A.F. Kamke. 1992. Cluster theory for water sorption in wood. *Wood Science and Technology,* 26:83-99

Hartley, I.D. and S. Avramidis. 1993. Analysis of the Wood Sorption Isotherm Using Clustering Theory. *Holzforschung*, 47:163-167

Havlin, S. and D. Ben-Avraham. 2002. Diffusion in disordered media. *Advances in Physics*, 51(1):187-292

Haykin, S. *Neural Networks*, A Comprehensive Foundation. McMillan College Publishing Company, New York (1994)

Hebb, D.O. The organization of behaviour, Wiley, New York (1949)

Hedges, O.L, Jack, L.R. Garrahan, P.J. and D. Chandler. 2009. Dynamic Order-Disorder in Atomistic Models of Structural Glass Formers. *Science,* 323:1309-1313

Hedström, J. Swenson, J., Bergman, R., Jansson, H. and Kittaka. 2007. Does confined water exhibit a fragile-to-strong transition? Eds: Koza, M. Frick,B. and R. Zorn. In: 3rd International Workshop on Dynamics in Confinement. *The European Physical Journal*. EPJ ST Special Topics. 141: 53-56

Hinton, G. E. and R. R. Salakhutdinov. 2006. Reducing the dimensionality of data with neural networks. *Science,* 313:504-507

Hofstetter, K, Hellmich, C. and J. Eberhardsteiner. Hierarchical organization of wood revisited in the framework of continuum micromechanics. In: European Congress on

Computational Methods in Applied Sciences and Engineering. Eds. Neittaanmäki et al. (2004).

Holcomb, T.R. and M. Morari. 1992. PLS/Neural Networks. *Computers and Chemical Engineering,* 16(4):393-411

Hollister, J.S. and N. Kikuchi. 1992. A Comparison of homogenization and standard mechanics. *Computational Mechanics*, 10(2):73-95

Horii, F. Structure of Cellulose: Developments in its Characterization. In Wood and Cellulosic Chemistry. Eds:Hon,N. S. D. and N. Shiraishi.. Marcel Dekker Inc. New York (2001)

Holland, J. H. 1973. Genetic Algorithms and the Optimal Allocation of Trials. *SIAM Journal on Computing*. 2(2): 88-105

Hopfield, J.J. 1982. Neural Networks and Physical Systems with Emergent Collective Computational Abilities. *Proceedings of the National Academy of Sciences*, 79:2554

Hopfield, J.J. 1984. Neurons with graded response have collective computational abilities. *Proceedings of the National Academy of Science*, 79:2554-2558

Hopefield, J.J. and D.W. Tank. 1985. Neural computation of decision in optimization problems. *Biological Cybernetics*, 52:141-152

Hopkinson, I., Jones, A.L.R., Black, S., Lane, M.D. and P.J. McDonald. 1997. Fickian and Case II diffusion of Water into Amylose: A Stray Field NMR Study. *Carbohydrates Polymers, 34*: 39-47

Howard, N. 1976. Exponential Dependency of the Moisture Diffusion Coefficient on Moisture Content, *Wood Science*, 8(3):174-181

Huangfu, D., Osafune, K., Maehr, R., Guo, W., Eijkelenboom, A., Chen, S., Muhlestein, W. and D. Melton. 2008. Induction of pluripotent stem cells from primary human fibroplasts with only Oct4 and Sox2. *Nature Biotechnology*. 26(11):1269-1275

Hunter, A.J. 1993. On movement of water through wood-The diffusion coefficient, *Wood Science and Technology*, 27:401-408

Hutter, K. and K. Jöhnk. *Continuum Methods of Physical Modeling. Continuum Mechanics, Dimensional Analysis, Turbulence*. Springer, (2004). pp 339-419

IUPAC. 1972. Manual of Symbols and Terminology, Appendix 2 – Pure and Surface Chemistry. *Pure and Applied Chemistry*, 31:578

Jacobs, H.M. 1967. *Diffusion Processes*. Springer-Verlag, New York Inc. 160p

Jarzynski, C. 1997. Nonequilibrium Equality for Free Energy Differences. *Physical Review Letters*, 78(14):2690-2693

Johnson, K.N. and F.J. Swanson. Historical Context of Old-growth in the Pacific Northwest-Policy, Practices, and Competing Worldviews. In: Old growth in a New World: a Pacific Northwest icon re-examined. Eds: Thomas A. Spies and Sally L. Duncan. Washington, DC: Island Press, (2009). p. 12-30

Johnstone, E.R. and Thring, W.M. *Pilot Plants, Models, and Scale-up Methods in Chemical Engineering.* McGraw-Hill Book Company, Inc, New York (1957).

Jonquiéres, A. and Fane, A. 1998. Modified BET models for Modeling Water Vapour sorption in Hydrophilic Glassy Polymers and Systems Deviating Strongly from Ideality. *Journal of Applied Polymer Science*, 67:1415-1430

Jozsa, L.A., Munro, B.D. and J.R. Gordon. 1998. Basic wood Properties of second-growth Western Hemlock. British Columbia. Forest Practices Branch and Forintek Canada Corp. *Special Publication* No. Sp–38.

Jozsa, L. A., J. E. Richards, and S. G. Johnson. 1987. Calibration of Forintek's Direct Reading X-Ray Densitometer. *Research Report CFS No. 36a*. Forintek Canada Corp., Vancouver, BC.

Joseph, B. Wang, H.F. and S.S.D. Shieh. 1992. Exploratory Data Analysis: A Comparison of Statistical Methods with Artificial Neural Networks. *Computer and Chemical Engineering,* 16 (4):413-423

Joshi, S.R and G. Astarita. 1979. Diffusion – Relaxation coupling in polymers which Show Two Stage Sorption Phenomena. *Polymers, 20:*455-461Kelsey, K.E. 1957. The sorption of water vapour by wood. *Australian Journal of Applied Science,* 8:42-54

Kalospiros, S.N., Raffaella, O., Astarita, G. and J.H. Meldon. 1991. Analysis of Anomalous Diffusion and Relaxation in Solid Polymers. *Industrial Engineering Chemical Research, 30*:851-864

Kantelhardt, J.W., Zschiegner, S.A., Koscielny, E., Havlin, S., Bunde, A. and H.E. Stanley. 2002. Multifractal detrended fluctuation analysis of nonstationary time series. *Physica A*. 316:87:114

Kennedy, R.W. 1961. Variation and periodicity of summerwood in some second-growth Douglas-fir. *Tappi*, 44:161-166

Kennedy, R.W. and W.G. Warren. 1970. Within tree variation in physical and chemical properties of Douglas-fir. In: *Second world consultation on forest tree breeding*, 1:393-417, Washington, DC.

Klopffer, H.M. and B. Flaconnè. 2001. Transport Properties of Gases in Polymers: Bibliographic Review. *Oil and Gas Science Technology-Rev. IFP*, 56(3):223-244

Kohler, R. Dück, Renate, Ausperger, B. A. Rainer. 2003. A numeric model for the kinetics of water vapour sorption on cellulosic reinforcement fibres. *Composite Interfaces*, 10(2-3):255-276

Kohnen, T. *Associative memory: a system theoretic approach*. Springer, New York (1977).

Kohnen, T. 1982. Self-organized formation of topologically correct feature maps, *Biological cybernetics*, 43:59-69

Kohnen, T. *Self-organization and associative memory*. First edition, Springer Verlag, Berlin (1984).

Kohnen, T. *Self organizing and associative memory*. Third edition, Springer Verlag, Berlin (1989)

Koubaa, A., Isabel, N., Zhang S.Y. and J. Beaulieu. 2005. Transition from juvenile to mature wood in black spruce (*Picea mariana* (mill.) B.S.P.). *Wood and Fiber Science,* 37(3):445 – 455

Koubaa, A., Zhang, S.Y.T. and S. Makni. 2002. Defining the transition from earlywood to latewood in black spruce based on intra-ring wood density profiles from X-ray densitometry. *Annals of Forest Sciences*, 59:511-518

Krabbenhøft, K. and L. Damkilde. 2004. A model for non-Fickian moisture transfer in wood. *Materials and Structures,* 37:615-622

Krabbenhøft, K. and L. Damkilde. 2004. Double porosity for the description of water infiltration in wood. *Wood Science and Technology*. 38: 641–659

Kränz, H., Vill, V. and B. Meyer. 1996. Prediction of Materials Properties from Chemical Structures. The Clearing Temperature of Nematic Liquid Crystals Derived from Their Chemical Structures by Artificial Neural Networks. *Journal of Chemical Information Computer Science*,36:1173-1177

Le, V.C. and N.G. Ly. 1992. Multilayer Adsorption of Moisture in Wool and Its Application in Fabric Steaming. *Textile Research Journal*, 62(11):648-657

Lecomte, V. Appert-Rolland, C. and F. van Wijland. 2005. Chaotic properties of systems with Markov dynamics. *Physical Review Letters.* **95 :**010601-4

Lightfoot, P.M., Bruce, J.G., McPherson, A.N. and K. Woods. 2005. The Application of Artificial Neural Networks to Weld-Induced Deformation in Ship Plate. *Welding Journal, Welding Research, Supplement to Welding Research*, pp. 23-30

Lin, H.S. 1990. Moisture Absorption in Cellulosic Materials. *International Journal of Engineering Sciences*, 28(11): 1151-1156
Liu, Y.J. 1989. A new method for separating diffusion coefficient and surface emission coefficient, *Wood and Fiber Science,* 21(2): 133-141

Liu, Y.J. and W.T. Simpson. 1996. Mathematical relationship between surface emission and diffusion coefficient. *Drying Technology*, 14(3&4):677-699

Lu, G. and E. Kaxiras. 2005. An overview of multiscale simulation materials. In *hand Book of Theoretical and Computational Nanotechnology*. Eds. Reith, M. and W. Schommers.

Luikov, A.V. *Heat and Mass Transfer in Capillary-porous Bodies*. Pergamon Press (1966).

Mandelbrot, B. B. *Fractals: Form, chance, and dimension*. San Francisco: W. H. Freeman, (1977).

Mandelbrot, B. B. *The fractal geometry of nature*. San Francisco: W.H. Freeman, (1982).

Mangel, A. 2000. Identifying physical and chemical phenomena with gravimetric water sorption analysis. *Journal of Thermal and Calorimetry*, 62:529-537

Mansfield, S. D., Iliadis, L. and S. Avramidis. 2007. Neural network prediction of bending strength and stiffness in Western Hemlock. *Holzforschung,* 61:707-716.

Mansfield, S.D, Parish, R., Di Lucca, C.M, Goudie, J. Kang, K-Y. and P. Ott. 2009. Revisiting the transition between juvenile and mature wood: a comparison of fibre length, microfibril angle and relative wood density in lodgepole pine. *Holzforschung*, 63: 449–456

Marchetti, M. C. Introduction to statistical and non-linear physics. In: Encyclopaedia of complexity. Ed- Meyers, R.A. Part-19 (S), Springer–Verlag (2009).

McCulloch, W.S. and W. Pitts. 1943. A logical calculus of the idea immanent in nervous activity. *Bulletin of Mathematical Biophysics*. 5:258-267

Marengo, E. Bobba, M. Robotti, E. and C.M. Liparota. 2006. Modeling of the polluting Emissions from a cement Production Plant by Partial Least-Squares, Principal Component Regression, and Artificial Neural Networks. *Environmental Science and Technology,* 40:272-280.

Masaro, L. and Zhu, X.X. 1999. Physical Models of Diffusion for Polymer Solutions, gels and Solids. *Progress in Polymer Science, 24*:731-775

Massen, C.H., Poulis, A.J. and E. Robens. 2000. Criticism on Jäntti's Three Point Method on Curtailing Gas Adsorption Measurements. *Adsorption*, 6:229-232

McMillan, F.P. 2004. Polyamorphic transformations in liquids and gases. *Journal of Materials Chemistry*. 14:1506-1512

Monson, A. P. 2005. Recent Progress in Molecular Modeling of Adsorption and Hysteresis in Mesoporous Materials. *Adsorption*, 11: 29–35

Newman, A.B. 1931. The drying of Porous Solids: Diffusion and Surface Emission Equations. *Transactions of American Institute of Chemical Engineers,* 27: 203-216

Nkano, T. Non-steady state water adsorption of wood. 1994. Part 1. A formulation of water adsorption. *Wood Science and Technology*, 28:359-363

Nkano, T. Non-steady state water adsorption of wood. 1994. Part 2.Validity of the theoretical equation of water adsorption. *Wood Science and Technology*, 28:450-456

Olek, W., Perré, P. and J. Weres. 2005. Inverse analysis of the transient bound water diffusion in wood. *Holzforschung*, 59: 38–45

Olek,W. and J. Weres. 2007. Effects of the method of identification of the diffusion coefficient on accuracy of modeling bound water transfer in wood. *Transport in Porous Media*, 66:135–144

Paass, G. 1992. probabilistic reasoning and probabilistic neural networks. *International Journal of Intelligent Systems*, 7:47-59

Pan, G. and Liss, S.P. 1998. Metastable-equilibrium adsorption theory: I Theoretical. *Journal of Colloid and Interface Science*, 201:71-76

Pang, S. and A. Herritsch. 2005. Physical properties of earlywood and latewood of *Pinus radiate* D. Don: Anisotropic shrinkage, equilibrium moisture content and fibre saturation point. *Holzforschung*, 59:654-661

Panshin, J.A. and C. De Zeeuw. *Textbook of Wood Technology – Structure, Identification, Properties, and Uses of the Commercial Woods of the United States and Canada*. Fourth Edition, (1980), pp 251-281.

Patterson, W.D. *Artificial neural networks-Theory and application*. Institute of system science, National University of Singapore, Prentice Hall (1996).

Peralta, P.N. 1995. Modeling wood moisture sorption hysteresis using the independent domain theory. *Wood and Fiber Science*, 27(3):250–257

Peralta, P.N. 1995. Sorption of moisture by wood within a limited range of relative humidities. *Wood and Fiber Science*, 27(1):13–21

Peralta, P. N. and A. P. Bangi. 1998. Modeling Wood Moisture Sorption Hysteresis Based on Similarity Hypothesis. Part 1. Direct Approach. *Wood and Fiber Science,* 30 (1): 48-55

Peralta, P. N. and A. P. Bangi. 1998. Modeling Wood Moisture Sorption Hysteresis Based on Similarity Hypothesis. Part II. Capillary-Radii Approach. *Wood and Fiber Science*, 30(2): 148-154

Pérre, P. 2007. Multiscale aspect of heat and mass transfer during drying. *Transport in Porous Media*, 66(1-2):59-76

Pérre, P. and É. Badel. 2003. Predicting of oak wood properties using X-ray inspection: representation, homogenization and localization. Part II: Computation of macroscopic properties and microscopic stress fields. *Annals of Forest Sciences*, 60:247-257

Pérre, P. and I. Turner. 2001. Determination of the Material Property Variation Across the Growth Ring of Softwood for Use in Heterogeneous Drying Model. Part 1. Capillary Pressure, Tracheid Model and Absolute Permeability. *Holzforschung*, 55:318-323

Pérre, P. and I. Turner. 2001. Determination of the Material Property Variation Across the Growth Ring of Softwood for Use in Heterogeneous Drying Model. Part 2. Use of Homogogenization to Predict Bound Liquid Diffusivity and Thermal Conductivity, *Holzforschung*, 55:417-425

Pfeifer, P., Wu, J.Y., Cole, W.M. and J. Krim. 1989. Multilayer Adsorption on a Fractally Rough Surface. *Physical Review Letter*, 62:17

Poole, H.P., Sciortino, F., Essmann, U. and E.H. Stanley. 1992. Phase behaviour of metastable water. *Nature*. 360:324

Popovski, D. and V. Mitrevski. 2004. Some New Four Parameter Models for Moisture Sorption Isotherms. *EJEFChe.* 3(3)

Popovski, D. and Mitrevski, V. 2004.A Method for Extension of the Water Sorption Isotherm Models. *EJEFChe.* 3(6)

Qin, J.S. and J.T. McAvoy. 1992. Nonlinear PLS Modeling Using Neural Networks. *Computers and Chemical Engineering,* 16(4):379-391

Rawat, S.P.S. and P.D. Khali. 1999. Studies on adsorption behaviour of water vapour in lignin using the Brunaur-Emmett-Teller theory. *Holz als Roh- und Werkstoff*, 57:203-204

Rayirath, P, Avramidis, S. and S. Mansfield. 2008. The effect of Wood Drying on Crystallinity and Microfibril Angle in Black Spruce. *Journal of Wood Chemistry and Technology*, 28: 167-179

Ripa, M. and L. Frangu 2004. A survey of Artificial Neural Networks Application in Wear and Manufacturing Processes. *Tribiology. The Analysis of University 'Dunârea de Jos' of Galati*, Fascicle VIII: 35-42

Ritort, F. 2004. Work and heat fluctuations in two-state systems: a trajectory thermodynamics formalism. *Journal of Statistical Mechanics: Theory and Experiment.* P10016:1-33

Robens, E., Krebs, F.K., Meyer, K. and K.K. Unger. 1999. Standardization of sorption measurements and reference materials for dispersed and porous solids. In: *Adsorption and its Application in industry and Environmental Protection*, 120:95-116

Robertsen, L. and B. Lönnberg. 1991. Diffusion in Wood-Part 1. Theory and apparatus. *Paper and Timber*, *73*(6):532-535

Scarselli, F. and A.C. Tsoi. 1998. Universal approximation Using Feedforward Neural Networks: A survey of some Existing Methods, and Some New Results. *Neural Networks*, 11:15-37

Robinson, W.J. Dendrochronology in Western North America: The Early Years. In *Methods of Dendrochronology*, Applications in the Environmental Sciences. Eds: Cook, R.E. and A. Kairiukstis. Kluwer Academic Publishers (1990)

Rogers, C.E. 1985. Permeation of Gases and Vapours in Polymers. In: *Polymer Permeability*, Comyn, J. (Ed), Elsevier Applied Science, pp. 11-73

Rosen, H.M. 1978. The influence of external resistance on moisture adsorption rates in wood. *Wood and Fiber Science*, 10(3):218-228

Rosenblatt, F. 1958. The perceptron; a probabilistic model for information storage and organization in the brain. *Psychological Review*, 65:386-408

Rouvray, H.D. 1992. Definition and Role of Similarity Concepts in the Chemical and Physical Sciences. *Journal of Chemical Informatics and Computer Science*, 32:580-586

Roy, S., Xu, X.W., Park, J.S. and K.M. Liechti. 2000. Anomalous Moisture Diffusion in Viscoelastic Polymers: Modeling and Testing. *Journal of Applied Mechanics, 67*:391-396

Rumelhart, E.D., Hinton, E.G. and R.J. Williams. Learning internal representations by error propagation. In *Parallel and distributed processing: Exploration in microstructures of cognition, Vol 1: Foundations*, Eds: Rumelhart, E.D. and J.L. McClelland, MIT Press, Cambridge, MA (1986)

Rumelhart, D. and J. Mclelland. *Parallel distributed processing: Exploitation in the micro structure of cognition*, Volume1, MIT Press, Cambridge (1986).

Saka.S. Chemical Composition and Distribution. In *Wood and Cellulosic Chemistry*. Eds:Hon,N. S. D. and N. Shiraishi.. Marcel Dekker Inc. New York (2001)

Salin, G.J. 2003. External Heat and Mass transfer- Some Remarks. *8th International IUFRO Wood Drying Conference*. 343-348

Sánchez-Maroñoz, N., Fontenla-Romero, O., Casteillo, E. and A. Alonso-Betanzos. 2005. Modeling Engineering Problems Using Dimensional Analysis for Feature Extraction. In: *Artificial Neural Networks: Formal Models and Their Applications ICANN 2005*. Eds: Duch, W., Kacprzyk, J., Oja, E. and S. Zadrozny.15th International Conference, Warsaw, Polland, Proceedings, Part II: 949-961

Schmidt, M. and H. Lipson. 2009. Distilling Free-Form Natural laws from Experimental Data, *Science*, 324(81): 81-85

Shiyatov, S., Mazepa, V. and P.D. Jones. Data analysis. In *Methods of Dendrochronology, Applications in the Environmental Sciences*. Eds: Cook, E.R. and L.A. Kairiukstis. Kluwer Academic Publishers (1990).

Siau, F.J. 1995. *Wood: Influence of Moisture on physical Properties*. Department of Wood Science and Forest Products Virginia Polytechnic Institute and State University, pp 111-188

Siau, J.F. and Avramidis, S. 1993. Application of a Thermodynamic Model to Experiments on Nonisothermal Diffusion of Moisture in Wood. *Wood Science and Technology, 27*:131-136

Simmons, S.C. Nielson, R.D. and W. Biggar. 1979. Scaling of Field Measured Soil-water Properties: I. Methodology, II Hydraulic Conductivity and Flux. *Hilgardia*, 47(4):77-173

Simpson, W.T. 1973. Predicting equilibrium moisture content of wood by mathematical models. *Wood and Fiber Science*. 5:41-49

Simpson, W.T. 1979. Sorption Theories for wood. In: *Proceedings of symposium on wood moisture content and humidity relationships*. Virginia polytechnic Institute, State University, Blacksburg VA, US FPL, Madison WI: 36-46

Simpson, W. and A. TenWolde. Physical Properties and Moisture Relations of Wood. In: *Wood handbook*: wood as engineering material, Forest Products Laboratory, *General technical report* FPL; GTR-113: 3.1-3.23, Madison, WI : USDA Forest Service (1999).

Sing, K.S.W, Everett, D.H., Haul, R.A.W., Moscou, L., Pierotti, R.A., Rouquérol and R.A. Siemieniewska. 1985. Reporting physisorption data for gas/solid systems with special reference to the determination of surface area and porosity. *Pure and Applied Chemistry*, 57(4):603-619

Sivanandam, S.N. and S.N. Deepa. *Introduction to genetic algorithms*. Springer, Berlin Heidelberg (2008)

Skaar, C. 1958. Analysis of Methods for Determining the Coefficient of Moisture Diffusion in Wood. *Forestry, 278*:1-8

Skaar, C. 1958. Moisture movement in beech below the Fiber saturation point. *Forest Products Journal,* 8:352-357

Skaar, C. *Water in Wood*. Syracuse University Press (1972).

Skaar, C. *Wood-Water relations*. Springer Verlag. Berlin, Heidelberg, New York, London, Paris and Tokyo (1988).

Sonin, A.A. 2004. A generalization of the π-theorem and dimensional analysis. *Proceedings of the National Academy of Science*, 101(23):8525-8526

Sornette, D. 1994. Power Laws without Parameter Tuning: An Alternative to Self-Organized Criticality. *Physical Review Letters*, 72(14):2306

Spalt, H.A. 1957. The sorption of water vapour by domestic and by domestic tropical species. *Forest Products Journal*, 7:331-335

Squire, G.B. 1967. *Examination of cellulose-lignin relationships within coniferous growth zones*. PhD thesis, University of BC

Stahl, R.W. 1962. Similarity and Dimensional Methods in Biology. *Science*, New series, 137(3525):205-212

Stamm, A.J. 1960. Combined bound-water and water vapour diffusion into Sitka spruce, *Forest Products Journal*, 10:644-648

Stamm, J.A. 1964. *Wood and cellulose Science*. The Ronald Press Company, New York, pp 410-440

Starkweather, H.W. 1963. Clustering of water in polymers. *Polymer Letters*. 1: 133-138

Starkweather, H.W. 1975. Some aspects of water clusters in polymers. *Macromolecule*, 8(4):476-479

Suykens, A.K.J., Vanderwalle, P.L.J. and B.L.R. De Moor. *Artificial Neural Networks for Modeling and Control of Non-Linear Systems*. Kluwer Academic Publishers. Boston (1996)

Tekleyohannes, T.A. and S. Avramidis. 2009. Two-level self-organization of properties of wood. A new paradigm for dimensional analysis and scaling. *Wood Science and Technology*. Published online first, DOI 10.1007/s00226-009-0279-9.

Todes, D. 2009. Global Darwin: Contempt for competition. *Nature*, 462:36-37

Tolman, C.R. 1914. The principle of Similitude. *Physical Review*, 3:244-255

Vesely, D. 2008. Diffusion of liquids in polymers. *International Materials Review*. 53 (5):299-315

Vaganov, A.E, Hughes, K.M. and Shashkin, V.A. 2006. Growth Dynamics of Conifer Tree Rings, Images of Past and Future Environments. In *Ecological Studies*, *Analysis and Synthesis.* Eds: Caldwell, M.M., Heldmaier, G., Jackson, R.B., Lange, O.L., Mooney, H.A., Schulze, E.-D., and U. Sommer, 183:1-19

Vahey, D. W., Zhu, J. Y. and C. T. Scott. 2007. Wood density and anatomical properties in suppressed-growth trees: comparison of two methods. *Wood and Fiber Science,* 39(3):462 – 471

Verleysen, M., Francois, D., Simon, G. and V. Wertz. 2003. On the effects of dimensionality on data analysis with neural networks. In: Artificial *Neural Nets Problem Solving*. Eds**:** Mira, J. and J.R. Álvarez, Proceedings of the 7th International Work-Conference on Artificial and Natural Neural Networks: Part II: 1044-1052

Von Storch, H. Zorita, E., Jones, M.J., Dimitriv, Y., González-Rouco, F. and S.F.B. Tett. 2004. Reconstructing Past Climate from Noisy Data, *Science*, 306:679-682

Wadsö, L. 1992. A critical Review on Anomalous or Non-Fickian Vapour Sorption. *Internal Report 7017*, Division of Building Materials Lund University

Wadsö, L. 1993. Surface mass transfer coefficients for wood. *Drying Technology*, 11(6):1227-1249

Wadsö, L. 1994. Describing non-Fickian Water –vapour Sorption in Wood. *Journal of Materials Science, 29*:2367-2372

Wadsö, L. 1994. Unsteady-state water-vapour adsorption in wood – an experimental-study. *Wood and Fiber Science, 26*(1):36–50

Wangaard F. and L. Granados. 1967. The effect of Extractives on Water-Vapour Sorption by Wood. *Wood Science and Technology,*1: 253-277

Wautelet, M. 2001. Scaling laws in the macro-, micro- and nanoworlds. *European Journal of Physics*. 22:601-611

West, G.B., Brown, J.H. and B.J. Enquist. 1999. A general model for the structure and allometry of plant vascular systems. *Nature*, 400: 664-667

Whitehead, L., Whitehead, R., Valeur, B. and M. Berberan-Santos. 2009. A simple function for the description of near-exponential decays: The stretched or compressed hyperbola. *American Journal of Physics*. 77(2):173-179

Williams, G.P. *Chaos Theory Tamed*. Taylor & Francis limited, London (1997).

Winkel, K., Elsaesser, S. M., Mayer, E. and T. Loerting. 2008. *The Journal of Chemical Physics*. 128

Wu, J. and H. Li. Concepts of scale and scaling. In *Scaling and Uncertainty Analysis in Ecology*. Eds: Wu, J., Jones, B.K., Li,H. and O.L. Loucks. Springer (2006).

Yamanaka, S. 2009. Elite and stochastic models for induced pluripotent stem cell generation. *Nature*, 460: 49-52

Zimm, H.B. 1953. Simplified relations Between Thermodynamics and Molecular Distribution Functions for a Mixture. *Journal of Chemical Physics*. 21: 934-935

Zimm, H.B. and Lundberg, L.H. 1956. Sorption of Vapour by High Polymers. *Journal of Physical Chemistry*. 21: 425-428

Zobel, B J.and J. P. van Buijtenen. *Wood Variation – Its Causes and Control*. Springer-Verlag (1989).

Zobel, B.J. and J.B. Jett. *Genetics of Wood Production*. Springer-Verlag (1995).

APPENDIX

A metaphor made on the basis of sexual reproduction would perhaps be helpful in rendering a generic insight to the analogy of two-level systems in chemical composition and physical properties of wood. During biological fertilization, an egg cell (inactive or static component) interacts with sperm cells (active component) to form an emergent property known as a pluripotent cell that is capable of differentiating into an organism. The inactive component is mainly single while the active component consists of many viable sperm cells. It would be very simple if the fertilization can take place by an egg cell and a single viable sperm cell and the biological event becomes very certain and deterministic. However, in real life fertilization becomes successful based on the interaction of a single egg cell and more than forty millions of sperm cells.

This study utilizes the analogy from biological reproduction without going to any significant depth in the mechanisms of fertilization and also with out any discourse as to what should be anatomical and other qualitative aspects of the sperm cells. It is possible to create an emergent property having many active components as far as the active and inactive interaction components are viable, which is a situation when both components are having powers or exponents almost close to each other in magnitude. From a pool of diverse egg and sperm cells few but hand picked and viable can be taken and allowed to interact and the fertilization can be successful. Similarly, without the need for selection and knowledge of the viability of sperm cell, many of them can be grabbed and allowed to interact with an egg cell and the fertilization can be as successful as the one made with meticulous selection. By raising the active state to larger powers the diversity between members of the second components is increased at the expense of similarity while the ability of the inactive and active component to form an emergent property remains invariant. Raising the second or the active component to larger and larger powers repeats the same physical behaviour by increasing diversity and reducing similarity but keeping the behaviour to form an emergent property invariant.

The two level-system, therefore, becomes more and more populated with dissimilar but synergistic components as the power of the active or second component is increased implying that the exponent of the active component or level to be a parameter that controls the field strength analogy to complexity. This analogy is in harmony with the technical capability recently obtained in getting induced pluripotent stem cells (iPPS) by Huangfu *et al*. (2008) from human fibroblasts using only two factors and low molecular chemical activation; however, it may be essential to point out that our analogy is not quite the same as the elitist model of Yamanaka (2009) which is put forward to explain the inefficiency in iPPS production in general. Generally, the two-component and two-level approach can render solutions to problems in any realm ranging from biomaterials to ecosystem where there is synergy or complimentarity between interacting components. It may not be, though, straight forward the analogy of the two-component and two-level system, as it has been discussed, has therefore a deep biological consequence.

The dual nature of the two-level and two-component approach can be generalized by the schematic diagram in Figure A.1 (on the next page) that depicts existence of invariant (identity) property in interactions ranging from homogeneous to complex and heterogeneous, using the Sierpinski gasket. The diagram also depicts two levels of mechanisms in which the first type is unifying or can be seen as self-organization to form a unified and synergistic whole. The second level is the highest in which components interact complexly and can be explained by scale invariant mechanisms or identities. The transition from similarity to identity through unity may not be hard to conceive; however, the transitions from diversity or complexity to identity are long range walks that can be accomplished by any of the routes leading to identity and the leap from diversity or complexity to identity is difficult with more of that involves back slides. This research was conceived, proposed and carried out based on the metaphor discussed and helped to solve the complex problem of water vapour sorption in wood in a unified approach. The concept may some how seem incompatible with certain aspects of “survival of the fittest” as it treats interaction as mainly synergistic but for a system that creates a unified and self-optimized whole like wood, it can work as elegantly discussed by Todes (2009) in the journal of Nature.

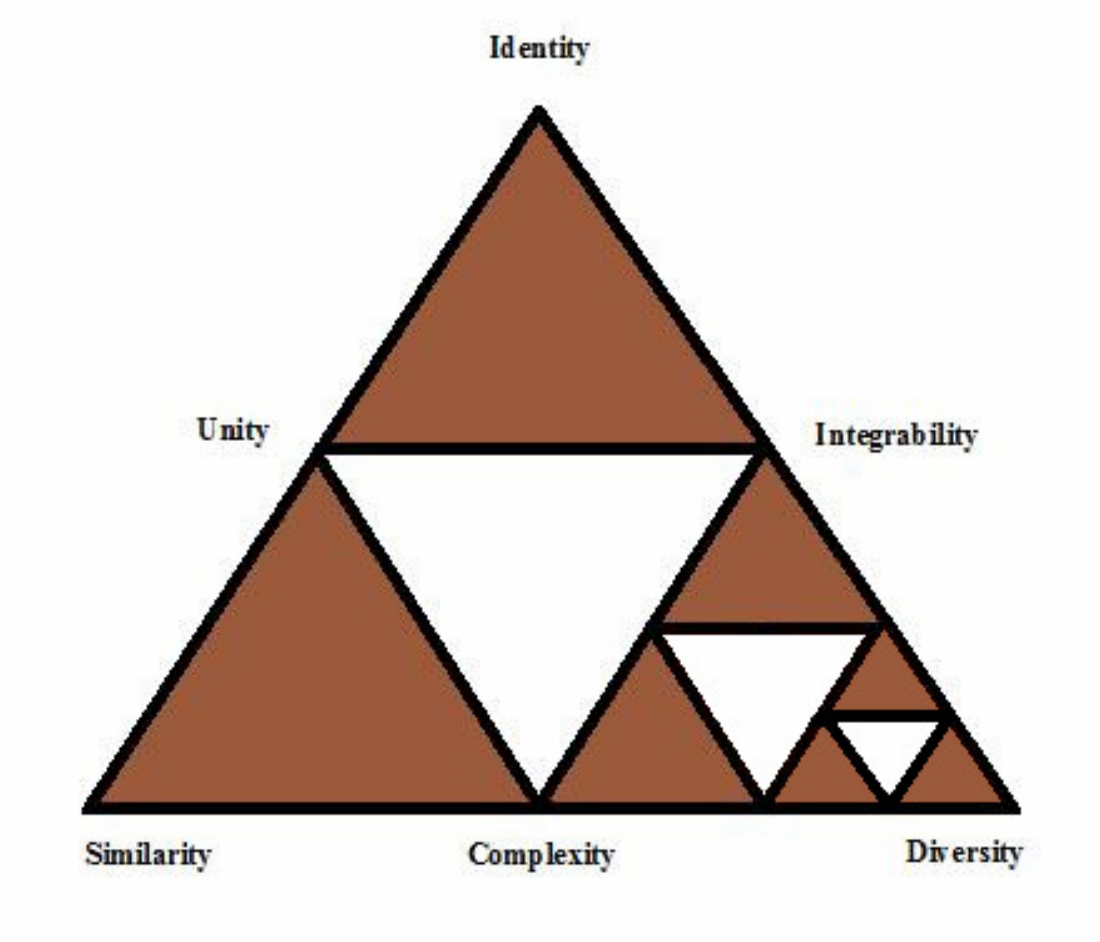

Figure A.1 General schematic representation of the invariant (identity) relationship arising from the interaction of homogeneous (similar) to diverse (heterogeneous) components using the Sierpinski gasket